

Experimental and Computational
Study of
Flames Venting Externally
During Full Scale Flashover Fires



Suzana Klopovic

A thesis submitted to Victoria University of Technology for the
Doctor of Philosophy Degree (Mechanical Engineering)

Victoria University of Technology

1999

FTS THESIS
628.9222 KLO
30001005875242
Klopovic, Suzana
Experimental and
computational study of
flames venting externally

DEDICATION

Mama i Tata

Za ljubav, pomoć i pašnju kroz godine

vaša kćerka

ACKNOWLEDGMENTS

I would especially like to thank my principle supervisor Dr. Özden Turan for her kind support and invaluable guidance. Her dedication and professionalism helped me develop both as researcher, and academic. Her sincere encouragement, patience and friendship have been an inspirational example during the arduous task of completing this thesis.

I must thank my co-supervisor Prof. Vaughan Beck for his assistance and commitment. The world class experimental fire facility created by him via the Centre for Environmental Safety and Risk Engineering, allowed the study of full scale fires, without which none of my research would have been possible. As such I wish to extend my sincerest thanks to Scott Steward and Martin Cole, who run the facility. Their experience in experimental testing and instrumentation has shown me the difficulties and challenges associated with researching flashover fires. I must also acknowledge the efforts of Dr. Mingchun Luo in the computer modelling aspects of this thesis, of Dr. Yaping He for his help in finding references along with the discussions we had, and of Prof. Paula Beever for her invaluable insight and guidance in reviewing this thesis. Finally, I must extend my thanks and appreciation to Teresa Alam whose project management skills and professionalism, along with her support and friendship helped considerably.

I would like to thank the Department of Mechanical Engineering for their unrelenting belief in my abilities. I am especially grateful to Dr. Michael Sek who first suggested I do a PhD. It was his initial encouragement and his thirst for knowledge and understanding which allowed me to see the rewards of doing research. I should also thank Denise Colledge, Marlene Schutt, Ray McIntosh, and all the other teaching and technical staff of the Department. Finally, my gratitude must be extended to my fellow postgraduate students and friends, Ben Bruscella, Katya Nyankina, Julie Han, Dana Stanca, Simone Lewis, Anthony Fernando and Jeremy Anderson who helped me keep my sanity.

Of course, recognition must be given to my family and friends for supporting me throughout the years, not just during my PhD but for all the years of preparation that naturally come before it.

ABSTRACT

In this study, externally venting flames have been examined during two series of full scale flashover fires. The purpose of the work is to investigate the likelihood of external fire spread from a burn room window with standard glass, when the external facade is non-combustible. The effects on externally venting flames of internal ventilation conditions, burning rate, burn room size and wind have been studied in detail. Secondary fires and glass breakage have been examined.. Repeatable experimental data and reliable information on externally venting flames have been generated for numerical model validation and performance based design code development.

During the first series of tests, polyurethane fuel was used in a standard burn room. With the results of the first series, the second series of tests were designed to be repeatable to generate reliable data. The second series of tests were performed in a larger burn room with furniture as fuel. In addition to repeatability, a new data averaging method was developed. Extensive comparisons were made with available experimental data and empirical approximations from the literature. Curve fits to the experimental data were developed for communication purposes. The experimental results were compared with limited numerical predictions.

SUMMARY

This thesis focuses on the effect of compartment ventilation conditions on flames as they emerge/vent from window openings in buildings with non-combustible external facades during full-scale flashover fires. As such, it is the first comprehensive full-scale study which focuses on the characteristics of emerging flames in a three-dimensional region above the window opening. The three major reasons for carrying out this work were to investigate the likelihood of external fire spread from a burn room window with standard glass, to produce repeatable experimental data for numerical model validation and to provide reliable information for performance based design code development and evaluation.

Two series of full-scale flashover experiments were designed to investigate externally venting flames. The first series of four tests was designed as a preliminary investigation into the venting of external flames during flashover fires, with polyurethane (PU) as the fuel source in a standard size burn room with a glazed window. This particular feature is rarely discussed elsewhere in the literature. The slabs of PU were arranged to mimic a bed and carpet, and the effects of a closed or open door on the growth of the fire were studied. As the fire developed, the burn room window failed, although it was closed initially. Failing of the glass allowed flames and smoke to vent from the window opening. Temperatures were measured on a *two-dimensional* cross section of the plume above the burn room window. The centre plane had been chosen for this purpose, between the burn room window and the window above. Total and radiative heat flux measurements on the external facade of the building were also taken, along with velocity and gas composition measurements. The effect of two different window arrangements were investigated, with a constant window size and fuel load.

During the first series of tests several important factors become apparent in relation to experimental set-up, instrumentation and measurements. These tests highlighted the random effects of glass breakage (burn room window) and the influence of environmental conditions, such as wind speed and direction on the venting flames. The appearance of flames outside the burn room window was due to continued combustion, but excess fuel factor could not be used as a means to quantify external flaming. Failure of the window above the burn room window during one of the tests, suggested that a secondary fire was

possible on the floor above. Observations of flame envelope were consistent with earlier empirical approximations for residential type buildings based on full-scale tests using mostly wood crib fires. However, the centre-line temperatures were over-estimated using similar approximations, most likely due to the tilting of the plume with respect to the external 2D thermocouple rack. The tilting caused the rack to miss the centre plane of the venting plume. This result was one of the reasons for developing a 3D external thermocouple grid for the second series of tests.

The second series of eight tests was designed based on the results of the first series. The second series also focused on the effects of the internal ventilation conditions on the venting flames and plume. To produce more realistic results, a larger burn room, representative of a living or lounge room was used, with commercially available (real) furniture. Temperature measurements were expanded to allow a *three-dimensional* map of the venting plume to be made. The new three-dimensional thermocouple grid extended approximately along the width of the burn room window, up to the window above and away from the external facade. Externally, total and radiative heat flux measurements were also taken. Internally, flow velocities into the burn room, gas composition, temperature and mass loss rates were recorded. The Smoke Management System (SMS) was activated during two of the tests to determine how it would influence the fire. Also, combustible lining was mounted in the corridor for one of the tests.

To eliminate the effects due to random glass breakage, and consequently to ensure repeatability, certain criteria were established to decide when the entire window should be lowered (Window Lowering Criteria, WLC#1 & WLC#2) during the second series of tests. The need to eliminate such randomness to produce repeatable results had become apparent during the first series. Similarly, for repeatability, tests were limited to days with low wind speeds, and they were completed while weather conditions remained almost constant, so that these conditions would have negligible effect on the plume. More importantly, a data analysis method has been developed based on averaging the time series data at a given grid point over the *Consistent External Flaming* (CEF) period. The external temperature data were subsequently non-dimensionalised with respect to the ambient and maximum external temperatures. These measures allowed comparison of the experimental results from tests with similar ventilation conditions. As a result, the second series of tests were grouped into two main ventilation classes. In this thesis, Class 1 refers to when the burn room door is open, and the window is opened according to the corresponding WLC,

and Class 2 is when the burn room door is closed, and the window is opened according to another WLC. Depending on the internal ventilation conditions, the standard glass in the burn room window affected fire spread differently. During Class 1 tests, failure of the burn room window resulted in external fire spread, while during Class 2 tests, the window did not fail on its own. However, flashover was facilitated by lowering the entire window to determine what would have happened if the window had failed (such as due to type or manufacturing defects). Consequently, bowing of the burn room window was an important factor due to its possible contribution to window failure.

Consistent External Flaming, CEF, covers a period during the fully developed phase, where externally venting flames consistently cover the region above the opening. This time period was determined for each test using burn room temperature and mass loss data, external temperatures and visual observations. Once CEF was defined, all external temperature and heat flux data were averaged over this period. Given the large volume of instantaneous data collected during these series of tests, CEF averaging allowed the data to be compiled into a form compatible with model outputs. It also eliminated randomness of the data over time due to turbulence.

The 3D external temperature measurements were presented using contour plots which focused on three specific planes: the centre plane (Plane 3), which corresponds to the same region as used during the first series of tests; a plane parallel to the external wall above the burn room window (Face 1), and a horizontal plane (Level 4) corresponding to the centre of the window above the room of fire origin. Three-dimensional temperature contour plots were also generated to provide an overall impression of the venting plume.

CEF averaged external temperature measurements allowed the evaluation of empirical approximations. In fact, the experimental results of the first series of tests were re-analysed to include CEF averaging. The same empirical approximations as the ones used with the results of the first series of tests, resulted in flame envelopes similar to the experimental ones for the second series, too, although by the very nature of the venting plume, its boundaries were recognised as being dynamic. Centre-line temperature approximations were found to overestimate the temperature along the flame axis. Modified equations were developed based on the experimental results gathered here. In addition, 3D polynomial equations were developed to describe the temperature variation that exists across the entire plume.

The conclusions reached at the end of the second series of tests were as follows. The implementation of the WLC, CEF averaging, non-dimensionalisation and grouping the tests according to specific internal ventilation conditions allowed repeatability to be gauged. It was found that the tests were very repeatable, with the exception of two tests which were unduly influenced by external wind.

Temperature and heat flux results were evaluated in terms of the initiation of secondary fires, and it was found that direct flame contact posed a greater risk than radiative heat transfer alone, through the window above the room or level of fire origin. The activation of the smoke management system (SMS) was observed to facilitate flashover during a Class 2 test which would not have otherwise progressed into a fully developed fire, by contributing to the bowing and subsequent failure of the burn room window. Bowing of the burn room window was also observed during these tests when external wind speeds were higher than anticipated. Such winds also contributed to the substantial swirling of the venting plume during three of the tests. The swirling plume was observed to have a diameter of approximately the width of the burn room window with a period of just over 1 second. Finally, the use of combustible wall linings in the corridor were not found to significantly influence the externally venting flames, however, within the building, higher temperatures and smoke levels were recorded.

The work concluded with a series of computer simulations which described the venting fire plume. The CFD code, CESARE-CFD, was modified from its original 'burn room' analysis to include a larger adjacent 'compartment' which represented the outside environment. Due to computational limitations, it was not possible to use as large a heat release rate as those of the Real Furniture Burns. However, due to the availability of more extensive experimental data, longer CEF periods and proven repeatability associated with these tests, it was still more appropriate to compare the numerical trends with the Real Furniture Burn results. While the experimental and computational results agreed globally, several aspects of the Real Furniture Burns were missing in the predicted results. These included the bellying of the plume, indicative of a greater horizontal reach, the effects of flame impingement and higher temperatures on the window above the burn room window. Comparison with the computational results further confirmed the appropriateness of the chosen CEF averaging and non-dimensionalisation of the experimental data.

CONTENTS

DEDICATION	ii
ACKNOWLEDGMENTS	iii
ABSTRACT	iv
SUMMARY	v
TABLE OF CONTENTS	ix
LIST OF TABLES	xiv
LIST OF FIGURES	xvi
NOMENCLATURE	xxii
1. INTRODUCTION	1
<hr/>	
1.1 THE DEVELOPMENT OF TWO SERIES OF TESTS	2
1.1.1 VENTILATION CONDITIONS	3
1.1.2 TEST METHODOLOGY	4
1.2 CONSISTENT EXTERNAL FLAMING (CEF)	6
1.3 THESIS STRUCTURE	7
2. BACKGROUND	8
<hr/>	
2.1 COMPARTMENT FIRES	9
2.1.1 THE PRE-FLASHOVER COMPARTMENT	10
2.1.2 FLASHOVER/FULLY DEVELOPED FIRES	11
2.2 FIRE SPREAD BEYOND THE ROOM OF FIRE ORIGIN	13
2.3 FIRE PLUMES	15
2.4 EARLY EXPERIMENTAL STUDIES ON EXTERNALLY VENTING FLAMES	18
2.4.1 THE VENTING PLUME	23
2.4.1.1 Rate of Burning	23
2.4.1.2 External Plume Shape	24
2.4.1.3 Centre-Line Temperature	26
2.4.1.4 Convective & Radiative Heat Transfer	27
2.4.1.5 Excess Fuel Factor	29
2.5 EXTERNALLY VENTING FLAMES REVISITED	30

2.6 EXTERNALLY VENTING FLAMES - ADDITIONAL CONSIDERATIONS	33
2.6.1 SMOKE MANAGEMENT SYSTEMS	33
2.6.2 GLASS BREAKAGE	34
2.6.3 HORIZONTAL AND VERTICAL PROJECTIONS	35
2.6.4 ENVIRONMENTAL EFFECTS	36
2.7 NUMERICAL MODELLING	39
2.7.1 MODELLING OF EXTERNALLY VENTING FLAMES	39
3. EXPERIMENTAL SETUP	43
<hr/>	
3.1 POLYURETHANE BURNS	43
3.1.1 THE BUILDING AND THE BURN ROOM	43
3.1.2 FUEL CONFIGURATION	47
3.1.3 EXPERIMENTAL CONDITIONS	48
3.1.4 INTERNAL INSTRUMENTATION	49
3.1.4.1 Mass Loss Platform	50
3.1.5 EXTERNAL INSTRUMENTATION	50
3.1.5.1 The Co-ordinate System for the 2D External Rack	50
3.1.5.2 Thermocouples	51
3.1.5.3 Heat Flux Transducers	53
3.1.5.4 Velocity Probes	55
3.1.5.5 Gas Analysis	55
3.2 REAL FURNITURE BURNS	56
3.2.1 THE BURN ROOM	56
3.2.2 WINDOW LOWERING CRITERIA	56
3.2.3 FUEL CONFIGURATION	57
3.2.4 EXPERIMENTAL CONDITIONS	61
3.2.5 INTERNAL INSTRUMENTATION	62
3.2.5.1 Mass Loss Platforms	65
3.2.5.2 Velocity Probes	65
3.2.5.3 Ignition Source	65
3.2.6 EXTERNAL INSTRUMENTATION	66
3.2.6.1 The Co-Ordinate System for the 3D External Thermocouple Grid	66
3.2.6.2 Heat Flux Transducers	67
3.2.7 EXTERNAL DATA ACQUISITION AND ANALYSIS	69

3.2.7.1 Data Logging System	69
3.2.7.2 Data Analysis Using MATLAB	71
3.2.8 COMBUSTIBLE LINING IN THE CORRIDOR	72
3.2.9 AIR HANDLING AND SMOKE MANAGEMENT SYSTEMS	72
4. POLYURETHANE BURNS - DISCUSSION OF RESULTS	74
4.1 INTRODUCTION	74
4.2 EXTERNAL TEMPERATURE RESULTS	76
4.2.1 TEMPERATURES ABOVE THE CENTRE OF THE BURN ROOM WINDOW	76
4.2.2 TEMPERATURE CONTOUR MAPS OF THE 2D RACK AND 3D GRID	80
4.2.3 EXCESS FUEL FACTOR	87
4.2.4 ESTIMATING FLAME ENVELOPE AND CENTRE-LINE TEMPERATURES	88
4.3 EXTERNAL HEAT FLUX RESULTS	93
4.3.1 VERTICAL AND HORIZONTAL HEAT FLUX VARIATION	93
4.3.2 HEAT FLUX ALONG THE BOTTOM OF W1M02	95
4.3.3 TOTAL AND RADIATIVE HEAT FLUX AT THE BOTTOM CENTRE OF W1M02	98
4.3.4 CALCULATED HEAT FLUX	99
4.4 WINDOW GLASS BREAKAGE	103
4.5 EXHAUST FLOW VELOCITIES	105
4.6 OXYGEN CONCENTRATIONS/GAS ANALYSIS	107
4.7 CONCLUSIONS FROM THE POLYURETHANE BURNS	110
5. REAL FURNITURE BURNS - DISCUSSION OF RESULTS	115
5.1 INTRODUCTION	115
5.2 VENTILATION CLASSES AND THE VENTING PLUME	117
5.3 CONSISTENT EXTERNAL FLAMING (CEF)	127
5.4 TEMPERATURE CONTOUR PLOTS	130
5.4.1 VENTILATION CLASS 1A - BURN 1 & BURN 2	132
5.4.1.1 Plane 3	132
5.4.1.2 Face 1	133
5.4.1.3 Level 4	134
5.4.1.4 Level 1 to Level 5	135

5.4.2 VENTILATION CLASS 1B - BURN 5 & BURN 8	138
5.4.2.1 Plane 3	138
5.4.2.2 Face 1	139
5.4.2.3 Level 4	140
5.4.2.4 Level 1 to Level 5	140
5.4.3 VENTILATION CLASS 2 - BURN 4 & BURN 7	142
5.4.3.1 Plane 3	142
5.4.3.2 Face 1	143
5.4.3.3 Level 4	143
5.4.3.4 Level 1 to Level 5	144
5.5 REPEATABILITY	146
5.5.1 MASS LOSS RATES	146
5.5.2 REPEATABILITY OF EXTERNAL TEMPERATURE MEASUREMENTS	149
5.5.3 QUANTIFYING THE REPEATABILITY OF EXTERNAL TEMPERATURE MEASUREMENTS	155
5.6 ESTIMATING PLUME FLAME ENVELOPE AND CENTRE-LINE TEMPERATURE	157
5.6.1 THE FLAME ENVELOPE AND COMPARISON WITH OTHER WORK	157
5.6.2 THE CENTRE-LINE TEMPERATURE AND COMPARISON WITH OTHER WORK	163
5.6.3 FURTHER COMPARISONS WITH OTHER WORK: CENTRE-LINE TEMPERATURE, RE-ATTACHMENT, SPANDREL LENGTH AND EXCESS FUEL FACTOR	168
5.6.4 CENTRE PLANE TEMPERATURE DISTRIBUTION ON FACE 1, FACE 2 & FACE 3	175
5.6.5 TEMPERATURE DISTRIBUTION ACROSS EACH FACE OF THE GRID	178
5.7 SECONDARY FIRES	184
5.7.1 DIRECT FLAME CONTACT	184
5.7.1.1 Window Cracking Times ~ W101 and W1M02	185
5.7.2 HEAT TRANSFER	187
5.8 EFFECTS DUE TO WIND AND SMOKE MANAGEMENT SYSTEM	194
5.8.1 BURN 3	194
5.8.2 SWIRLING	197
5.8.3 SMOKE MANAGEMENT SYSTEMS	201
5.8.4 BOWING OF THE BURN ROOM WINDOW AND SMS	202
5.9 CONCLUSIONS FROM THE REAL FURNITURE BURNS	204

6. NUMERICAL PREDICTION OF THE EXTERNAL TEMPERATURE FIELD 212

6.1 INTRODUCTION	212
6.2 NUMERICAL RESULTS AND COMPARISON WITH EXPERIMENTAL DATA	214
6.3 CONCLUSIONS FROM THE NUMERICAL PREDICTIONS	221

7. CONCLUSIONS 222

REFERENCES	228
-------------------	------------

APPENDICES 237

Appendix A: Calculated Spandrel Heights	238
Appendix B: Experimental Building Fire Facility Plans	239
Appendix C: Fuel Load and Layout for Burn 1	246
Appendix D: MATLAB Programs	247
Appendix E: Estimating Compartment Temperature	267
Appendix F: Co-efficients for each Face for Burns 2, 4 and 8	269
Appendix G: Sample Input and Output from CESARE-CFD	271

FOLDOUTS

Foldout 1: Polyurethane Burns: Summary Information	284
Foldout 2: Real Furniture Burns: Summary Information	285

List of Tables

<i>Table 1.1: Class distinctions for the Polyurethane and Real Furniture Burns.</i>	3
<i>Table 3.1: Fuel load for each of the PU tests.</i>	47
<i>Table 3.2: Environmental conditions and test durations for PU1 to PU4.</i>	48
<i>Table 3.3: Ventilation conditions.</i>	49
<i>Table 3.4: Fuel breakdown for Burn 2.</i>	58
<i>Table 3.5: Fuel load, ventilation conditions and additional factors.</i>	61
<i>Table 3.6: Environmental conditions.</i>	61
<i>Table 4.1: Calculated flame envelope.</i>	88
<i>Table 4.2: Observed flame shape during the CEF period.</i>	89
<i>Table 4.3: Measured burn room and external centre-line temperatures during CEF period.</i>	90
<i>Table 4.4: Calculated centre-line temperatures on Face 2.</i>	90
<i>Table 4.5: Flame emissivity determined using constant and variable flame thickness.</i>	100
<i>Table 4.6: Center-line temperatures and burning rates measured during the CEF period.</i>	100
<i>Table 4.7: Calculated radiative, convective and total heat flux and measured total and radiative heat flux in kW/m², at Level 1, Level 3 and Level 5 on the external wall.</i>	102
<i>Table 4.8: Measured heat flux, h_f, in kW/m², averaged over the CEF period.</i>	102
<i>Table 4.9: Time from ignition to initial cracking for PU1 to PU3 and to lowering for PU4 of the burn room window, W102, and time to dislodgment of the window in the floor above, W1M02.</i>	104
<i>Table 4.10: Summary of information gathered for the Polyurethane Burns.</i>	110
<i>Table 5.1: Summary of fuel load, environmental conditions, WLC and Class specifications, based on Table 3.5* and Table 3.6*.</i>	118
<i>Table 5.2: Class 1a event/time histories.</i>	118
<i>Table 5.3: Class 1b event/time histories.</i>	119
<i>Table 5.4: Class 2 event/time histories..</i>	120
<i>Table 5.5: Duration of CEF, T_{max} and T_{amb} used in non-dimensionalisation of the data.</i>	128
<i>Table 5.6: Statistical analysis of experimental data of external temperature contours to determine repeatability.</i>	156
<i>Table 5.7: Calculated flame envelope.</i>	159
<i>Table 5.8: Observed flame shape.</i>	159
<i>Table 5.9: Measured peak and average burn room temperatures and external centre-line temperatures averaged over CEF.</i>	164
<i>Table 5.10: Calculated center-line temperatures using Equation 2.15.</i>	165

<i>Table 5.11: Coefficients and variables of the 3D polynomial.</i>	180
<i>Table 5.12: Time from ignition to window cracking, flashover and CEF. Failure times include time of initial crack and of initial dislodgment of the Floor 1M window.</i>	187
<i>Table 5.13: Flame emissivity determined using constant and variable flame thicknesses..</i>	188
<i>Table 5.14: Center-line temperatures and burning rates measured during the CEF period.</i>	189
<i>Table 5.15: Calculated radiative, convective and total heat flux, kW/m², at Level 1, Level 3 and Level 4.</i>	189
<i>Table 5.16: Measured heat flux, hf, in kW/m².</i>	190
<i>Table 5.17: Bowing of the burn room window, W102.</i>	203
<i>Table 5.18: Summary of information gathered for the Real Furniture Burns.</i>	204
<i>Table A1: Calculated values of the necessary spandrel height</i>	238
<i>Table C1: Fuel Breakdown for Burn 1</i>	246
<i>Table F1: Co-efficients for Faces 2, 3 and 4 for Burn 2.</i>	269
<i>Table F2: Co-efficients for Faces 2, 3 and 4 for Burn 4.</i>	269
<i>Table F3: Co-efficients for Faces 2, 3 and 4 for Burn 8.</i>	270

List of Figures

Figure 2.1: Stages of a fire's development in an enclosure.	9
Figure 2.2: Features of a fire plume.	15
Figure 2.3: Regions of a fire plume.	16
Figure 2.4: Buoyant flow out of a window opening during a room fire.	17
Figure 2.5: Top view of an emerging plume for a through draft - Class 1 ventilation condition.	25
Figure 2.6: Side view of an emerging flame for a through draft - Class 1 ventilation condition.	25
Figure 2.7: Top view of an emerging plume for a no-through-draft Class 2 ventilation condition.	26
Figure 2.8: Side view of an emerging plume for a no-through-draft Class 2 ventilation condition.	26
Figure 2.9: Modified flame shape used to determine heat transfer effects to the external wall from the emerging plume.	28
Figure 2.10: Original and modified shapes of a venting plume due to horizontal and vertical projections.	36
Figure 3.1: Floor 1 - Plan view including instrumentation within the standard burn room for PU1 to PU3.	45
Figure 3.2: Plan view of the standard burn room, R102, and fuel load positions, and the external 2D thermocouple rack for PU1 to PU3.	45
Figure 3.3: Plan view of the large burn room, R102, fuel load positions and the external 3D thermocouple grid for PU4.	46
Figure 3.4: Window construction.	46
Figure 3.5: Bed fuel configuration.	47
Figure 3.6: Chair fuel load.	47
Figure 3.7: External 2D thermocouple rack.	51
Figure 3.9: Southern elevation - external instrumentation.	53
Figure 3.10: Plan view of burn room.	56
Figure 3.11: Fuel distribution in the burn room for Burn 2 to Burn 8.	59
Figure 3.12: Burn room layout showing the internal N-S thermocouple rack, bookshelf and arm chair, for Burn 2 to Burn 8.	60
Figure 3.13: Burn room layout showing window, couch and ignition source, tables, arm chairs and the internal N-S and E-W thermocouple racks, for Burn 2 to Burn 8.	60
Figure 3.14: Internal instrumentation layout on Floor 1.	63
Figure 3.15: Dimensions of the North-South and East-West thermocouple racks in the burn room.	64
Figure 3.16: Instrumentation layout on the mezzanine floor, Floor 1M.	64
Figure 3.17: Front view of the external grid and burn room window.	68
Figure 3.18: Side view of the external grid and building.	68

<i>Figure 3.19: External 3D thermocouple grid.</i>	68
<i>Figure 3.20: Locations of the external</i>	68
<i>Figure 3.21: The original HP VEE program which performed temperature scans.</i>	69
<i>Figure 3.22: The modified HP VEE program which collected voltages and cold junction temperature.</i>	70
<i>Figure 3.23: Combustible lining locations in Floor 1 corridor.</i>	72
<i>Figure 3.24: Supply (S/A) and return (R/A) air grill locations on Floor 1.</i>	73
<i>Figure 4.1: PU1 - Vertical temperature distribution along the external wall.</i>	78
<i>Figure 4.2: PU2 - Vertical temperature distribution along the external wall.</i>	78
<i>Figure 4.3: PU3 - Vertical temperature distribution along the external wall.</i>	79
<i>Figure 4.4: PU4 - Vertical temperature distribution along the external wall.</i>	79
<i>Figure 4.5: Burning Rate during PU1.</i>	81
<i>Figure 4.6: Burning Rate during PU2.</i>	82
<i>Figure 4.7: Burning Rate during PU3.</i>	82
<i>Figure 4.8: Burning Rate during PU4.</i>	82
<i>Figure 4.9: PU1 - temperature contour plot from the 2D rack.</i>	84
<i>Figure 4.10: PU2 - temperature contour plot from the 2D rack.</i>	84
<i>Figure 4.11: PU3 - temperature contour plot from the 2D rack.</i>	84
<i>Figure 4.12: PU4 - temperature contour plot of the Centre Plane, Plane 3 of the 3D grid.</i>	85
<i>Figure 4.13: PU4 - temperature contour plot of Face 1 of the 3D grid.</i>	85
<i>Figure 4.14: PU4 - temperature contour plot of Level 4 of the external 3D grid.</i>	85
<i>Figure 4.15: CEF averaged and non-dimensionalised temperature contours from Level 1 to Level 5 of the external grid for PU4, viewed from inside the burn room.</i>	86
<i>Figure 4.16: The plume envelope as it vents from the burn room window opening.</i>	89
<i>Figure 4.17: Schematic view of the soot pattern on the external facade during PU1.</i>	92
<i>Figure 4.18: PU1 - Vertical distribution of the total heat flux along the external wall.</i>	94
<i>Figure 4.19: PU2 - Vertical distribution of the total heat flux along the external wall.</i>	94
<i>Figure 4.20: PU3 - Vertical distribution of the total heat flux along the external wall.</i>	94
<i>Figure 4.21: PU4 - Vertical distribution of the total heat flux at the centre and bottom centre of W1M02.</i>	95
<i>Figure 4.22: PU1 - Horizontal distribution of the total heat flux along the bottom of W1M02.</i>	96
<i>Figure 4.23: PU2 - Horizontal distribution of the total heat flux along the bottom of W1M02.</i>	97
<i>Figure 4.24: PU3 - Horizontal distribution of the total heat flux along the bottom of W1M02.</i>	97
<i>Figure 4.25: PU4 - Horizontal distribution of the total heat flux along the bottom of W1M02.</i>	97
<i>Figure 4.26: PU4 - Total (hf4) and radiative (hf11) heat flux at the bottom centre of W1M02.</i>	98
<i>Figure 4.27: PU1 - Velocity across the top of W102 at $x = 0m$ and $y = -0.1m$.</i>	105
<i>Figure 4.28: PU2 - Velocity across the top of W102 at $z = 0m$ and $y = -0.1m$.</i>	106
<i>Figure 4.29: PU3 - Velocity across the top of W102 at $x = 0m$ and $y = -0.1m$.</i>	106

Figure 4.30: PU4 - Velocity at the centre of the burn room door (D1) where y is the distance above the floor. A positive velocity indicates flow into the burn room from the corridor. _____	106
Figure 4.31: PU1: Gas composition measured at the top centre of W101 on the external wall. _____	108
Figure 4.32: PU2: Gas composition measured at the top centre of W101 on the external wall. _____	108
Figure 4.33: PU3: Gas composition measured at the top centre of W101 on the external wall. _____	108
Figure 4.34: PU4: Gas composition measured at the centre of the burn room door, 2m above the floor. _____	109
Figure 5.1: Bowing of the burn room window at approximately 3½ minutes after ignition during Burn 7 (just prior to window failure). _____	121
Figure 5.2: Growth at approximately 3½ minutes after ignition during Burn 8. _____	121
Figure 5.3: Growth phase, side view, at approximately 6½ minutes after ignition during Burn 8. _____	122
Figure 5.4: Fully developed phase, front view, at approximately 8 minutes after ignition during Burn 8. _____	122
Figure 5.5: Fully developed phase, side view, at approximately 8 minutes after ignition during Burn 8. _____	123
Figure 5.6: Decay at approximately 14 minutes after ignition during Burn 8. _____	123
Figure 5.7: Velocity histories at the centre of the burn room door and at the indicated heights above the burn room floor for Burn 2. _____	125
Figure 5.8: Velocity histories at the centre of the burn room door and at the indicated heights from the burn room floor for Burn 5. _____	125
Figure 5.9: Burn 2 - CEF averaged temperature contours of Plane 3. _____	126
Figure 5.10: Burn 5 - CEF averaged temperature contour of Plane 3. _____	126
Figure 5.11: Burn 2 - 19 point smoothed upper layer temperature. The dashed line marks the beginning of flashover in the burn room. _____	128
Figure 5.12: Burn 2 at $x = 1.2m$, $y = 0m$ and $z = 0.5m$ at grid location P3/L1/F2. _____	128
Figure 5.14: Temperature during the CEF period for Burn 2 at $x = 1.2m$, $y = 0m$ and $z = 0.5m$, grid location P3/L1/F2. _____	129
Figure 5.15: Histogram of the temperature data given in Figure 5.14 (collected during the CEF period of Burn 2 at $x = 1.2m$, $y = 0m$ and $z = 0.5m$, grid location P3/L1/F2). _____	129
Figure 5.16: BURN 1 - Plane 3. _____	132
Figure 5.17: BURN 2 - Plane 3. _____	132
Figure 5.18: BURN 1 - Face 1. _____	134
Figure 5.19: BURN 2 - Face 1. _____	134
Figure 5.20: BURN 1 - Level 4. _____	135
Figure 5.21: BURN 2 - Level 4. _____	135
Figure 5.22: BURN 1 over the CEF period from Level 1 to Level 5 of the external grid. _____	137
Figure 5.23: BURN 2 over the CEF period from Level 1 to Level 5 of the external grid. _____	137
Figure 5.24: BURN 5 - Plane 3. _____	138
Figure 5.25: BURN 8 - Plane 3. _____	138
Figure 5.26: BURN 5 - Face 1. _____	139

<i>Figure 5.27: BURN 8 - Face 1.</i>	139
<i>Figure 5.28: BURN 5 - Level 4.</i>	140
<i>Figure 5.29: BURN 8 - Level 4.</i>	140
<i>Figure 5.30: BURN 5 over the CEF period from Level 1 to Level 5 of the external grid.</i>	141
<i>Figure 5.31: BURN 8 over the CEF period from Level 1 to Level 5 of the external grid.</i>	141
<i>Figure 5.32: BURN 4 - Plane 3.</i>	142
<i>Figure 5.33: BURN 7 - Plane 3.</i>	142
<i>Figure 5.34: BURN 4 - Face 1.</i>	143
<i>Figure 5.35: BURN 7 - Face 1.</i>	143
<i>Figure 5.36: BURN 4 - Level 4.</i>	144
<i>Figure 5.37: BURN 7 - Level 4.</i>	144
<i>Figure 5.38: BURN 4 over the CEF period from Level 1 to Level 5 of the external grid.</i>	145
<i>Figure 5.39: BURN 7 over the CEF period from Level 1 to Level 5 of the external grid.</i>	145
<i>Figure 5.40: Total mass loss history during Burn 1 and Burn 2.</i>	148
<i>Figure 5.41: Total mass loss history during Burn 5 and Burn 8.</i>	148
<i>Figure 5.42: Total mass loss history during Burn 3, Burn 4 and Burn 7.</i>	148
<i>Figure 5.43: Class 1a: Plane 3.</i>	151
<i>Figure 5.44: Class 1b: Plane 3.</i>	151
<i>Figure 5.45: Class 2: Plane 3.</i>	152
<i>Figure 5.46: Class 1a: Face 1.</i>	152
<i>Figure 5.47: Class 1b: Face 1.</i>	153
<i>Figure 5.48: Class 2: Face 1.</i>	153
<i>Figure 5.49: Class 1a: Level 4.</i>	154
<i>Figure 5.50: Class 1b: Level 4.</i>	154
<i>Figure 5.51: Class 2: Level 4.</i>	154
<i>Figure 5.52: Schematic side view of the plume.</i>	161
<i>Figure 5.53: Schematic top view of the plume.</i>	161
<i>Figure 5.54: Burn 4 Face 1 temperature variation across a venting plume.</i>	161
<i>Figure 5.55: Schematic representation of the emerging flame showing flame axis (plume centre-line), flame height (H) and width (W), and flame (T_p), opening (T_o) and ambient (T_{amb}) temperatures.</i>	164
<i>Figure 5.56: Measured and calculated center-line temperature distribution for Burn 1 and Burn 2.</i>	166
<i>Figure 5.57: Measured and calculated center-line temperature distribution for Burn 5 and Burn 8.</i>	166
<i>Figure 5.58: Measured and calculated center-line temperature distribution for Burn 4 and Burn 7.</i>	167
<i>Figure 5.59: Measured and calculated (Equation 2.1 with total and modified Q) centre-line temperature distributions for Burn 1 to Burn 8.</i>	169
<i>Figure 5.60: Data plotted using variables from Equation 2.26.</i>	170
<i>Figure 5.61: Trajectories of hot gas ejected from various rectangular windows.</i>	171
<i>Figure 5.62: Yokoi's Test #4 - mean temperatures during maximum intensity phase.</i>	173

Nomenclature

A_T	area of enclosed surface excluding the window (m^2)
A_t	area of enclosed surface including the window (m^2)
A_w	area of burn room window/opening (m^2)
b	emission co-efficient (m^{-1})
c_p	specific heat ($kJ/kg\ K$)
C_{temp}	co-efficient for excess temperature ($^{\circ}C$)
C_{vel}	co-efficient for upward velocity (m/s)
D	equivalent window diameter (m)
D	depth of the venting plume (m)
D_c	depth of compartment/enclosure (m)
E	Young's Modulus (MPa)
f_{ex}	excess fuel factor
g	acceleration due to gravity, $9.81\ m/s^2$
h	height of the burn room window from which the plume emerges (m)
h	height of the burn room window/opening (m)
H	height of the venting plume (m)
I	radiant heat flux density (kW)
k	constant ($kWm^2K[m^2/kg/s]^{0.6}$) used in Equation 2.21
l	distance along flame axis X (m)
l_f	flame length (m)
L	total mass of the fire load (kg)
m	mass inflow rate of air (kg/s)
n	parameter ($w/1/2h$)
Q	heat release rate (kW)
Q_{rec}	dimensionless heat release rate
r	stoichiometric ratio
R	rate of burning (kg/min or kg/s)
T	temperature ($^{\circ}C$ or K)
T_o	window/opening temperature ($^{\circ}C$ or K)
T_f	flame temperature ($^{\circ}C$ or K)
ΔT_m	centre-line temperature rise above ambient ($^{\circ}C$)
T_{FDF}	average temperature during the fully developed phase ($^{\circ}C$ or K)
T_{wall}	wall temperature ($^{\circ}C$ or K)
T_{max}	maximum temperature ($^{\circ}C$ or K)
T_{amb}	ambient temperature ($^{\circ}C$ or K)
u	wind speed producing through-draft (m/s)
u^*	velocity based on heat release rate (m/s)
U_m	centre-line velocity (m/s)
V	upward velocity (m/s)
V_{wind}	wind velocity (m/s)
w	width of the burn room window/opening (m)
W	width of the venting plume (m)
W_c	width of compartment/enclosure (m)
X	flame axis

z	height above window/opening (m)
Z	height above virtual source (m)
α	convective heat transfer co-efficient ($\text{kW}/\text{m}^2\text{K}$)
β	co-efficient of linear expansion (K^{-1})
ϵ	flame emissivity
η	parameter ($A_T/A_w\sqrt{h}$)
ϕ	plume tilt angle ($^\circ$)
κ	constant ($\text{kgm}^{-5/2}\text{s}^{-1}$)
λ	flame thickness (m)
θ_1 to θ_5	multiplication factors (see Appendix E)
ρ_{amb}	ambient density (kg/m^3)
σ	Stefan-Boltzmann constant, $5.6699 \times 10^{-8} \text{ Wm}^{-2}\text{K}^{-4}$
σ_b	breaking stress (MPa)
τ_F	free burning duration (min)
Υ	wind correctional factor used in Equation 2.26
Θ	dimensionless temperature
N	North
S	South
E	East
W	West
CEF	consistent external flaming
hf	heat flux
ΔH_c	heat of combustion
HRR	heat release rate
NA	neutral axis
PU	polyurethane
WLC	window lowering criterion, WLC #1 or WLC #2
Plane	vertical section of the 3D external thermocouple grid perpendicular to the external wall
Face	section of the 3D external thermocouple grid parallel to the external wall
Level	horizontal section of the 3D external thermocouple grid and perpendicular to the external wall
Class 1	through-draft ventilation condition (burn room door and window are open)
Class 2	no-through draft ventilation condition (burn room door is closed, window is open)

1. INTRODUCTION

Legend has it that Prometheus stole the knowledge of fire, craft and sacrifice from the gods and gave it to the human race in an attempt to save them from the wrath of Zeus. As punishment for his betrayal, Zeus chained Prometheus to a mountain peak and plagued humankind with Pandora and her box of evil. The human race lost its innocence and barbarism but gained knowledge at the expense of its mortality.

Such sacrifice seems unworthy of such a gift, however Prometheus believed that without the knowledge of fire, the human race could not have progressed[1].

Until recently, research on fire characteristics has concentrated on the ‘room of fire origin’. The amount of data collected in this area of fire research is significant[2,3]. The effects of fire and smoke spread beyond the room of fire origin (burn room), on the other hand, have not been investigated to the same extent. In this respect, one interesting characteristic of fire is the way it spreads out of openings, such as windows of buildings. The appearance of flames through windows in buildings is caused by the venting of unburnt gases from the burn room and their continued combustion beyond the opening where a reservoir of fresh air exists[4]. External flaming is characteristic of fires that have undergone a transition to flashover[5] and entered a ventilation controlled state.

The amount of emerging/venting flames and combustion products, and the risk they pose to the external facade of a building are at their highest during the fully developed phase of a fire[6]. It is during this phase that temperatures both inside the room of fire origin and outside on the facade are also at their highest. As a result, a secondary fire may initiate, either in the upper levels of the building[7] or adjacent structures[8] via direct flame contact or radiative heat transfer from the venting plume. Consequently, this thesis was undertaken with the objective of studying, quantifying and understanding the nature of flames as they vent from window openings in a building with non-combustible external facades, during flashover fires. This work is the first comprehensive full-scale study of the phenomena associated with venting flames, in which realistic fuel types have been used.

The need to have a detailed analysis of the venting plume stems from the recent emergence of performance based fire codes[9,10]. In the past, most fire safety design systems and specifications were based on empirical relationships[11]. The use of CFD (computational fluid dynamics) and Zonal Models[12] has become an alternative means to predict the effects of a fire, both inside and beyond the room of fire origin. However, before such numerical models can be used in conjunction with performance based codes and risk assessment models[13], their predictions need to be validated against results taken during full-scale experiments[14]. Hence, while it is possible to use some small scale fire tests for full-scale fire prediction[15,16], the use of full-scale experiments eliminates the difficulties associated with such small scale correlations[17, 18]. Hence, well planned full-scale tests are still needed in developing better designs to minimise fire loss. These tests need to be representative of realistic living and working environments and more importantly they must be repeatable.

1.1 THE DEVELOPMENT OF TWO SERIES OF TESTS

As part of this study, two comprehensive series of full-scale flashover fires were conducted to investigate the effect of external flames venting from openings in a building during the flashover/fully developed phase of a fire. The two series were, *Polyurethane Burns*[†] and *Real Furniture Burns*[‡]. The primary intention of these experiments was to determine the effects of ventilation conditions on the venting plume and the likelihood of secondary fires. Although external combustible cladding can also contribute to the likelihood of secondary fires[19,20], this topic is beyond the scope of the thesis. In total, four Polyurethane and eight Real Furniture tests were performed.

In the first series of Polyurethane (PU) Burns, three of the four tests were carried out in a *standard sized burn room*, while the last test was performed in a *large burn room*, similar to a residential living room. The *Polyurethane Burns* should be viewed as a preliminary set of experiments, developed as a precursor to the second series of tests,

[†] The Polyurethane Burns were conducted through a CESARE contract with the National Research Council of Canada (NRCC).

[‡] The Real Furniture Burns were performed in conjunction with CESARE's contract with the Fire Code Reform Centre (FCRC) of Australia.

the Real Furniture Burns. These preliminary tests helped in developing an understanding of the nature of externally venting flames during flashover fires. The second series of Real Furniture Burns was designed on the basis of the understanding of the venting plume developed during the Polyurethane Burns. The Real Furniture Burns were conducted with commercially available furniture in the larger size (living) room where the fourth polyurethane test took place. All tests were grouped according to specific ventilation conditions that existed within the building.

1.1.1 Ventilation Conditions

The ventilation conditions during both series of tests can be grouped into two classes, each having a distinct effect on the way the plume vents from the window opening[21]. A *through-draft-condition* implies that air may flow through a room, such as from an open door to an open window. This ventilation condition is referred to as *Class 1* in this thesis. A *Class 2, no-through-draft-condition*, implies that there is no such flow of air through the room, such as when the door is closed. In a Class 1 test, air in the burn room is supplemented with air from adjacent rooms or a corridor. This allows the flames to vent from the entire window opening. Class 1 tests have been further grouped into Class 1a and Class 1b tests, according to the internal ventilation conditions within the building. In a Class 2 test, the combined effect of a closed door and a closed window may suffocate the fire if the window does not fail. However, if the window fails, the supply of air from outside will help sustain the fire, causing the flames to vent from the upper half to two-thirds of the opening, while air is drawn in from the lower half to third. In both these classes, if a sufficient amount of fuel and air is available, the fire can grow to a fully developed condition, where all the combustible material in the room becomes involved. For both series of tests, Table 1.1 lists the ventilation conditions which existed for each test.

Table 1.1: Class distinctions for the Polyurethane and Real Furniture Burns.

	POLYURETHANE BURNS				REAL FURNITURE BURNS							
	PU1	PU2	PU3	PU4	B1	B2	B3	B4	B5	B6	B7	B8
CLASS 1a												
CLASS 1b												
CLASS 2												

1.1.2 Test Methodology

During the first three PU tests, the temperature field in a 2D cross section of the plume was mapped, above the top centre of the burn room window, perpendicular to the external wall. This region of space was chosen for the preliminary investigation, as the majority of work in this field[8,20,22] had focused on this region. The mapped area covered a 2.78m high and 1.5m deep section of the plume, which included its centre-line, with 20 temperature sample locations. Total and radiant heat flux, velocity and gas composition measurements were also taken during each of the tests.

After the completion of the PU tests, several influential factors regarding fire development and test structure became apparent. These factors, listed below, had to be considered when designing the second series of tests:

1. randomness of glass breakage,
2. natural wind movement on the venting plume,
3. seemingly subtle differences in internal ventilation conditions,
4. temperature variation across the height, depth and width of the plume,
5. likelihood of a secondary fire,
6. repeatability of external and internal experimental results.

As a result, the following measures were taken before the second series of tests. Firstly, to eliminate partial cracking/dislodgment of glass in the burn room window, two window lowering criteria were established. These criteria were first implemented during the last polyurethane test, PU4. This practice resulted in the entire window being lowered when either one of the two sets of conditions was met. The Window Lowering Criteria (WLC) were based on the onset of window failure as determined by glass and gas temperatures for Class 1 tests, and from mass loss rate for Class 2 tests where the window was lowered to facilitate flashover. The specifics of each window lowering criterion are detailed in *Section 3.2.2*. As a result, some measure of repeatability was established between similar tests. Secondly, to overcome variations in wind speed and direction, which alter the path of the venting plume, all tests were carried out on 'still' days, where a wind speed of no more than 10km/hr (2.8m/s) was expected. Thirdly, given the influence of ventilation conditions on the development and subsequent venting of the flames, it became apparent that these effects needed to be studied in detail. This objective was achieved by having pairs of tests, providing repetitions.

The fourth measure was that given the variations in temperature with *height* and *depth* observed in a two-dimensional section of the venting plume, it was necessary to investigate the temperature variations across the *width* of the venting plume as well as along the height and depth. This was achieved by constructing a three-dimensional external thermocouple grid, instead of the two-dimensional rack used earlier. The three-dimensional grid was positioned on the external wall, above the window opening of the burn room. The new grid extended over a region expected to be covered by the venting plume (2.4m wide, 3.9m high and 1.5m deep), and it had a total of 140 temperature sample locations. Although this arrangement complicated the data acquisition and subsequent analysis, it helped clarify the physics of externally venting flames.

The occurrence of severe cracking and dislodgment of the glass in the window on the level above the burn room during one of the PU tests, was an indication of the overall severity of the fire and its potential to initiate a secondary fire, either through direct flame contact or radiative heat transfer. As a fifth objective, this point needed to be studied further. Finally, the need for repeat tests stemmed from the uniqueness of each of the PU tests during which invaluable insight was gathered, but some of the information was inconclusive. Consequently, the second series of tests was designed to have at least two repeat tests in each ventilation class for comparison. The Real Furniture Burns, BURN 1 to BURN 8, incorporated all of the above mentioned modifications.

As mentioned earlier, the increased number of temperature measurements for the second series of tests complicated both the data acquisition process and the data analysis. To remove random variation in time of the measured temperatures during the fully-developed phase and for comparison with numerical models, a time averaging method was developed. This method consisted of time averaging the experimental data over the Consistent External Flaming (CEF) period of each test, and it allowed comparison of the large amount of data collected during repeat tests. For the purpose of gauging repeatability, further spatial averaging was used. In part, the reason for developing the CEF averaging method was similar to those of Janssens *et al.*[23] and He[24] for data reduction with spatial averaging for zone model comparison. The averaging of experimental data over the Consistent External Flaming (CEF) period is discussed in *Section 1.2* below.

1.2 CONSISTENT EXTERNAL FLAMING (CEF)

The flow of hot gases and smoke in the burn room is mainly buoyancy driven and turbulent. The temperature field is controlled by natural convection, forced convection (for a through-draft ventilation condition) and radiation, in addition to being coupled with the velocity field. The externally venting plume is also driven by buoyancy, and air entrainment exists along its free boundaries. Both internally and externally, the velocity and temperature fields are turbulent. Turbulence alters the moment to moment development of a fire, but the stages of a fire's progress remains the same. The fire begins at ignition, moves through flashover to the fully developed phase, and then eventually decays as the fuel source is consumed. Consequently, the comparison of *instantaneous* results for similar locations both within the burn room and outside is inappropriate due to the random nature of turbulence. An averaging method has been developed here based on the time averaging of experimental data over the Consistent External Flaming period, described next. Subsequently, the external temperature data were non-dimensionalised using the ambient and maximum external temperatures during the CEF period, to consolidate the data according to the stage of fire development. The same averaging and non-dimensionalisation were applied to each test to allow the data to be interpreted.

Consistent External Flaming (CEF) refers to the portion of *the fully developed fire* when externally, strong consistent flames exist. In determining this time period, several factors were considered. These factors are,

- ◆ burn room temperatures
- ◆ mass loss data
- ◆ temperature just outside the opening
- ◆ visual observations

Flashover acts as a precursor to the onset of CEF. As such, factors such as burn room temperatures and the appearance of external flames, provide a convenient marker as to the onset of CEF. However, as CEF corresponds to *consistent* external flaming, some time lapses before the flames which first appear at flashover exist continually beyond the window opening. The amount of time lapse depends primarily on the ventilation conditions. A detailed explanation of how the CEF duration was decided on is given in *Section 4.2.2* and *Section 5.3* with respect to PU and Real Furniture tests, respectively.

1.3 THESIS STRUCTURE

In the following, the background information on flashover fires and externally venting flames is summarised in Chapter 2. Chapter 3 contains the details of the experimental arrangements used for both series of tests. Chapters 4 and 5, respectively, contain the experimental results* from the Polyurethane Burns and Real Furniture Burns. Chapter 6 contains the numerically predicted results of the external temperature field using CESARE-CFD and comparison with experimental data. The conclusions of this thesis are listed in Chapter 7.

Appendix A contains information to estimate the necessary spandrel height to prevent fire spread through an upper level window. The building plans of the Experimental Fire Building Facility where the experiments were conducted, are included in Appendix B. A detailed fuel load breakdown of the first test (Burn 1) of the second series of Real Furniture Burns is given in Appendix C. The eight main MATLAB computer programs developed in this thesis for data analysis are listed in Appendix D. The details of a compartment temperature calculation are given in Appendix E. Appendix F contains the temperature contours of each Face of the venting plume for the second series of tests. Appendix G contains sample input and output data files from CESARE-CFD for the numerical predictions presented in Chapter 6.

For easier reference to internal instrumentation, burn room configuration, external instrumentation consisting of both thermocouple and heat flux transducer locations, fuel load, environmental conditions and ventilation conditions, two foldouts are located after the Appendices. Foldout 1 and Foldout 2 contain the above information for the Polyurethane Burns and Real Furniture Burns, respectively.

* The experimental results referred to in this thesis are available from the author and CESARE (Centre for Environmental Safety and Risk Engineering).

2. BACKGROUND

As discussed in the *Introduction*, the fully developed fire is of interest here, since the maximum amount of externally venting flames and combustion products exists during this phase of the fire[6]. This stage of the fire also poses a significant risk, in terms of exterior structural damage[25] and fire spread to the external facade of the building and to adjacent structures[8]. As such, an understanding of the ability of a fire to achieve flashover[26,27] and the progress from a flaming fire to a fully developed fire is necessary with respect to external flames.

Factors affecting a fire are primarily the fuel source (type, load and distribution), ventilation conditions, such as the size of openings, and rate of burning. These in turn influence the likelihood of external flames. Once the fire extends beyond the compartment, window geometry and the presence of other openings, affect the shape of the external plume and whether or not re-attachment to the facade occurs[28 and 49, pp. 189-194], while the environmental conditions influence both swirling of the plume and air entrainment into it. The external plume can be considered in terms of flame shape (height, width and depth), temperature and velocity distribution[28] within the plume and heat flux received by external[29] or adjacent[8] walls, where all of the above mentioned factors play an important role.

This chapter discusses briefly the development and spread of fire within a compartment in *Section 2.1*. This is followed in *Section 2.2* by the early experimental work in the area of externally venting flames and the subsequent development of a Design Guide[30] which is still being used to determine the shape and temperature distribution of venting plumes. *Section 2.3* summarises works on fire plumes, while the limited number of earlier studies on venting flames is discussed in *Section 2.4*. Numerical modeling of externally venting flames is discussed in *Section 2.7*. Once the fire changes from a localised to a fully developed fire, factors specifically affecting externally venting flames are discussed in *Section 2.6*. These include, Controlled Ventilation Systems, Glass Breakage, Horizontal and Vertical Projections and Environmental Effects. In *Section 2.5*, additional experimental work on externally venting flames is discussed.

2.1 COMPARTMENT FIRES

The birth of the fire occurs at ignition, and if conditions are favourable, the temperature in the compartment will continue to rise. Depending on the first item ignited and ventilation conditions, the fire may either continue to grow, spreading to other items, or it may die out, and as such, the transition into a fully developed fire may not occur. However, if the fire continues to grow, the transition from a localised fire to complete room involvement occurs. Figure 2.1 illustrates the stages of the fire's development within a compartment from ignition to decay[31,p. 278]: ignition, growth, flashover, fully-developed and decay.

Although the presence of external flames is directly related to the conditions within the compartment, including entrainment, ventilation conditions and heat transfer effects, these factors are not generally discussed with respect to their effect on externally venting flames. The limited number of works discussed in *Section 2.4* and *Section 2.5* relate the compartment conditions to the external plume.

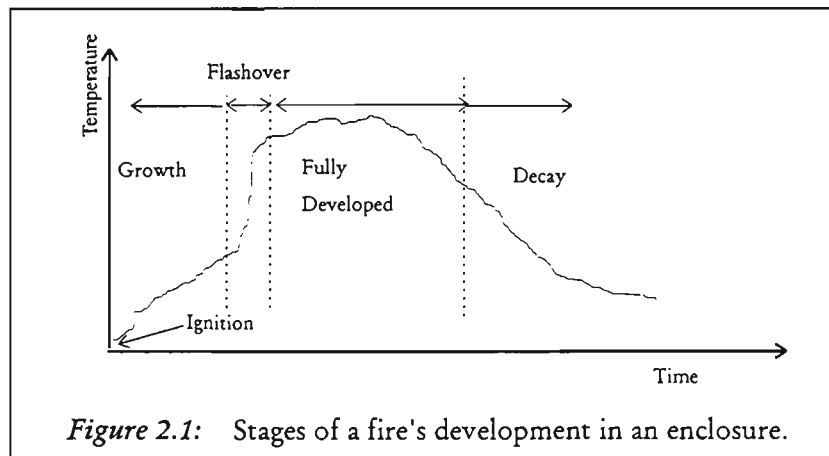


Figure 2.1: Stages of a fire's development in an enclosure.

Compartment fires can be divided into three main stages, pre-flashover, flashover/fully developed and decay. Quintiere[2,3] provides an extensive review of compartment fires with respect to fundamental fluid mechanics, heat transfer and combustion processes, as well as the corresponding models that exist. He begins with a discussion of the differences in entrainment into a fire plume when the fire source is unbounded or cornered, as well as some of the differences between wood crib and real furniture fires. Vent flows, convective and radiative heat transfer are discussed with respect to fire scenarios, from the item first ignited to the second item, to wall/ceiling spread. This is followed by a discussion of the effect of ventilation openings on the fire and the

spread to adjoining spaces. Overall, the areas where further experimental and computational work is required are indicated. Quintiere points out that many individual aspects pertaining to compartment fires have been examined and effectively modelled. These aspects include plume development and entrainment, describing vent flows and given sufficient data, computing ignition of primary and secondary items. However, certain areas still need to be addressed, one of which is the modelling of fire spread outside windows.

2.1.1 The Pre-flashover Compartment

Ignition of an item is associated with the onset of combustion, a rapid exothermic reaction, manifesting as flames and an increase in temperature[32]. After ignition, the flame will spread along the combustible surface of the fuel source. Surface flame spread is described as the '*phenomenon of a moving flame in close proximity to its source of fuel*'[33], a solid or liquid, unlike a pre-mixed flame which spreads through an air-fuel mixture. Flame propagation across the fuel surface is sustained by the transfer of heat to the surface which causes the pyrolysis of the region directly before the flame front. The interdependence of heat transfer and continuous gasification of fuel is the primary interaction which defines surface flame spread. Williams[34] and Thomas[35] have provided extensive reviews of flame spread and its dependence on pressure, temperature, oxygen concentration, fuel type, geometry and orientation, as well as flame spread over continuous or discrete surfaces, effects of ventilation and upward spread. Their works have focused on spread along fuel sources and can be applied to the spread of flames along vertical combustible surfaces, such as external cladding. This aspect of flame spread is not within the scope of this thesis.

The fire can spread from the item first ignited to other items either through direct flame spread or due to radiative heat transfer. Direct flame spread can occur along carpets or other floor, wall or ceiling linings[36] (within the enclosure, to adjacent enclosures and outside the building). If radiation is sufficiently high from hot smoke and combustion products which have accumulated under the ceiling, combustible items may ignite[37]. The transition from a localised to complete room involvement is referred to as flashover and leads to the fully developed stage of the fire.

2.1.2 Flashover/Fully Developed Fires

Several theoretical approaches have been developed to predict if and when a fire would achieve flashover. Graham *et al.* based their work on heat balance considerations within the hot upper layer of a two-zone model and classical thermal explosion theory[26]. Babrauskas' method[37] calculates the heat release rate necessary to cause flashover, as a fraction of the stoichiometric heat release rate, using ventilation factors and a modified radiative heat transfer equation. The McCaffrey, Quintiere and Harkleroad method[37] and the Thomas method[37], also use a combination of these, placing different emphasis on the effect of ventilation with respect to the room. McCaffrey *et al.* correlate experimental data to obtain energy release rates required for flashover, while Thomas focuses on the minimum rate of energy release necessary for flashover using an energy balance of the upper layer.

While a theoretical means exists to predict whether or not flashover will occur, an explicit definition has not yet been agreed upon. It is understood that flashover is *'the rapid transition to a state of total surface involvement in a fire of combustible materials within an enclosure'* [38]. Contained within this description are several mechanisms which have been associated with the transition into a fully developed fire. These are[5]:

- ◆ an increase in the burning rate
- ◆ the spread of flames over all exposed surfaces
- ◆ burning of the hot smoke/gas layer under the ceiling

Each of these mechanisms can be associated with either quantifiable or physical manifestations. These are[5]:

- ◆ when gas temperatures under the ceiling in the room of fire origin reach between 500°C to 600°C
- ◆ when a radiation heat flux of 20kW/m² at floor level is measured ~ Waterman's Criterion
- ◆ external flaming as a result of the ignition of unburnt fuels within the smoke layer ~ Hugglund's Criterion

Each of the above points has been linked to the onset of flashover and has been used as an indicator of the transition into a fully developed fire. However, given that a precise definition of flashover has yet to be decided upon, it has become accepted practice to associate compartment temperatures in the upper layer of 500 to 600°C with the onset of flashover[27]. Waterman's Criterion[39] refers to the ignition of strips of paper at floor level, which was based on earlier work associated with the rapid pyrolysis or 'flameover' of cellulosic floor coverings[35, p.317], and has been found to be conservative[5]. Finally, the appearance of flames from available openings was originally specified as Hugglund's Criterion[31, p.284] and a definition of flashover. However, as indicated by Walton[37], the appearance of flames may not correspond to flashover. Although external flaming may not be 'flashover', it has been observed in this study that the appearance of external flames can provide a clear and convenient indication of the fire's having progressed to the fully developed stage.

In general, the fully developed stage is usually ventilation controlled as the amount of pyrolised fuel produced exceeds the oxygen available in the enclosure. Flashover produces conditions favourable for external flaming, such as through cracking and failure of windows. Windows can be said to act as '*barriers*'[40] to prevent or delay the passage of flames during the initial stages of the fire and may delay the onset of flashover. However, they also have the potential to become vents, and in doing so, supply the fire with air. Openings such as doors to adjacent rooms and enclosures provide a means for the hot gases to move around the building[41]. The spread of fire can be caused by the spontaneous ignition of a surface or fuel due to exposure of radiative heat from hot smoke and combustion gases which have accumulated under the ceiling in adjacent enclosures, or through direct flame spread. Following the fully developed phase, as the remaining fuel is consumed, the fire begins to die.

The flashover and fully developed phases of a fire pose the greatest risk of fire spread throughout a building. With the highest temperatures and strongest flames generated during this stage, the resulting interior and structural damage is the most severe, as is the risk associated with external flaming and external spread.

2.2 FIRE SPREAD BEYOND THE ROOM OF FIRE ORIGIN

During the fully developed phase, spread of the fire beyond the room of fire origin becomes possible, either to adjacent enclosures within the building or externally through window openings[42].

Mechanisms of fire spread *within the building* can occur either:

- ◆ by surface or direct flame spread along carpets or other floor, wall, or ceiling linings, or
- ◆ by the build-up of a hot layer in an adjacent enclosure, which increases the temperature and causes the ignition of its contents.

While *external spread* of the fire can occur either:

- ◆ by *leap frogging* of flames which emerge from a lower level opening and ignite combustible material on the inside of the level above by radiative heat transfer or by direct flame contact if the window is opened or has failed,
- ◆ by the spread to adjacent buildings, or
- ◆ by the ignition of combustible exterior walls.

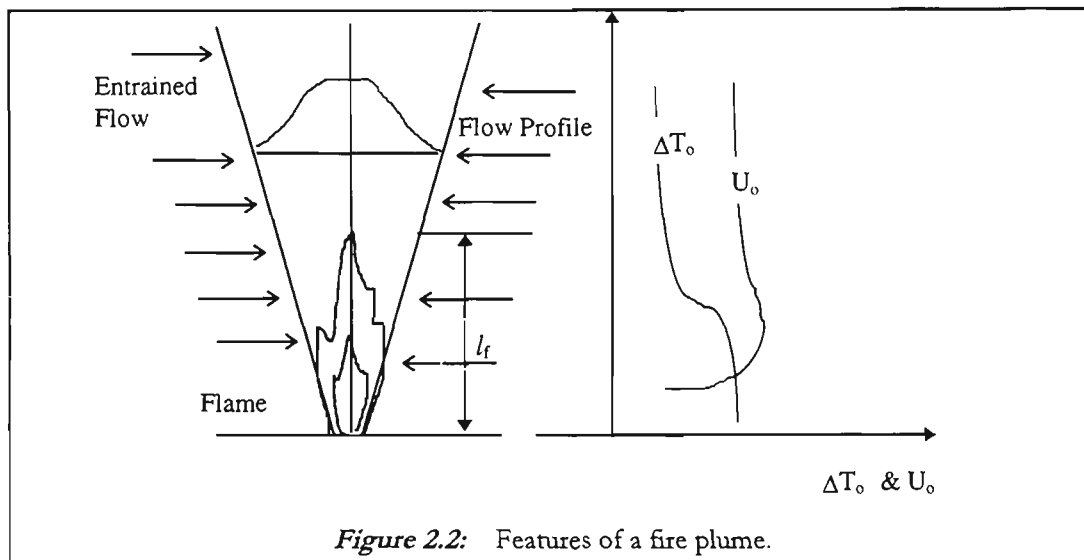
The risk of room to room spread and ceiling/floor spread can be minimised by the implementation of proper design codes and the use of fire doors. The spread and accumulation of hot gases in adjacent enclosures or to higher levels via stairwells, can also be reduced by *controlled venting systems*[43]. A controlled venting system implies active removal of hot gases and smoke, through the use of an air handling system in a modified mode of operation, as opposed to the escape of gases and smoke through vents due to natural pressure and temperature differentials.

On the other hand, external fire spread poses a threat which many conventional fire protection schemes and efforts neglect to address. The danger of a fire *leap frogging*[44] between levels of a building is greater at present, due to the numerous and continued construction of apartment buildings in both city and suburban areas. Leap frogging is where flames emerging from a lower level window reach the window on the level

above (where the external wall does not participate) and cause ignition of combustibles in the level above. Sprinklers can reduce the size of external flames by limiting the size of the fire, by cooling the upper gas layer in the enclosure[45] or by cooling the glazing[46]. When sprinklers are not present, the Building Code of Australia (BCA) and other international codes require certain spandrel heights to prevent leap-frogging. The spread to adjacent buildings can be limited by ensuring effective separation distances[47]. Another factor to be considered is the use of external combustible cladding. Although it is limited in Australia, the push for its use is increasing due to cheaper production costs. However, before its use is increased further, flame spread across a combustible medium needs to be investigated in more detail. This issue of flame spread over combustible exterior cladding is not within the scope of the present study.

2.3 FIRE PLUMES

Buoyant flow consisting of heated gas, smoke and flames, which rise from a burning item into a region of essentially uncontaminated air is referred to as a fire plume[48]. Inside an enclosure, a plume is said to exist through all the early stages of a fire's development, until just before flashover. Conventional analysis considers the plume to be axisymmetric and surrounded by uncontaminated air of uniform temperature as shown in Figure 2.2, where l_f is the mean flame length, ΔT_o is the mean excess temperature and U_o is the mean velocity.



Generally, plume temperatures are the highest within the combustion region. The temperature decreases with increased height and air entrainment into the plume, which cools the flow. Velocities within the plume peak in the intermittent region of the flame, slightly below the mean flame length, and drop-off with increased distance above the burning item. The total heat release comprises of convective flux which is carried away by the plume and radiative flux which radiates away from the combustion region.

Parameters of interest in fire plumes *within an enclosure* are: its height, the top of which oscillates vertically making flame height definition difficult; the entrainment rate of air into each distinctive region which controls the mass flux and ceiling plume development; species and enthalpy fluxes, and radiant energy flux which effects the rate of fire growth[49]. The fire plume has three distinctive regions[31, pp. 123-124] where the presence of flames can be described as persistent, intermittent or buoyant, as shown in Figure 2.3. The persistent or flame zone, occurs above the burning surface where flaming

combustion continually produces heat addition due to chemical reactions, accelerating the flow of burning gases. The intermittent region is an unsteady region at the top of the flame where flaming combustion is intermittent and flow velocity is almost constant. In the buoyant or far-field region, temperature and velocities decrease with increased height due to lack of chemical reactions.

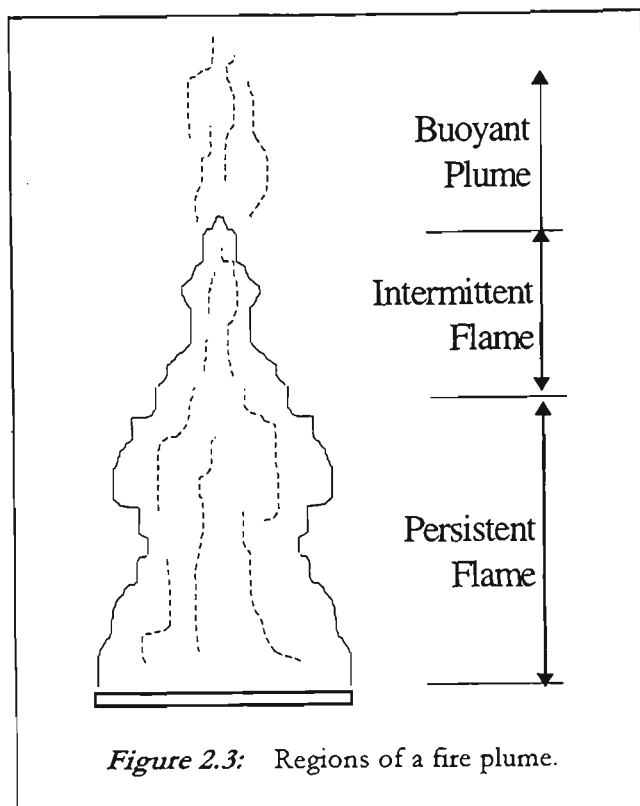


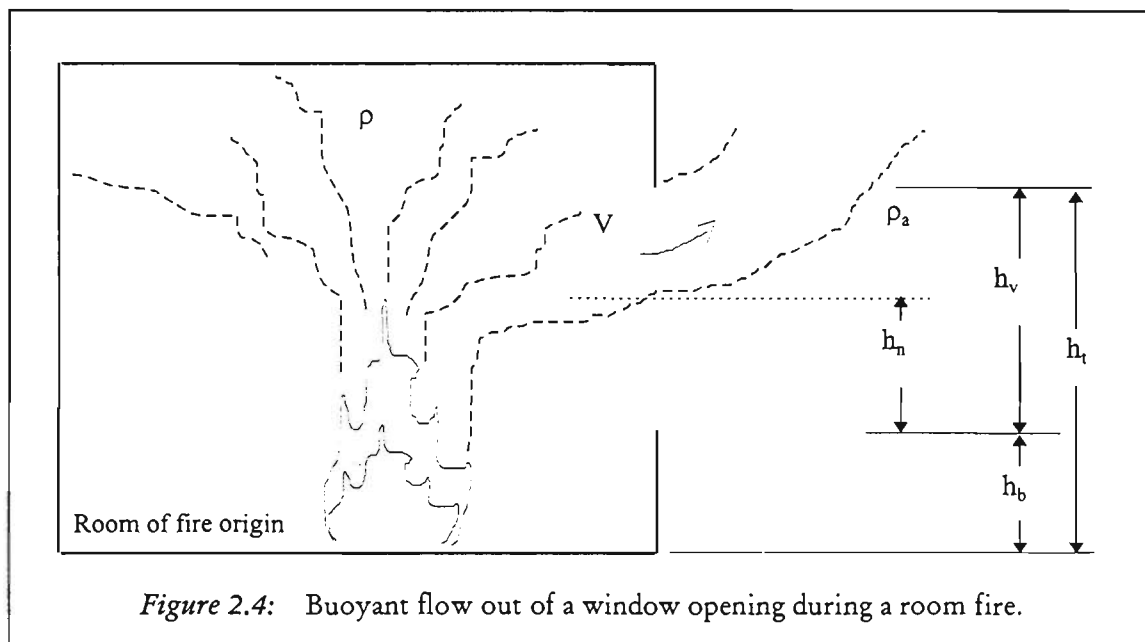
Figure 2.3: Regions of a fire plume.

The study of air entrainment into fire plumes plays an important role in the growth and spread of the fire. Cetegen *et al.*'s[50] work focuses on air entrainment into each of the three regions of the fire plume. To aid in the modeling of air entrainment into each of these regions, experimental measurements of plumes rising from natural gas burners of varying diameters were carried out. At the base or fire zone, entrainment rates were found to be almost proportional to burner diameters and independent of fuel flow.

In the intermediate region, entrainment rates were similar to that of a turbulent plume, where plume mass flux was dependent on heat release rate and height above the fire source. In the far-field or buoyant region, a point source plume model was used to predict entrainment rates. The work by Quintiere *et al.*[51] looked at the effect of room openings, such as door and windows on entrainment rates in fire plumes, and they found that such flow through the room tilted the fire plume, similar to external wind effects. Also, increased flow through the room was linked to both the strength of the plume and the size and location of the opening, with corresponding increases in entrainment rates.

A review of the development of fire plumes and ceiling jets was carried out by Beyler[52], where expressions describing both the temperature and velocity distribution within the fire plume are provided in terms of heat release rate and height above a virtual source. In addition, calculations for flame height above the fuel source and entrainment rates are given.

While the study of fire plumes within an enclosure was been carried out in detail, the study of the fire plume beyond the room of fire origin has received little attention. Thomas[53] briefly mentions the flow of flames out of openings, using the fundamental work of Yokoi[28] who identified mean flame length with an isotherm rather than using a virtual source, given the difficulties in defining an origin for external plumes. Yokoi's work is discussed in detail in *Section 2.4*. However, while the study of external fire plumes during real fires had been limited, some understanding of this phenomenon has been possible through the study of vent flows[54]. Figure 2.4 shows the buoyant flow out of the room of fire origin as a result of the heating of gases in the room. When the hot-layer is deep enough to fall below a vent opening, such as the top of a window or door, some gas will flow out. As the fire continues to grow, the buoyant flow will surpass gas expansion in the room resulting in the pressure dropping below atmospheric at the floor level in the room. When this occurs, air is drawn in from the lower portion of the vent/opening while flames and gases flow out from the top. This buoyant flow into the burn room provides the oxygen necessary for the continued combustion of the fire. Velocity and mass flow rates of the buoyant flow through the vent are determined using temperature (density) variations across the opening.



In Figure 2.4, ρ and ρ_a are the density of the fire plume and ambient air respectively; V is the velocity of the buoyant outflow; h_v and h_n are the height of the vent and the height to the neutral axis, respectively; h_t and h_b are the total height to the top of the vent and the height of the sill, as measured from the floor, respectively.

2.4 EARLY EXPERIMENTAL STUDIES ON EXTERNALLY VENTING PLUMES

Fundamental work on plumes was carried out by Yokoi[28] in the 1960's to assess the risks associated with fire spread from window openings in buildings. Yokoi performed both small scale and full scale experimental testing during his investigation of hot upward currents and venting plumes. His investigations began with a series of simple tests using alcohol as a fuel source, and preliminary investigations into temperature and velocity distributions within upward currents generated from a point and line source were carried out. These tests were followed by investigations into velocity distribution in air jets flowing from circular and rectangular orifices. The analysis lent itself to the flow of hot-currents ejecting from circular and rectangular heat sources. The intention was to understand hot-currents, such as flames, venting through window openings. Yokoi then described a burning wooden house as a rectangular heat source and derived the vertical temperature distribution above this heat source. He identified the sensitivity of the temperature and velocity distributions to a ratio of the window's width (w) to half of the height from which the plume emerges from the opening (h) in terms of a parameter n . In a table, Yokoi[28, p.87] provided a means to determine the height, h , as a function of the compartment temperature during the maximum intensity phase of the fire and the neutral axis (NA) of the window (above the NA, flames emerge from the window, and below it, air is drawn in). The parameter, n , defined as $n = w/(1/2h)$, was used also to determine whether or not re-attachment of the plume would occur. He noticed that both the presence of a wall above a window opening, as well as the shape of the window, affected the path of the ejecting plume. When a wall exists above wide openings, it absorbs heat from the flames as well as restricting air entrainment on the wall side. This restriction causes the plumes to be longer and makes the plume travel along the wall (re-attachment). Narrower windows eject the plume away from the wall, allowing entrainment from all sides, shortening the plume.

Following his preliminary investigations and analysis into hot-currents, Yokoi carried out a series of four full-scale fire tests in concrete buildings, using rooms with the following three sets of dimensions: 13.35m x 9.7m x 3.5m high, 4.3m x 3.48m x 2.47m high and 5m x 2.5m 1.67m high, with windows sizes of 0.91m x 1.67m, 0.82m x 1.55m

and 3m x 1m, respectively; the fuel source was wood with fuel load densities of 42kg/m², 53kg/m² and 40kg/m², respectively. All tests were carried out on calm days when the wind speed was 1.5m/s or less. During these tests temperature of the burn room and temperature and velocity of the ejected flames were measured. Once again, the importance of window geometry was observed. He noted that the standard glass windows of 3mm thickness, mostly cracked when subjected to hot gases at 400°C with dislodgment at 500°C, while wired-glass windows did not crack even when gas temperatures reached 600°C.

Following the full scale work, Yokoi performed a series of small scale (model) experiments with the intention of applying his full-scale formulations to the results of the small scale tests. Once again, alcohol was used as a fuel source, and windows of various sizes were used. The effect of window geometry, and the presence of a wall above the opening were investigated, and good correlations were found to exist between the full scale and model test results over the period of maximum intensity. To correlate experimental results obtained with small scale tests to full scale conditions, consideration was given to the differences of the thermal properties of the wall above the window, the emissivity of the flames, and the continued combustion of gases when ventilation conditions were restricted.

Once the trajectory path (line marking the hottest temperatures) of the plume was verified, it could be used to determine the effectiveness of spandrel walls and balconies. By setting the critical temperature at which standard glass fails at 500°C, Yokoi developed a means to estimate the spandrel length necessary between window openings to prevent the ignition of an upper level by flames emerging from lower levels. Balconies deflected the trajectory path, and as a result, were found to be highly effective in preventing the spread of the fire.

In summary, the following equations were developed using Yokoi's data. Where possible, these equations are compared with the results of the Real Furniture Burns, in Chapter 5, *Section 5.6.3*.

Trajectory along plume axis:

Temperature and Velocity:

$$\Delta T_m = 24.6 Q^{2/3} Z^{5/3} \quad \text{Equation 2.1}$$

$$U_m = 1.17 Q^{1/3} Z^{-1/3} \quad \text{Equation 2.2}$$

where ΔT_m = centre-line temperature rise above ambient ($T_{amb} = 293 \text{ K}$)

U_m = centre-line velocity (m/s)

Q = heat release rate (kW)

Z = height above the virtual source (m)

Equation 2.1 and Equation 2.2 are based on Beyler's[52] calculations using Yokoi's data. Only Equation 2.1 can be compared with the present experimental results, as given in *Section 5.6.3*, because plume velocity measurements are not available.

Re-attachment parameter n:

$$n = w / (\frac{1}{2}h) \quad \text{Equation 2.3}$$

where w = the width of the window (m)

h = the height of the window from which the plume emerges (m)

$n < 3.4$ plume will rise close the wall, but it will not re-attach. The closer this number gets to 1, the further away from the wall the plume will tend.

$n > 6$ plume will strongly deflect towards the wall.

Spandrel length necessary to prevent a secondary fire:

The necessary distance between the top of the window on one level and the bottom of the window on the level above to prevent a secondary fire, can be determined if the window size and the quantity of combustibles (kg/m^2) within the room are known. Yokoi provides a table (Table 9.9, p. 117) to determine when the temperature along the trajectory of the emerging plume reaches 500°C (based on glass breakage considerations). This table is duplicated in Appendix A, for comparison with Chapter 5, *Section 5.6.3*, results.

Horizontal Projections (balconies):

The necessary length of horizontal projections can be determined once again based on window size and quantity of combustibles (kg/m^2) in the room. For example, the information presented[28] in Table 10.5 (p. 135) is for when a 50cm deep balcony is attached above the window. For this case, the plume is deflected away from the wall, and the impact (temperature) on the wall is lessened. Also, the effect of multiple balconies and the corresponding spandrel lengths can be determined from Table 10.5. This table is not duplicated here, since no direct comparison was possible with the present results.

Similar to Yokoi's investigation into air ejected through circular and rectangular orifices, Seigel[4] considered the plume as a horizontal jet, to predict the size of flames during building fires. This was done with the intention of assessing the use of external structural steel elements without fire protection. Thirty experiments were carried out in a 3.05m x 3.66m x 3.05m high chamber with wood crib fuel load density ranging from 24.4 - 97.7 kg/m^2 (5-20 lbs/ft^2), with a single window opening of sizes 0.61m wide x 1.83m high or 1.83m wide x 2.44m high. For tests with multiple (two) window openings spaced 1.22m apart, horizontally, flames emerging from the 0.61m x 1.83m windows tended to merge together during the peak burning phase of the fire. Temperature measurements were made in the test room and in the external flames using thermocouple grids. Seigel noted that the rate of temperature drop away from the opening was small and attributed this to continued combustion outside the opening. Consequently, additional ventilation was provided, other than the opening, by connecting an external air supply to the test room. This allowed the fire to burn freely in a well ventilated room, therefore increasing the rate of burning and the length of the flames. Seigel's correlation for flame length can be used when fuel load and burning rates are known. This correlation for flame length assumes a flame tip temperature of 538°C (1000°F). This value was selected as flame temperatures below this value will not pose a significant risk to exposed steel structures.

Recognising the importance of investigating the effect of external flames on structural steel, Thomas and Law[55] re-examined earlier work by Yokoi, Seigel and Webster. Similarities and differences amongst the findings were discussed, and once again several

important points were highlighted. These included the effect of window geometry on flame trajectory, definition of visible flame length at 540°C, the need to consider radiation losses, the effect of 'no wall' and 'wall' above the window opening, and the effect of supplying air to the room which enhances the burning rate. Correlations were developed which allowed the height of the flame tip above an opening to be determined. Due to the sensitivity of flame temperature measurements to radiation, this work indicated that radiative heat transfer from flames should be measured directly, rather than estimating from thermocouple measurements.

Adding to the work of Thomas and Law[55], Law[21] produced a comprehensive guide to assess the fire safety of external building elements. Incorporated into the Design Guide[21] were additional full-scale experimental results on fires using timber, wood crib and office furniture as the fuel source, where the room size and openings were varied. Correlations for free and restricted burning rates, the dimensions (height, depth and width) of the external flame, based on through-draft and no-through draft conditions, as well as whether or not there is a wall above the opening are presented. In addition, temperature along the flame axis and a model of the heat transfer from the flames to the external steel structure are given. This publication was followed by a manual by Law and O'Brien[30], which simplified the information presented previously by Law[21]. Law's procedure is presented in *Section 2.4.1*.

Law's procedure is still used as a guide for determining the shape of the venting plume, centre-line temperatures and heat transfer effects. As such, a comparison of the experimental work carried out in this thesis with her predictions provides an opportunity to test these correlations (see *Section 4.2.4* and *Section 4.3* for the Polyurethane Burns and *Section 5.6* and *Section 5.7* for the Real Furniture Burns). Overall, while Law's work deals with emerging or venting flames, her focus has been on the effect of those flames on external structural steel members. On the other hand, as described earlier in this section, Yokoi's contribution was to describe the trajectory of the venting plume in terms of temperature and velocity distribution along the plume axis. The work presented in this thesis expands on his analysis and considers the variations within the *entire plume*, using full-scale test fires, as well as examining the existing correlations.

2.4.1 The Venting Plume

As discussed above, Law and O'Brien[30] produced a Design Guide to predict both the shape and centre-line temperature of externally venting flames. Based on this work, the venting plume is described by the rate of burning, the plume shape, centre-line temperatures and heat transfer effects. Heat transfer effects developed by Law are in relation to determining the effect of the venting flames on external structural steel members. Oleszkiewicz[29] modified Law's plume shape and used the heat transfer equations in relation to the effect of the plume on the external wall. Oleszkiewicz's equations are presented here. In addition to the work of Law and O'Brien, and Oleszkiewicz, the work of Bullen and Thomas[56] is included in this section in relation to the size of external flames and the excess fuel factor.

The equations presented in this section are used in Chapter 4 and Chapter 5 of this thesis for comparison with the results from two different series of full scale fires using polyurethane and real furniture as fuel. Given the current usage of the design guide of Law and O'Brien, the results from these series of tests provide an opportunity to compare the correlations, which were primarily developed from wood crib and office furniture tests, with the fuel used here.

2.4.1.1 Rate of Burning

The ventilation conditions within a room directly affect the burning rate of the fuel[57,58] which in turn affects the severity of a venting fire plume and its shape. Important parameters are the window area, A_w (m^2), window height h (m), area of the enclosed surface, A_T (m^2), excluding the window area, the ratio of the compartment's depth (m) to width (m) (D_c/W_c)[6]. The rate of burning in kg/s, derived from experimental studies with wood cribs, can be determined for restricted ventilation conditions using Equation 2.4[6] or Equation 2.5 and Equation 2.6[30].

$$R \approx 0.1A_w\sqrt{h} \quad \text{Equation 2.4}$$

$$R = [0.18(1 - e^{-0.036\eta})/(D_c/W_c)^{1/2}].(A_w\sqrt{h}) \quad \text{Equation 2.5}$$

where $\eta = A_T/(A_w\sqrt{h}) \quad \text{Equation 2.6}$

When there is sufficient ventilation, the rate of burning can be expressed in terms of the fire load, L , and free burning duration, τ_F . The free burning or effective duration allows the burning rate, during the fully developed portion of the fire to be determined. The free burning duration is about 20 minutes for most types of furniture found in buildings[59]. The rate of burning is given by:

$$R = L / \tau_F \quad \text{Equation 2.7}$$

The fully developed phase of a fire can also be linked to the rate of burning. Based on mostly small scale tests, it has been reported that the fully developed phase of a fire begins when the fuel mass falls to 80% of its original load and ends when approximately 30% of the fuel remains. This extends over about half of the overall burning time of the fire[6].

2.4.1.2 External Plume Shape

As a plume vents from an opening, its shape is affected by the enclosure's ventilation conditions as well as the window shape[30]. The plume often surges out of the window, curling back to make contact with the external wall[44] some distance above the opening, depending on its aspect ratio[28]. The overall height and width of the venting flame will depend on the window aspect ratio, as well as whether there are any horizontal or vertical projections above or beside the window. In general, flames that emerge from narrow windows are expected to project up a distance of half of the window height, only, while flames emerging from wide or square windows can project one and a half times the window's height[42]. The Design Guide[30] produced by AISI (American Iron and Steel Institute) in conjunction with Law[21] at Ove Arup & Partners, investigated the effect of *no-through* and *through-draft* conditions on flame shape and behaviour using mostly cellulosic fuel. Correlations of flame height and width were developed for both of these ventilation conditions as a function of compartment and window size, and burning rate. Generally, the flame for a through-draft condition was said to emerge from the entire window area, its width being slightly wider than the window width, as shown in Figure 2.5, and at an upward angle as shown in Figure 2.6. In these figures, the top and side views, respectively, of the plume are given as it emerges from a window when a through draft - Class 1 ventilation condition exists.

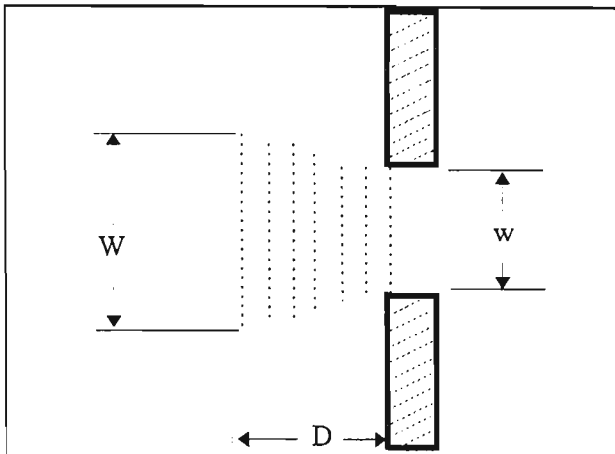


Figure 2.5: Top view of an emerging plume for a through draft - Class 1 ventilation condition.

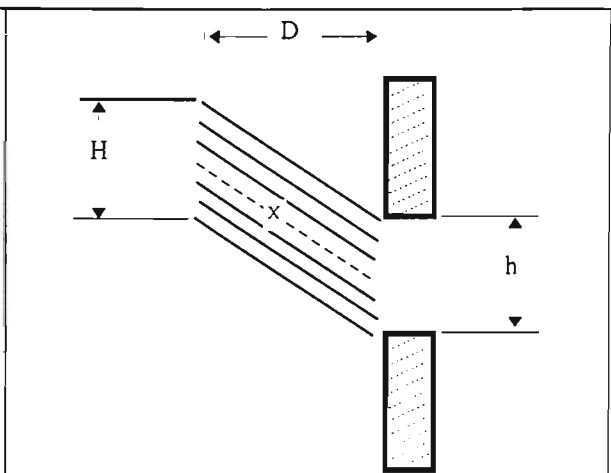


Figure 2.6: Side view of an emerging flame for a through draft - Class 1 ventilation condition.

Empirical approximations to specify the venting plume's envelope have been developed by Law and O'Brien[30] for both Class 1 and Class 2 ventilation conditions. These are summarised as follows for Class 1 ventilation conditions for flame height above the top of the window, H (m), flame width W (m) and depth, D (m), and illustrated in Figure 2.5 and Figure 2.6 above.

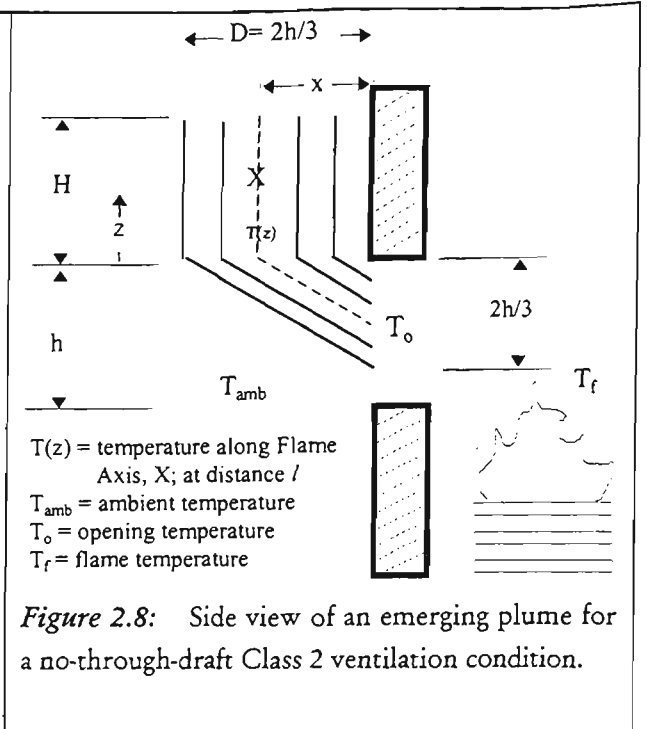
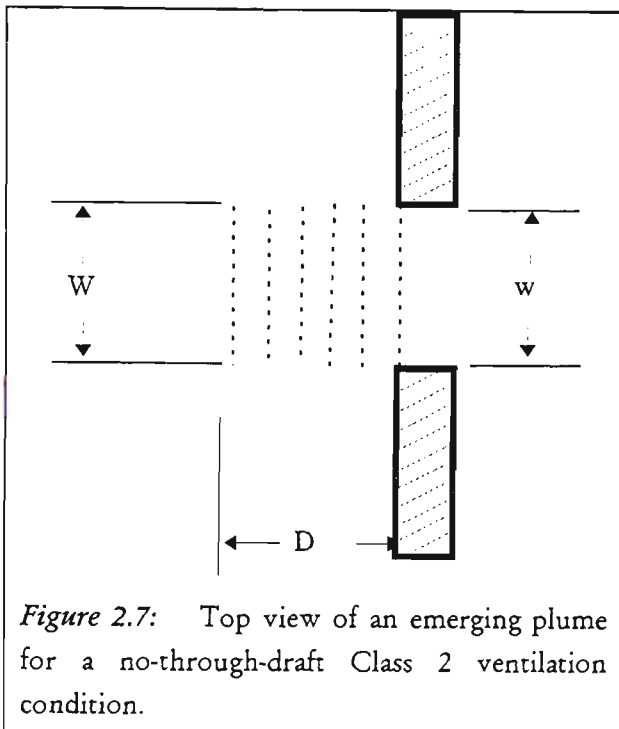
$$H = 23.9(1/u)^{0.43} (R/A_w^{1/2}) - h \quad \text{Equation 2.8}$$

$$D = 0.605(u^2/h)^{0.22} (H+h) \quad \text{Equation 2.9}$$

$$W = w + 0.4D \quad \text{Equation 2.10}$$

where u = wind speed producing the through draft (m/s), R = burning rate (kg/s), A_w = window area (m^2), h = height of window opening (m) and w = width of window opening (m).

When the window provides the only source of air, the flames emerge from the upper two-thirds or half of the window and travel up (or beside) the external wall, with a uniform thickness as shown in Figure 2.7 and Figure 2.8. In these figures, top and side views are given as the plume emerges from a window for a no-through draft - Class 2 ventilation condition.



Empirical approximations for Class 2 ventilation conditions, when a wall exists above the opening, are summarised as follows for flame height, H (m), flame depth, D (m) and width W (m).

$$H = 12.8 (R/w)^{2/3} - h \quad \text{Equation 2.11}$$

$$D = 2h/3 \quad \text{Equation 2.12}$$

$$W = w \quad \text{Equation 2.13}$$

where R = burning rate (kg/s), h = height of window opening (m) and w = width of window opening (m).

2.4.1.3 Centre-Line Temperature

The *flame axis* corresponds to the centre-line of the venting plume, beginning at the window opening and extending vertically up the external wall, in the middle of the plume as indicated by the dashed lines in Figure 2.6 and Figure 2.8. In Law and O'Brien's[30] work, the temperature along the flame axis $T(z)$ for Class 1 and Class 2 ventilation conditions, respectively are given by:

$$\frac{T(z) - T_{amb}}{T_o - T_{amb}} = 1 - 0.019 \frac{l A_w^{0.5}}{R} \quad \text{Equation 2.14}$$

$$\frac{T(z) - T_{amb}}{T_o - T_{amb}} = 1 - 0.027 \frac{l w}{R} \quad \text{Equation 2.15}$$

where T_{amb} and T_o are the ambient and opening temperatures ($^{\circ}\text{C}$) as indicated in Figure 2.8. l (m) is the distance along the flame axis X , w (m) is the window width and R (kg/s) is the rate of burning. As provided by Law[6], the average temperature in the compartment during the fully developed period, T_{FDP} is:

$$T_{FDP} = \frac{6000(1 - e^{-0.01\eta})}{\sqrt{\eta}} (1 - e^{-0.05\psi}) \quad \text{Equation 2.16}$$

and

$$\psi = L / (A_w A_T)^{0.5} \quad \text{Equation 2.17}$$

where L is the total mass of fire load (kg), A_w is the window area (m^2), A_T is the area of the enclosure excluding the window (m^2), and η is defined in Equation 2.6.

Hence, Law's procedure provides a means to describe the flame envelope, along with the plume's centre line temperature, where aspects of the plume's shape are functions of the rate of burning, room and window geometry and ventilation conditions.

2.4.1.4 Convective & Radiative Heat Transfer

The original flame shape proposed by Law[21] has been modified by Oleszkiewicz[29], changing the conservative assumption of a flame of constant thickness to a tapered (triangular) flame as shown in Figure 2.9 (taken from [29]). Based on this modified flame shape, Oleszkiewicz found that the calculated radiant and total heat flux at the flame tip, where temperatures were 520°C above ambient temperature[4], were more realistic. These equations are summarised below for flame emissivity, $\varepsilon(z)$, radiant heat flux density, $I(z)$, and convective heat flux density, $q(z)$:

$$\varepsilon(z) = 1 - \exp(-b\lambda) \quad \text{Equation 2.18}$$

where the emission co-efficient $b = 0.3 \text{ m}^{-1}$ [29], z is the vertical distance from the top of the window and λ is the flame thickness at height z (and $\lambda = 2h/3$ at the top of the opening);

$$I(z) = \varepsilon(z) \sigma [T(z)]^4 \quad \text{Equation 2.19}$$

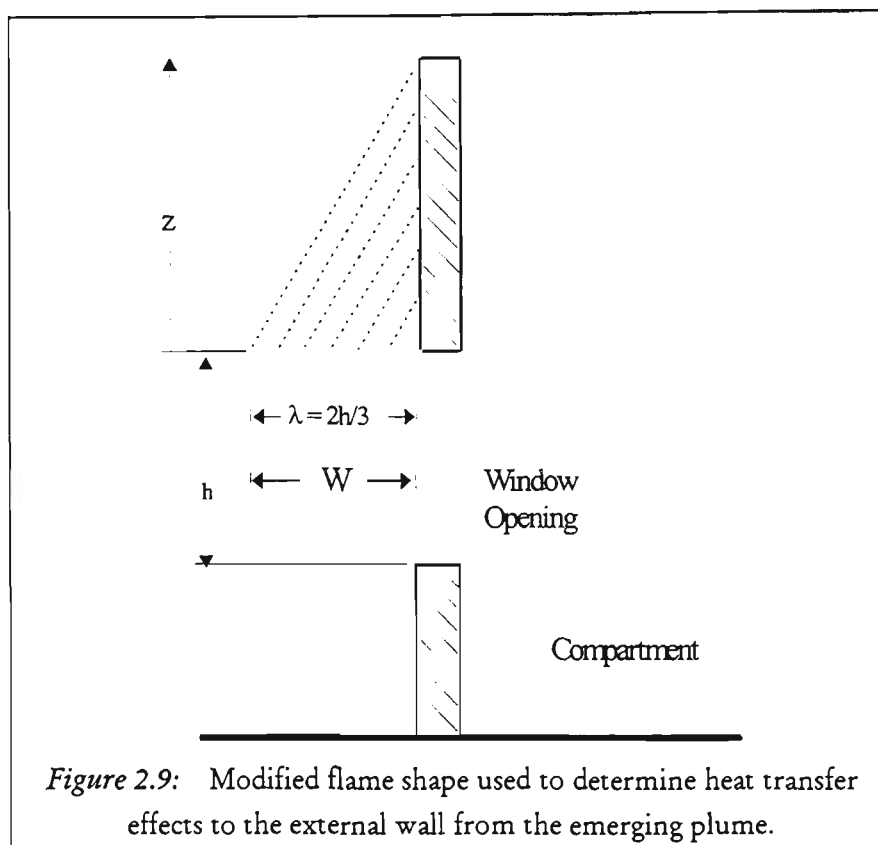
where σ is the Stefan-Boltzmann constant and $T(z)$ is the absolute plume temperature at its centre;

$$q(z) = \alpha [T(z) - T_{\text{wall}}] \quad \text{Equation 2.20}$$

where α is the convective heat transfer coefficient ($\text{kW}/\text{m}^2 \text{K}$) given in Equation 2.21, T_{wall} is the wall temperature. Equation 2.21 below is a variation[29] developed from Law's[21] model. The modification is to calculate the convective heat transfer to the external wall above the burn room window[29] from the venting flames, rather than to an exposed steel structure[21].

$$\alpha = k (R / A_w)^{0.6} \quad \text{Equation 2.21}$$

where k is a dimensional factor ($k = 0.013 \text{ kW}/\text{m}^2\text{K}[\text{m}^2/\text{kg}/\text{s}]^{0.6}$).



2.4.1.5 Excess Fuel Factor

Excess fuel factor was used by Bullen and Thomas[56] to aid in their explanation of external flames. They linked the height of the external flames (and radiative heat flux to the facade) to the amount of unburnt fuel leaving the compartment. The larger the positive excess fuel factor is, the higher the flame height must be. The excess fuel factor, f_{ex} , is defined by :

$$f_{ex} = 1 - \dot{m}/rR \quad \text{Equation 2.22}$$

where air mass flow rate, \dot{m} is in (kg/s), r is the stoichiometric ratio and R is the rate of burning (kg/s). The following expression[31, p. 315] is used for the air mass flow rate into the room:

$$\dot{m} = 0.5A_w h^{1/2} \quad \text{Equation 2.23}$$

where A_w is the window area (m^2) and h is the height of the opening (m).

Calculations of excess fuel factors are given in *Section 4.2.3* and *Section 5.6.3* for the Polyurethane Burns and Real Furniture Burns, respectively.

2.5 EXTERNALLY VENTING FLAMES REVISITED

The following papers on fire spread are not grouped with *Section 2.4*, “Early Experimental Studies on Externally Venting Flames”, because unlike the ones given in *Section 2.4*, these papers were not used in the development of the Design Guide[30]. As a result, these more recent papers give an indication of the developments in this area since 1981. In essence, the fundamental work carried out by Yokoi and expanded upon by Thomas and Law, and Oleszkiewicz is still used as the benchmark for the study of externally venting flames as indicated by the 1994 paper by Quintiere and Cleary[60]. While the effect of venting flames has been the focus of much work, especially at the National Research Council of Canada (NRCC), detailed studies of the plume itself, such as Yokoi’s[28], have not been performed until the present thesis.

Quintiere and Cleary[60] examined the heat transfer from flames to vertical surfaces, collating much of the work carried out in this area. Their emphasis was on determining a correlation between heat flux and flame height based on fundamental experiments such as heat generated from a line source and a corner burner. They found that complicating factors included window geometry and the need to take into account that heat fluxes from venting plumes on the external wall were generally higher than those of internal wall fires. Summarising the work on window flames developed by Thomas and Law, and Oleszkiewicz, they provide the following equation, Equation 2.24, for flame length.

$$l_f = 0.0321(Q/D)^{2/3} \quad \text{Equation 2.24}$$

where l_f = flame length measured from the bottom of the window opening (m); Q = heat release rate out of the window and D = characteristic fire dimension - side of square burner or equivalent window diameter.

Equation 2.24 taken from Thomas and Law, was based on Yokoi’s original formulations which require the heat release rate at the window to be known. As such, no consideration is made for heat loss to the room. Such losses would undoubtedly affect flame lengths. Also, effects of window shape may not be fully accounted for when using equivalent window diameter.

Oleszkiewicz[19, 22, 29, 44, 42], Yung and Oleszkiewicz[20] and Lougheed and Yung[8] at the NRCC have carried out extensive work in the areas of external fire spread, testing of combustible linings, spread to adjacent structures and development of smaller-scale testing procedures of external wall assemblies. In general, tests were carried out in two different sized burn rooms (standard and larger) with wood cribs or propane as the fuel source. The *standard burn room* measured 2.4m x 3.6m x 2.4m high, with an extended external facade with overall dimensions of 3.6m wide, 6.1m high. The size of the window opening was varied while providing approximately equivalent ventilation, using $A_w\sqrt{h}$, for wood cribs. In the *larger facility*, the burn room measured 5.95m x 4.4m x 2.75m high with a variety of window sizes. The fuel source was either evenly distributed wood cribs equalling approximately 25kg/m² (fuel load) or propane gas. The mass flow rate of the four linear (evenly spaced) propane diffusion burners, 0.6m above the floor, was controlled manually and monitored by a hot wire anemometer. Wood cribs were used as they produced flames with emissivities similar to that of real fires and as such allowed the radiant component of heat flux to be determined. The propane tests were designed to study the impact of heat release rate and window configuration on heat transfer to the external wall. Also, the effect of horizontal and vertical projections on the heat transfer to the external wall was studied. Similar to the present study, the external facade was instrumented with total heat flux transducers, thermocouples above the top centre of the opening, air purged radiometers and an oxygen probe.

Oleszkiewicz's[22] results indicate that higher radiant heat flux was measured just above the window opening for a square window (peak of 50kW/m²) compared to a narrow window (peak of 30kW/m²). On the other hand, total heat flux was higher (peak of 120kW/m²) for a narrow window than for a square window (peak of 80kW/m²), indicating higher convective heat transfer in the case of the narrow window. No specific attempts were made to explain why different window shapes caused these differences. Subsequent discussions on the effect of horizontal and vertical projections which deflected and channelled the venting plume, respectively, were only with respect to their contribution to fire spread. While it is acknowledged by Oleszkiewicz[44] that the venting flames curl back and impinge on the external wall, specific effects due to window shape, entrainment effects and resulting plume shape were not considered.

The focus of most of the NRCC work has been on assessing the effect of the plume on combustible exterior assemblies by varying the heat release rates. The window size and details of plume characteristics have not been considered or discussed. As a result, direct comparison of most of the present results with the NRCC results is not possible, with the exception of the heat flux measurements on the external wall taken during the Real Furniture Burns. This comparison is given in *Section 5.7.2* in relation to Oleszkiewicz's[29] work.

2.6 EXTERNALLY VENTING FLAMES - ADDITIONAL CONSIDERATIONS

Factors which directly influence the shape and severity of externally venting flames can be linked to the internal and external conditions of the building, which act in combination, and as such are inseparable from each other. Internally, many factors influence if flashover will occur, and this determines whether or not external flaming occurs. Assuming that flashover occurs, then factors such as smoke management systems (controlled venting systems) and the likelihood of glass breakage will affect the externally venting flames. In addition, window shape, projections such as horizontal balconies or vertical shades, as well as environmental conditions, such as wind speed and direction will influence the emerging flames.

2.6.1 Smoke Management Systems

The movement of air in a building plays a pivotal part in how a fire grows, spreads and the form it takes outside the building. Air movement is affected by the air handling/smoke management system of the building, its floor plan and the location of openings with respect to one another, the height of the building and external wind[61].

Controlled venting involves re-direction of hot gases and smoke from the upper layer of a compartment to the outside, to introduce fresh air into its lower layer[43]. The design of a building's ventilation system must be integrated with other precautionary fire designs, such as escape routes and sprinklers. The ventilation system when employed as a Smoke Management System (SMS), can reduce the spread of hot smoke within a compartment and to adjacent ones. A properly designed SMS can reduce smoke and hot gas damage, and in controlling the spread of smoke, provide additional time for a building's occupants to escape. Although doors to individual enclosures may be fire rated, the breaking of windows and the venting of hot smoke/gases and flames across the external facade of a building pose a different risk. Rather than the fire spreading from one enclosure to the next on the same level, the fire may now reach upper levels, via *leap frogging*[44]. In addition, SMS has been found to facilitate flashover in compartments with Class 2 ventilation conditions (closed door and window) as discussed further in *Section 5.7*.

2.6.2 Glass Breakage

During the course of a fire, a window may act as a barrier, preventing the spread of flames and combustion products. However, upon failure the window acts as a vent, providing a source of fresh air which stimulates fire growth. The works carried out by Joshi and Pagni[62,63,64], Skelly *et al.*[65], and Keski-Rahkonen[66] suggest that glass breakage is caused by thermally induced stresses which arise from a difference in temperature of the glass pane from its centre to its shaded edge (portion of glass supported within the window frame). The time to breakage corresponds to when the shaded edge reaches the breaking stress. The temperature difference required can be approximated by the following equation[64]:

$$\beta \Delta T = \sigma_b / E \quad \text{Equation 2.25}$$

where ΔT is the temperature difference in K between the glass edge and centre; β is the thermal co-efficient of linear expansion of the glass, $\beta \approx 3.6 \times 10^{-6} \text{ K}^{-1}$; σ_b is the breaking stress, $\sigma_b \approx 40 \text{ MPa}$; and E is Young's Modulus for glass, $E \approx 70 \times 10^3 \text{ MPa}$.

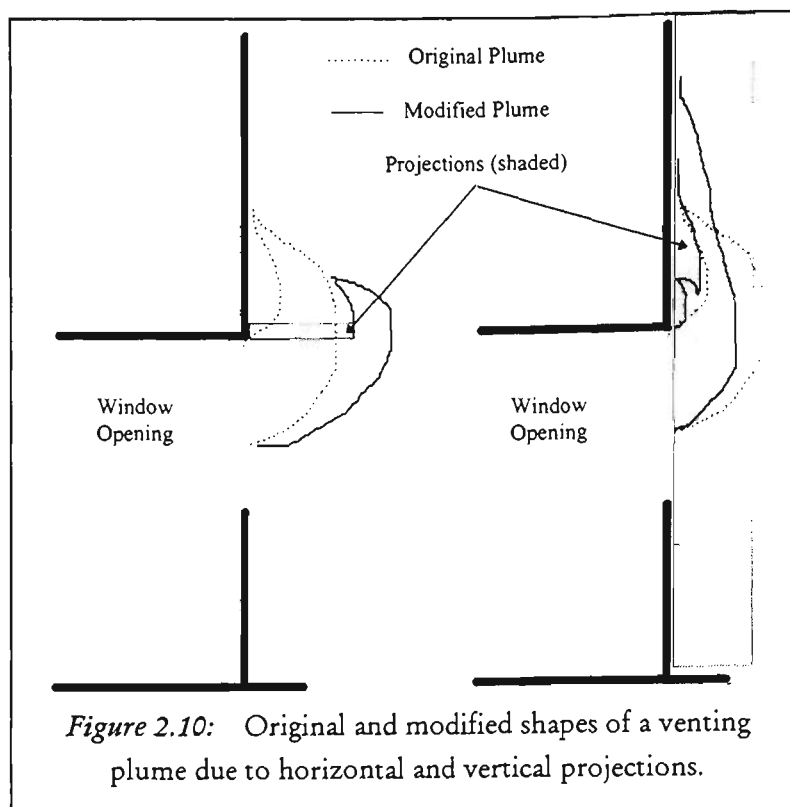
Experiments by Joshi and Pagni approximate the breaking stress of glass to 40 MPa, acknowledging that this value is suitable for common window sizes. Larger window panes will have a lower breaking stress than smaller window panes. Their results also suggest that fractures propagating through the glass are initiated due to edge imperfections rather than surface flaws. This result is confirmed experimentally by Skelly *et al.* on small samples of glass. They found that none of the cracks which lead to breaking initiated or travelled along any surface flaws. Determination of breaking stress and application of Equation 2.25 lead to the development of a means of estimating the time to window breakage. This corresponded to a temperature differential between the shaded and centre pane of the glass of about 70°C for Skelly, Roby and Beyler, and 90°C for Joshi and Pagni. The variation between these results was attributed to the use of slightly different values for breaking stress, Young's Modulus and coefficient of thermal expansion of glass. Specifically, Joshi and Pagni[64] found that differences in glass properties could result in temperature differences necessary to cause cracking, ranging from 30K to 110K. However, Silcock[67] suggests that the methods used to predict the temperature difference necessary to cause failure of compartment windows must be re-evaluated for slowly developing fires.

When determining the time to window breakage, time histories of the average burn room temperatures as well as glass temperatures are required. However, it is generally accepted that as a first approximation, when the temperatures in the hot gas layer which covers the upper portion of the window, reach between 300 and 450°C, the glass breaks.

2.6.3 Horizontal and Vertical Projections

The shape of a plume as it vents from a window is also affected by any projection which may enhance or diminish the reach of the flames, as shown in Figure 2.10 (taken from [19]), and as verified by Oleszkiewicz[19] and Harmathy[68]. Although this particular aspect was not covered during the present experiments, a brief review is provided here due the importance of projections on external fire spread.

Vertical projections such as shadings and other design features on the external walls of buildings, limit side-ways air entrainment, channelling the venting plume and extending the reach of the flames. Flames travel out along horizontal projections, and once over it, return to their original path. At this stage, temperature along the flame axis is reduced, and any damage caused to the wall above the horizontal projections is generally minimised compared to an undeflected flame. It has been suggested[69,70] that the effectiveness of a horizontal projection may also be improved by altering the angle the projection makes with the external wall. While the implementation of a horizontal deflector, such as a balcony may be an effective means of limiting flame spread, it is considered aesthetically unappealing[71] for high-rise/multi-storey buildings. In addition, direct changes to the architectural design of a building facade may not always be possible.



2.6.4 Environmental Effects

Another important and often neglected aspect, due to its uncontrollability, is the effect of wind speed and direction on externally venting plumes. Cross winds may skew a venting fire plume, forcing it towards other windows along the same level as the burn room, or diagonally across to upper level windows, thus placing them at risk. Some small scale experimental work has been carried out by Sugawa and Takahashi[72] highlighting the dependence of the plume trajectory on wind speed, window shape (narrow or wide) and heat release rate. They found that the plume trajectory tended more towards the wall for wider openings compared to narrower openings, and increased heat release rates (without wind effects) resulted in a wider and longer plume. Also, direct (front-on) wind tended to push the plume back against the wall. Sugawa and Takahashi also developed the following equations, Equation 2.26 and Equation 2.27, as a simple model for estimating temperature and velocity along the plume trajectory when front wind is present:

$$\Delta T_m / T_{amb} = C_{temp} Q_{rec}^{2/3} z^{-(2/3)Y} \quad \text{Equation 2.26}$$

$$V / \sqrt{gD} = C_{vel} Q_{rec}^{1/3} z^0 \quad \text{Equation 2.27}$$

where $\Delta T_m/T_{amb}$ is the ratio of the rise in centre-line temperature above ambient temperature, divided by ambient temperature; V is the upward velocity of the venting plume (m/s); C_{temp} and C_{vel} are coefficients for excess temperature and upward velocity, respectively. Υ is a correctional factor to take into account wind. It is given that $\Upsilon = 0.23(V_{wind})^2 + 1$ (where V_{wind} is the external wind speed) and $\Upsilon = 1$ when there is no wind. z is assumed to be the height above the top of the window opening (m). Q_{rec} , the dimensionless heat release rate is given as follows: $Q_{rec} = Q / (\rho c_p \theta \sqrt{(gD) D w})$; ρ is density (kg/m^3); c_p is the specific heat of the gases (kJ/kg K); θ is the difference between the plume and ambient temperatures ($^{\circ}\text{C}$); g is acceleration due to gravity (m/s^2); D is the depth of the ejected plume/flame (m) and w is the window width (m). Comparison between the present full scale experiments using Real Furniture and Sugawa and Takahashi's formulation is given in *Section 5.6.3*, Chapter 5.

Following from their earlier work, Sugawa *et al.*[73] investigated the effect of side winds on plumes venting from openings and developed an expression to determine the flame angle along the trajectory. The flame angle, ϕ , is the angle from the vertical centre of the plume to the horizontal, and it is given by Equation 2.28.

$$\sin\phi = V_{wind} / u^* (h/w)^{1/3} \quad \text{Equation 2.28}$$

where V_{wind} is the wind velocity (m/s); u^* is the velocity based on heat release rate given by $u^* = (Qg/\rho_{amb}T_{amb}c_p w)^{1/3}$; h and w are the height and width of the opening (m), respectively. An evaluation of Sugawa *et al.*'s flame angle is given in *Section 5.8.1* of Chapter 5 using Real Furniture results.

An example of the effect of wind during full scale fires is discussed by Bechtold[74]. He carried out a full scale fire test on a four storey building, placing combustible items at various locations, including on several balconies. The purpose of the work was to study the fire behaviour on the external facade of a building and the effect of wind on the spread of the fire from one level to the balconies on higher levels. He noted that during the fully developed phase, the temperatures of the hot gases venting through the window (measured along the window's centre line) were comparable to the maximum temperatures reached in the compartment. Even as this phase ended, the

temperature on the external facade, just outside the window, was essentially the same as the room's mean temperature. The importance of wind effects was also shown in a series of constant temperature curves which skewed according to the direction of the wind. In one case, this caused the wood cribs to ignite on a balcony on the level above. Bechtold observed that well over half of the total heat produced during the course of a fire can vent through a window, and that continued combustion of unburnt gases can further increase the temperature just beyond the compartment's window.

2.7 NUMERICAL MODELLING

The internal conditions of a compartment have a significant effect on the venting flames. Although this thesis is on externally venting flames, the importance of the conditions in the burn room are not neglected, since internal data are needed for the interpretation of external phenomena. Several works exist in the literature on the modelling of the internal conditions during a compartment fire. Modelling of smoke movement[75,76,77], fire plume dynamics[78,79], combustion[80,81], modelling of flame spread[82,83,84,85], compartment fires[86,87] and spread to adjacent enclosures[88] describe internal conditions. In the following, the works on modelling of externally venting flames are treated in detail.

2.7.1 Modelling of Externally Venting Flames

Numerical modelling of external fire spread in high rise buildings was carried out by Satoh and Kuwahara[89], using a two-dimensional finite difference code based on micro-control volume scheme and pressure correlation algorithms. Time-dependent flow behaviour of externally venting flames was studied for nine cases where the length of the horizontal balcony and soffit were varied, along with the height of the window opening. For all cases, the two-dimensional cross-section of the room was 3.43 x 2.25m (high) and externally, the region extended vertically upwards by 6 floors. The outside region was divided into 131 x 151 (vertical) uniform grids, each cell measured 0.098m x 0.098m and each run took approximately 60hrs on a SUN 3-260 workstation. Initial temperature and air speed were set to 15°C and 0m/s, respectively. Heat release was divided into stages for simplicity, with a linear increase over the first 20 seconds, after which it remained constant. The heat release rate was 1.5MW corresponding to a rise in room temperature of 700K. Also, by varying the heat release rate, corresponding changes in the periodic motion within the venting gas flow could be investigated. The periodic motion referred to here, is upward moving coherent structures in the plume.

Temperatures along the external wall were found to range from approximately 400-500°C up to 1m above the opening without a balcony, and dropping to around 200°C at 2m and 50°C at 4m. They also investigated the effect on the venting plume when the window above the room of fire origin was open. Temperature and velocity profiles were found to be similar even when balcony and soffit lengths were varied. However, window sizes were found to cause the plume to tend either towards (wide windows) or away from (narrow windows) the external wall, based on Yokoi's[28] earlier work. However, the effect of entrainment from the side of the plume was not considered in this 2D simulation. The presence of an open window above the room of fire origin tended to partially draw the plume into the room, and the plume partially continued to travel up along the external wall. Finally, a connection was made between the development of vortices created when hot and cold gases interact. The resulting entrainment process was found to produce an oscillatory motion with a period of 1.8 seconds, independent of balcony length. In addition, it was found that the oscillatory motion of the plume accelerated with increased heat release rate. Observations on the oscillatory behaviour of energy, flow and pressure fields within *compartments* were reported in an earlier finite-difference study by Satoh *et al.*[90]. This phenomena has been observed both numerically[91,92] and experimentally[93,94] and has been associated with inherent instabilities in the fluid dynamic processes at the base of the fire which contribute to the entrainment of air, the effectiveness of combustion, the resulting flame height and the radiation field.

To overcome current computational limitations associated with simulations, Galea *et al.*[95] proposed the use of parallel processing techniques to shorten processing time. Applications ranged from external fire spread in buildings to aircraft fires. For a building fire, both 2D and 3D simulations were performed when fire spread out of both wide and narrow window openings. It was found that the wider window geometry using a 3D simulation produced results that corresponded more closely to the 2D case. Differences between the 2D and 3D simulations were linked to window geometry and corresponding air entrainment into the side of the plume which were not considered in the 2D case, indicating the three-dimensional nature of the venting plume.

Continuing from earlier work, Galea *et al.*[96] also studied the effect of horizontal balconies on fire plume emerging from wide window openings. Their entire 3D flow domain measured 16.8m deep, 22.8m high and 22m wide encompassing a compartment measuring 4.75m x 4m x 2.5m high. The heat source was ramped up to 1MW until it occupied the floor area of the compartment. The non-uniform grid was divided into 63 x 63 x 26 cells, with smaller cells along the external wall. Three dimensional modelling of a full 60 second simulation on CFD5-FLOW3D took approximately 25 days with a time step of 0.5 seconds using parallel processing. Three cases were run with wide windows, and with and without protrusions at ceiling level. Each window was 4m wide (matching the width of compartment) and 0.88m high located at ceiling level. As a result, plume emerged from the entire opening. Galea *et al.* estimated Yokoi's[28] re-attachment parameter n to be 9.1 for their window geometry, and re-attachment occurred as expected.

Results indicate a strong tendency for the emerging plume to adhere to the external wall when there are no protrusions. Temperature contours plotted on the vertical symmetry plane show core temperatures reaching 530°C just over 1m above the top of the opening and dropping off to 400°C at 2m and 200°C at 4m above the opening when there are no protrusions. Corresponding contours at the window edge have significantly lower temperatures: 400°C just at the opening, and 40°C for over 4m up the external wall. Just a little away from the wall, temperatures of 200°C are measured at 0.5m and 100°C just below 2m after which they also drop to 40°C.

Generally, protrusions deflect the plume away from the wall, and if reattachment occurs there is a significant drop in temperature. For protrusions 1m in depth, there is a greater drop in temperature compared to 0.5m depth protrusions as there is little reattachment. As such, protrusions of 1m in depth minimise the chances of flame spread along the external wall. Approximations of the velocity of the hot gases venting from the opening are also presented. *Peak velocities* at the plane of symmetry of 3m/s and 5m/s were calculated, with and without protrusions, respectively. At the window edge, peak velocities fell to 2.5m/s and 3.5m/s, with and without protrusions. However, while higher local velocities were calculated when there were no protrusions, on the whole, average exit velocities were higher across the width of the opening when there were protrusions.

The work of Satoh and Kuwahara[89] and Galea *et al.*[96] show certain similarities. Temperature predictions and the effects of horizontal protrusions (balconies) were found to contribute to a decrease in temperature measured along the external wall. Satoh and Kuwahara highlighted the periodic nature of the venting plume while Galea *et al.* acknowledged the horizontal variations in temperature of the venting plume as well as the vertical variations. These works have admittedly neglected combustion and radiation effects which would certainly alter the temperature contours presented and have also used relatively small fires. In Chapter 6, comparison is presented between the present numerical predictions and the external ones discussed in this section.

3. EXPERIMENTAL SETUP

Four flashover fires were carried out using polyurethane to simulate a mattress and carpet, as explained in the *Section 3.1*. The first three tests (PU1, PU2 and PU3) were in a standard burn room with standard and alternative window arrangements. The fourth polyurethane test (PU4), was performed in the large burn room in which the subsequent Real Furniture Burns were carried out. The standard and larger burn room layouts are discussed in *Section 3.1.1*, followed by the fuel configuration, experimental conditions and instrumentation.

Following the Polyurethane Burns was a series of eight full scale flashover tests, referred to as the Real Furniture Burns, during which real furniture was used in a living or lounge room arrangement. The corresponding setup is given in *Section 3.2*. Two window lowering criteria were established to eliminate the uncertainty associated with glass cracking and dislodgment, as detailed in *Section 3.2.2*. Although the influence of air handling systems and combustible lining in the corridor were investigated, the effects of ventilation conditions on the venting plume were the primary focus during both of these series of tests.

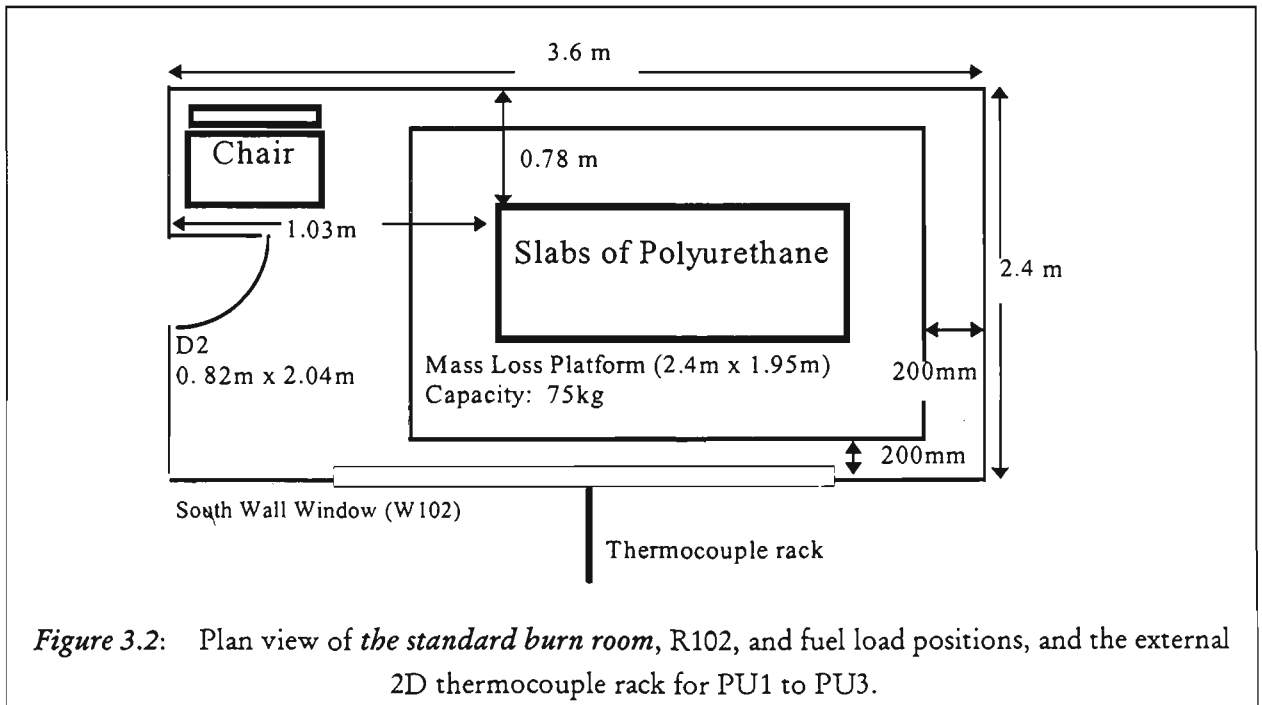
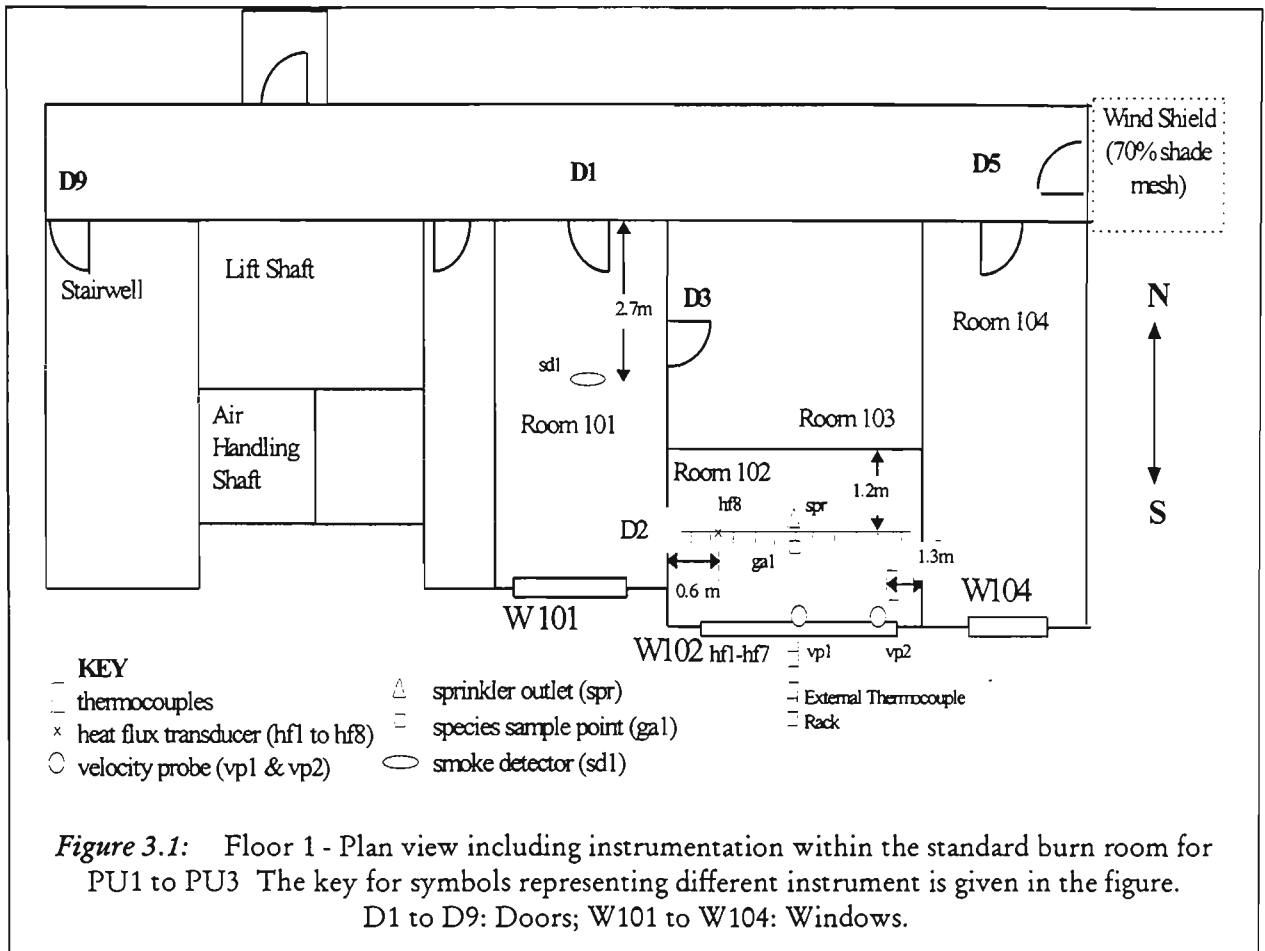
3.1 POLYURETHANE BURNS

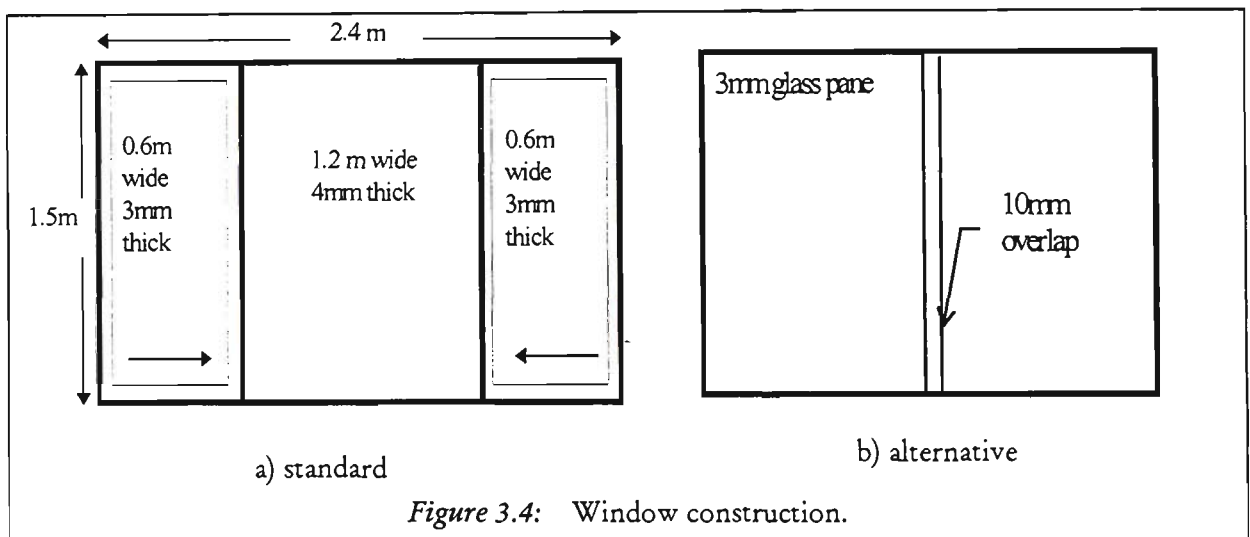
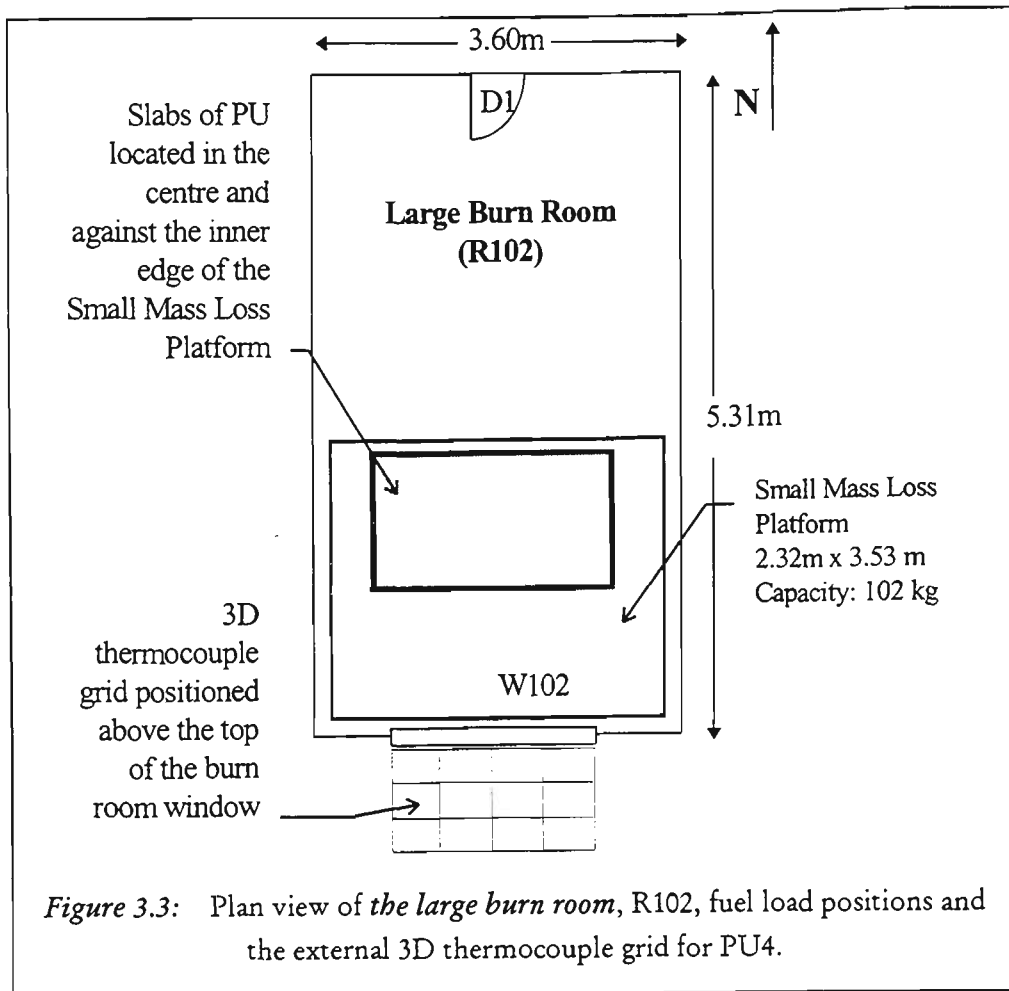
3.1.1 The Building and The Burn Room

The burn room (R102) is located on the first floor (Floor 1) of a three storey steel and concrete building, called the EB-FF (Experimental Building-Fire Facility), 12m in height with a floor area of 21m x 15m. A schematic plan of the burn room within Floor 1 including instrumentation is illustrated in Figure 3.1. The building plans are given in Appendix B. A mezzanine floor, Floor 1M, is included to produce a suitable room height between the first floor (Floor 1) and the second floor (Floor 2) of the building. The external South wall facade consists of 9mm compressed cement sheeting, and it is along this wall that the effects of the venting fire plume are measured.

Figure 3.2 shows the plan view of *the standard burn room* (R102) including fuel load positions used for PU1 to PU3. The room was 2.4m x 3.6m x 2.4m high, with a window opening of 2.4m x 1.5m placed in the centre of the Southern wall, 0.5m above the floor and a 0.82m x 2.04m door opening in the centre of the Western wall. Figure 3.3 shows the plan view of *the large burn room* (R102) including fuel load positions used for PU4. This larger burn room is a combination of the original burn room, R102, and R103, originally located between R102 and the corridor, as illustrated in Figure 3.1. The larger burn room is 5.31m x 3.6m x 2.4m high, with a *standard* window opening of 2.4m x 1.5m placed in the centre of the Southern wall, 0.5m above the floor and a 0.82m x 2.04m door opening in the centre of the Northern wall.

The window consists of an aluminium frame with two 600mm sliders located on each side. The first window construction, shown in Figure 3.4a, included a centre glass pane, 4mm thick, with two 3mm glass pane on each side, both 600mm wide. This *standard window arrangement* was used for PU1, PU2 and PU4. Figure 3.4b shows the *alternative window arrangement* that was employed for the third test, PU3, where two approximately equal glass panes, 3mm thick with an overlap of 10mm were positioned in the window, completely supported by 16mm fire-stop plasterboard reveals. This alternative window construction was used in the third test, PU3, in anticipation that both sheets of glass would break-away together. As a result, an '*open window*' of constant size in the burn room would be created. However, although the panes cracked and dislodged, the glass did not fall away completely, but the '*overlap*' section of the glass remained intact until the fully developed phase of the fire. Glass Breakage during the Polyurethane Burns is discussed further in *Section 4.4*.



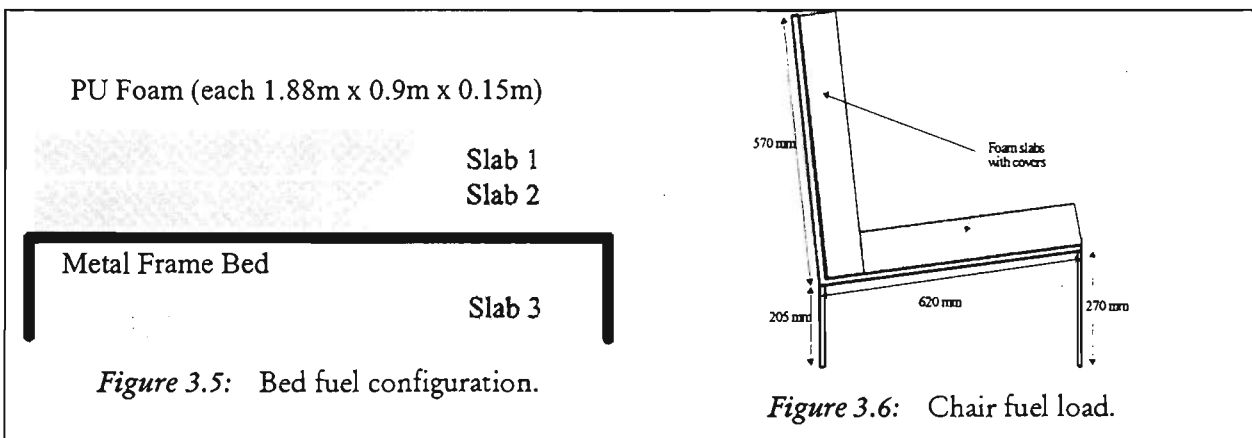


3.1.2 Fuel Configuration

The fuel used was polyurethane foam (A23-130) manufactured by Dunlop, having a density of 23 kg/m³ and an average initial hardness of 130 Newtons. Table 3.1 details the fuel load for each of the polyurethane tests, including PU4. Figure 3.2 and Figure 3.3 show the approximate location of the fuel in the burn room for PU1 to PU3 and PU4, respectively. Of the three slabs used, two were placed on top of a metal frame bed, to represent a mattress and other possible combustible items that might be found in a typical bedroom. The third slab, placed beneath the bed, was considered to be equivalent to a floor covering, such as a carpet, as shown in Figure 3.5. As well as the three slabs used, an additional fuel load was included in PU1, characterised as a chair, shown here in Figure 3.6. Ignition with a gas torch was in the approximate centre of the top PU slab, Slab 1.

Table 3.1: Fuel load for each of the PU tests.

Test	PU Slab 1 (kg)	PU Slab 2 (kg)	PU Slab 3 (kg)	Chair Slab (kg)	Total (kg)
PU1	6.12	6.14	4.04	1.48	17.78
PU2	6.04	6.08	3.90	0	16.02
PU3	5.86	5.78	3.96	0	15.06
PU4	5.93	5.93	4.36	0	16.22



3.1.3 Experimental Conditions

The environmental conditions during the experiments, such as barometric pressure, temperature, wind speed and direction are given in Table 3.2. These were measured with a *Weather Monitor II*, a weather monitoring station developed by DAVIS Instruments Corp., Hayward, California, located approximately 17 meters South of the burn room window, W102. The ventilation conditions for each test are described in Table 3.3. This table refers to various ventilation conditions and the corresponding Window Lowering Criteria and Class distinctions which were associated with these conditions. The Window Lowering Criteria and Class definitions are introduced in Chapter 1, *Introduction* (and they are discussed in detail in *Section 3.2.2* and *Section 5.2*, respectively). Class 1 and Class 2 refer to when the door D1 is open and closed, respectively, creating through-draft and no-through-draft ventilation conditions. Class 1a and Class 1b correspond to when the stairwell door, D9, is open or closed, respectively, and D1 is open, as indicated in Figure 3.1. Table 3.3 can be viewed in conjunction with either the first floor (Floor 1) plan provided in Appendix B, or Figure 3.1. As seen from a comparison of Figure 3.2 for PU1 to PU3 with Figure 3.3 for PU4, the layout of the room and openings for PU4 correspond to those of PU1 to PU3 with the exception of D1 which is now the burn room door. A complete floor plan for PU4 can be seen in Appendix B. In addition, Appendix B contains the floor plans for Floor 2 and Floor 3, and the facade plan of the Southern elevation of the building, along which the effects of the venting plume were measured.

Table 3.2: Environmental conditions and test durations for PU1 to PU4. Ambient temperatures were measured within $\pm 2^\circ\text{C}$ throughout the course of each test. Average wind speeds were determined over the entire duration of a test, and wind direction was as stated for 90% of the duration.

Test	Start Time	Duration (min)	Ambient Temperature ($^\circ\text{C}$)	Barometric Pressure (mbar)	Average Wind Speed (m/s)	Average Wind Direction
PU1	11:30 am	20	23.1	1007.17	4.33	WNW
PU2	3:46 pm	19	26.5	1023.56	2.53	ENE
PU3	8:56 pm	15	15.4	1014.78	3.72	ENE
PU4	11.43 am	8	15.4	1013.44	2.98	NNE

Table 3.3: Ventilation conditions. Other doors on the first floor (Floor 1) not listed below were closed, except D3. Due to the large burn room size, D2 did not exist during PU4. The Southern exposure window W102 in R102, was closed at the beginning of the test and failed during the course of PU1 to PU3. W102 was lowered using WLC #1 during PU4. WLC and ventilation classes are discussed in Chapter 1, *Introduction*. WLC#1 is detailed in *Section 3.2.2*. The distinction between Class 1a and Class 1b is given in *Section 5.2*.

Test	D2	D1	D9	D5	W102	Ventilation Class
PU1	Open	Closed	Closed	Closed	Closed	Class 2
PU2	Open	Open	Open	Closed	Closed	Class 1b
PU3	Open	Open	Closed	Open	Closed	Class 1a
PU4	--	Open	Open	Closed	Closed	Class 1b

3.1.4 Internal Instrumentation

The emphasis in this study is on the external plume characteristics. Although these characteristics depend on the burn room conditions, the internal data that define the burn room conditions are not discussed in detail in this thesis. Only the mass loss data, velocity measurements and gas analysis in the burn room door are provided. These and all other internal results of the Polyurethane Burns are given in a CESARE report by Beck *et al.*[97]. The internal instrumentation used during the Polyurethane Burns is listed here for completeness and also to indicate which other internal results are available for these tests.

The plan view of the instrumentation layout inside the building used for PU1 to PU3 is shown in Figure 3.1. A four-tiered thermocouple rack, made of 6mm stainless steel rods, 3.4m long was placed at the centre of the burn room (R102), 0.25m from the ceiling. The spacing between the top and successive rows was 0.5m, 0.45m and 0.2m, and the rack consisted of 11 columns each spaced 0.34m apart. A total of 44 Nickel-Chromium, Nickel Aluminium, 1.5mm diameter K-type thermocouples which were mineral insulated and metal sheathed (MIMS), were used. Also located in the centre of the burn room ceiling was a sprinkler outlet (to record activation time) and a species sample point 1.9m above the floor. A total heat flux transducer was placed in the centre of the burn room at floor level, 0.6m away from the door opening. An ionisation type (Kambrook SD28) smoke detector was mounted on the ceiling in R101, 2.7m away from the door (D1) and activation times were recorded. For PU4, the internal instrumentation had an arrangement similar to that of the Real Furniture Burns. A detailed description of this arrangement is provided in *Section 3.2.5* (and it is shown in Figure 3.14).

3.1.4.1 Mass Loss Platform

For PU1 to PU3, a 2.4m x 1.95m weighing platform, with a 5mm compressed cement sheet floor and a capacity of approximately 75 ± 15 kg was built in the burn room to determine the burning rate of the fuel. The platform was suspended by load transfer rods which connected the platform to three load cells located on the mezzanine floor, Floor 1M, the room above the burn room. This location was chosen to ensure minimal fire exposure to the load cells during the test. The platform was calibrated prior to each test. For PU4, the small mass loss platform discussed in *Section 3.2.5.1* was used.

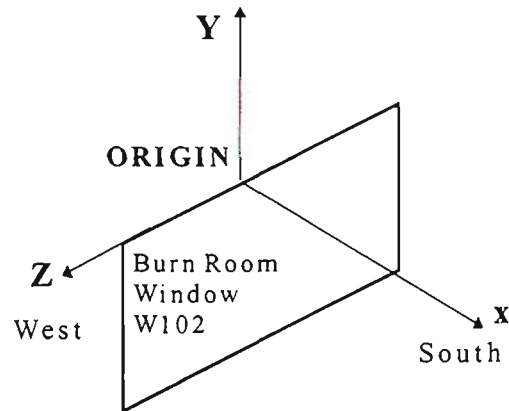
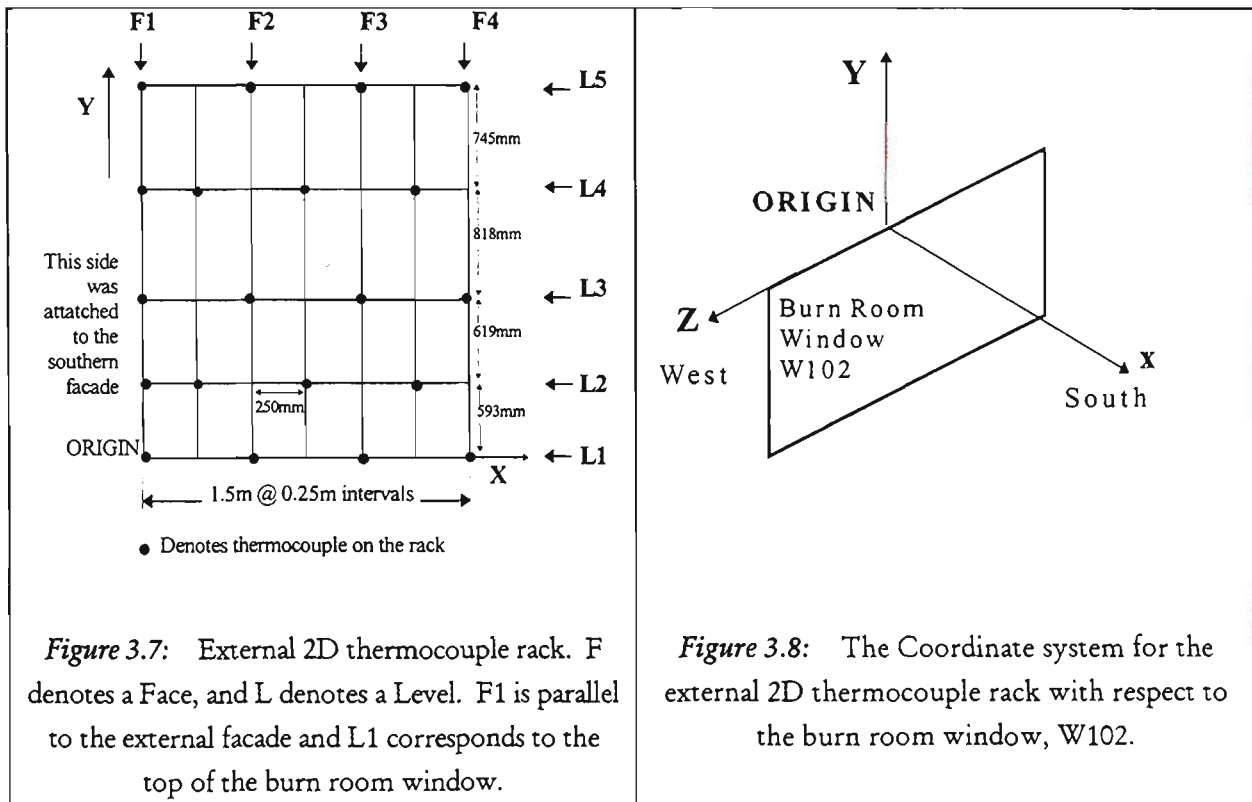
3.1.5 External Instrumentation

The external instrumentation consisted of thermocouples, heat flux transducers (total and radiative), velocity probes and gas samplers. Externally, the thermocouples were arranged on a 2D rack (PU1 to PU3) or on a 3D grid (PU4). The external instrumentation is described in detail next.

3.1.4.1 The Co-ordinate System for the 2D External Rack

Prior to the present study, the focus of most experimental investigations of the external plume had been along the plume's centre plane. The centre plane corresponds to the region of space in the centre of the burn room window, both vertically up and perpendicularly away from it. To begin a preliminary investigation of the plume, it was decided to take measurements along the centre plane with the 2D thermocouple rack shown in Figure 3.7 during PU1 to PU3. For this configuration, the origin of the Cartesian co-ordinate system, as shown in Figure 3.8, was placed on the external facade of the Southern wall at the top-centre of the burn room window (W102). The y-axis represented the vertical height above the window. The x-axis extended South and away from the wall. The positive and negative z-axes ran along the top of the window to the West and East, respectively. The 2D thermocouple rack was constructed with 6mm outer diameter 2mm wall thickness steel tubing. Each thermocouple was mounted at least 5cm from a node of the thermocouple rack to minimise the effect of heat capacitance of the node (consisting of two joining rods and welding). For PU4, a 3D thermocouple grid was located on the external facade of the

building as shown in top view in Figure 3.3. The experience gained during PU1 to PU3 highlighted the need for a 3D investigation of the external plume. The details of the 3D grid are provided in *Section 3.2.6.1* (and Figure 3.19). In fact, the results and conclusions of the second series of tests, the Real Furniture Burns rely heavily on the 3D thermocouple grid.



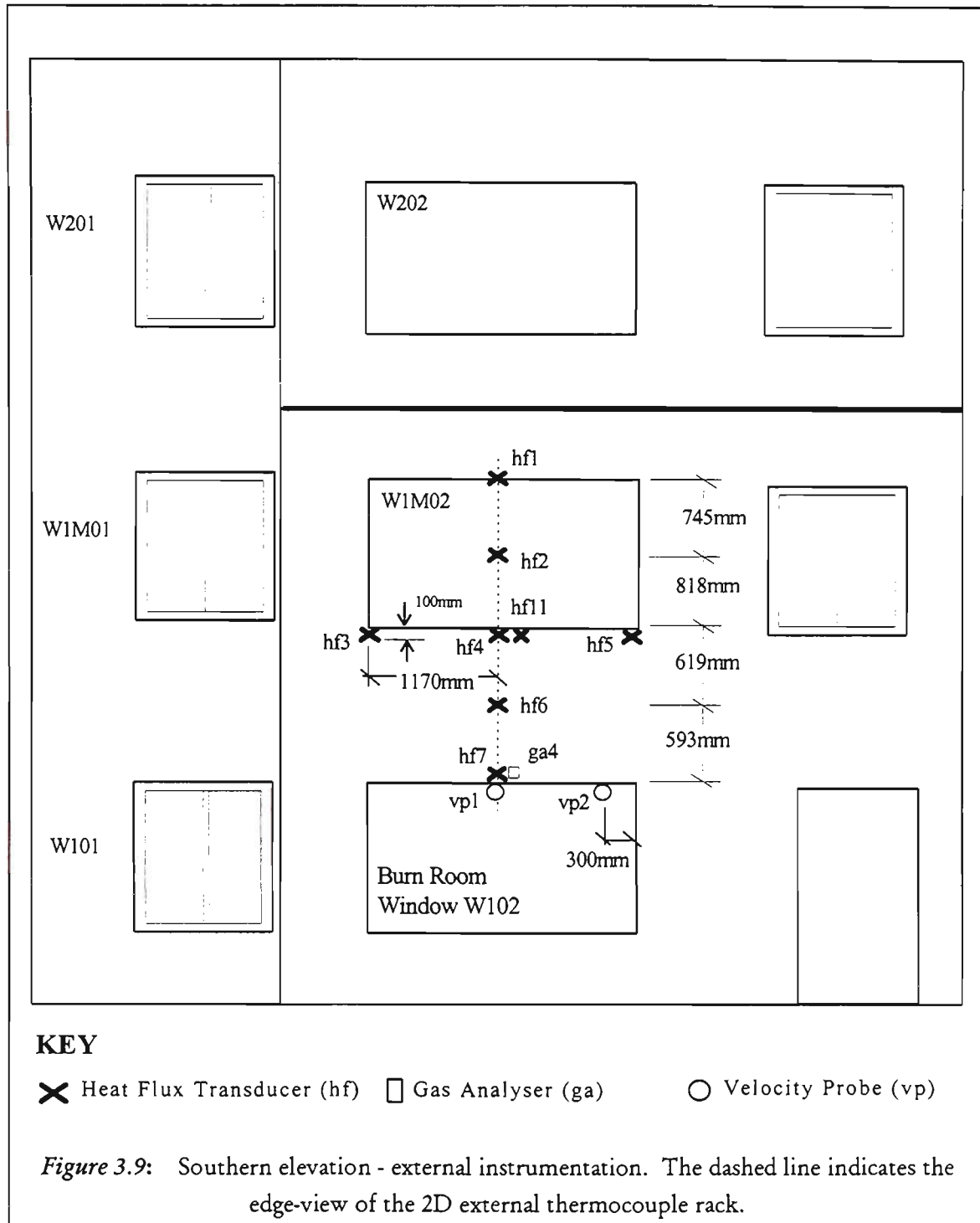
3.1.5.2 Thermocouples

One corner of the two-dimensional (2D) external thermocouple rack shown in Figure 3.7, was aligned with the origin of the coordinate system as shown in Figure 3.8. The rack extended vertically to a height of 2.78m above the origin, taking it to the top of the window on the floor above (W1M02), as well as 1.5m away from the wall to allow a two dimensional section of the fire plume to be mapped.

All internal and external temperatures were measured with Nickel-Chromium, Nickel Aluminium, 1.5mm diameter K-type thermocouples which were mineral insulated and metal sheathed (MIMS). The thermocouples were mounted on 6mm stainless steel rods. All thermocouples used in these series of tests were purchased with NIST calibration certificates. The manufacturer specified uncertainty in temperature measurements was $\pm 2.2^{\circ}\text{C}$ or 0.75% of the reading, whichever is higher. Selected

thermocouples were tested in a calibrated furnace after the completion of the tests. With measurements at 500°C, no more than a $\pm 2^\circ\text{C}$ error was recorded at this stage. Thermocouple outputs were sampled nominally at 1 Hz and then averaged over 12 consecutive sample points after the data were converted into appropriate physical quantities.

Accurate temperature measurements are complicated by the effects of radiation which contribute to either increasing or decreasing the indicated temperature, depending on the temperature of the gas/flame surrounding the thermocouple and the adjacent wall/environment temperature[98]. As pointed out by Jones[99], based on a simplified heat balance equation, these errors can be significant. In an attempt to quantify such effects Luo *et al.*[100]. performed experiments to compare measurements taken with a thermocouple protected by a suction pyrometer with those obtained using a bare thermocouple wire. A constant fire size of 650kW was achieved with a propane burner in the large burn room (described in *Section 3.2.1*), Luo *et al.* concluded that a difference of at most $\pm 30^\circ\text{C}$ in the measured temperature caused by radiation is expected within the compartment when temperatures are between 400°C to 600°C. In the present study, compensating for the effects of radiation on the temperatures indicated by the thermocouples located outside the burn room, is further complicated by the variation in radiation within the plume itself and the stage of the fire's development. Based on Luo *et al.*'s work, the indicated temperatures under 600°C are considered acceptable within $\pm 30^\circ\text{C}$.



3.1.5.3 Heat Flux Transducers

In Figure 3.9, each ✕ corresponds to a heat flux transducer, hf. All but two of the seven heat flux transducers were positioned along the centre-line of the burn room window (W102), corresponding to the thermocouple locations. The remaining transducers were located 1.17m on either side of the centre line, 100mm from the bottom of W1M02, to determine the variation in the total heat flux along the bottom of the window above the burn room window. For PU1 to PU3, hf1 to hf7 were total

heat flux transducers. For the last PU test, PU4, data were sampled only from four of the seven original total heat flux transducers. These four transducers were labelled as hf2, hf3 hf4 and hf5 in Figure 3.9. A radiometer, hf11, was added beside hf4 to measure radiative heat transfer at the bottom centre of the Floor 1M window, W1M02.

Total and radiative heat transfer was measured using Gardon Gauge type transducers from the Medtherm 64 Series. The total heat flux transducers were water cooled, with ranges varying from 57 kW/m^2 to 227 kW/m^2 , with a manufacturer quoted accuracy of typically $\pm 3\%$ at full range for new transducers, and a field use accuracy of typically $\pm 5\%$ at full range. The sapphire windowed radiometer was nitrogen gas purged, and it measured radiative heat transfer. Calibrations have been performed annually on a randomly selected group of transducers in a furnace. The transducers used in this study were found to perform within manufacturer specifications. Whenever the output from a transducers was considered 'questionable', the transducer was checked in the same furnace. Depending on the outcome, the data were either accepted or rejected, and the transducer was replaced if necessary (and possible). Re-calibration by the manufacturer was not carried out due to the high cost associated with shipping components overseas[101].

For the three total heat flux transducers embedded in the wall just below the Floor 1M window, the experimental uncertainty is not expected to exceed the manufacturer specification of $\pm 3\%$. For these transducers, no correction was needed, because the wall temperature matched the transducer temperature[29]. For transducers not embedded in the external wall, Oleszkiewicz[29] states that for an average air temperature of 650°C and a cold wall temperature of 100°C , approximately *11% error* can be expected in the *convective heat flux* measurements. This error corresponds to 4.4% uncertainty in the total heat flux, if 40% of the total is due to convective heat transfer. Oleszkiewicz's calculation details are given in *Section 4.3.4* for the Polyurethane Burns.

High frequency fluctuations in the measured heat flux data on the external wall was reduced by the same averaging process as used for the thermocouple outputs.

3.1.5.4 Velocity Probes

For PU1 to PU3, two bi-directional probes were mounted 100mm below the top edge of the burn room window opening (W102) outside the glass. The first probe, vp1, was positioned in the centre of the window while the second probe, vp2, was positioned 1.2m away from vp1, as indicated in Figure 3.9. These two probes registered the velocity of the venting plume when the window began to crack along the top. They were connected to Veltron differential pressure transducers to determine the velocity of gases venting from the burn room window. Positive velocity indicated flow towards the fire, into the burn room, while negative velocity indicated flow away from the fire and out of the burn room. These readings were temperature compensated. For PU4, velocity measurements were taken only at the centre of the burn room door (D1), as discussed further in *Section 3.2.5.2*.

3.1.5.5 Gas Analysis

Levels of O₂, CO and CO₂ were taken during the course of each test on the ceiling in the centre of the burn room and just outside the burn room window opening, as shown in Figure 3.1 and Figure 3.9 for PU1 to PU3. For PU4, gas samples were taken only at the top centre of the burn room door, 2.0m above the floor. The CO and CO₂ transducers were infra-red optical bench-type made by Analytical Development Co. The O₂ sensor, a galvanic cell, was manufactured by Japan Storage Battery. The analysis system was calibrated against a sample with known concentrations prior to the series of experiments.

3.2 REAL FURNITURE BURNS

3.2.1 The Burn Room

Figure 3.10 shows the plan view of the Burn Room for the Real Furniture Burns. This burn room was an enlarged, and hence, more realistic version of the one used for the first three PU tests, located on the first floor (Floor 1) of the three-storey steel and concrete building. The construction and dimensions of the South external facade was the same as in the PU Burns. The burn room was lined with 2 layers of 16mm fire rated plaster, except for the ceiling which had an extra layer. The room measured 5.31m x 3.6m x 2.4m high, with a window opening (W102) of 2.4 x 1.5m placed in the centre of the Southern wall, 0.5m above the floor.

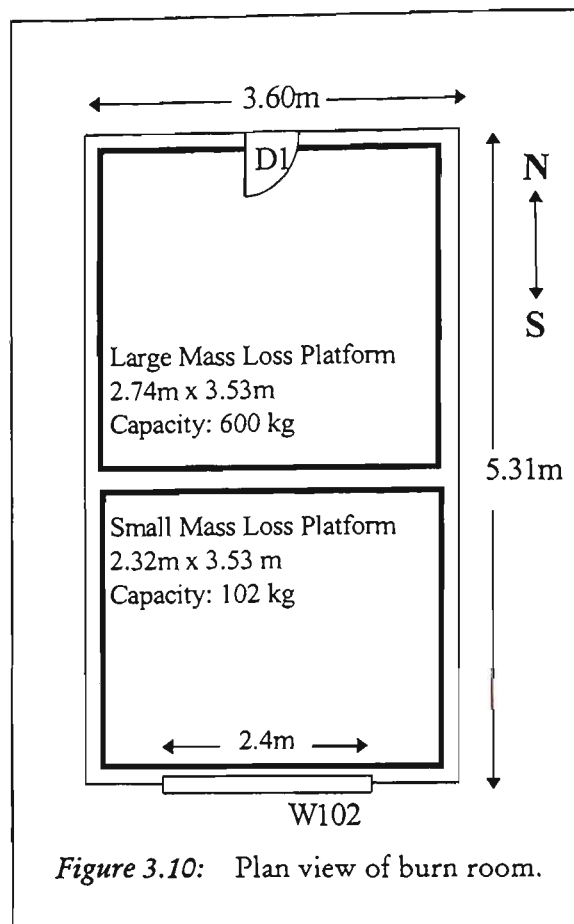


Figure 3.10: Plan view of burn room.

The standard three-pane window was the same as in PU1, PU2 and PU4, shown in Figure 3.4a. The 0.82m x 2.04m door opening (D1) was located in the centre of the Northern wall which lead to the corridor. This was a standard fire rated door, and when fitted into the frame, it had a 15mm clearance from the floor.

3.2.2 Window Lowering Criteria

The cracking of glass in a window is a random phenomenon which may result in partial or complete dislodgment of the glass during various stages of a fire. To eliminate this variable, the following window lowering criteria were used. The first criterion was established to produce an 'open window' during Class 1 tests. The second criterion was designed to *facilitate* flashover for tests where the door to the burn room was closed during Class 2 tests. The distinction between Class 1 and Class 2 tests are given in the *Introduction* (and also in *Section 5.2*).

Window Lowering Criterion #1 (WLC #1): to lower the entire window and frame when either a fast response thermocouple, glued to the inner surface of the glass window and shielded by a calcium-silicate base block, indicated a glass temperature of 250°C, or when a MIMS thermocouple, approximately 15cm away from the centre of the glass window indicated a gas temperature of 450°C. The window was lowered as soon as either one of these two conditions was met.

Window Lowering Criterion #2 (WLC #2): to lower the entire window/frame when the mass loss rate reached 0.1 kg/min.

The temperature and mass loss rate values quoted above were decided on after an examination of the experimental data obtained at CESARE[102, Appendix 4]. These experiments indicated that when the burn room door was open, Class 1, initial glass cracking/dislodgment occurred when the glass temperature reached between 200°C to 250°C, or equivalently, after the gas temperature close to the window approached 450°C. When the burn room door was closed, Class 2, the window was lowered to *facilitate* flashover. Otherwise, the fire would have extinguished itself.

3.2.3 Fuel Configuration

During the Real Furniture Burns, the fuel load and distribution were selected and designed to mimic a lounge or living room situation, with a fuel load density (per unit floor area) of approximately 28kg/m² (wood equivalent), considered to be representative of a typical residential environment[102, Appendix 1]. The load consisted of a 3 seater couch, two arm chairs, coffee tables and bookcases, as detailed in Table 3.4, for Burn 2 to Burn 8. Burn 1 had a slightly different fuel load distribution. The furniture included an additional side-cupboard on the large mass loss platform and a lamp table on the small mass loss platform. For the later test, the weight of the side-cupboard was replaced by telephone books, and the lamp table by another coffee table. The detailed load breakdown and distribution for Burn 1 are given in Table C1 and Figure C1, respectively in Appendix C. All items placed in the burn room were conditioned at 20°C for seven days prior to each test.

Table 3.4: Fuel breakdown for Burn 2. A similar breakdown existed for all other tests, except Burn 1. The fuel breakdown for Burn 1 is given in Table C1, Appendix C.

	Mass (kg)	Heat of Combustion (MJ/kg)	Wood Equivalent (kg)
SMALL PLATFORM			
3 Seater Couch	46.04	14.6	36.53
Coffee Table	21.90	18.4	21.90
Carpet & Underlay	17.22 & 16.7	53.7	99.0
TOTAL	101.86		157.43
LARGE PLATFORM			
Chair x 2	22.72 & 22.82	14.6 x 2	36.14
Coffee Table	20.56	18.4	20.56
Carpet & Underlay	19.78 & 19.66	53.7	115.11
Bookcase x 2	33.54 & 31.44	18.4 x 2	64.98
Books on Shelf & on Coffee Table	138 + 3.9	18.4	141.9
TOTAL	439.62		378.69
BURN ROOM TOTAL	541.48		536.12
Wood Equivalent Fuel Load Density in the burn room: 28.05 kg/m²			

Both the coffee tables and the bookcases were made of untreated pine. Unused and outdated telephone books were used to simulate real books on the book cases. These were spaced evenly on the shelves, and each weighed *approximately* 1.95 ± 0.05 kg. Two books were also placed on the coffee table closest to the bookcases. A total of 110 telephone books was used. The carpet was a “Domestic Heavy Duty”, fibre blend with 80-20 wool-polypropylene, and was untreated, while the underlay was made of natural latex rubber. A strip of carpet and underlay (approx. 1.56kg) were also placed between the weighing platforms, to ensure that the entire floor was covered continuously with carpet, without gaps between the weighing platforms. The couch setting consisted of kiln dried radiata pine, plywood, Dacron which is 100% polyester fibre, webbing and filling consisting of a blend of rubber, polyolefin and polyurethane foam, with a blend of nylon and acrylic fabric cover [102, Appendix 3]. The total mass (wood equivalent) for each test is given in Table 3.5 along with the ventilation conditions, and the distribution of the fuel inside the burn room is shown in Figure 3.11 to Figure 3.13, for Burn 2 to Burn 8. For Burn 1, the fuel distribution in the burn room was similar, as shown in Figure C1, Appendix C. Differences in the fuel load for each test can be attributed to manufacturing technique and materials, along with variations in the total weight of the telephone books, which constituted a significant portion of the overall weight.

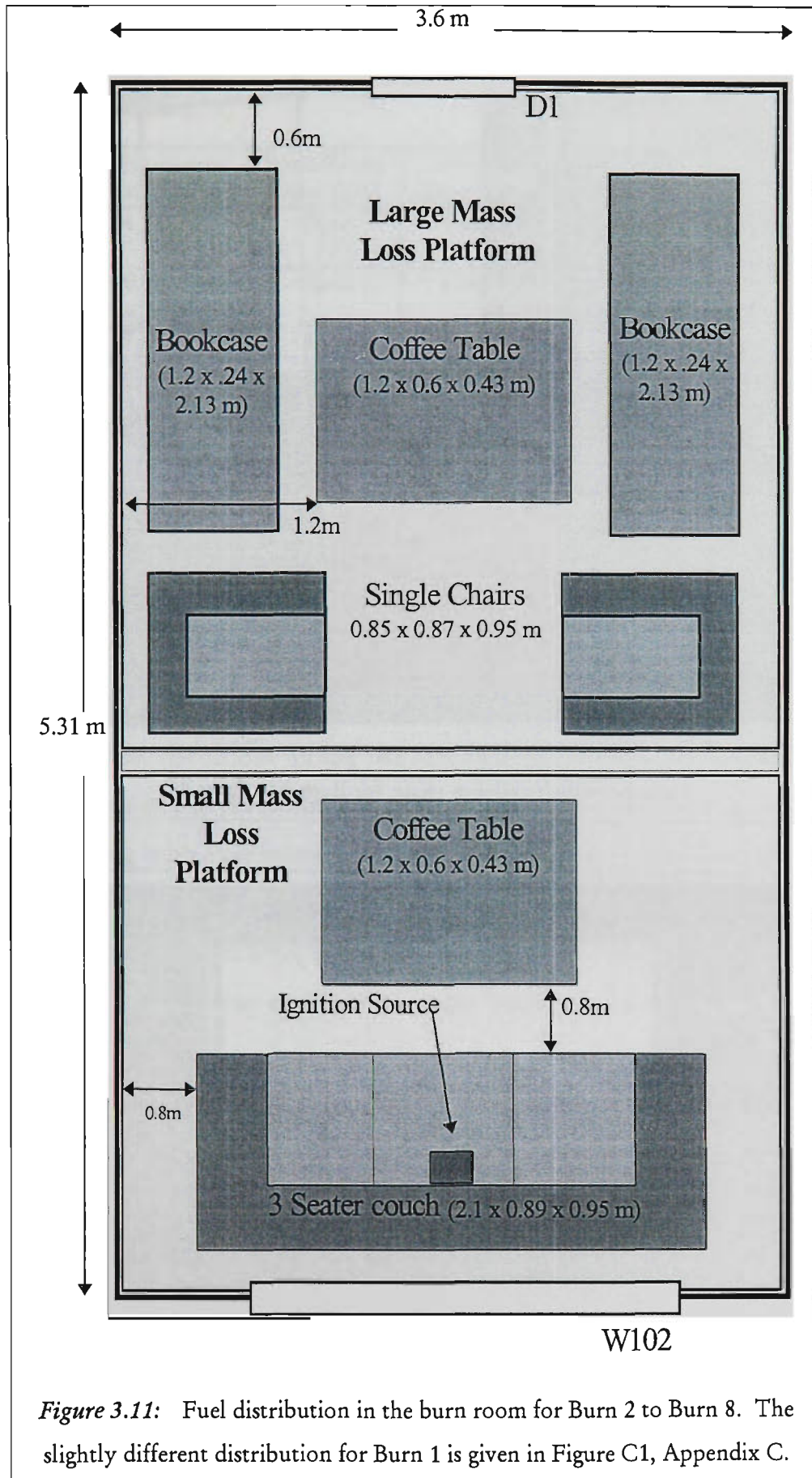


Figure 3.11: Fuel distribution in the burn room for Burn 2 to Burn 8. The slightly different distribution for Burn 1 is given in Figure C1, Appendix C.

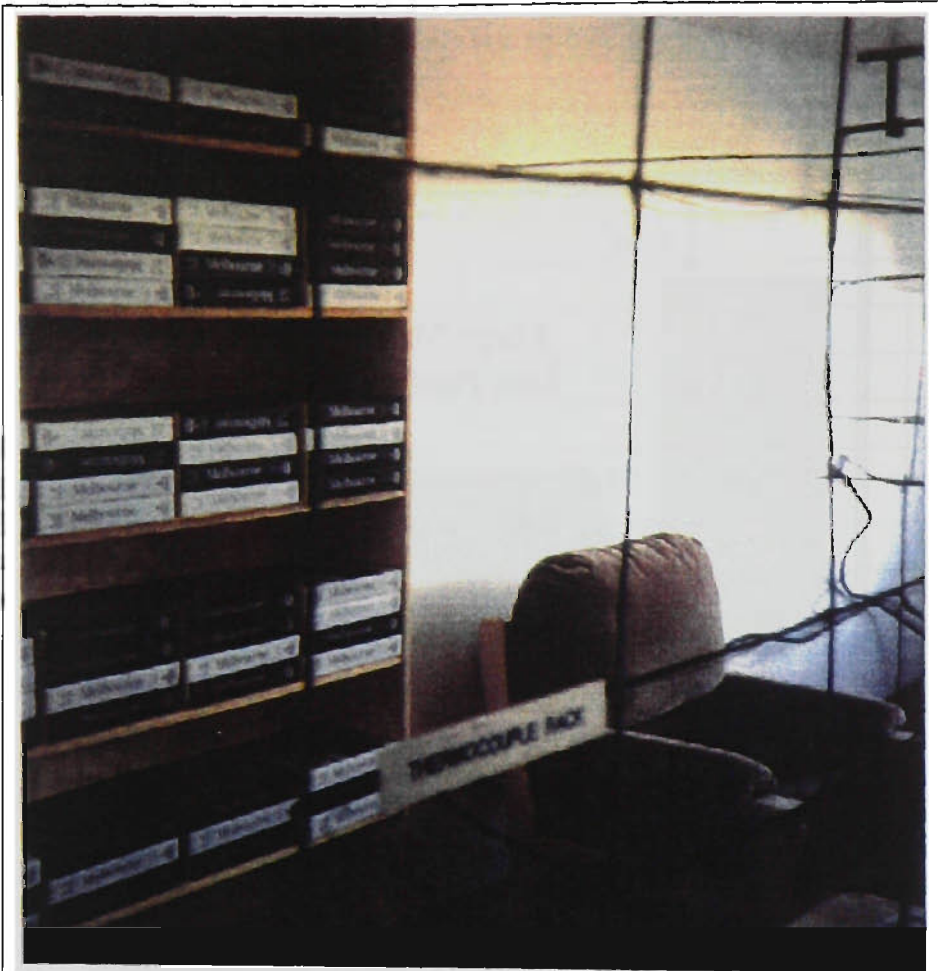


Figure 3.12: Burn room layout showing the internal N-S thermocouple rack, bookshelf and arm chair, for Burn 2 to Burn 8.



Figure 3.13: Burn room layout showing window, couch and ignition source, tables, arm chairs and the internal N-S and E-W thermocouple racks, for Burn 2 to Burn 8.

Table 3.5: Fuel load, ventilation conditions and additional factors. Fuel load and distribution remained the same for Burn 2 to Burn 8. Burn 1 details are in Appendix C. WLC refers to window lowering criteria as explained in the *Introduction* and in detail in *Section 3.2.2*. Flashover occurred during all of the tests except for Burn 6. Class definitions are given in the *Introduction* as well as in *Section 5.2*.

Test	Wood Equivalent Fuel Load (kg/m ²)	Burn Room Door (D1)	Stairwell Door (D9)	Additional Factors
BURN 1	26.36	Open	Closed	Window opened, fuel type and distribution in Appendix C, Class 1a
BURN 2	28.05	Open	Closed	New fuel distribution, with similar fuel load as Burn 1, WLC#1, Class 1a
BURN 3	27.65	Closed	Closed	WLC#2, Class 2
BURN 4	28.32	Closed	Closed	WLC#2, Class 2
BURN 5	28.21	Open	Open	Window failed, Class 1b
BURN 6	27.90	Open	Open	WLC#1, Smoke Management System on, no flashover, Class 1b
BURN 7	27.95	Closed	Closed	WLC#1, Smoke Management System on, flashover occurred, Class 2
BURN 8	28.48	Open	Open	WLC#1, combustible linings in corridor, Class 1b

3.2.4 Experimental Conditions

The environmental conditions during the second series of tests (ambient temperature, pressure, wind speed and direction) are given in Table 3.6. The ventilation conditions for each test along with Equivalent Fuel Loads are specified in Table 3.5, which can be viewed in conjunction with the floor plan of Floor 1, given in Figure 3.14 or Figure B2 in Appendix B. These tests were carried out on ‘still’ days, where a wind speed of 2.8 m/s (10km/hr) or less was expected to cause minimal disturbance of the venting plume.

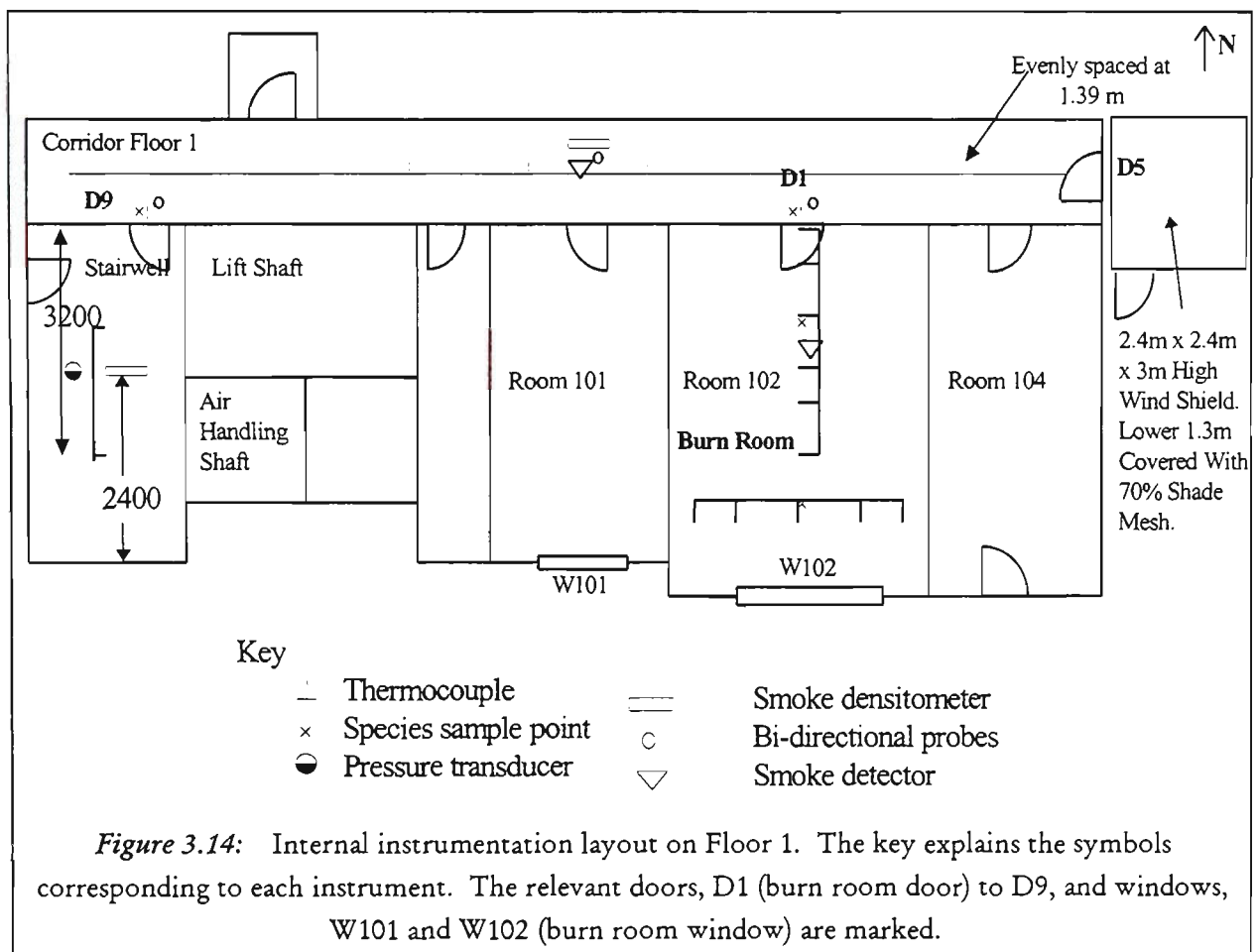
Table 3.6: Environmental conditions. Ambient temperatures were measured within $\pm 2^{\circ}\text{C}$ throughout the course of each test. Averaged wind speeds were determined over the entire duration of a test, and wind direction was as stated for 90% of the duration.

Test	Start Time	Duration (min)	Ambient Temperature (°C)	Barometric Pressure (mbar)	Average & Peak Wind Speed (m/s)	Average Wind Direction
BURN 1	7:17 pm	32	15.4	1019.04	1.5 : 2.5	ENE
BURN 2	7:20 pm	32	12.1	1023.59	1.6 : 2.8	SSE
BURN 3	4:11 pm	32	14.1	1023.35	3.5 : 5.8	S-SSW
BURN 4	5:44 pm	32	11.0	1025.15	1.6 : 2.9	NE
BURN 5	5:24 pm	29	8.3	1025.38	2.1 : 2.8	W
BURN 6	9:52 am	21	7.5	1020.48	2.5 : 5	WNW
BURN 7	5:05 pm	24	7.7	1015.40	1.2 : 2.1	SW
BURN 8	11:56 am	54	8.0	na	1.3 : 2.2	NNW

3.2.5 Internal Instrumentation

Similar to the Polyurethane Burns, the emphasis during the Real Furniture Burns was the external plume characteristics. The importance of the burn room conditions in producing external plume characteristics must be acknowledged again. As such, the internal instrumentation has been listed here both for completeness and to give an indication of what additional data were collected during this series of tests. The internal results are provided by Alam and Beever[102]. Only mass loss data and burn room temperatures are included in this thesis.

The burn room, Floor 1 corridor and stairwell were instrumented as shown in Figure 3.14 during PU4 and the Real Furniture Burns. In the burn room, two thermocouple racks were placed in the centre of each of the mass loss platforms. The thermocouples were fibreglass-fibreglass (K-type) and mineral insulated-metal sheathed (K-type MIMS), based on casing material and insulation type, respectively. Across the large and small mass loss platforms were a North-South rack, and a East-West rack, respectively, each with a total of 35 thermocouples as shown in Figure 3.15. A smoke detector was also located in the burn room. Down the centre of the burn room door was a thermocouple tree, 2m high, with eight branches at 0.25m intervals (As opposed to a *thermocouple rack* which is used to represent a 2D thermocouple arrangement, as illustrated in Figure 3.15, a *thermocouple tree* refers a *single column* of thermocouples.). A series of eight bi-directional velocity probes were located at the same heights as the thermocouples. This arrangement allowed the velocity results measured with the bi-directional probes to be temperature compensated. Samples of O₂, CO and CO₂ were taken at 1.9m above floor level at the centres of the burn room, R102, burn room door, D1, small mass loss platform and the stairwell door, D9. Unlike the first three polyurethane tests, gas samples were not collected outside the burn room window.



Ten thermocouple trees were located along the centre-line of the corridor, each 2m high, and spaced 1.39m apart. Thermocouples were attached to each of the four branches of the tree which were 0.5m apart. A smoke detector, species sample point measuring oxygen and a smoke densitometer were located in the centre of the corridor at ceiling level.

Seven velocity probes with corresponding thermocouples, were evenly spaced, 0.204m from the top of the centre of the stairwell door along with a species sample point measuring O_2 , CO and CO_2 , at a height of 1.7m above the floor. A pressure transducer and smoke densitometer were located in the centre of the stairwell shaft, also at a height of 1.7m above the floor. Finally, two thermocouples were placed in the centre of the stairwell, 1.39m and 3.2m away from the door D9, at a height of 1.7m above the floor.

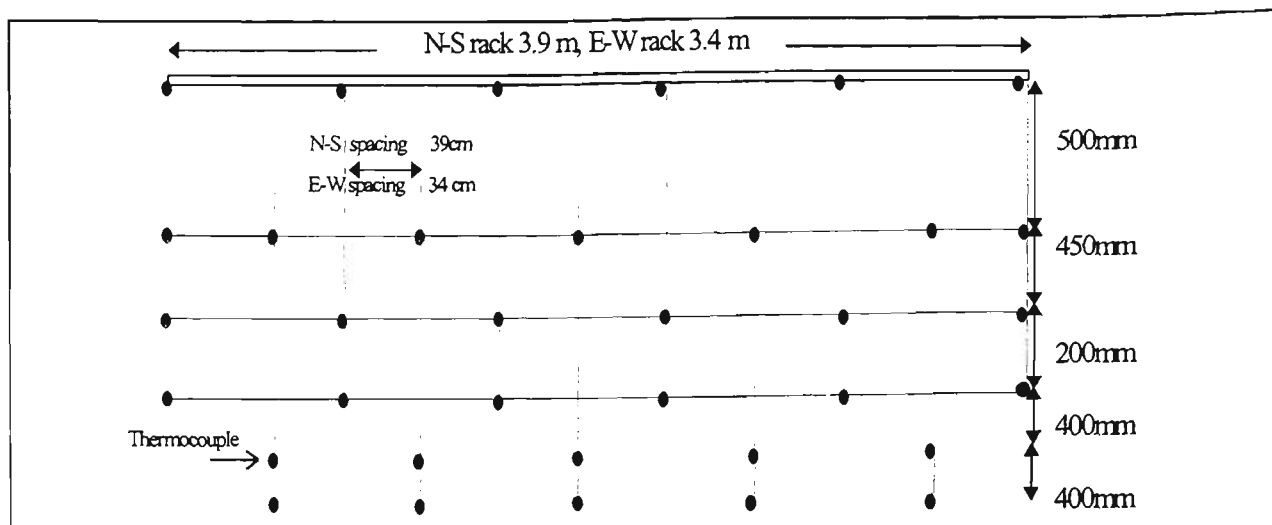


Figure 3.15: Dimensions of the North-South and East-West thermocouple racks in the burn room.

As indicated in Figure 3.16, the instrumentation in the floor above the burn room, the mezzanine floor (Floor 1M) consisted of a row of thermocouples down the centre of the corridor at a height of 1.7m above the floor, spaced evenly at 1.39m apart, with a gap of 1.39m from the East end of the corridor. The centre of the stairwell door and the stairwell shaft were instrumented as in Floor 1, without the velocity probes.

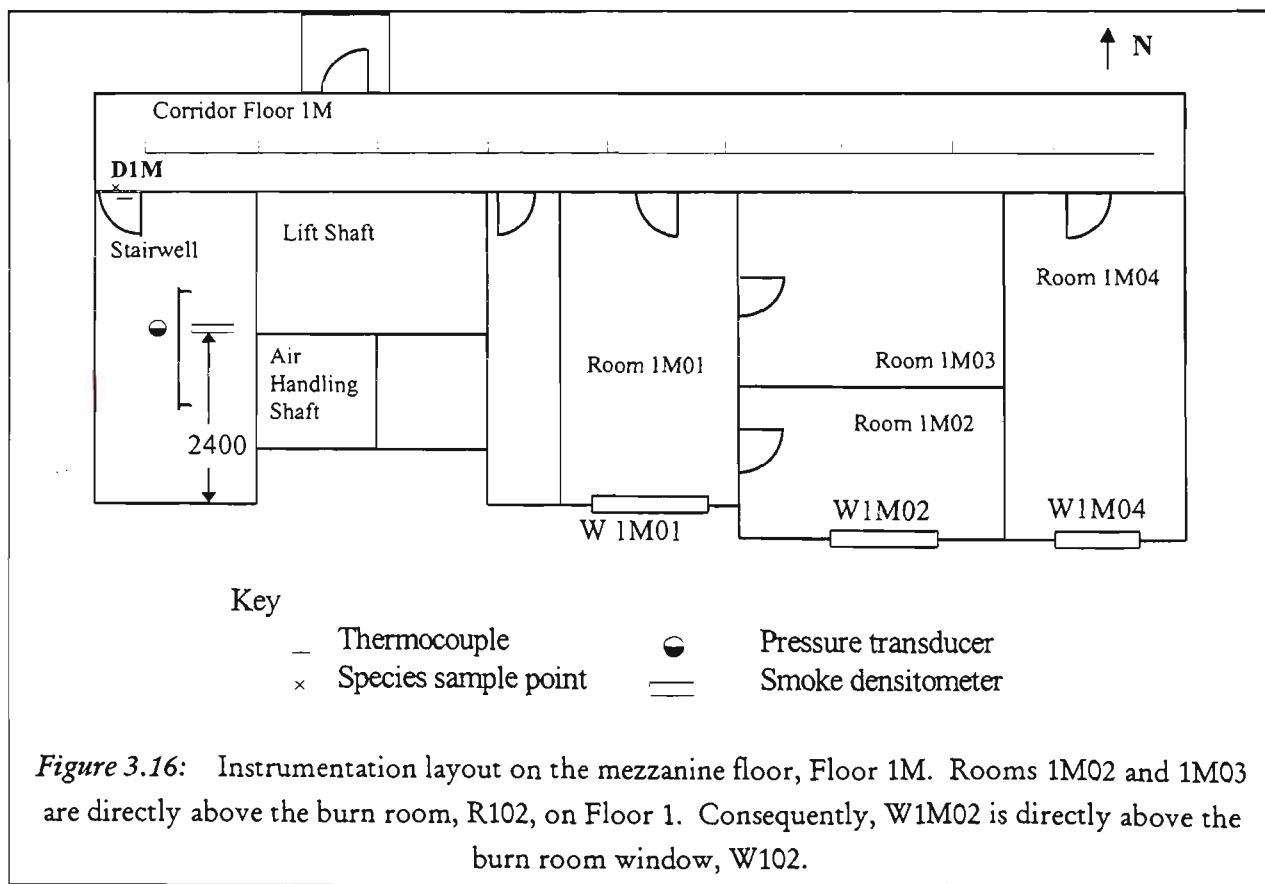


Figure 3.16: Instrumentation layout on the mezzanine floor, Floor 1M. Rooms 1M02 and 1M03 are directly above the burn room, R102, on Floor 1. Consequently, W1M02 is directly above the burn room window, W102.

3.2.5.1 Mass Loss Platforms

The contents in the burn room were distributed between the two mass loss platforms shown in Figure 3.10. The platforms had areas of 2.74m x 3.52m and 2.32m x 3.52m and capacities of 600kg and 102kg, respectively. Each platform had a resolution of 30g at full scale. The connection of the platforms' load cells was similar to that of the one used during the Polyurethane Burns.

3.2.5.2 Velocity Probes

Air flow velocity, in and out of the burn room door, was measured by the same type of bi-directional probes as those used for the PU Burns. These were located in the centre of the burn room door as shown in Figure 3.14 and spaced 2, 1.75, 1.5, 1, 0.75, 0.5 and 0.25m above the floor. Unlike PU1 to PU3, velocity measurements were not taken at the burn room window during PU4 and the Real Furniture Burns.

3.2.5.3 Ignition Source

For each of the tests of the Real Furniture Burns, a standard ignition source was used to ensure repeatability. This took the form of a wooden crib which was conditioned for 7 days at 20°C prior to each test. Each crib weighed approximately 150g and was carefully constructed with 200mm x 3.5mm sticks. A seven layered crib was constructed, each layer consisting of seven sticks. The sticks orientation was altered by 90° for each layer. The crib was placed against the back and in the centre of the three-seater couch shown in Figure 3.11, and it was ignited with a gas torch.

The three-seater couch was considered to be the most likely item of furniture to ignite[103] in a residential living room following a typical scenario of a cigarette falling between the back and seat of the couch. The layout of the room and mass loss platforms restricted the possible location of the couch to in front of the window. As a result, the ignition source had to be located close to the burn room window. This arrangement gave rise to certain effects during the growth of the fire, including the presence of flames beyond the opening prior to flashover. In addition, the location of the ignition source is suspected to have contributed to the bowing of the glass in the centre pane of the window to varying degrees during certain tests, as discussed in *Section 5.8.4*. The position of the ignition source may also have accelerated the time to when Window Lowering Criterion # 1 was met.

3.2.6 External Instrumentation

Externally, thermocouple and heat flux (total and radiative) measurements were taken during the Real Furniture Burns. In Figure 3.17 and Figure 3.18, the 3D external thermocouple grid is shown on the external facade in front and side views. A schematic view of the 3D external thermocouple grid is given in Figure 3.19 to illustrate its dimensions. It was constructed of 6mm diameter stainless steel rods welded to form a seven-level structure. With respect to the building, this grid structure formed five planes *perpendicular* to the external facade and four faces *parallel* to it as explained next in Section 3.2.6.1. A total of 140 thermocouples was used in a volume of 2.4m (width) x 3.9m (height) x 1.5m (depth), covering on the external facade the width of the burn room window, and extending from just above the burn room window, W102, to the bottom of the second level window, W202. These external thermocouples were K-type MIMS, the same type as those used in the Polyurethane Burns. The centre plane of the 3D grid, Plane 3, corresponded to the 2D rack used in the first three PU tests.

3.2.6.1 The Co-Ordinate System for the 3D External Thermocouple Grid

The external thermocouple grid consisted of vertical PLANES, parallel FACES, and horizontal LEVELS with respect to the external wall as shown in Figure 3.19. The 3D thermocouple grid was made of 6mm steel rods. Each thermocouple wire was located approximately 5cm away from the corresponding node of the grid within each Plane, Face and Level, similar to the Polyurethane Burns.

- ◆ The far left and right planes correspond to Plane 1 and Plane 5, respectively. Each plane is 0.6m apart, which divides the area across the 2.4m wide window, evenly. Each Plane is 1.5m wide and 3.9m high. As indicated before, between Level 1 and Level 5, Plane 3 corresponds to the 2D thermocouple rack used during the first three polyurethane tests. This similarity can be observed by comparing Figure 3.8 for the location of the 2D rack with Figure 3.17 for the 3D grid.

- ◆ Level 1 begins 15cm above the top of the burn room window, W102, while the subsequent levels, from Levels 1 to 7 are spaced 0.59m, 0.62m, 0.82m, 0.75m, 0.56m and 0.56m apart. Each Level is 2.4m wide, matching the width of the window and it extends 1.5m away from the external wall.
- ◆ Four Faces run parallel to the external wall. They are spaced 0.5m apart and end with Face 4, 1.5m away from the external wall. Face 1 lies directly on the external wall and covers an area of 2.4m x 3.9m.

3.2.6.2 Heat Flux Transducers

A total of six heat flux transducers were mounted either in (hf3, hf4 and hf5) or on (hf1, hf2 and hf6) the external wall as illustrated in Figure 3.20, and most of these positions corresponded to the original transducer locations used in the Polyurethane Burns. These transducers were also the same type of transducers as the ones used in the PU Burns. As with the PU Burns, all measured total heat flux, except for one radiometer now located at Position 1 in Figure 3.20, at the centre of the Floor 1M window, rather than at the bottom. A sapphire window was placed on this transducer to eliminate convective heat transfer to the radiometer.

In Figure 3.20, heat flux transducers at Positions 1 and 2 (hf1 and hf2) at the approximate centre of the Floor 1M window, also correspond to Level 4, Plane 3 and Face 1 of the 3D external thermocouple grid. Along the bottom of the Floor 1M window, were three transducers as marked by Positions 3, 4 and 5, corresponding to the same locations as used in the PU Burns. Position 6, indicates the last transducer whose location corresponds to Level 1, Plane 3, Face 1 of the thermocouple grid.

The uncertainty for total heat flux transducers embedded in the wall is not expected to exceed $\pm 3\%$ as discussed in *Section 3.1.5.3* for the Polyurethane Burns. Similar to the Polyurethane Burns, Oleszkiewicz's[29] uncertainty analysis is applied to data from the Real Furniture Burns in *Section 5.7.2* to estimate the experimental error associated with the other total heat flux transducers.



Figure 3.17: Front view of the external grid and burn room window.

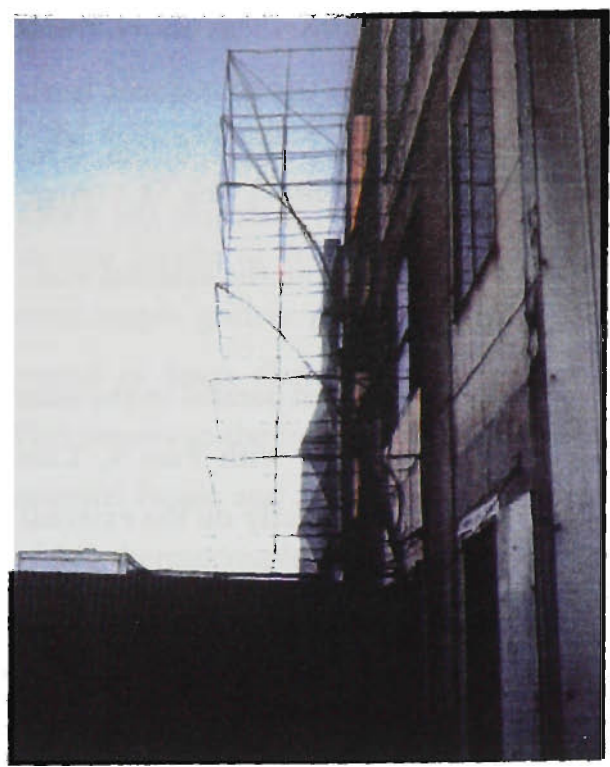


Figure 3.18: Side view of the external grid and building.

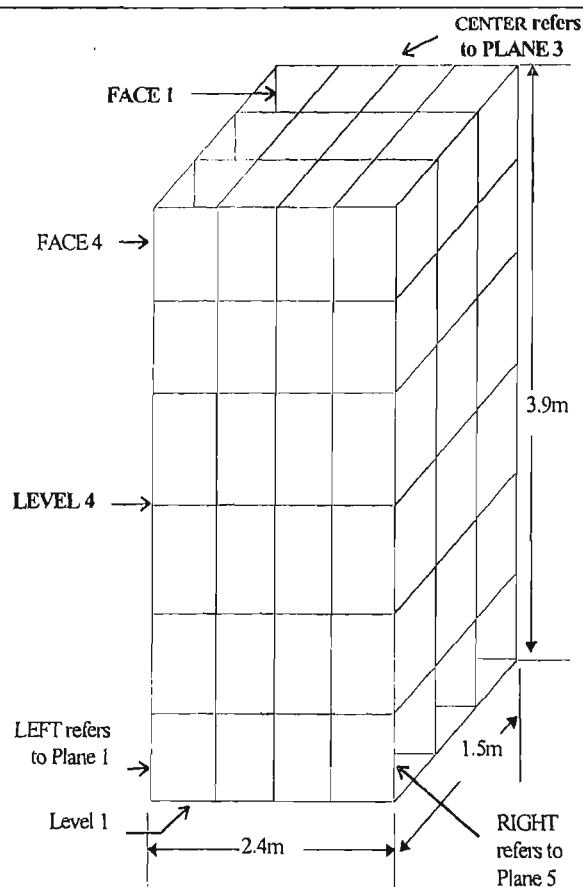
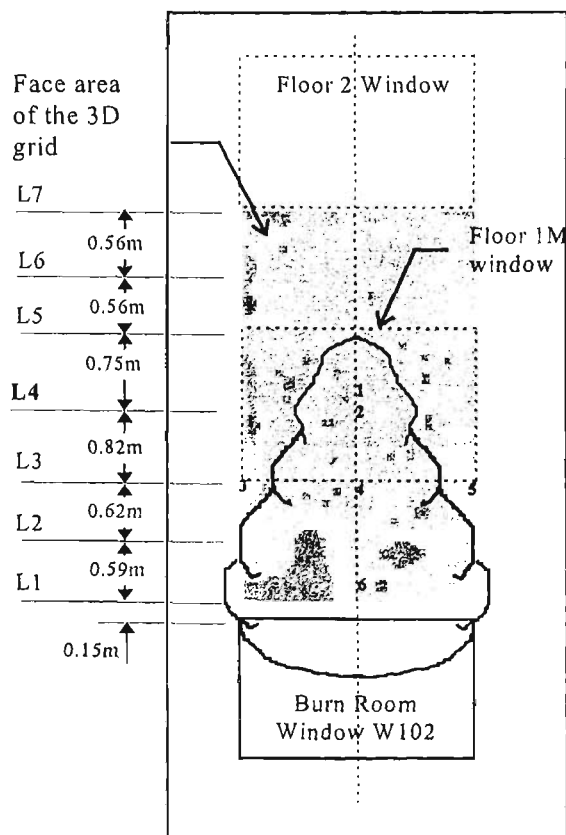


Figure 3.19: External 3D thermocouple grid. A thermocouple was attached 5cm away from each grid point.



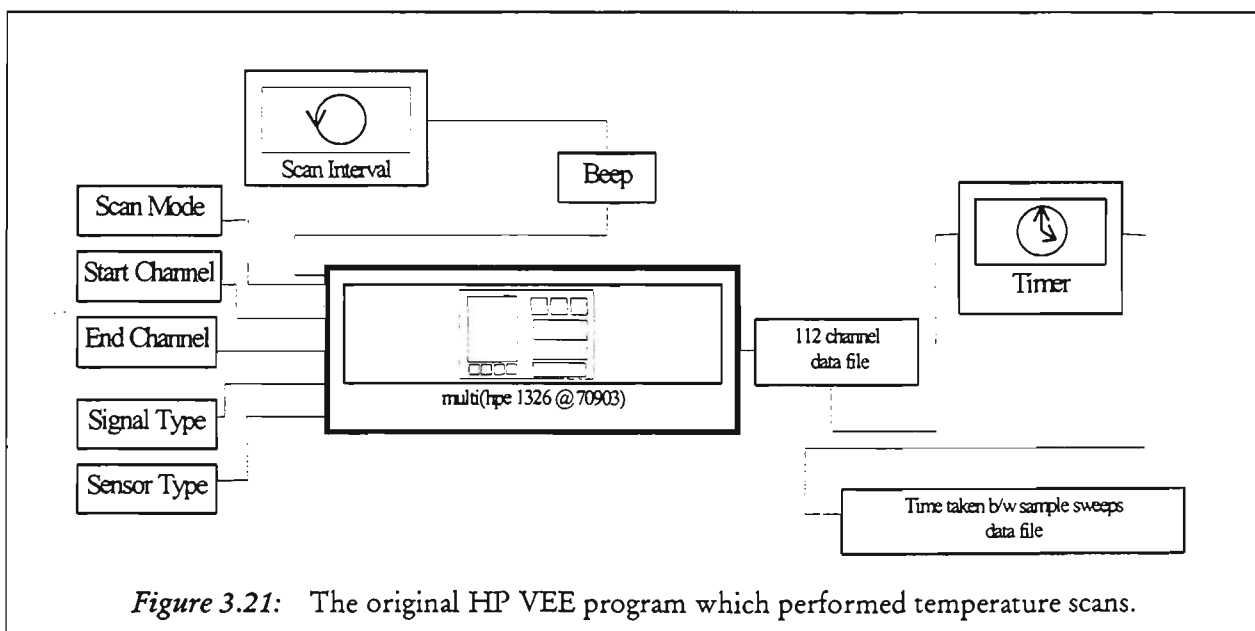
1-6: Heat Flux Transducer Locations

Figure 3.20: Locations of the external heat flux transducers.

3.2.7 External Data Acquisition and Analysis

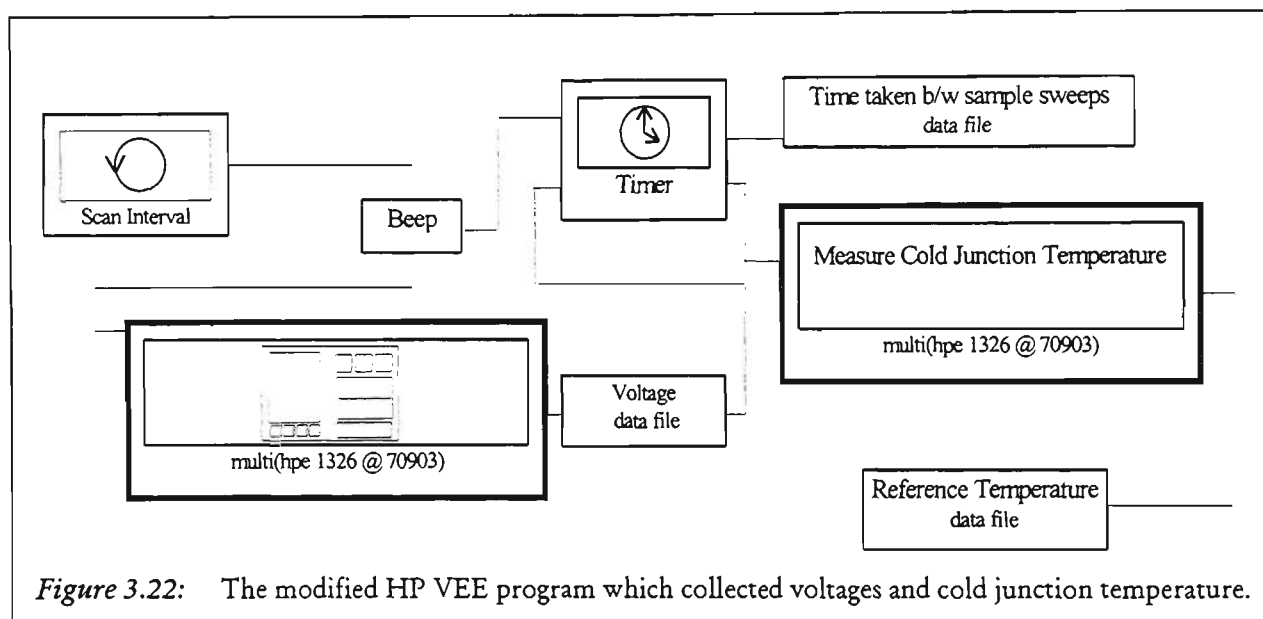
3.2.7.1 Data Logging System

Seven 16-Channel Relay Multiplexer modules (HP E1347A) were connected to a HP 75000 Series B Mainframe which has a in-built digital multi-meter (DMM), HP E1326B. These ran in conjunction with a HP VEE (Hewlett Packard Visual Engineering Environment) program to sample the data from up to 112 channels. Three data files were generated to store the data for post-processing. All internal and the remainder of the external data (28 temperature channels and all heat flux measurements) were collected by CESARE's *Process Program* written by E. Szmalko. The external data sampled this way included the first 28 locations on the external grid along with heat flux measurements. During Burn 4 and Burn 5, data were sampled from only Levels 1 through 5 of the 3D external thermocouple grid, and for all other tests, data were sampled from all seven Levels. All 112 channels were sampled every second, except during Burn 1 and Burn 5. During Burn 1, data were sampled once every six seconds per 112 channels, and during Burn 5, every half-a-second. These changes in the sampling speed did not affect the measured temperature patterns. The reason was the overall slow variation in temperature histories.



The original HP VEE program shown in Figure 3.21 was designed to sample all of the channels and convert the results directly into temperature. Input to the digital multi-meter (DMM) included *Scan Mode*, *Start and End Channel*, *Signal* and *Sensor Type*. In

accordance with the HP VEE program, Scan Mode was set at '2', to indicate a continuous scan of the channels. Start and End Channels corresponded to the 16-Channel Relay Multiplexer Modules, beginning with Board 1 Channel 0 (100) and ending with Board 7 Channel 15 (715). Each board had 16 channels. Signal Type was set to temperature measurement, while Sensor Type was equated to K-type thermocouples. When these were selected, the cold junction temperature compensation was applied automatically. The conversion process into temperature along with cold junction correction slowed down the sample speed to one sweep every six seconds. To increase the sample speed, the program interface was modified to Direct I/O as shown in Figure 3.22. As a result, the output signal was measured as a DC voltage. The sampling speed hence increased to at most 112 channels every half a second. The conversion equations from voltage to temperature, including cold junction correction are given in *Program 1* of Appendix D.



The DMM was set to scan through all of the multiplexer modules continuously, switching from channel 100 through to channel 715 again and again until the program was terminated manually. The measurements were stored in voltage instead of temperature. The cold junction (reference) temperature was monitored and stored in a separate data file to allow for compensation. Therefore, three data files were created: DC voltage for each channel, stored sequentially; reference temperature and time taken to complete each sweep, gauged by the triggering of the timer at each sweep. A beep provided an audible signal that the program was running.

3.2.7.2 Data Analysis Using MATLAB

For processing and conversion of voltage measurements, eight MATLAB programs were written. The program listings are given in Appendix D. The processing began with the conversion of the data from a sequentially sampled single column to a 112-column matrix, where each column represented the output of a single thermocouple. Once the voltage was in this format, it was converted to temperature using manufacturer specified equations. Following the conversion from voltage to temperature, cold junction correction was performed. This conversion resulted in a temperature (TEMP) and a time (TIME) matrix. These tasks were accomplished with *Program 1*. The TEMP matrix consisted of 112 columns, each corresponding to a location on the external grid. The program also combined the 28 locations sampled by CESARE's data acquisition program generating the corresponding pair of temperature (STEMP) and time (STIME) matrices. Both TIME and STIME were single column matrices.

Once the data were converted into matrix form, MATLAB programs allowed the analysis of the data to begin. *Program 2* to *Program 5* enabled any of the Planes, Levels or Faces to be viewed at any time, with or without averaging, as either a contour plot or a shaded plot, which could also be non-dimensionalised to take into account the average ambient and the maximum external temperatures. Instantaneous temperature versus time plots for either a single location or any row of thermocouples could also be plotted. The temperature results were also animated with *Program 6*, using existing MATLAB commands which allowed the growth and movement of the plume to be viewed in real time. In *Program 7*, temperature data obtained across each Face of the experimental grid was used to develop a series of 3D fourth order polynomial equations which described the variation in the CEF (consistent external flaming) averaged and non-dimensionalised temperature results in terms of the burn room window width and height. *Program 8*, allowed the transfer of the CESARE-CFD data (referred to in Chapter 6) to be analysed in MATLAB.

3.2.8 Combustible Lining in the Corridor

In Burn 8, a portion of the corridor wall in the first floor, Floor 1, from floor to ceiling, was covered with 4mm three-ply Lauan panel board, as shown in Figure 3.23. This lining was used to determine what additional effects the extra fuel in the corridor would have on the burn room fire and spread to the carpet in the corridor, as well as smoke spread and untenability within the building. Burn 8 is included here to report the effect on externally venting flames of combustible lining in the corridor.

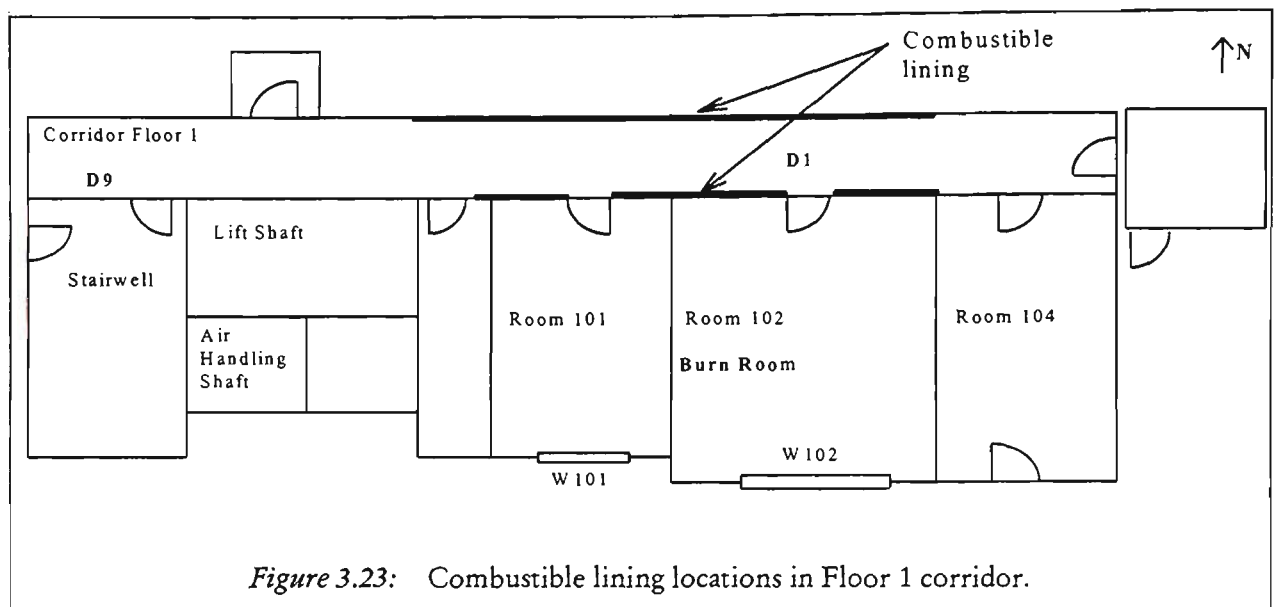


Figure 3.23: Combustible lining locations in Floor 1 corridor.

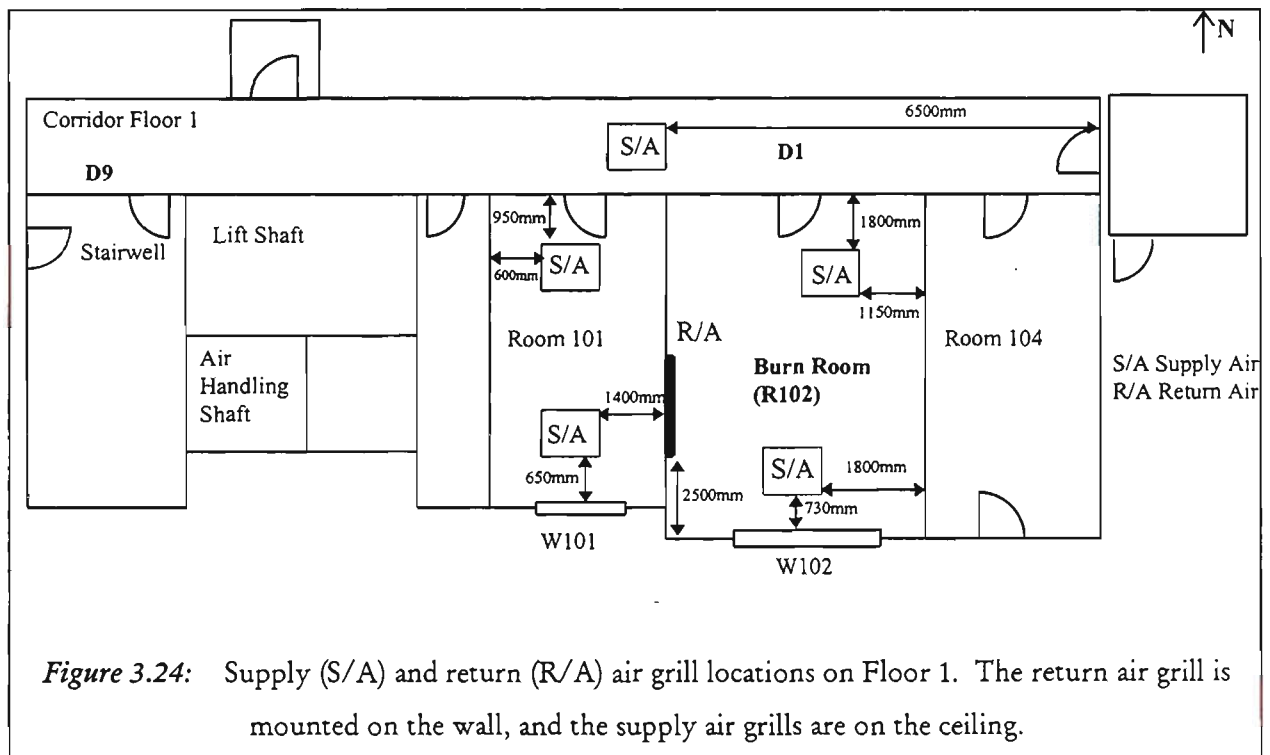
3.2.9 Air Handling and Smoke Management Systems

In normal operation mode, the air handling system recycled air, via the supply and return ducts within the building, with no fresh air intake. In smoke management mode, the air handling system took in 100% fresh air and supplied it to all levels of the building, except the level of fire origin, Floor 1. At Floor 1, the exhaust system was in operation in conjunction with a stairwell pressurisation system which used separate fans.

For Burn 6 and Burn 7 with the Air Handling system specified as “on”, the normal supply and return air were switched on prior to the commencement of the test. The smoke management system was initiated only when a high sensitivity photo-optical detector, located inside the return air duct, was activated. Upon activation, all supply

air (S/A) dampers were closed with the return air (R/A) dampers open for smoke extraction from the first floor. The supply and return air grills on Floor 1 are shown in Figure 3.24. Conversely, on the higher levels, the reverse was applied; all supply air dampers remained open, and all return air dampers were closed. After the activation, it took approximately 2 minutes for the dampers to fully open or close, and both the stair pressurisation and smoke extraction fans were switched on high. This resulted in supply air rates from 46 to 50 l/s. Return air rates were 494 l/s for D1 and D9 both open for Burn 6, and 1321 l/s for D1 closed and D9 open for Burn 7.

Supply and return air ducts were typically 210mm x 215mm in cross-section. As indicated in Figure 3.24, there was only a single return air duct, measuring 440mm x 330mm, located on the left North-South wall running between R101 and the burn room, R102, 240mm from the ceiling in the centre of the wall.



4. POLYURETHANE BURNS - DISCUSSION OF RESULTS

4.1 INTRODUCTION

After a review of the existing literature, it became clear that the centre plane of the venting plume had to be investigated first. The centre plane corresponded to a cross-section of the plume, directly above the centre of the burn room window, and perpendicular to the external wall. As indicated in *Section 3.1.5.1*, the 2D external thermocouple rack was designed to provide temperature and heat flux measurements on this plane during the first three polyurethane tests, PU1 to PU3. The temperature measurements at one cross-section of the plume were expanded using a 3D external thermocouple grid to obtain a more detailed picture of the venting plume during PU4. Hence, as explained briefly in the *Introduction* and again in detail in *Section 3.1*, the set-up for PU1 to PU3 differed from that of the last PU test, PU4. Another significant difference was the size of the burn room. PU1 to PU3 were carried out in a standard burn room, while the size of the burn room for PU4 was more than double the standard size. The reason was to represent a more realistic living environment. The total fuel load was comparable for each test. In this chapter, the first three PU tests are discussed with respect to one another, followed by the corresponding PU4 results.

As indicated in Chapter 1, *Introduction*, PU1 to PU4 represent the learning experience of the author. The following series of tests, the Real Furniture Burns: Burn 1 to Burn 8, was designed with the knowledge gained from PU1 to PU4. In fact, PU1 to PU4 data were re-examined after the analysis of Burn 1 to Burn 8 data presented in Chapter 5. Two important points that were added to the original Chapter 4 analysis of PU1 to PU4 were the ventilation class distinctions and the use of the Consistent External Flaming (CEF) period in averaging the experimental data.

Unlike Burn 1 to Burn 8, the author was not involved in planning PU1 to PU4. The purpose of PU1 to PU4 was to obtain internal experimental data for model validation[104]. The author was given the opportunity to add the external components, that is, the external temperature, heat flux, velocity and gas measurements, to an already designed set of tests. As a result, some of the findings

presented in Chapter 4 are not as conclusive as those in Chapter 5. There are two major reasons for this outcome. The first reason is that more than one variable was allowed to change during these four PU tests, making each test distinct. As such, this series had no measure of repeatability (Given that these tests were not repeated, no attempt was made to curve-fit PU data). The second reason is that only a 2D external thermocouple rack was used to map the temperature field within the plume, which was insufficient to provide detailed analysis of the venting plume. The other reasons which also became clear after completing PU1 to PU4 are listed in Section 4.7, Conclusions of Chapter 4.

During PU1 to PU4, both the burn room and the external facade were instrumented to measure temperature, heat flux, velocity and species concentrations. The following discussion focuses on the external results, only. The corresponding internal measurements are given by Beck *et al.*[97]. In the following, *Section 4.2* begins with an analysis of the temperatures measured across the 2D rack, detailed in Figure 3.7, during PU1 to PU3. Subsequently, temperature results obtained with the 3D external grid are presented for PU4. This section is concluded by a comparison of the measured temperatures with empirical approximations. Heat flux measurements at the Floor 1M window (W1M02), which is above the burn room window (W102), are discussed in *Section 4.3*. This discussion is with respect to the vertical variation along the centre and the horizontal variation along the bottom of the Floor 1M window. A radiometer was placed at the bottom centre of this window for PU4, and the radiation results are discussed in terms of Secondary Fires. *Section 4.4*, *Section 4.5* and *Section 4.6* contain window breakage, exhaust flow velocities and gas analysis, respectively. The conclusions reached as a result of PU1 to PU4 are presented in *Section 4.7*.

For easy reference to internal instrumentation and burn room configuration, external instrumentation consisting of the 2D thermocouple rack and heat flux transducer locations, fuel load, environmental conditions and ventilation conditions of the polyurethane tests, a foldout is given (Foldout 1) after the Appendices. Foldout 1 contains Figure 3.1, Figure 3.7, Figure 3.9, Table 3.1, Table 3.2 and Table 3.3. Wherever these figures and tables are referred to in Chapter 4, they are accompanied by an asterisk.

4.2 EXTERNAL TEMPERATURE RESULTS

4.2.1 Temperatures above the Centre of the Burn Room Window

The vertical temperature variations at five locations ($y = 0\text{m}$, 0.59m , 1.21m , 2.03m and 2.78m) along the external wall ($x = z = 0\text{m}$), are shown in Figure 4.1 to Figure 4.3 for PU1 to PU3, respectively. With respect to the 2D external thermocouple rack shown in Figure 3.7*, these measurements were obtained above the centre of the burn room window to the bottom of the window on the floor above. In Figure 4.1 to Figure 4.3, the horizontal time scale ranges from the third minute, just before the window begins to crack, to the thirteenth minute.

In general, all three figures show an increase in temperature just after the window began to crack, approximately 3 minutes after ignition. Over the next minute, the cracks in the glass became more pronounced, until sections of glass were dislodged from the window frame, providing access to a reservoir of fresh air. Regarding the impact of the venting plume on the wall, the highest temperatures occurred at the origin, the top centre of the burn room window. The temperature dropped off with increased vertical distance along the wall. Flashover occurred approximately four minutes after ignition, and this also corresponded to most of the remaining glass falling away. As a result, there was an overall increase in temperature at all measurement points, as the region directly beyond the window opening was covered with flames, smoke and exhaust gases. After flashover and during the fully developed phase, the remaining glass was dislodged from the window frame, with the bulk of the flames and smoke venting outside, causing the external temperatures to increase. Gradually, temperatures dropped off as the remainder of the fuel was consumed.

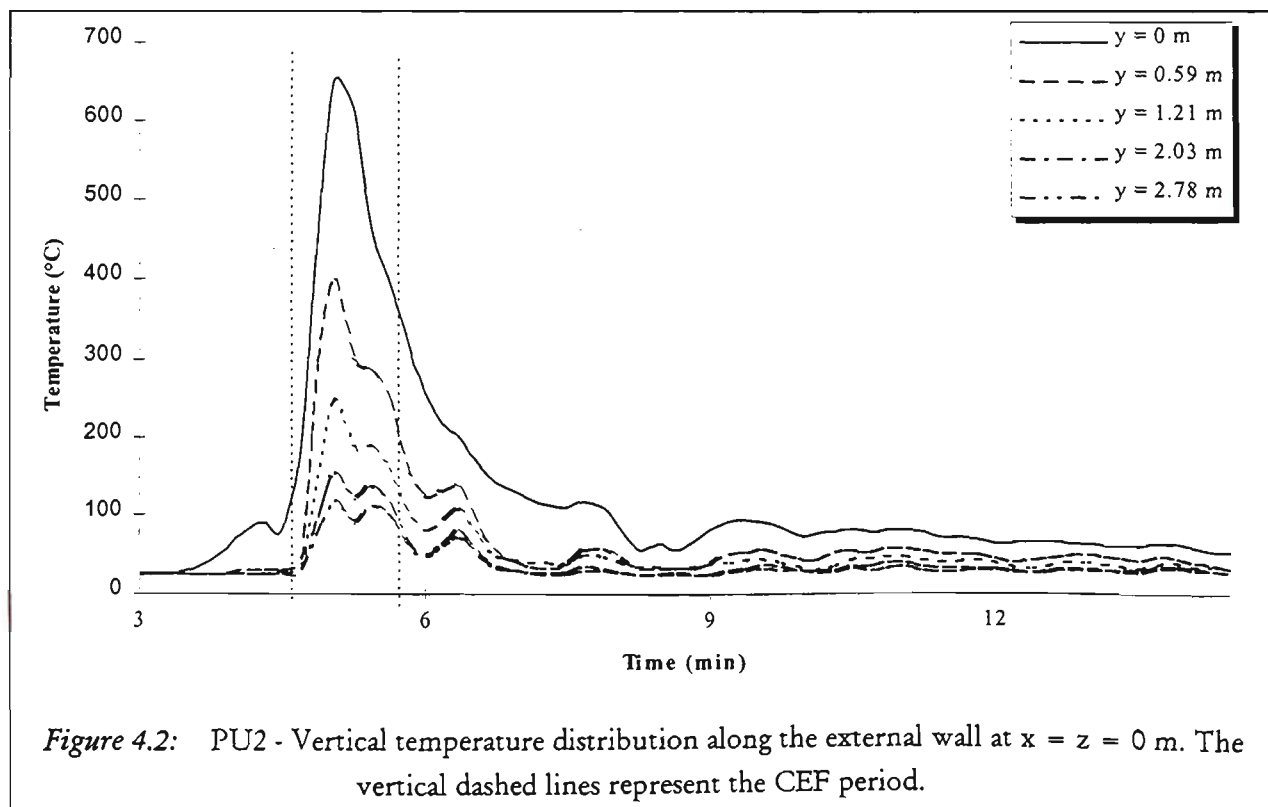
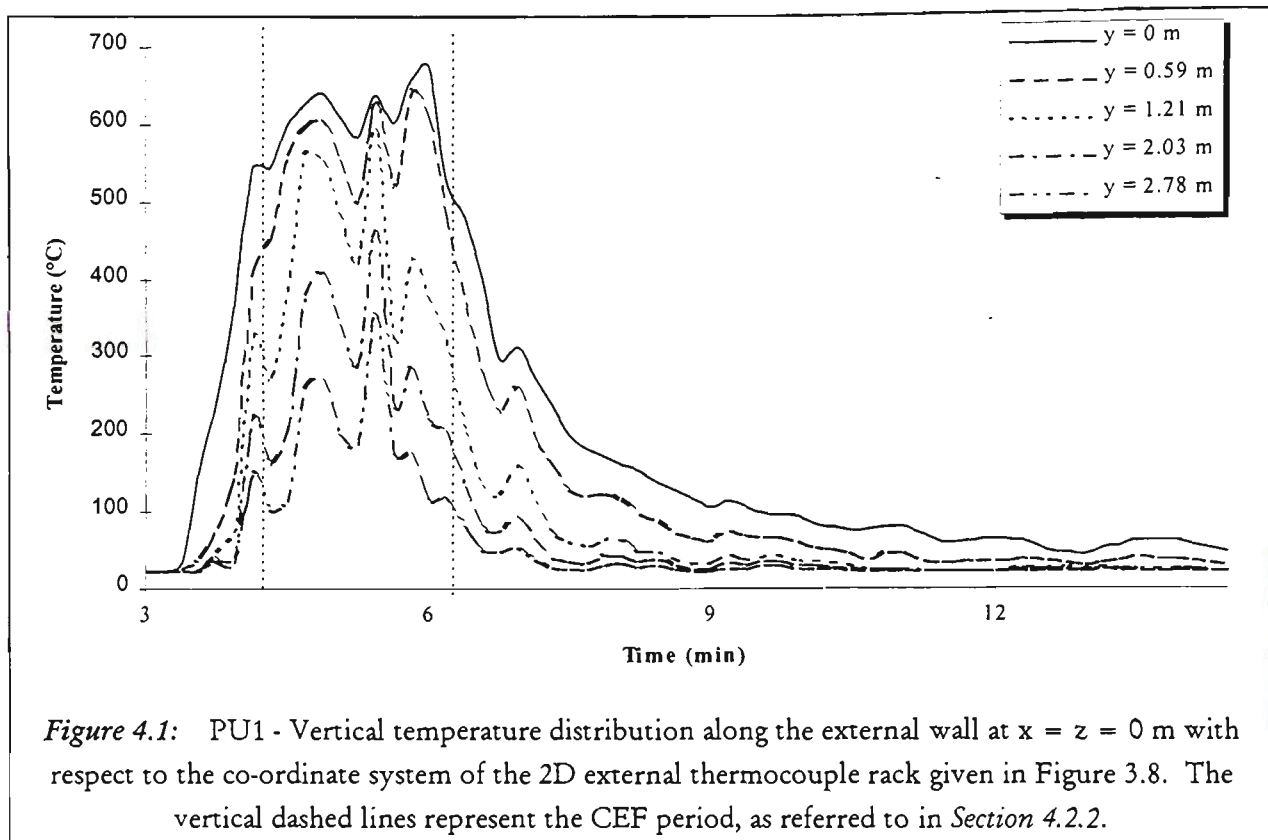
The internal ventilation conditions have a significant effect on the progress of the fire and the severity of the external flames with respect to measured temperatures on the external wall. As listed in Table 3.3*, during PU1 to PU3, the burn room door (D2) was always open, and the window (W102) was allowed to fail on its own. As shown in Figure 3.1*, D2 connected the burn room (R102) to an adjacent room (R101). Only during PU1, the door to the corridor, D1, of room R101, was kept closed. D1 was open during PU2 and PU3. It can be seen in Figure 4.1 that the external temperatures

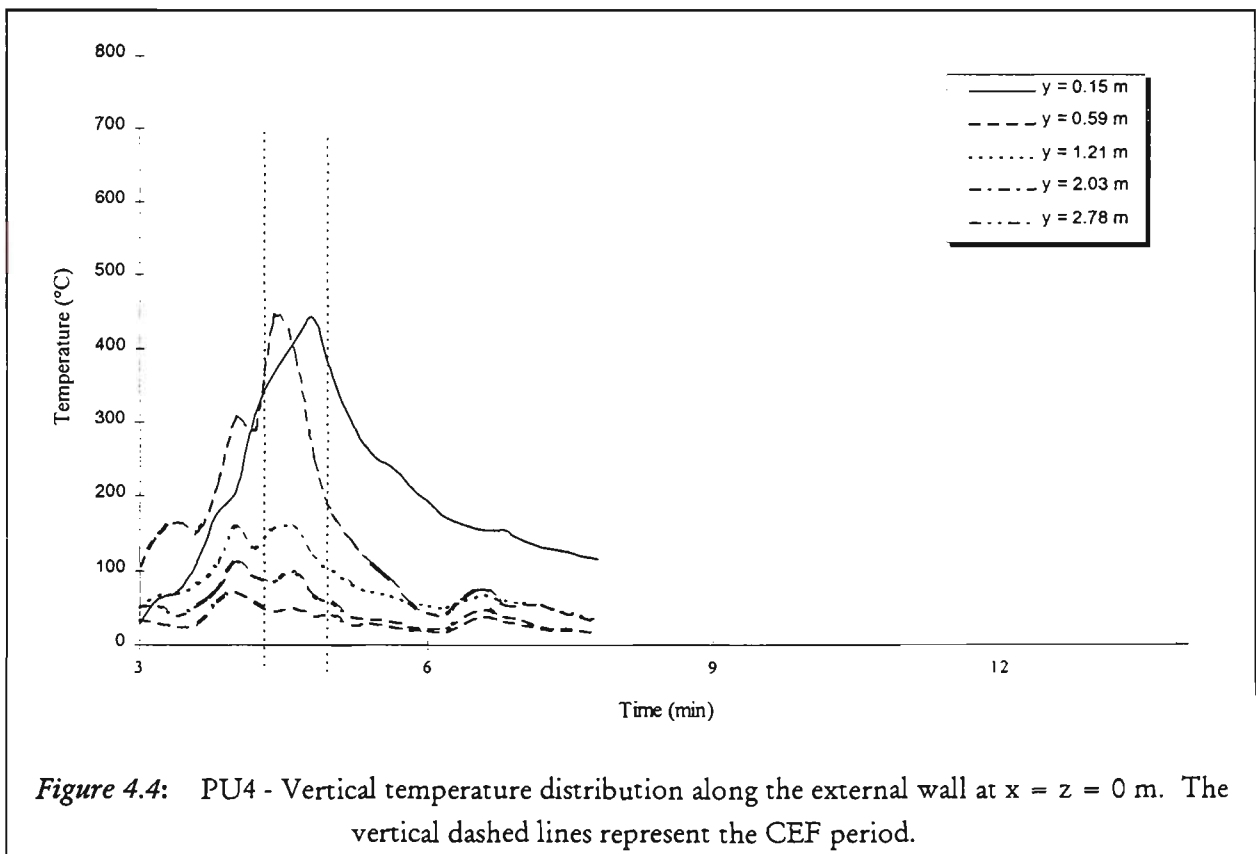
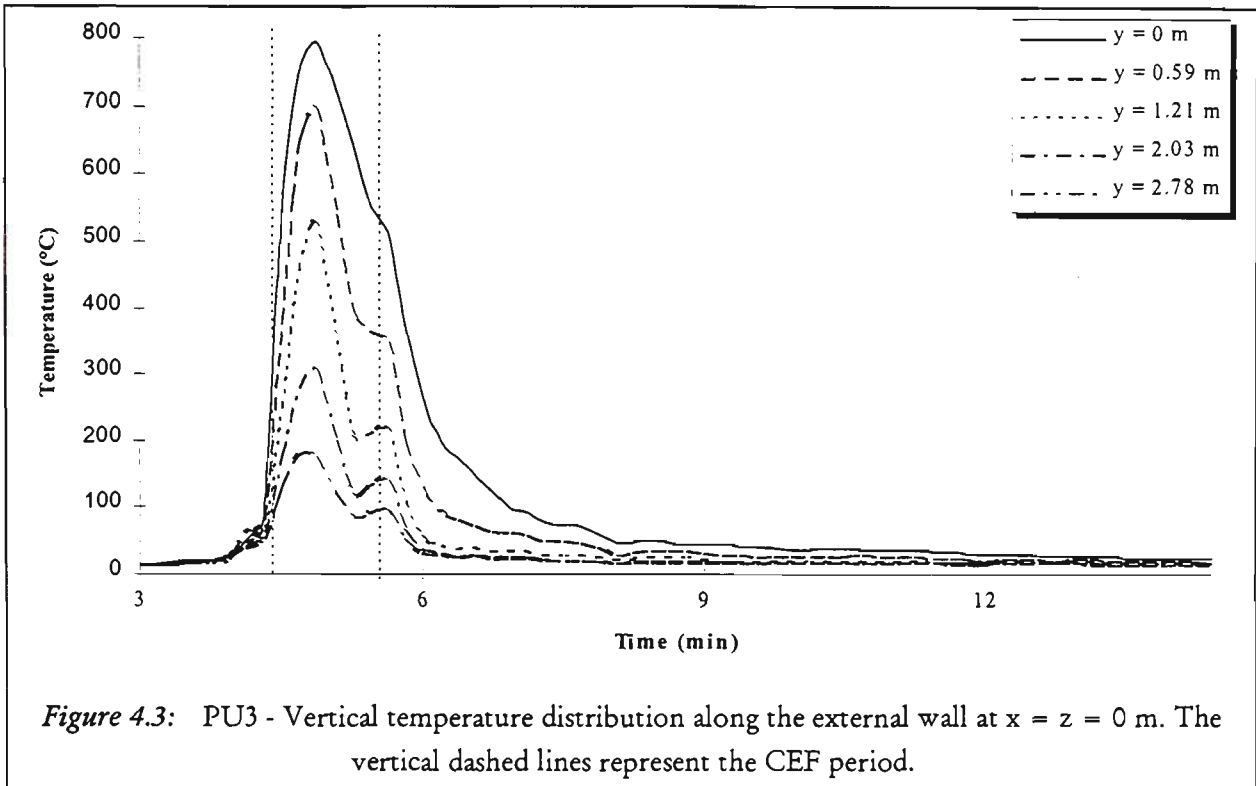
in PU1 have a broader peak than those of PU2 and PU3, given in Figure 4.2 and Figure 4.3, respectively. This broader peak, during PU1, has been attributed to having the door to the corridor, D1, closed, leaving the window (W102) as the only available vent, once it began to crack/dislodge. The cracked window allowed the accumulated combustion products (flames, smoke/hot gases) to vent from the burn room for the duration of the test. Unlike PU1, the temperature histories of PU2 and PU3, given in Figure 4.2 and Figure 4.3, respectively, show a narrower peak soon after the window failed. This is because the open door, D1, in these two tests allowed the combustion products to vent into the corridor as well as out of the window, thus reducing the size (height and depth) and duration of the externally venting flames. The maximum temperatures were comparable, 600°C to 800°C during these three PU tests due to the similarity in fuel loads. Although PU1 had a slightly higher fuel load, as listed in Table 3.1*, this difference is marginal, and the increased duration of the fully developed phase in PU1 must be mainly due to the ventilation conditions. From a comparison of Figure 4.2 and Figure 4.3, no conclusion can be drawn as to the effect of D5 and D9 on the venting plume during PU2 and PU3. D5 and D9 are the doors at the end of the corridor and to the stairwell, respectively, as shown in Figure 3.1*. D5 and D9 were closed and open, respectively, during PU2 and open and closed, respectively, during PU3 as shown in Table 3.3*.

During PU4, the burn room, R102, was larger than the one used during PU1 to PU3, as shown in Figure 3.14. The burn room door, D1, was kept open during PU4, and the window, W102, was lowered according to the Window Lowering Criterion #1 (WLC #1, as explained earlier in *Section 3.2.2*). As indicated in Table 3.3*, the ventilation conditions during PU4 were similar but not identical to those of PU2 and PU3. The reason for the similarity was that D1 connected both sized burn rooms to the corridor: during PU4 directly, and during PU2 and PU3 via R101. This similarity can also be observed from the temperature histories of PU2 to PU4, given in Figure 4.2 to Figure 4.4, respectively, that all display narrower peaks than that of Figure 4.1.

The external temperatures measured during PU4, were lower than those measured during PU1 to PU3. The lower external temperatures can be attributed to having almost the same fuel load as in PU1 to PU3, but in a larger burn room. The larger burn room for PU4 resulted in more of the combustion taking place within the burn

room as compared to PU1 to PU3, and consequently lower external temperatures were measured along with slightly lower flame height. This point is re-visited in *Section 4.2.4*. In addition to the larger burn room in PU4, the direct link to the corridor, through D1, helped with increased combustion within the burn room, although the ventilation conditions were similar to those of PU2 and PU3.





4.2.2 Temperature Contour Maps of the 2D Rack and 3D Grid

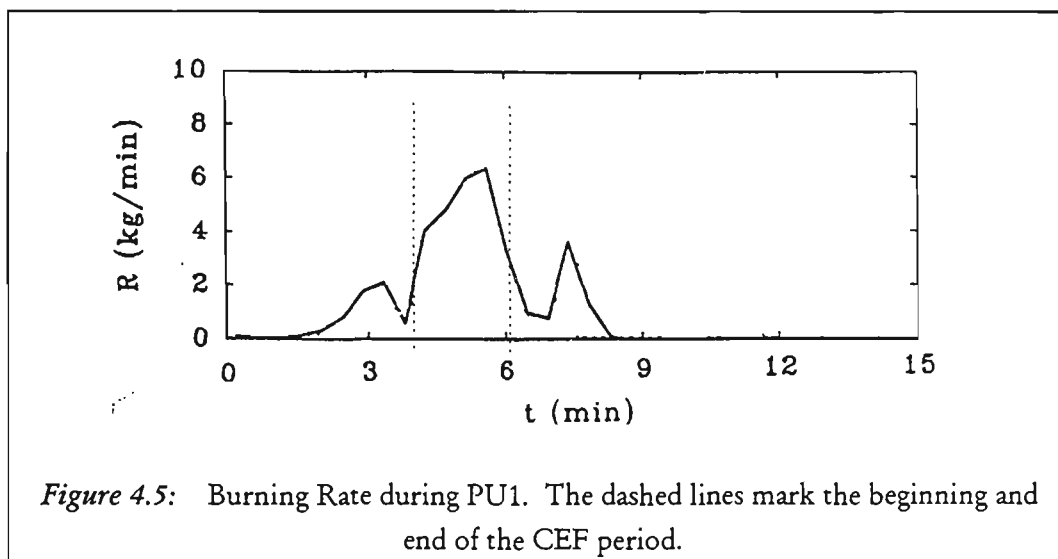
The 2D thermocouple rack, perpendicular to the external wall provided a cross-section of the venting plume for PU1 to PU3. The rack began at the top of the burn room window, W102, and extended to the top of the Floor 1M window, W1M02, as indicated in Figure 3.9*. The rack extended 1.5m away from the external wall as shown in Figure 3.7*. To present fully the results of this cross-section of the plume, temperature contour plots were generated. There are three important points regarding the data analysis leading to these contour plots. The first point is that the results were time averaged over the Consistent External Flaming (CEF) period. This averaging method is described in detail in *Section 1.2*, and it was developed during the second series of tests, the Real Furniture Burns*. The need to develop an averaging method stemmed from the larger amount of data collected during the Real Furniture Burns. As a result, the temperature results from the 2D rack were re-analysed after the Real Furniture Burns for consistency. The second point is that these contours were non-dimensionalised to take into account differences in the ambient, T_{amb} , and maximum, T_{max} , temperatures recorded for each of the tests by using $(T - T_{amb}) / (T_{max} - T_{amb})$. As illustrated in Chapter 5, with comparison of repeat tests, this non-dimensionalisation removed from the data slight variations due to ambient and maximum external temperature changes. Thirdly, because of the staggered thermocouple configuration on the 2D rack, as shown in Figure 3.7*, a cubic-spline interpolation was used with the existing data[105]. This interpolation filled in data between existing data points based on the spatial resolution of the 2D rack.

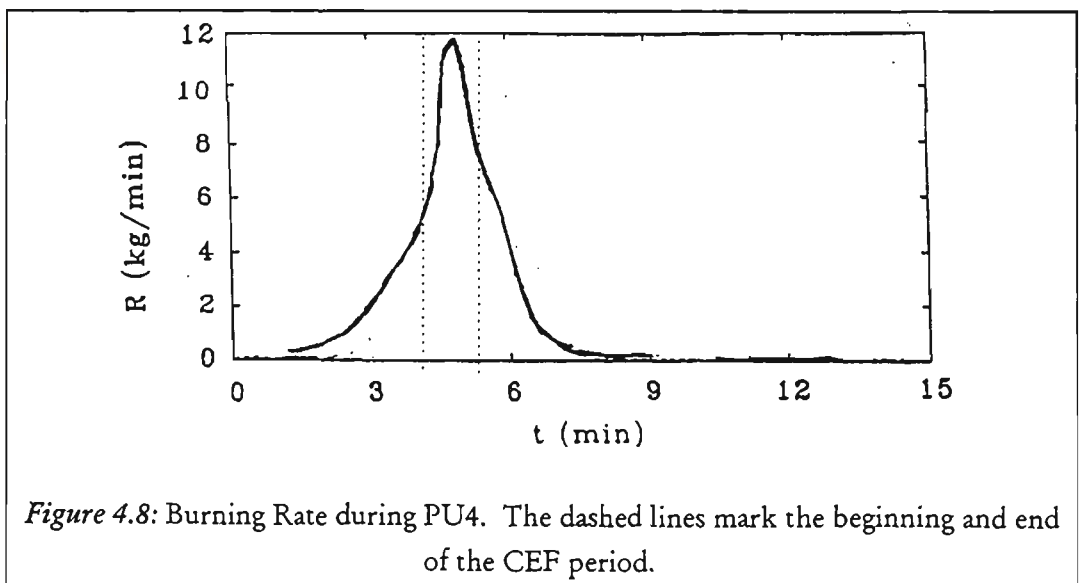
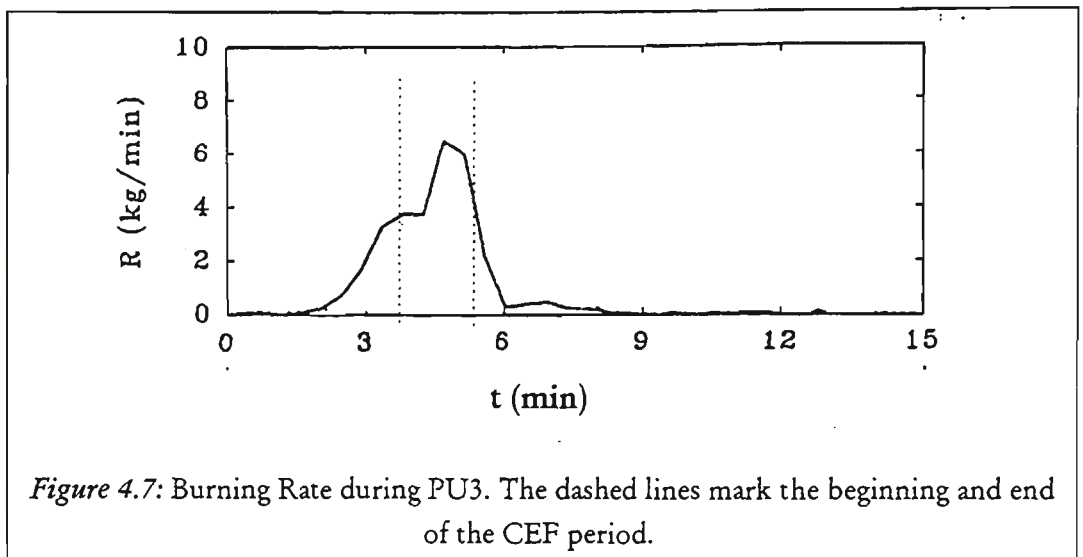
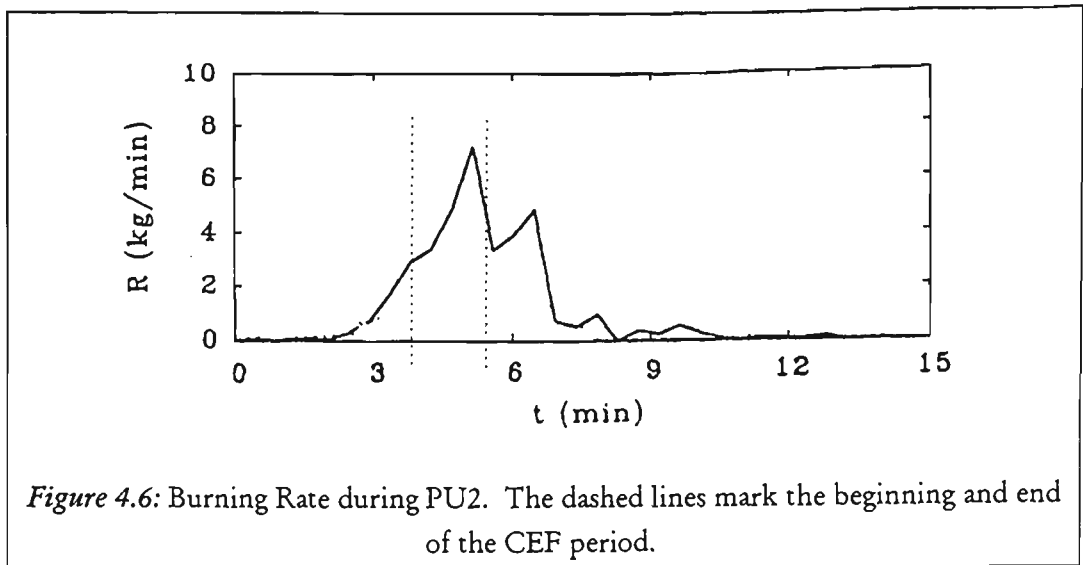
The CEF period corresponds to approximately 2 minutes, 1.5 minutes, 1.5 minutes and 1 minute for PU1, PU2, PU3 and PU4, respectively. The beginning and end of the CEF period is marked with vertical dashed lines in Figure 4.1 to Figure 4.4. The CEF period was much shorter for the Polyurethane Burns than for the Real Furniture Burns due to the higher fuel load during the latter series. The CEF period was determined by combining burning rate information[97], given here in Figure 4.5 to Figure 4.8, internal and external temperature measurements and observations made during each of the tests. In each case, the beginning of the CEF period corresponded to an increase in the burning rate, accompanied by internal temperatures of 600°C or

* As a result, the CEF concept is revisited in *Section 5.3*.

above, and externally, temperatures in excess of 540°C just above the window opening indicating visible flames, and the presence of consistent flames. CEF ended when all these parameters began to decline.

From Figure 4.5 to Figure 4.8, CEF averaged burning rates of 5, 5.5, 5 and 6 kg/min can be determined. The patterns in Figure 4.5 to Figure 4.8 reflect the internal ventilation conditions. In Figure 4.5, as the fuel began to burn, the first peak was registered. However, with the closed door to the corridor, D1, the supply of air was restricted until the window began to dislodge partially, after the third minute. As more of the glass was dislodged from the burn room window, more fresh air became available, contributing to the continued burning of the fuel and the presence of the central peak. The maximum burning rate occurred during this stage. With the open burn room door for PU2 and PU3, the supply of air into the burn room was not as restricted as in PU1. As a result, in Figure 4.6 and Figure 4.7, the burning rates increase to the maximum without a decrease, similar to the first dip shown in Figure 4.5. For PU4, the larger burn room, open burn room door and lowering of the burn room window allowed almost unrestricted burning. Consequently, this test had the highest peak burning rate.





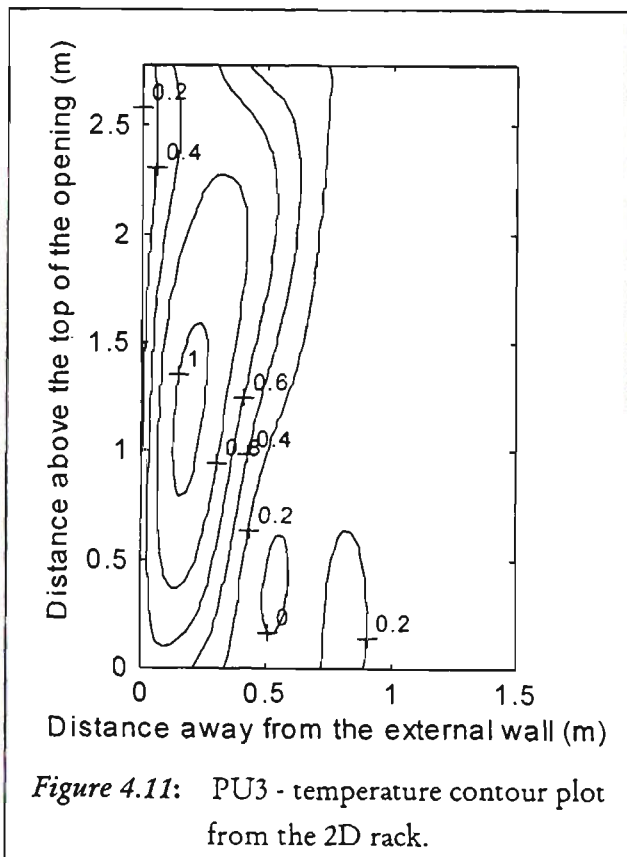
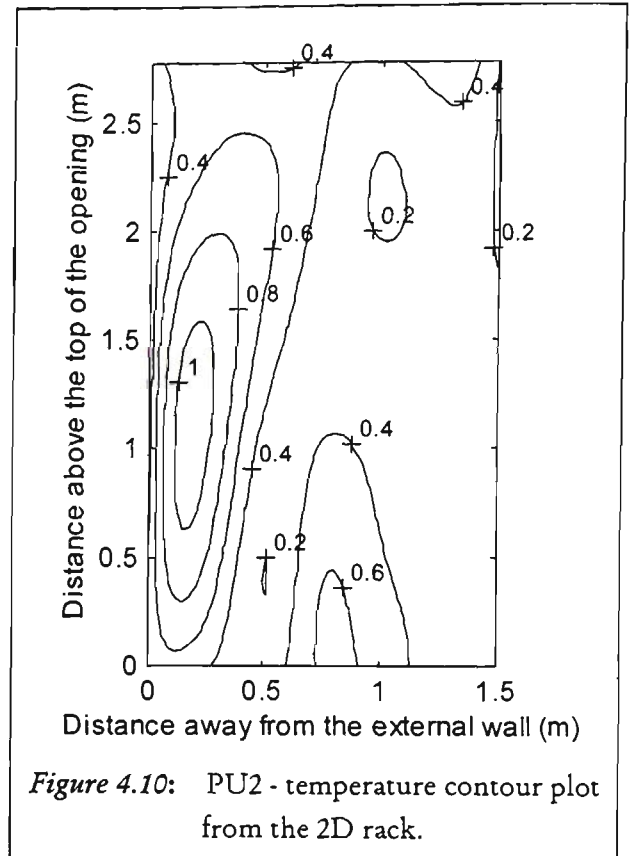
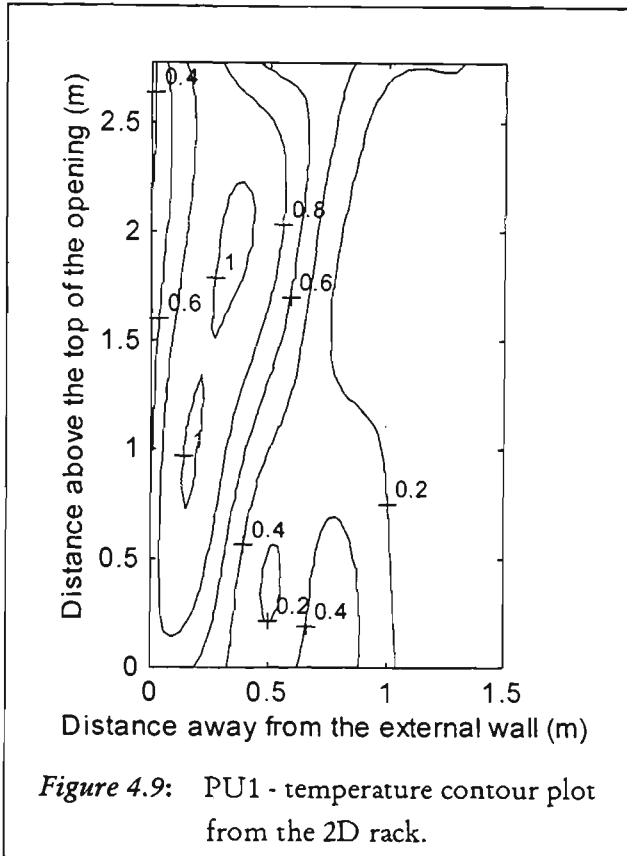
For PU4, the 3D thermocouple grid shown in Figure 3.19 was used. As indicated in the *Introduction*, the need for a 3D grid became obvious after a close first examination of the external temperature results of PU1 to PU3. The new 3D grid provided a more

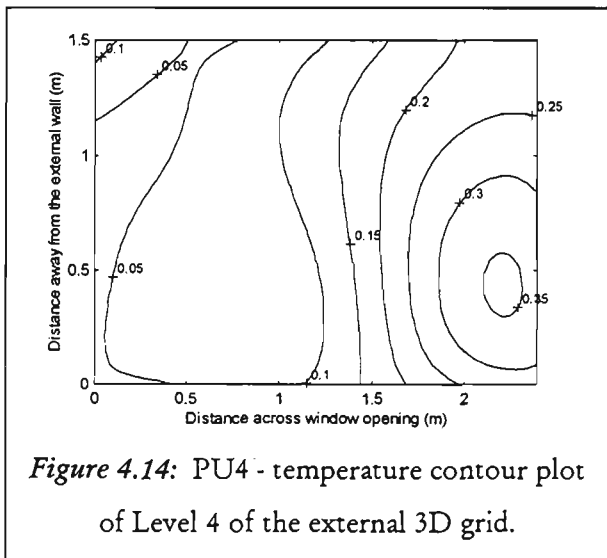
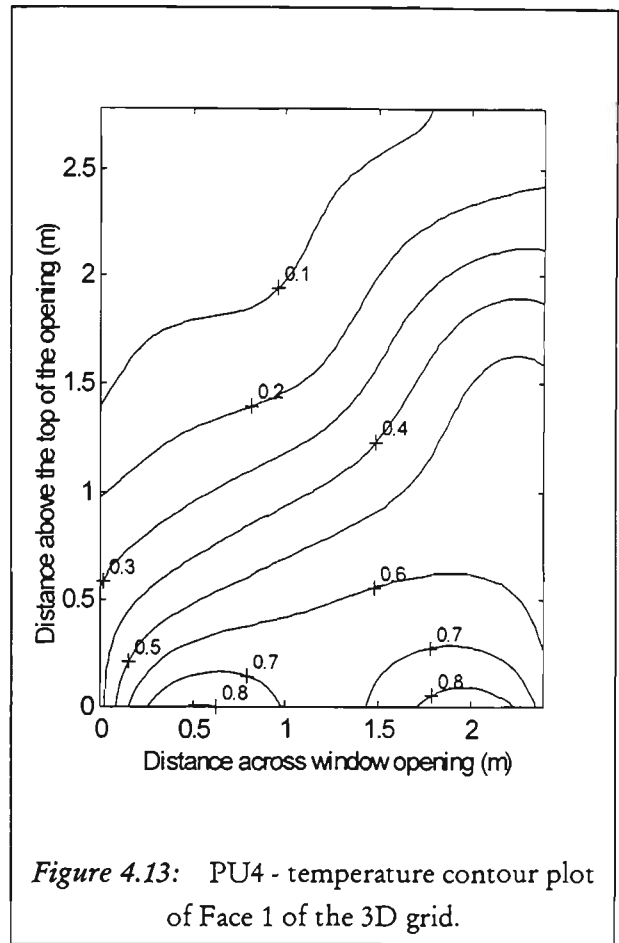
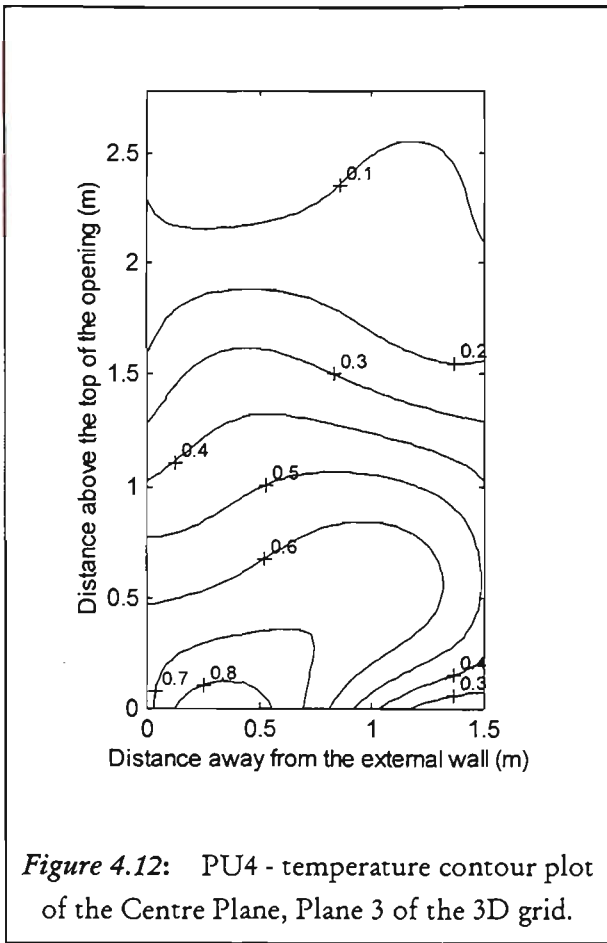
detailed picture of the venting plume. The sections included for discussion here are the centre plane of this grid, P3, which corresponds to the 2D rack used in PU1 to PU3, Face 1 of the grid, F1, which lies just on the external wall, and Level 4, L4, which corresponds to the middle of the Floor 1M window. P3, F1 and L4 are marked in Figure 3.19. Face 1 provides an overall impression of the impact of the venting plume on the external wall, while Level 4 allows the effects of the venting plume on the window above the burn room window to be gauged. The contour plots generated for PU4 were also averaged over the CEF period and non-dimensionalised with respect to the ambient and maximum temperatures measured during the test.

The CEF averaged and non-dimensionalised temperature contour plots for PU1 to PU3 are shown in Figure 4.9 to Figure 4.11, respectively. Table 3.2 contains the ambient temperature values used in non-dimensionalising the temperature as $(T-T_{amb})/(T_{max}-T_{amb})$. The corresponding maximum external temperatures for PU1, PU2 and PU3 were, 697°C, 776°C and 795°C, respectively. Figure 4.9 to Figure 4.11 show the path of the flames out of the opening, which travel up beside the external wall. Visible flaming corresponds to 1.0 and 0.8 contours in these figures. These contours indicate temperatures above 540°C, and hence, they denote the paths of visible flaming. These figures indicate that for PU1 to PU3, the flames reached at least the centre of the window above the burn room window, corresponding to approximately 2m, with a depth of approximately 0.5m. Using Figure 3.7 which details the dimensions of the 2D thermocouple rack, these flame dimensions correspond to between Level 4 (2.03m) and Level 5 (2.78m), and Face 2 (0.5m). Figure 4.12 corresponds to the centre plane, P3, of the 3D grid for PU4 during the CEF period. A more complete thermocouple grid provided a better picture of the entire venting plume. The ambient temperature during PU4 is also given in Table 3.2. The corresponding maximum external temperature was 804°C.

For PU4, the CEF averaged and non-dimensionalised temperature contour plot of Face 1, which covers a 2.4m x 2.78m region above the burn room window, is shown in Figure 4.13. This figure indicates that the venting plume was slightly cooler along the centre of Face 1 compared to its sides. Visually, flames were observed to vent from either side of the opening, confirming the temperature contour pattern of Figure 4.13. Flames had greater vertical reach on the right side of the opening compared to the left.

This difference between the right and the left hand sides of the plume is also apparent in Figure 4.13. As expected, the temperatures gradually decrease with increased vertical distance above the opening.

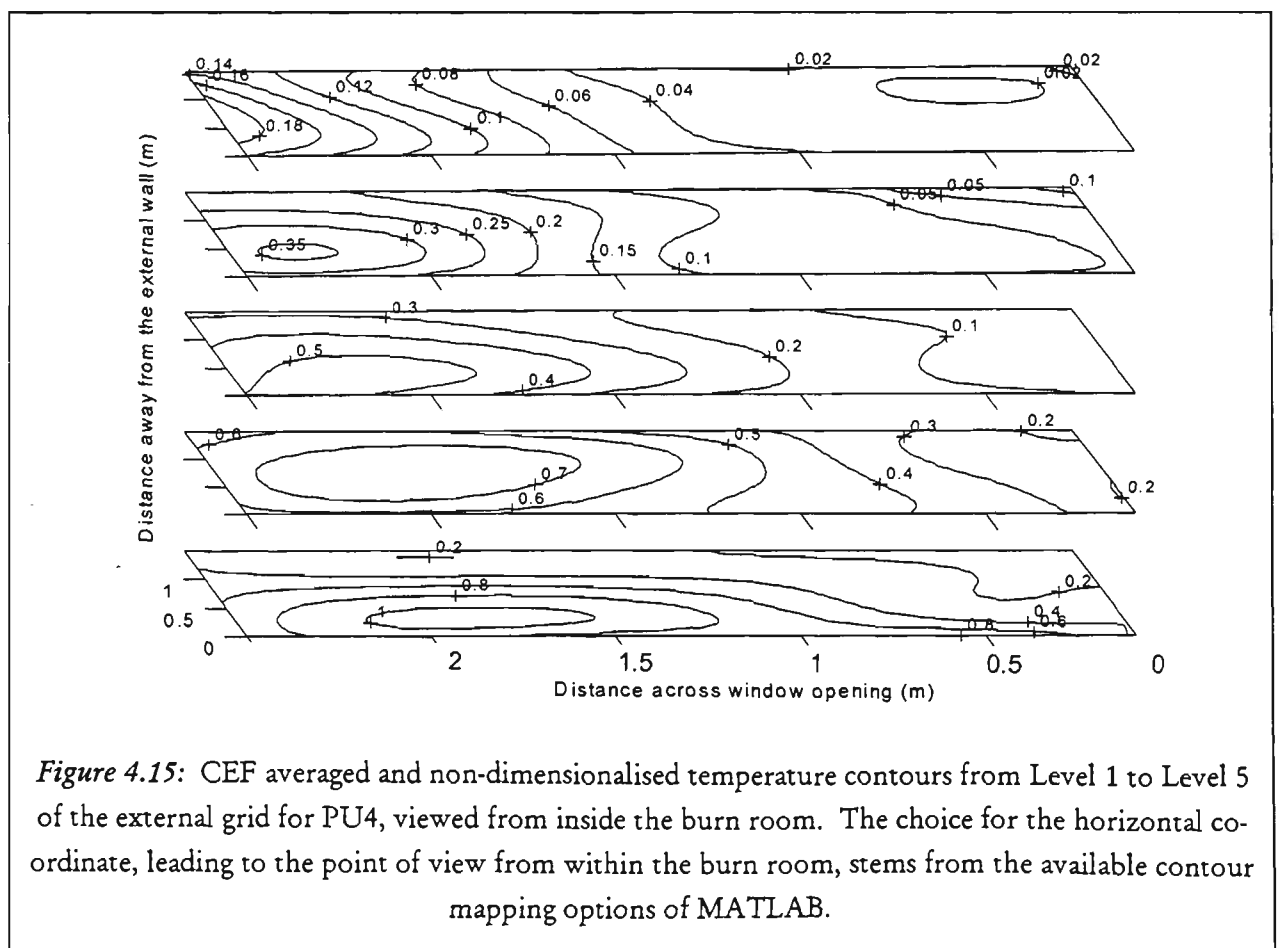




Level 4 covers a horizontal region of space across the centre of W1M02 and extends 1.5m away from the wall. The temperature contour plot of Level 4 is shown in Figure 4.14, for PU4. The lower edge of this figure corresponds to the centre of the Floor 1M window. Figure 4.14 shows a slight variation in temperature across the length of the glass, from 5 to 35% of the maximum measured temperature. In this case, such a small variation was not sufficient to cause the glass to crack in W1M02. With the plume venting more predominantly from the right of the opening compared to the left, a

slightly hotter region, marked by the 0.35 contour, was formed on the right side of Level 4.

The temperature contours over the 3D thermocouple grid are given in Figure 4.15 to show the entire plume as it vents from the opening. The maximum temperature contour of 1.0 exists on Level 1, centred around Plane 4 (1.8m). Level 1, Plane 3 and Plane 4 are shown in Figure 3.19 of the Experimental Setup. The fact that this contour is missing in the Plane 3, Face 1 and Level 4 contours given in Figure 4.12, Figure 4.13 and Figure 4.14, respectively, is an indication of the need for the 3D external thermocouple grid. Figure 4.15 also indicates that the *average* flame height for PU4 was above Level 2, 0.59m above the top of the burn room window. This height is determined assuming a visible flame tip temperature of 540°C . As such, the 0.7 contour corresponds to 564°C with a maximum temperature of 804°C . Based on visual observations, the *maximum* flame height was determined to be between Level 3 and Level 4 (2.03m), as discussed in Section 4.2.4.

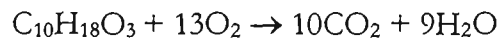


4.2.3 Excess Fuel Factor

The concept of excess fuel factor was developed by Bullen and Thomas[56] as a measure of the amount of unburnt fuel that exits the burn room through an opening during a fire. The amount of excess fuel is linked to the amount of air that can flow into the burn room via the opening. As such, the larger the opening, the greater the inflow of air, and the more fuel can be burnt within the compartment.

From Equation 2.22 and Equation 2.23, it can be seen that the excess fuel factor is dependent on the flow of air into the room, the burning rate and the stoichiometric ratio. To determine the flow into the room, both the window width and height must be known. An average burning rate of 0.090 kg/s is calculated using the values presented in *Section 4.2.2*, for the PU tests. Using a window area and height of 3.6m² and 1.5m, respectively, in Equation 2.23 [$m_{\text{air}} = 0.5A_w\sqrt{h}$], the mass flow rate of air can be calculated to be 2.2 kg/s.

The stoichiometric ratio of polyurethane (C₁₀H₁₈O₃[106]) is calculated as follows.



Using molecular masses[107] of 1.008, 12.001 and 15.999 kg/kmol for Hydrogen, Carbon and Oxygen (O₂), respectively, the following values can be calculated for the fuel and air (approximately 21% oxygen) masses required for complete combustion.

$$m_{\text{fuel}}: 10 \text{ kmol} \times 12.001 \text{ kg/kmol} + 18 \times 1.008 + 3 \times (15.999) = 186.15 \text{ kg}$$

$$m_{\text{O}_2}: 13 \times 2 \times 15.999 = 415.97 \text{ kg}$$

$$m_{\text{O}_2}/m_{\text{fuel}} = 2.23$$

and therefore, $m_{\text{air}}/m_{\text{fuel}} = 2.23/0.21 = 10.64$. Using Equation 2.22, the excess fuel factor can be determined as follows.

$$f_{\text{ex}} = 1 - m/rR = 1 - 2.2/(10.64 \times 0.09) = -1.29$$

This negative value applies to PU1 to PU4. However, during each of these tests, external flaming was observed, and the presence of external flames was also verified with temperature measurements. Therefore, for the PU tests of the present work, there is a lack of experimental evidence to validate the excess fuel factor correlation given above. The presence of external flaming with a small negative excess fuel factor was also reported by Drysdale[31, p.347]. This point is revisited in *Section 5.6.3* with data from the Real Furniture tests.

4.2.4 Estimating Flame Envelope and Centre-Line Temperatures

The depth and height, the horizontal and vertical reach, respectively, of flames as they emerge from window openings is dependent on the internal ventilation conditions. According to Law's approximations[21], a Class 1 through-draft ventilation condition, with both the burn room door and window open, should result in flames which vent from the entire opening. A Class 2 no-through draft ventilation condition, with the burn room door closed and only the window open, should result in flames which vent from the upper half of the opening, while drawing air in from the lower half. However, due to the large burn room window size, during the Class 1 tests, PU2, PU3 and PU4, the external flames vented predominantly from the upper half of the opening, just like they did during the Class 2 test, PU1.

Approximations developed by Law[21] are summarised in *Section 2.4.1* of the *Background*. These approximations have been developed from tests using wood fuel. They were applied to the present results to see if it was possible to extend them to predict the flame envelope when the fuel source was polyurethane. These approximations describe the predicted flame envelope, shown in Figure 4.16, and centre-line temperature of a venting plume in terms of room and window geometry and burning rate. In the following section, Law's flame envelope approximations are compared with the observations made during each of the PU tests. Calculations based on her centre-line temperature equation (Equation 2.15) are also compared with CEF averaged temperatures measured during the PU test.

Table 4.1: Calculated flame envelope. The calculated numbers resulted from Equation 2.11 to Equation 2.13 in *Section 2.4.1*. In the calculations, $w = 2.4\text{m}$ and $h = 1.5\text{m}$ are the window width and height, respectively. The rate of burning was calculated using Equation 2.4 with $A_w = 3.6\text{m}^2$ as the window area. In the table below, L5 is 2.78m above the opening, F3 is 1m away from the external wall, and P1 to P5 cover the 2.4m wide window. na: not available

	Calculated (m)	Approximate locations on 2D rack and 3D grid
HEIGHT	2.4	L5 / L5
DEPTH	1.0	F3 / F3
WIDTH	2.4	na / P1-P5

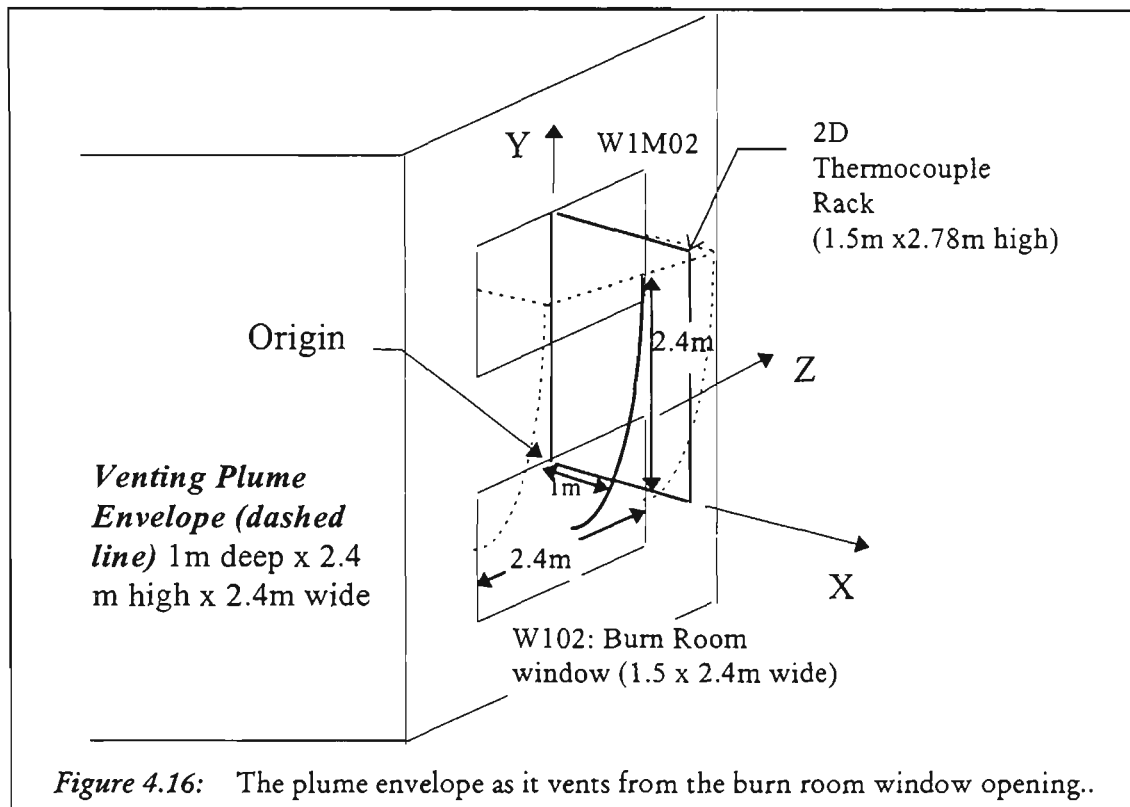


Figure 4.16: The plume envelope as it vents from the burn room window opening..

Table 4.2: Observed flame shape during the CEF period.

	Maximum Height (m)		Maximum Depth		Maximum Width	
PU1	L5	2.78m	0.5 - 1m		2.4m	
PU2	L4 - L5	2.03m - 2.78m	0.5 - 1m		2.4m	
PU3	L3 - L4	1.21m - 2.03m	0.5 - 1m		2.4m	
PU4	L3 - L4	1.21m - 2.03m	F2 - F3	0.5m - 1m	P1 - P5	2.4m

The estimated flame envelope, given in Table 4.1, was calculated using the equations for Class 2 ventilation conditions. Table 4.2 shows the observed flame shape. The estimated flame envelope compares reasonably well with the experimental PU1 results, a Class 2 no-through draft ventilation case. Although PU2, PU3 and PU4 are Class 1 tests, as mentioned above, the venting plume exhibited the no-through draft tendency during these tests. As a result, the estimated envelope also compares well with the observed flame shapes of PU2 to PU4.

High fuel loads and small compartments lead to a continuation of the combustion process outside the compartment's window, where an unlimited source of fresh air exists. Even though this point has been recognised, with the exception of Bullen and Thomas' excess fuel factor[56] concept, little work has been carried out in investigating the continued combustion aspect of a venting plume. In Law's procedure to estimate centre line temperatures, the flame temperature is assumed to be constant along the

width of the window, and across the depth of the plume. It is further assumed that the flame temperature varies linearly with distance along the flame axis.

Table 4.3 shows the Face 1 and Face 2 (as marked in Figure 3.7) temperatures at Plane 3, averaged over the CEF period. Plane 3 corresponds to the centre plane, perpendicular to the external wall, just above the window opening. Face 1 lies on the external wall ($y=0\text{m}$) and Face 2 is at the centre of the plume. The overall depth of the plume was determined to be 1.0m from the external wall, as shown in Table 4.1. Consequently, the centre of the plume was expected to be at 0.5m, parallel to the external wall. Hence, the centre of the plume corresponded to Face 2.

Table 4.3: Measured burn room and external centre-line temperatures during CEF period. The internal values listed in the first column are from Beck *et al.*[97]. Face 2 was selected to allow a comparison between calculated and measured temperatures, and the distance from the centre of the plume to the wall was determined to be 0.5m (Figure 4.16). Face 1 was included for comparison. The shaded cells denote the expected boundary of visible flame.

	Average Burn Room Temperature (°C)	EXTERNAL GRID - CENTRE PLANE (P3) Face 1 $x = 0\text{m}$ / Face 2 $x = 0.5\text{m}$ Temperatures (°C)				
		Level 1 $y = 0\text{m}$	Level 2 $y = 0.59\text{m}$	Level 3 $y = 1.2\text{m}$	Level 4 $y = 2.03\text{m}$	Level 5 $y = 2.78\text{m}$
		PU1	700	639 / 501	630 / na	594 / 448
PU2	790	649 / 703	402 / na	248 / 304	153 / na	118 / na
PU3	690	795 / 212	696 / na	528 / 158	305 / na	174 / 107
PU4	700	441 / 696	428 / 362	121 / 173	66 / 60	39 / 31

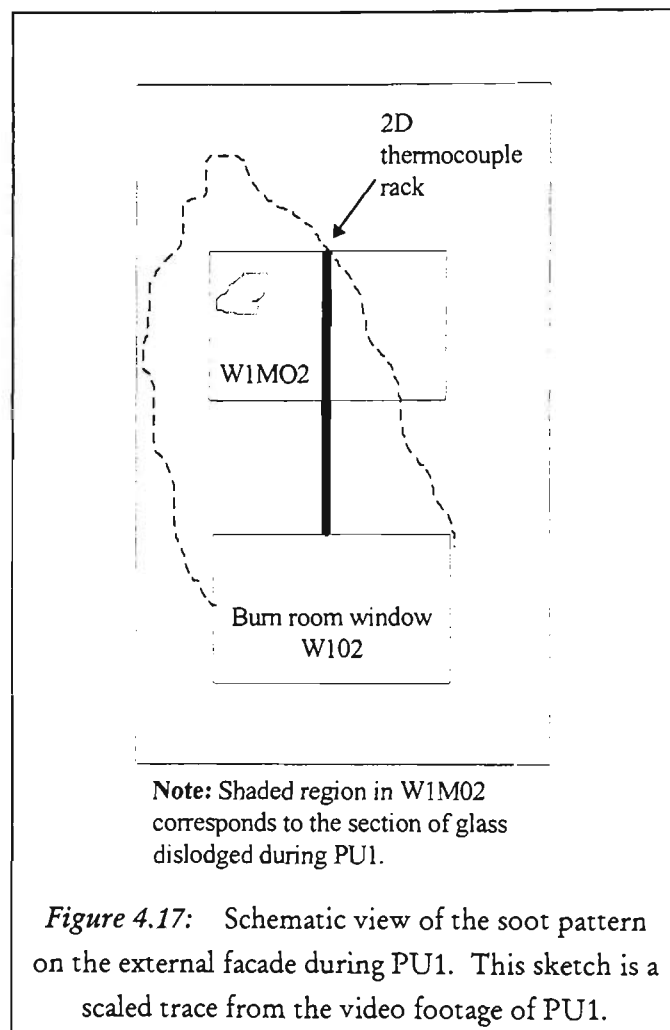
Table 4.4: Calculated centre-line temperatures on Face 2, using Equation 2.15 from Section 2.4.1. The average burn room temperatures listed in Table 4.3 were used as the *opening temperatures* in Equation 2.15. The average measured rates of burning during the CEF period for PU1 to PU4 are 5, 5.5, 5 and 6kg/min[97]. The shaded cells denote the expected boundary of visible flame.

	CALCULATED CENTRE-LINE TEMPERATURES on FACE 2 (°C)				
	Level 1	Level 2	Level 3	Level 4	Level 5
PU1	622	557	489	399	317
PU2	702	628	553	451	358
PU3	612	547	480	391	309
PU4	621	555	487	396	313

If a temperature of 540°C is used to indicate visible flame, then according to Table 4.3, on the average on Plane 3, flames reached up to Level 3 for PU1, Level 2 for PU3 and Level 1 for PU2 and PU4 above the top of the window opening, as indicated by the shaded cells. The observed maximum flame heights given in Table 4.2 indicate that larger flames existed on occasion. The difference between the observed flame heights and those expected based on the measured external centre-line temperatures, is due partly to the tilting of the flames as they vented from the window. Any tilting of the venting plume due to external wind conditions caused the upper portion of the plume to miss the 2D external thermocouple rack (and Plane 3 of the 3D thermocouple grid) positioned in the centre above the burn room window. For this reason, the temperatures measured along the centre-line of the plume during PU1 to PU4 indicate lower temperatures and shorter flames than those observed. A clear example of the tilting plume during PU1 is shown in Figure 4.17. The vent path extended across the left side of W1M02. Although similar patterns existed during PU2 to PU4, the plume vented across to the right. It is also in this portion of the window that a section of glass was dislodged during PU1, as discussed further in *Section 4.4*. The contact between the upper portions of the plume and the external wall was greatest during PU1. The soot covered the width of the burn room window, and reached above the top of W1M02.

Using Equation 2.15, external plume centre-line temperatures can be calculated. In this calculation, the average burn room temperatures from Table 4.3 are used as the opening temperature, T_o (T_o was not measured during PU1 to PU4). The ambient temperatures are taken from Table 3.2, and the average measured rates of burning during CEF for PU1 to PU4 are 5, 5.5, 5 and 6 kg/min, as given previously in *Section 4.2.2*. The window width is $w=2.4\text{m}$, and the height above the window opening, l , is taken at each Level, as indicated in Figure 2.6. The resulting external plume centre-line temperatures are listed in Table 4.4. These calculated temperatures indicate that flames would be expected to be present only up to Level 2 for all tests, except for PU2 where flames would reach Level 3, as shown by the shaded cells. These calculations underestimate the observed maximum flame heights listed in Table 4.2. This result can be due in part to using the average burn room temperature as the opening temperature in the calculations. On the other hand, the calculated centre-line temperatures given in Table 4.4 generally overestimate the measured centre-line

temperatures. The unfavourable centre-line temperature comparison can be attributed to the tilting of the venting plume leading to lower centre-line temperature measurements, as discussed above. Both of these conflicting comparisons can also be due to the fuel type used here, polyurethane, whereas Equation 2.15 was developed from wood crib fires[30]. A more appropriate comparison is given in *Section 5.6*. The measured Face 2 temperatures given in Table 4.3 and the calculated centre-line temperatures given in Table 4.4 decrease with distance for PU1 to PU4, as expected.



4.3 EXTERNAL HEAT FLUX RESULTS

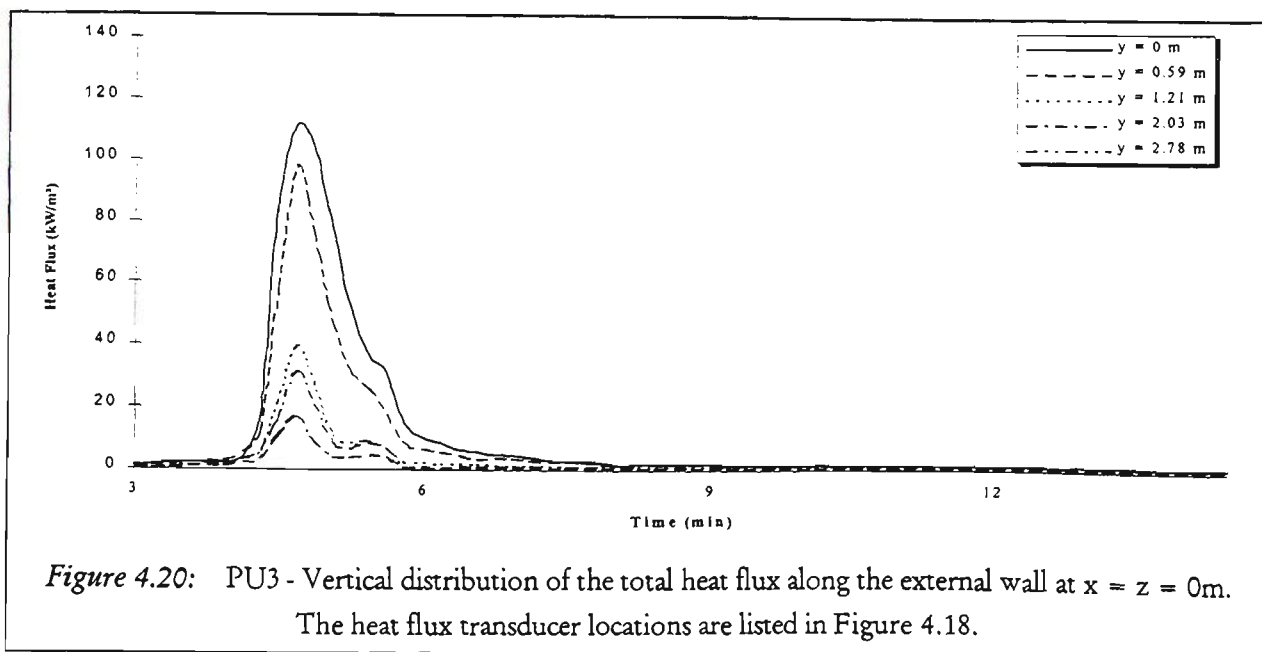
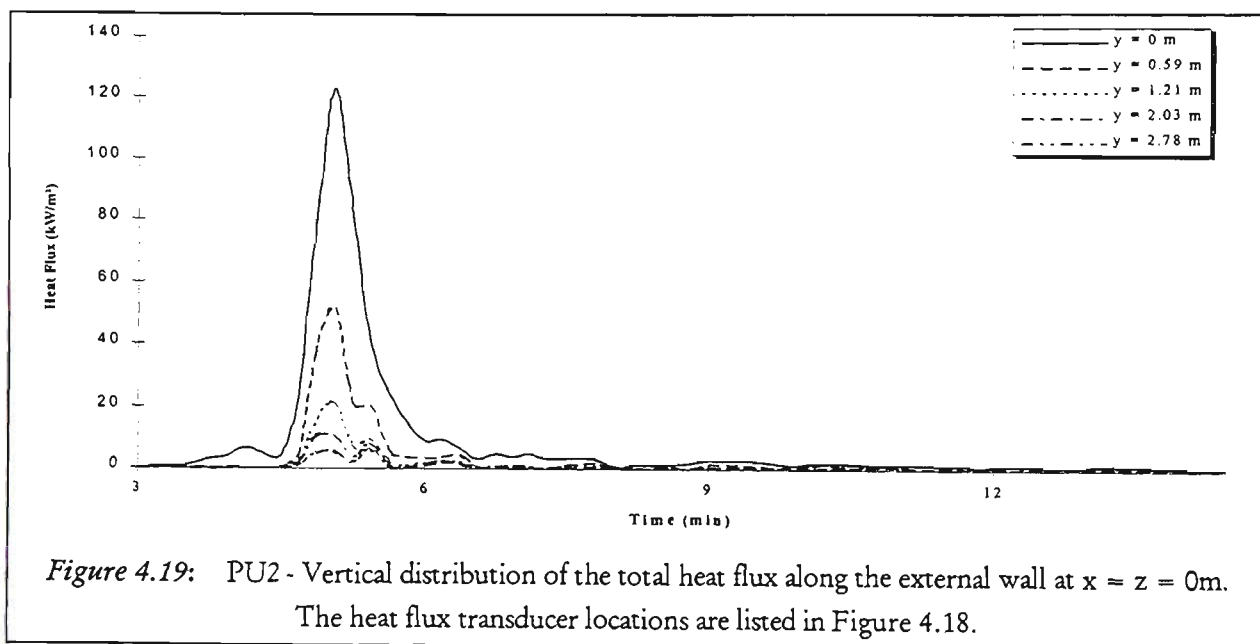
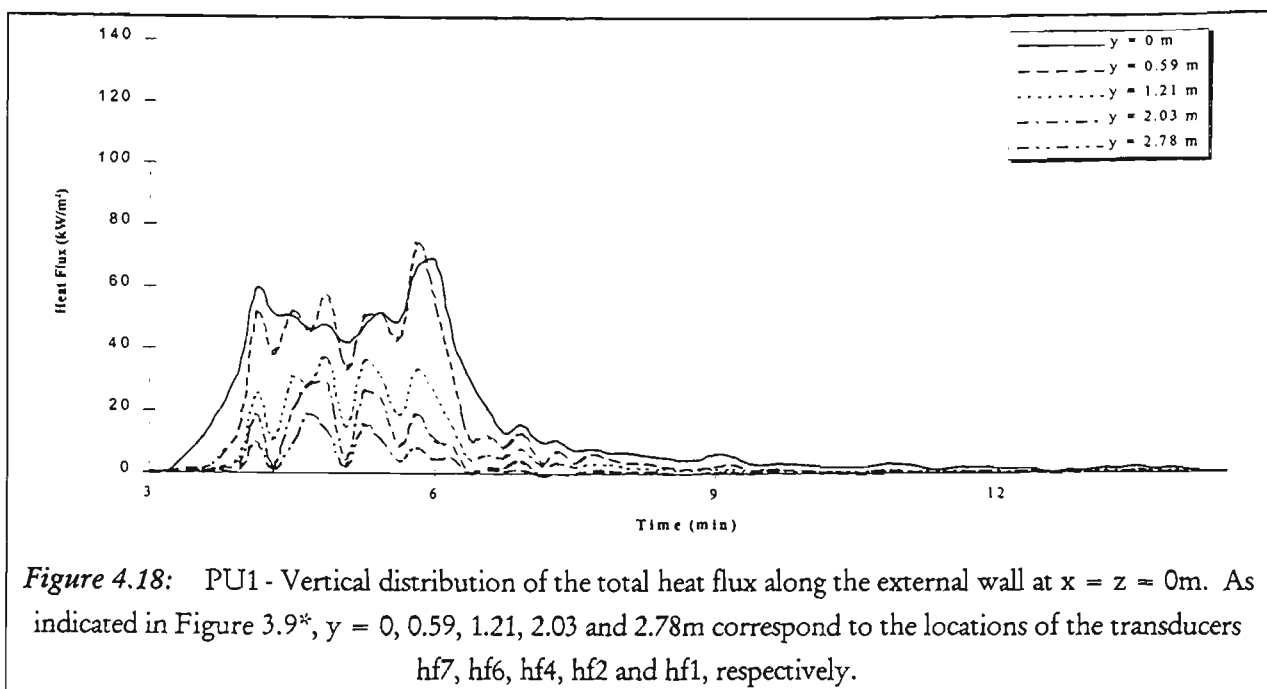
As indicated in *Section 3.1.5* the first three PU tests had seven *total heat flux* transducers located on the external facade of the building: five in a line above the centre of the window ($x=0\text{m}$), hf1, hf2, hf4, hf6 and hf7, and one to each side along the bottom of W1M02 (the mezzanine floor, Floor 1M window) at $z = \pm 1.17\text{m}$, hf5 and hf3, as shown in Figure 3.9. PU4 had an *additional* radiometer located at the bottom centre of W1M02, hf11, next to the total heat flux transducer, hf4. The top and bottom most transducers, hf1 and hf7, respectively, in Figure 3.9 were not in operation during PU4.

In this section, the vertical and horizontal variation in heat flux over the external wall is discussed. The inclusion of a radiometer during PU4, allowed the proportion of radiative and total heat transfer at the bottom centre of the W1M02 to be determined, to assess the possibility of a secondary fire.

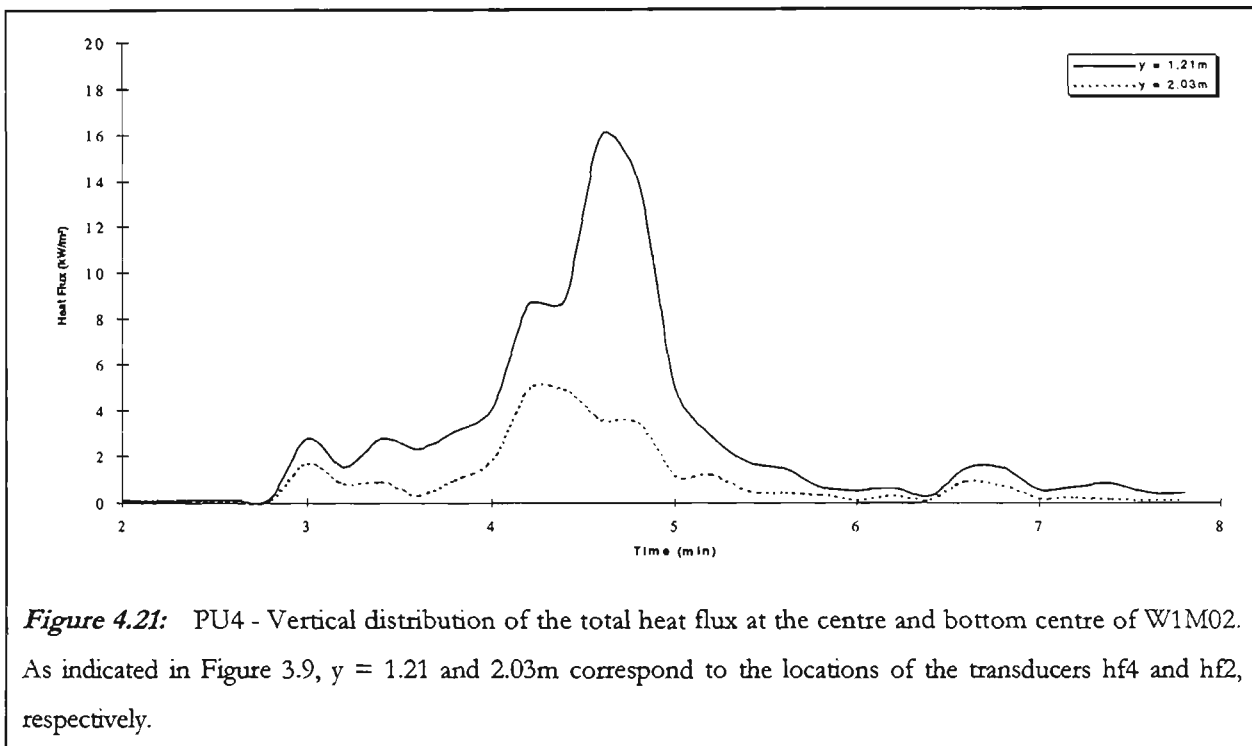
4.3.1 Vertical and Horizontal Heat Flux Variation

Figure 4.18 to Figure 4.20 show the measured total heat flux on the external wall at varying vertical positions during PU1 to PU3. The transducers began to register after the burn room window, W102, was broken. As expected, the greatest heat flux along the wall occurred at the origin. The heat flux decreased with increased vertical and horizontal distance away from the origin.

Similar to the external temperature measurements of PU1 given in Figure 4.1, the peak is broader for the total heat flux measurements in comparison with those of PU2 and PU3, however the maximum is much less. For PU1, the broadness of the peak can be explained by the ventilation conditions. With the door to the corridor closed during PU1, the only available vent path was the window. As a result, all combustion products vented through the window, instead of out into the corridor, as they did for PU2 to PU4, resulting in a slightly longer CEF duration for PU1. For similar heat release rates, the longer CEF duration resulted in lower heat flux measurements during PU1. For PU1 to PU4, the heat flux results peaked after flashover, similar to the external temperature results.



During PU4, the results obtained with two total heat flux transducers are presented in Figure 4.21. These transducers were both placed on the Floor 1M window (W1M02), one at the centre of the window (hf2) and the other at the bottom centre of the window (hf4) as shown in Figure 3.9. Figure 4.21 shows that between the fourth and fifth minute, hf2 peaked to approximately 5 kW/m^2 , while hf4 peaked at just over 15 kW/m^2 , showing an almost a two-third decline in total heat flux over a distance of 0.8 m . The peak total heat flux measured during PU4 is lower compared to PU1 to PU3 values at 1.2 m above the top of the burn room window, due to the larger burn room size used for PU4 (and this was the reason why a different vertical scale was used in Figure 4.21). With the larger burn room, more of the combustion took place within the room, in addition to increased heat loss to the walls, resulting in reduced continued combustion outside the burn room window.



4.3.2 Heat Flux along the Bottom of W1M02

Total heat flux measurements also varied horizontally along the bottom of the W1M02, where two transducers were located 1.17 m on either side of the centre-line. Similar to the vertical variation on the external total heat flux results presented in the previous section, broader peaks were obtained for the total heat flux measured along the bottom of W1M02 during PU1, compared to PU2 to PU4. The maximum heat

flux measurements for PU1, PU2, PU3 and PU4 were at about 35, 20, 60 and 24 kW/m², respectively, as indicated in Figure 4.22 to Figure 4.25. The maximum heat flux lasted approximately twice as long for PU1, compared to PU2 to PU4.

Having transducers along the bottom of W1M02 also allowed the wind direction to be gauged from heat flux histories. Generally, the centre of the plume ($z=0\text{m}$) was the hottest part of the venting plume, and therefore, the centre transducer registered the highest reading, while on either side of the plume ($z=\pm 1.17\text{m}$), the measured heat flux was proportionally less. However, if the wind tilted the plume, the reading of one of the side transducers exceeded the centre transducer readings. As seen in Figure 4.23 for PU2, Figure 4.24 for PU3 and Figure 4.25 for PU4, the tilting of the plume towards the East (right) resulted in an increase in the measured heat flux to the right of the centre. Whereas for PU1 as shown in Figure 4.22, the plume tilted towards the left, causing comparable heat flux readings from the centre and left transducers. The tilting of the venting plume as indicated by the heat flux measurements corresponds to the observed pattern during each test, in addition to being consistent with the wind directions given in Table 3.2.

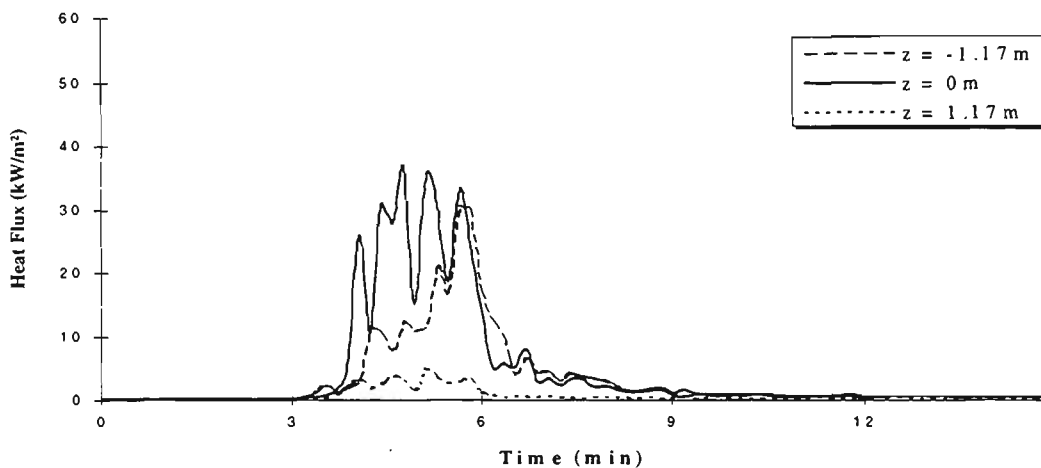


Figure 4.22: PU1 - Horizontal distribution of the total heat flux along the bottom of W1M02 at $x = 0\text{ m}$ and $y = 1.2\text{ m}$. The plume was tending to the West (to the left with respect to an observer facing the burn room window). As indicated in Figure 3.9, $z = -1.17, 0$ and 1.17m correspond to the locations of the transducers hf3, hf4 and hf5, respectively.

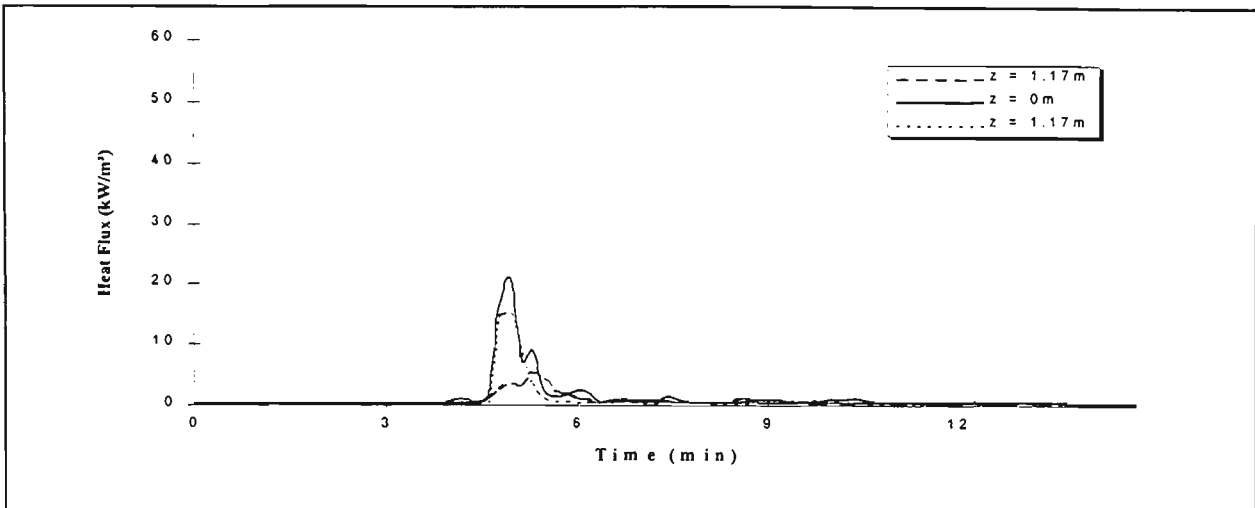


Figure 4.23: PU2 - Horizontal distribution of the total heat flux along the bottom of W1M02 at $x = 0$ m and $y = 1.2$ m. The plume was tending to the East (to the right with respect to an observer facing the burn room window). The heat flux transducer locations are listed in Figure 4.22.

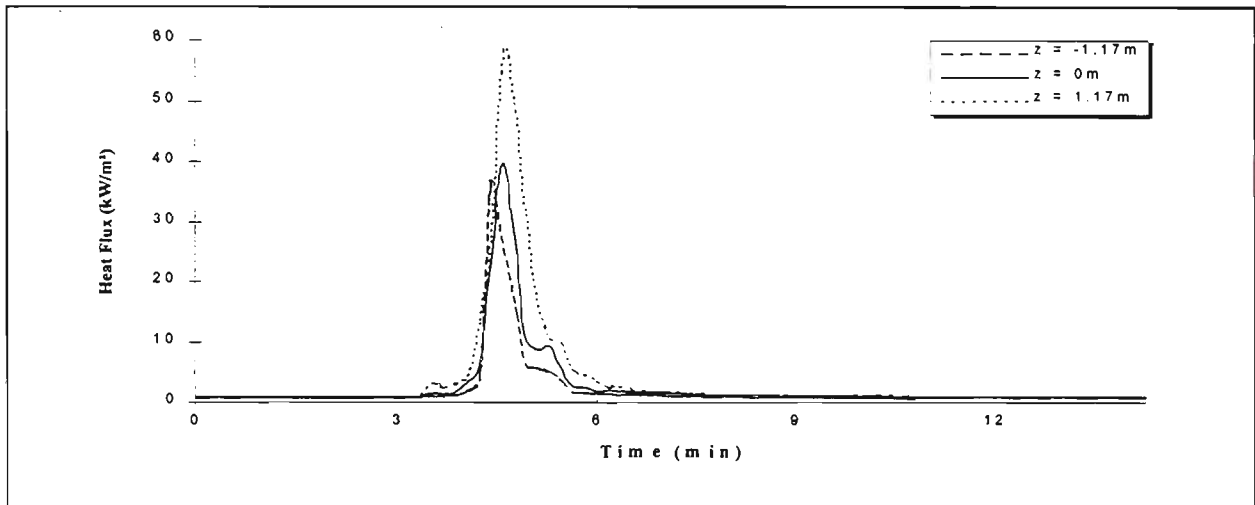


Figure 4.24: PU3 - Horizontal distribution of the total heat flux along the bottom of W1M02 at $x = 0$ m and $y = 1.2$ m. The plume was tending to the East. The heat flux transducer locations are listed in Figure 4.22.

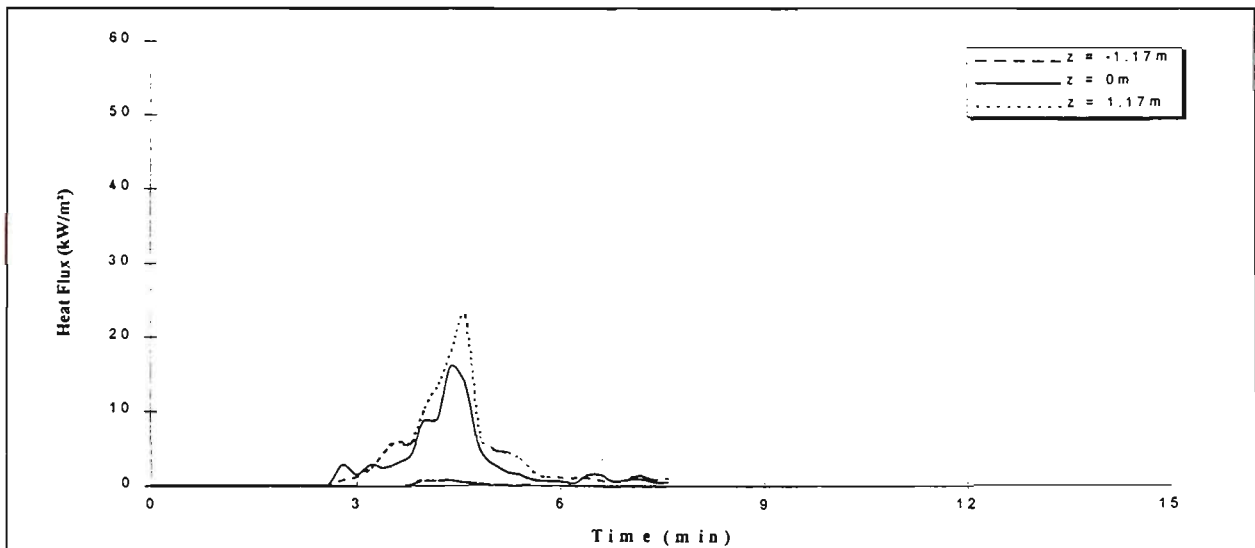
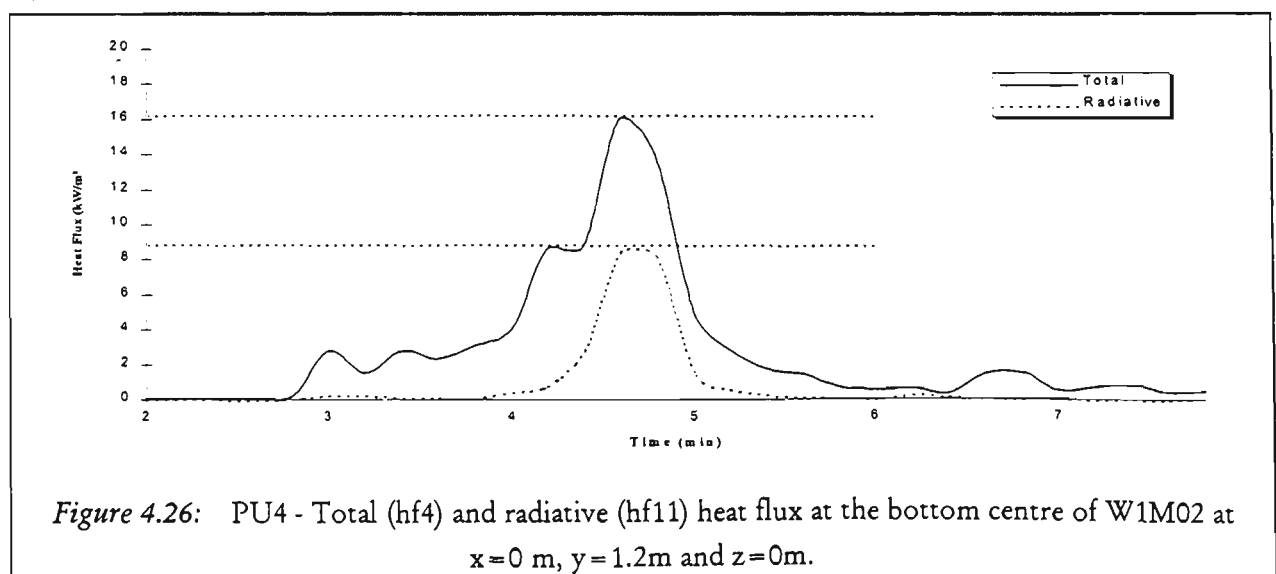


Figure 4.25: PU4 - Horizontal distribution of the total heat flux along the bottom of W1M02 at $x = 0$ m and $y = 1.2$ m. The plume was tending to the East. The heat flux transducer locations are listed in Figure 4.22.

4.3.3 Total and Radiative Heat Flux at the Bottom Centre of W1M02

For PU4, a nitrogen gas purged heat flux transducer with a sapphire window was placed next to a total heat flux transducer, to measure the radiative portion of heat flux at the bottom centre of W1M02. These transducers were approximately 0.1 m from the bottom of the window, corresponding roughly to Level 3 in Figure 3.7*, and they were embedded in the wall. During PU4, the peak total heat flux, as shown in Figure 4.26, was approximately 16 kW/m^2 at the bottom centre of the window ($z=0\text{m}$), with a corresponding maximum radiative component of approximately 9 kW/m^2 . At the peak, the radiative portion constituted 56% of the total measured heat flux. The corresponding CEF averaged total and radiative heat fluxes were 13 and 5 kW/m^2 , respectively. Therefore, even on the average, the radiative heat flux was about 38% of the total. A comparison is given in the next section, Section 4.3.4, between these measurements and heat flux calculations using measured temperatures.

With respect to the initiation of a secondary fire through the window in the floor above the room of fire origin, the radiation levels measured in PU4 are not high enough. Direct flame contact in this respect becomes an issue only after the window fails on the floor above the burn room. During PU4, the window on the mezzanine floor, W1M02, above the burn room did not fail. In addition, radiant heat flux levels of 10 and 20 kW/m^2 are necessary to ignite items such as thin curtains or loose newsprint and upholstered furniture, respectively[108]. Approximately 25% attenuation occurs through standard glass[109]. Consequently, radiative ignition would not be expected to occur during PU4.



4.3.4 Calculated Heat Flux

Using the temperatures measured at the centre-line (Face 2) given in Table 4.3, the convective and radiative heat flux can be calculated using Equation 2.18 to Equation 2.21. The radiant heat flux is calculated as a function of flame emissivity, ϵ , and consequently, the flame shape, Stefan-Boltzmann constant, σ , and temperature. In this case, constant and variable flame thicknesses (based on shape) are used to determine the flame emissivity at various heights above the burn room window. The temperatures along the centre-line are used to determine the radiant heat flux.

The emissive power of flames venting from the burn room window depends on the density of soot particles and the thickness of the flame. Therefore, the production of soot particles during the combustion process directly affects radiation measurements both within the room of fire origin and beyond it, by influencing the emission spectrum. Values of emission coefficients, b , are given by Drysdale[31, p.75] for a variety of materials, indicating that sootier flames result in higher emissivities. In addition, in Equation 2.18, the emissivity of the plume depends on flame thickness. Law[21] proposed a constant flame thickness which results in a constant flame emissivity, while Oleszkiewicz[29] proposed a triangular flame shape (variable flame thickness) resulting in variable flame emissivity determined based on the thickness of the flame at various heights. During this series of tests, a variable flame thickness was also observed.

Using Equation 2.18, emissivities were determined using an emission co-efficient of $b=0.37 \text{ m}^{-1}$ for polyurethane[110]. The first column of Table 4.5 shows the emissivity for a flame thickness of 1.0m as specified by Law. In the second column, a maximum flame thickness of $2h/3$ ($= 1\text{m}$) is used as specified by Oleszkiewicz. Based on his triangular flame shape (shown in Figure 2.7), the subsequent flame thickness at each level was determined. The flame thickness was taken to be zero at 0.56m above Level 5, 3.34m above Level 1 (this height corresponds to Level 6 in Figure 3.19). As indicated in Table 4.2, the flames reached at most Level 5. Therefore, the height at which the flame thickness drops to zero must be above Level 5. No flaming was observed at the next level, Level 6, and the external grid was used as a gauge for determining flame heights above the window.

Table 4.5: Flame emissivity determined using constant and variable flame thickness.

Constant Flame Thickness (LAW)	Triangular Flame Shape using $\lambda_{\max} = 2h/3 = 1\text{m}$ (OLESZKIEWICZ)	
$\lambda = 1\text{m}$	$\lambda (\max) = 1\text{m}$	emissivity
$\varepsilon = 0.31$	$\lambda_1 = 1\text{m}$	$\varepsilon_1 = 0.31$
	$\lambda_3 = 0.39\text{m}$	$\varepsilon_3 = 0.13$
	$\lambda_5 = 0.17\text{m}$	$\varepsilon_5 = 0.06$

To determine the radiative and convective heat transfer, the centre-line temperatures and burning rates are needed. This information is provided in Table 4.6. Using Equation 2.19 and Equation 2.20, the radiative and convective heat flux were calculated at Level 1, Level 3 and Level 5, and these values are listed in Table 4.7. In the last column of Table 4.7, the corresponding experimental values are given on the external wall. These Levels were selected as they correspond to where temperatures were measured along Face 2 (centre-line location) and where actual heat flux measurements were taken on the external wall. The location of Faces and Levels on the 2D thermocouple rack and the positions of the heat flux transducers on the external wall are indicated in Figure 3.7* and Figure 3.9*, respectively, in the *Experimental Setup*. All radiant and total heat flux measurements taken during the Polyurethane Burns were averaged over the CEF period to allow comparison with calculated radiation and total heat flux, and Table 4.8 lists all heat flux measurements taken during this series. Using Equation 2.20, $T_{\text{wall}} = 100^\circ\text{C}$ corresponds to Oleszkiewicz's assumption that a transducer will cease to function if its temperature exceeds 100°C , as the water used to cool the transducer will boil.

Table 4.6 Center-line temperatures and burning rates measured during the CEF period. Note: dna=data not available. Level 1, Level 3 and Level 5 are 0m, 1.2m and 2.78m above the top of the burn room window, respectively. dna=data not available.

	Temperature T(z) taken at Face 2 Plume Centre-Line ($^\circ\text{C}$)			Rate of Burning (kg/min)
	Level 1	Level 3	Level 5	
PU1	501	448	302	5
PU2	703	304	dna	5.5
PU3	212	158	107	5
PU4	696	173	31	6

The calculated total heat flux results presented in Table 4.7 differ greatly from those measured. Such differences can be attributed partly to the convective heat flux equations (Equation 2.20 and Equation 2.21) given by Oleszkiewicz. Oleszkiewicz[29] states that the expression for convective heat transfer coefficient, Equation 2.21, needs to be modified when faster burning materials, such as plastics are used. This equation has been found to be satisfactory when the fire burns at a moderate rate, such as when wood cribs, furniture or thicker charring materials are used. This point is confirmed by the application of these equations in *Section 5.7.2* to the Real Furniture tests. In addition, the observed tilt of the venting plume is expected to cause lower values of the calculated convective heat flux, even with a correct convective heat transfer coefficient. This effect is discussed further next with respect to radiative heat transfer calculations.

In Table 4.7 the shaded row contains the radiation measurement taken during PU4. A value of 5kW/m^2 for the CEF period is used in Table 4.7 for comparison with the calculations, rather than the peak radiative heat flux of 9kW/m^2 , as given in the previous section, *Section 4.3.3*. Calculations using Equation 2.18 and Equation 2.19 were found to result in lower radiative heat flux than measured. The reason can be attributed to the tilting of the plume as shown in Figure 4.15. To calculate the radiation values given in the shaded row of Table 4.7, the temperature measured at Level 3, Face 2, Plane 3 was used. This location corresponds to the centre-line of the plume at Level 3, if the plume has no tilt. Working backwards, an average radiative heat flux of 5kW/m^2 corresponds to a temperature of approximately 450°C which existed at Level 3, Face 3 and Plane 4 (0.5 temperature contour on Level 3 in Figure 4.15) indicating that the plume centre-line had tilted to the right during PU4 with respect to an observer facing the burn room window, as stated earlier. This result also indicates that better comparison could have been obtained with the calculated radiative (and convective) heat flux if the plume had not tilted during PU4.

Table 4.7: Calculated radiative, convective and total heat flux and measured total and radiative heat flux in kW/m², at Level 1, Level 3 and Level 5 on the external wall. Radiative heat flux is calculated with constant and variable emissivities, based on flame thickness. Note: Level 1 corresponds to the top of the burn room window, Level 3 is at the bottom of the mezzanine level window, Level 5 is at the top of the mezzanine level window. dna=data not available.

	PLANE 3	Using Constant ϵ			Using variable ϵ			Measured
		Radiation	Convective	Total	Radiation	Convection	Total	Total / Rad
PU1	Level 1	6.3	6.3	12.6	6.3	6.3	12.6	55
	Level 3	4.7	5.5	10.3	2.1	5.5	7.6	27
	Level 5	1.9	3.2	5.1	0.38	3.2	3.6	9
PU2	Level 1	15.9	10.1	26.1	15.9	10.1	26.0	57
	Level 3	1.9	3.4	5.4	0.84	3.4	4.3	8
	Level 5	dna	dna	dna	dna	dna	dna	3
PU3	Level 1	0.97	1.8	2.7	0.97	1.8	2.7	59
	Level 3	0.61	0.92	1.5	0.26	0.92	1.2	15
	Level 5	0.37	0.11	0.48	0.07	0.11	0.18	7
PU4	Level 1	15.5	10.5	26.0	15.5	10.5	26	dna
	Level 3	0.70	1.3	2.0	0.3	1.3	1.6	13 / 5
	Level 5	0.15	-1.2	-1.1	0.03	-1.22	-1.18	5

Table 4.8 Measured heat flux, hf, in kW/m², averaged over the CEF period. All heat flux measurements are total heat flux, with the exception of hf11 which measured radiative heat transfer during PU4. For PU1 to PU4, refer to Figure 3.9* for heat flux locations. NOTE: dna=data not available. P3 refers to the centre of the burn room window, and P1 and P5 correspond roughly to 1.17m on either side of P3. The designation of Planes, Levels and Faces was used to compare the information from the PU tests.

	Location	PU1	PU2	PU3	PU4
hf1	L5 / P3	9	3	7	dna
hf2	L4 / P3	18	5	12	5
hf3	L3 / P1	19	3	12	1
hf4/hf11	L3 / P3	27	8	15	13 / 5
hf5	L3 / P5	3	5	25	18
hf6	L2 / P3	50	21	42	49
hf7	L1 / P3	55	57	59	dna

4.4 WINDOW GLASS BREAKAGE

The work of Skelly and Roby[65] with small glass samples on how glass breaks when subjected to a heat source, shows remarkable similarity to the breaking of the glass during each of the first three PU tests, in that during PU1 to PU3, cracks initiated from the edge of the glass pane. As discussed in *Section 3.1.1*, PU1, PU2 and PU4 had a standard window arrangement, while PU3 had an alternative window arrangement. For PU1 and PU2, the smaller side panes of glass cracked first, as these were thinner (3mm thick) compared to the centre pane (4mm thick). Once cracking began in the smaller panes, it was usually followed by cracking of the larger pane. Initial cracks in the burn room window provided a means for hot exhaust gases and smoke to exit the burn room, resulting in a slight drop in the room temperature. However, as more pieces of glass were dislodged, the increased air flow caused the temperature to rise again, enhancing the combustion process. This repeated sequence of events, that of breaking glass allowing the hot gases to exhaust from the room as well as allowing fresh air into the room, was typical during the initial stages of PU1 and PU2. For PU3, the thinner sections of glass cracked at the edges, just like PU1 and PU2. However, the overlap between the two sections of glass in the centre of the window remained intact until just after flashover. For PU4, the window was lowered.

The window cracking times given in Table 4.9 are taken from the video records of the experiments. These times represent the duration from the ignition of the fuel to when the window first began to crack during PU1 to PU3. The time to initial cracking corresponded approximately to when the *average burn room temperature* approached 300°C with complete dislodgment occurring at 600°C[97]. These times were about the same, around 3 minutes after ignition, for PU1 to PU3.

As highlighted in Table 4.9, the burn room window (W102) was lowered for PU4 in accordance with the Window Lowering Criterion #1 as detailed in *Section 3.2.2*. This criterion implies that the entire window was lowered when *a gas temperature of 450°C was indicated next to the window*, because glass failure is expected at this temperature. As a result, the time shown in the first column of Table 4.9 corresponding to lowering of W102 in PU4, is different than the times given to initial cracking during PU1 to PU3. Consequently, it would be expected that PU4 was not at the same stage of development as PU1 to PU3 at the indicated time.

The times given for PU1 to PU3 in the first column of Table 4.9 indicate that neither the window configuration nor the ventilation conditions could be said to have had a significant effect on the time to glass cracking of the burn room window, W102. As indicated earlier, a standard window arrangement was used for PU1 and PU2; and for PU3, an alternative window arrangement was prepared, as shown in Figure 3.4. As far as the ventilation conditions are concerned, PU1 was a Class 2 type, and PU2 and PU3 were Class 1.

Dislodgment of glass from the mezzanine floor window, W1M02, located 1.21 m above the burn room window, occurred only during PU1. While some cracking of the glass in W1M02 occurred during PU2 and PU3, it remained intact during PU4. These results may be explained by the ventilation conditions. Given that the door to the corridor, D1, was closed for PU1, only W102 was available for the venting of combustion products such as flames, gas and smoke. Internal measurements during PU2 and PU3 showed that significant amounts of hot gases and smoke vented through the burn room door and down into the corridor[97]. For PU4, the larger burn room as well as the open burn room door reduced the overall impact of the external flames.

Table 4.9: Time from ignition to initial cracking for PU1 to PU3 and to lowering for PU4 of the burn room window, W102, and time to dislodgment of the window in the floor above, W1M02. The mezzanine floor window, W1M02, dislodged during PU1 after cracking as indicated below. W1M02 did not crack during PU4. dna: data not available.

Test	Cracking of W102	Dislodgment of W1M02
PU1	3 min 17 sec	7 min
PU2	3 min 10 sec	dna
PU3	3 min 12 sec	dna
PU4	2 min 30 sec	--

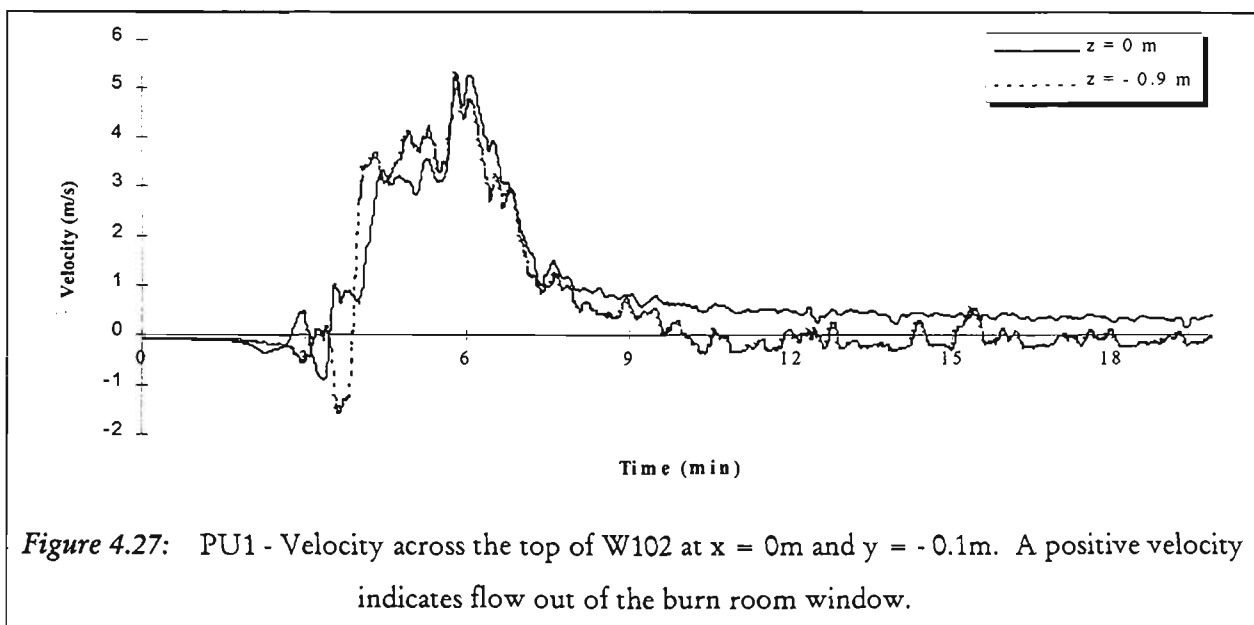
At the onset of cracking and dislodgment of the burn room window, the following observations were made about the release of hot gases and smoke:

- ◆ High concentrations of CO₂ and CO were measured outside the burn room window.
- ◆ The flow velocities across the window started to increase.
- ◆ The external temperatures above the burn room window rose sharply.
- ◆ The heat fluxes measurements across the Southern facade increased dramatically.

4.5 EXHAUST FLOW VELOCITIES

The exhaust flow velocity data collected with bi-directional velocity probes located just *outside the burn room window* (vp1 at $x=0\text{m}$, $y=-0.1\text{m}$, $z=0\text{m}$ and vp2 at $x=0\text{m}$, $y=-0.1\text{m}$, $z=0.9\text{m}$), are given in Figure 4.27 to Figure 4.29 for PU1 to PU3, respectively. As seen in these figures, the exhaust flows were extremely unsteady throughout each test and even reversed direction during the course of one experiment. During PU1 to PU3, maximum outflow (positive) velocities from the burn room window were between 4 to 6 m/s.

For PU4, velocities were measured along *the centre of the burn room door* (D1) at different heights, y , from the floor, instead of at the burn room window, as in PU1 to PU3. For completeness, these gas velocity histories during PU4 are given in Figure 4.30. During most of the CEF period, air was drawn in from the corridor at heights of 0.25, 0.75, 1.0 and 1.75m above the floor (positive flow). Hot gases/smoke flowed out of the burn room at heights of 0.5, 1.25 and 1.5m above the floor (negative flow). Peak flow velocity through the burn room door, towards the fire, was approximately 3m/s at a height of 1.75m.



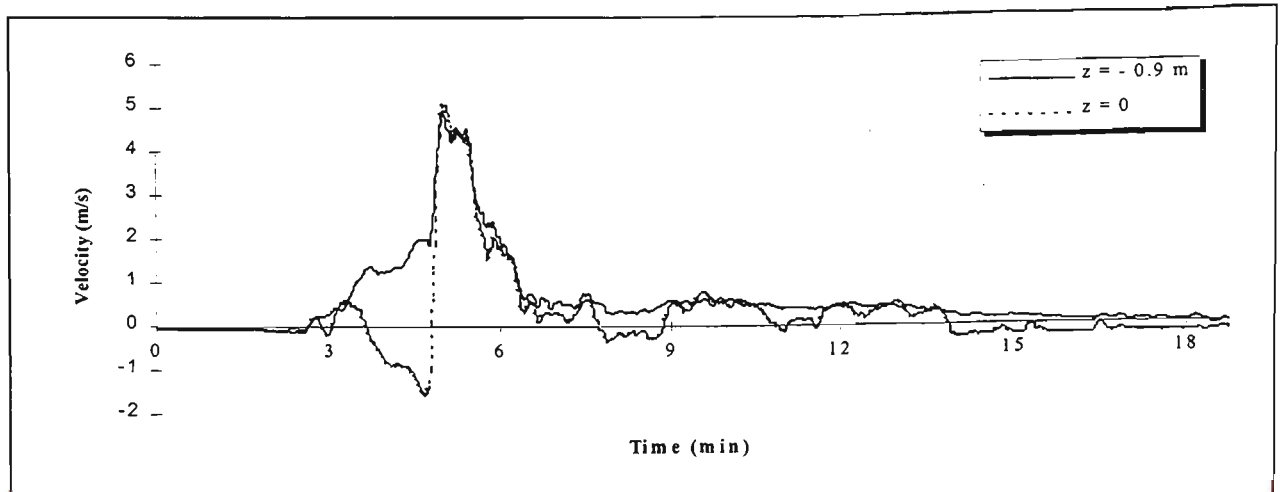


Figure 4.28: PU2 - Velocity across the top of W102 at $z = 0\text{m}$ and $y = -0.1\text{m}$.

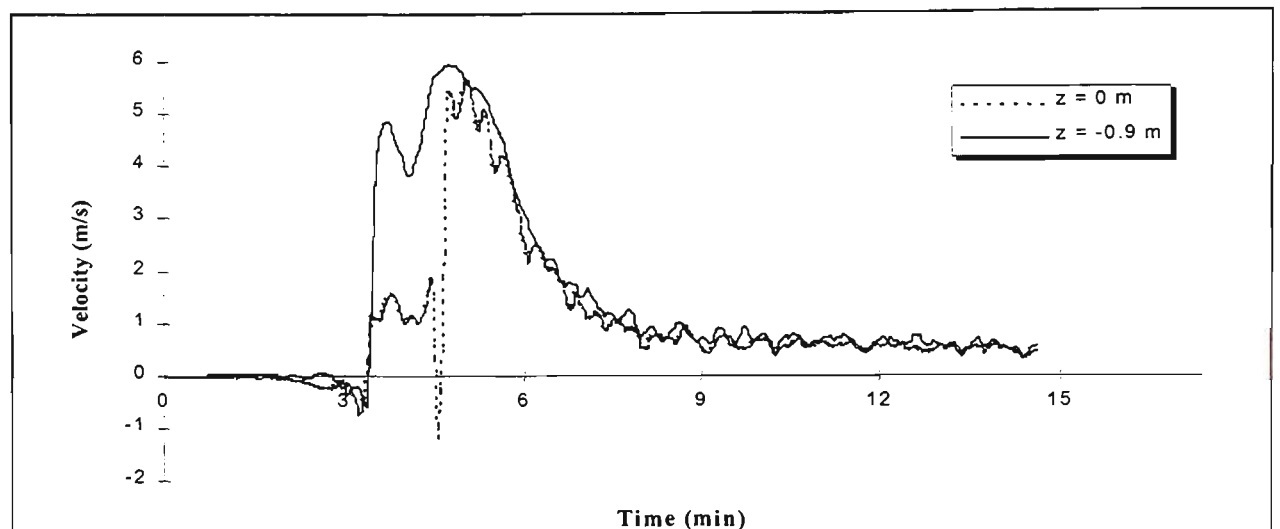


Figure 4.29: PU3 - Velocity across the top of W102 at $x = 0\text{m}$ and $y = -0.1\text{m}$.

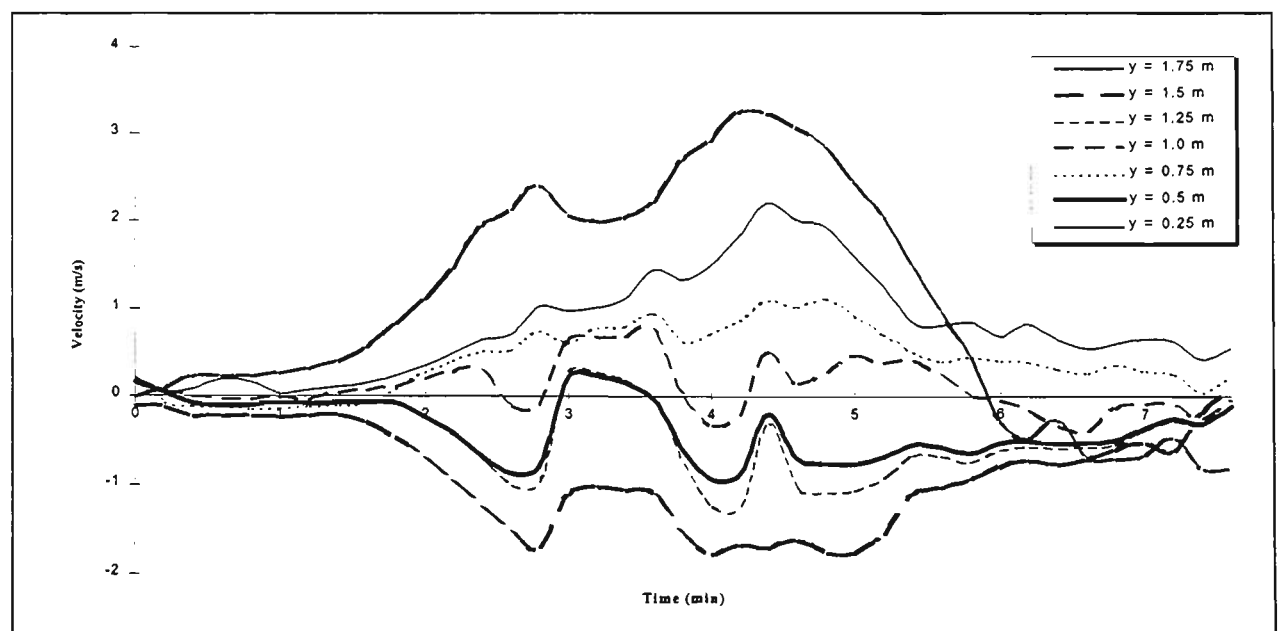


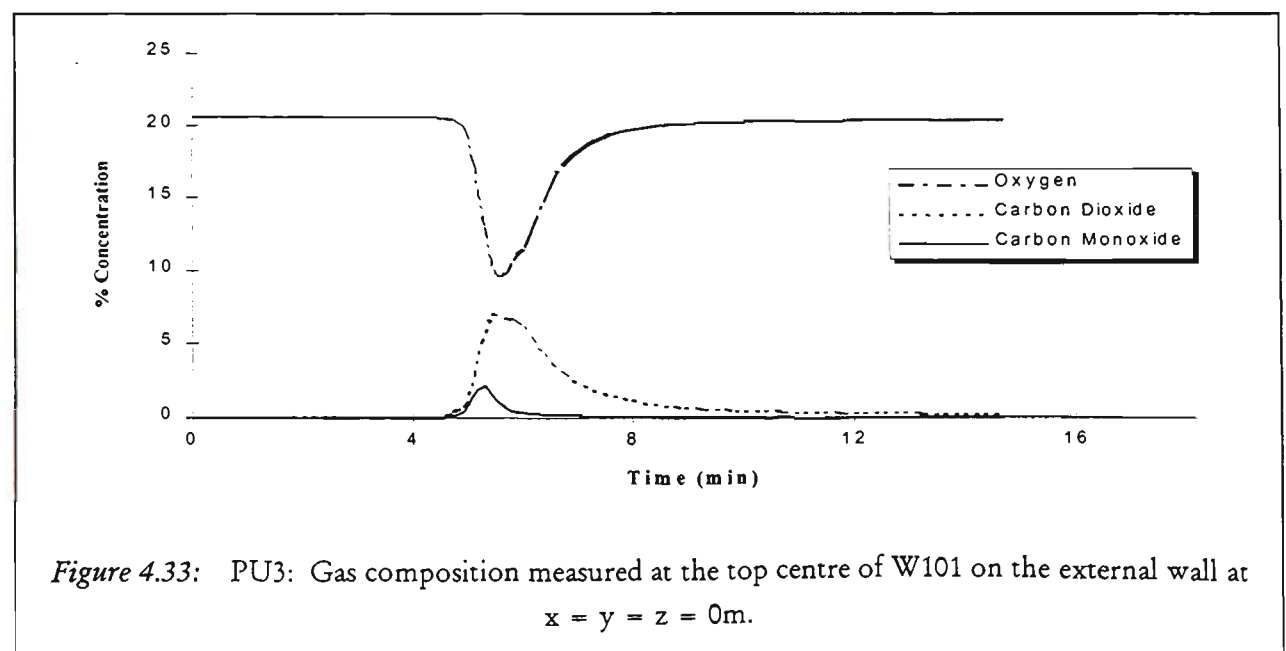
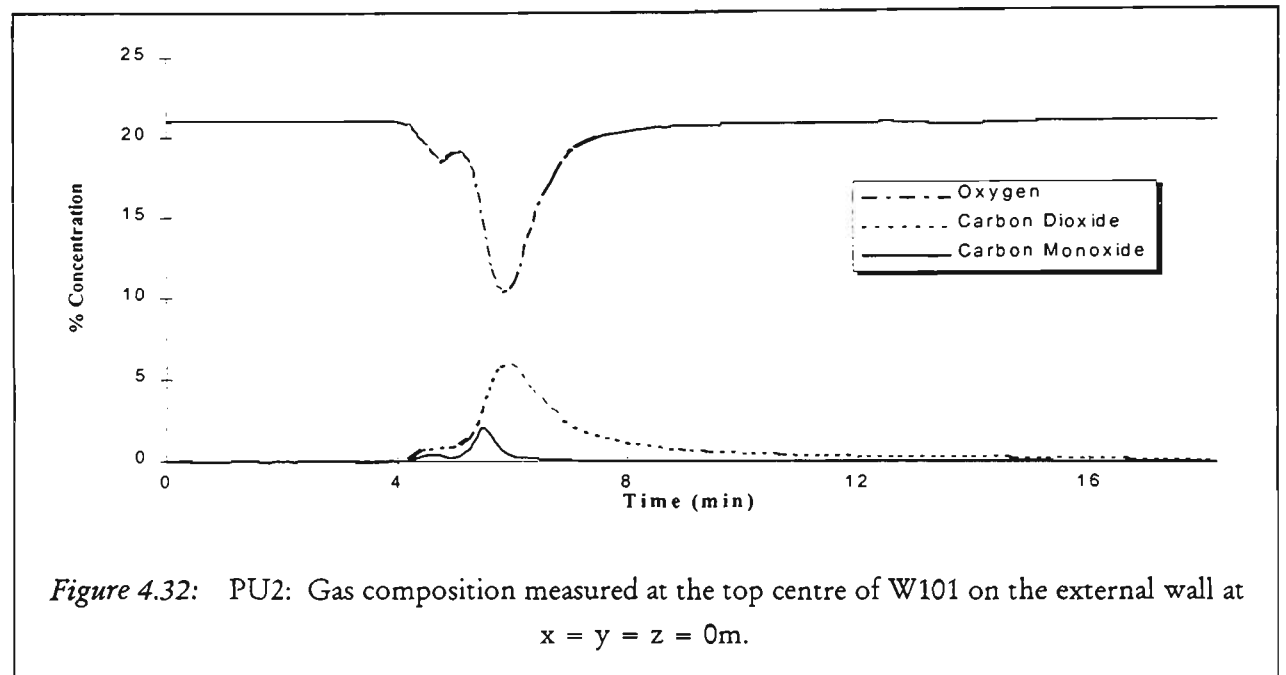
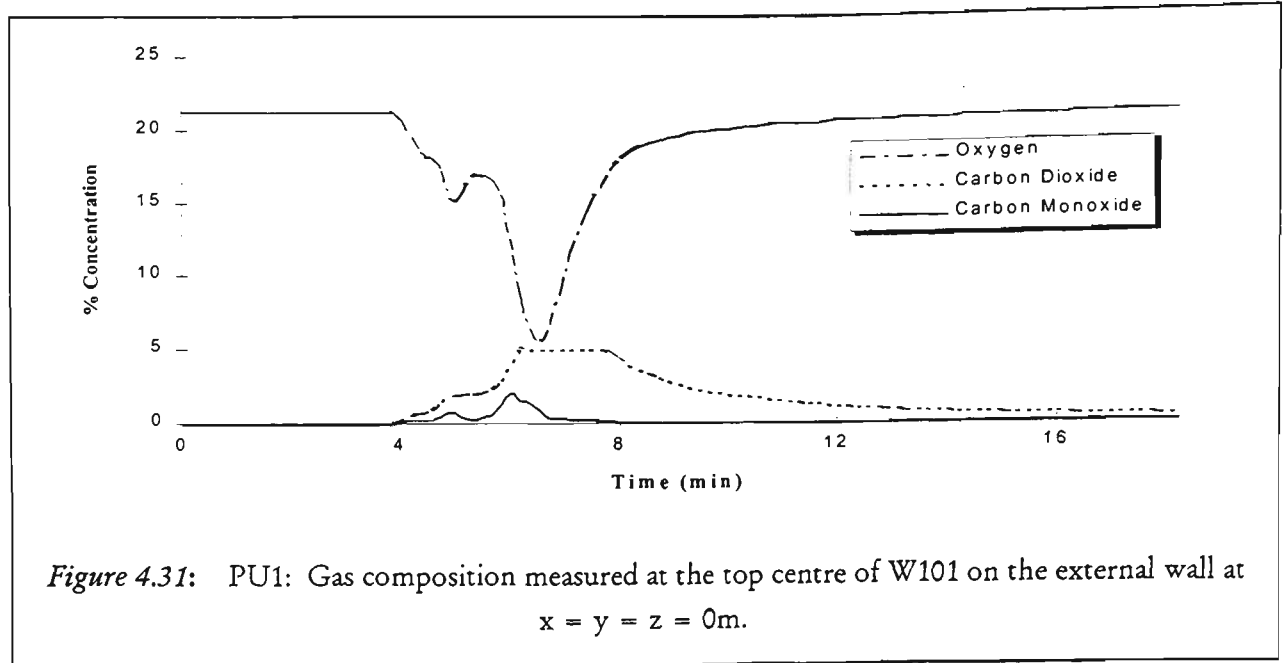
Figure 4.30: PU4 - Velocity at the centre of the burn room door (D1) where y is the distance above the floor. A positive velocity indicates flow into the burn room from the corridor.

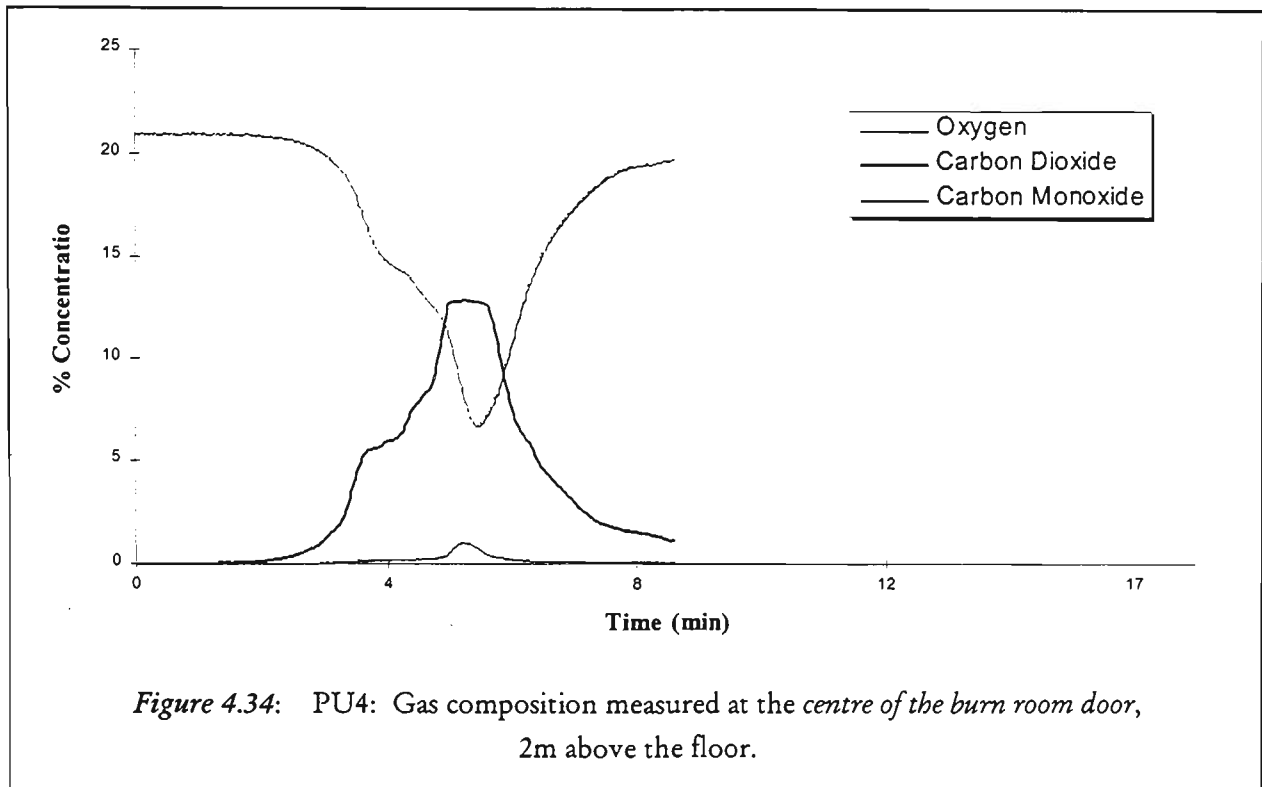
4.6 OXYGEN CONCENTRATIONS/GAS ANALYSIS

The external gas analysis results are reported here to provide data for numerical prediction purposes, only. The external gas analyser, located approximately at the top centre of W102, first registered a change in the species concentration when the window broke. Figure 4.31 to Figure 4.33 show the percentage concentrations of oxygen, carbon dioxide and carbon monoxide that were measured during PU1 to PU3. In general, the percentage of oxygen remained fairly constant (at approximately 21%) until glass started to dislodge from W102 in the third minute, causing the levels of oxygen to drop. The reason for this drop was the presence of external flames which vented from the dislodged sections of glass in the window. For PU1, the level of oxygen dropped to between 5 to 10% and between 10 to 15% for PU2 and PU3. The level of oxygen remained low until shortly after the fully developed phase, one to two minutes after flashover, and then it began to return to normal. As expected, the drop in oxygen corresponded to an increase in the levels of carbon monoxide (CO) and carbon dioxide (CO₂). The greatest increase in CO occurred just after flashover (around 2%), but also peaked slightly when the window broke.

During PU1, the maximum measurable increase in CO₂ was limited to 5%, due to equipment limitations. This corresponds to the 'plateau' in the CO₂ measurements shown in Figure 4.31. However, this was overcome in the following two tests, which produced an increase of approximately 7% in the levels of CO₂ for PU2 and PU3, as shown in Figure 4.32 and Figure 4.33, respectively. The levels of CO peaked as the levels of O₂ reached a minimum, after which O₂ levels began to return to normal and levels of CO fell off. The percentage of CO₂ took slightly longer to return to normal.

In the absence of external gas analysis results during PU4, the results at the burn room door are quoted here for completeness. For PU4, the gas sample point was located at the top centre of the burn room door, 2.0m above the floor. At this location, the concentrations of O₂ and CO₂ gave an indication of the air quality between the burn room and corridor. Just over four and a half minutes from ignition, and over the next two minutes, the level of oxygen dropped to around 12%, reaching a minimum of approximately 6%. This corresponded to an increase in carbon dioxide to at most, 12%, and in carbon monoxide of approximately 1% over the same time period, as shown in Figure 4.34.





4.7 CONCLUSIONS FROM THE POLYURETHANE BURNS

Results from the Polyurethane Burns have highlighted the effects of the internal ventilation conditions, burn room size and rate of burning on the venting flames. These aspects affect the external temperature and heat flux measurements, as well as the reach of the venting plume on the external wall and window directly above the room of fire origin. Summaries of PU1 to PU4 are given in Table 4.10. Included in this table are the environmental conditions, such as wind speed and direction, and ambient temperature recorded for each of the tests. Also included are the fuel load, ventilation conditions, room and window configurations and the time to initial glass cracking of W102, the burn room window. The conclusions regarding these aspects are discussed next, along with the temperature and heat flux results.

Table 4.10: Summary of information gathered for the Polyurethane Burns. Note BR = Burn Room

POLYURETHANE BURNS					
Test	Environmental Conditions	Fuel Load (kg)	Ventilation Conditions	Burn Room/Window Configuration	Time to Glass cracking of W102
PU1	WNW @ 4.22 m/s 23.1°C	17.78	Closed: D1, D9, D5, W101 & W102 Open: D2 Class 2	Standard BR Standard Window	3 min 17 sec
PU2	ENE @ 2.53 m/s 26.5°C	16.02	Closed: D5, W101 & W102 Open: D1, D2 & D9 Class 1b	Standard BR Standard Window	3 min 10 sec
PU3	ENE @ 3.72 m/s 15.4°C	15.06	Closed: D9, W101 & W102 Open: D1, D2 & D5 Class 1a	Standard BR Alternative Window	3 min 12 sec
PU4	NNE @ 2.98 m/s 15.4°C	16.22	Closed: D5, W101 Open: D2, D1 & D9 Class 1b	Large BR Standard Window	2 min 30 sec Window lowered

These tests were carried out on days without consideration given to WIND SPEED or DIRECTION. Consequently, given the test-to-test variation in wind, it was difficult to quantify the impact of wind on the venting plume/flame. However, tilting of the venting plume was observed during each of the tests. As a result, flames missed the 2D thermocouple rack which was positioned in the centre above the burn room window. Therefore, temperature measurements and subsequent comparisons based on centre-line temperatures were affected, as discussed below. From a repeatability point of view, tests needed to be carried out on days when wind effects were minimal.

The effect of the internal VENTILATION CONDITIONS on the venting flames can be seen from the vertical temperature distributions and heat flux results. For PU1, the door leading to the corridor, D1, was closed. As a result, the temperature and heat flux histories had broader peaks, as all combustion products vented through the window alone. The corresponding temperature and heat flux results for PU2 and PU3 showed narrower peaks. This result can be attributed to the combustion products being able to vent through both D1 and W102, the burn room window, once it failed. This trend is also matched in PU4 results. Hence, Class 1 (PU2 to PU4) and Class 2 (PU1) ventilation conditions lead to different external temperature and heat flux patterns. However, with the limited data available, it was not possible to distinguish between Class 1a (PU3) and Class 1b (PU2 and PU4) ventilation conditions. This distinction is revisited in *Section 5.2*.

With all tests having approximately the same FUEL LOAD, the slight differences in burning rate can be linked to the ventilation conditions and the SIZE of the BURN ROOM. PU2 and PU3 were carried out in the standard burn room, and they had the same ventilation condition (door to the corridor open). As a result, the CEF averaged burning rates were the same. While for PU1, also carried out in the standard burn room, the burning rate was slightly lower given that the door to the corridor, D1, was closed, restricting the flow of air into the room. However, for PU4, the larger burn room resulted in a the fastest burning rate, given the greater volume of air in the room, along with the burn room door being open.

Total heat flux measurements were taken during all of the Polyurethane Burns. However, only during PU4, radiative measurements were taken. Consequently, ignition of certain target fuels via radiation can only be assessed against the measurements taken during PU4. During PU4, the maximum radiation constituted 56% of the maximum total measured heat flux. A peak radiative heat flux of 9kW/m^2 was measured at the bottom centre of W1M02, the window directly above the burn room window, W102. The positioning of the radiometer at the bottom of W1M02 was with the intent of establishing the amount of radiation impinging on the second floor window, with respect to SECONDARY FIRES. As discussed previously, the glass in W1M02 cracked for the first three PU tests, and glass was dislodged only during PU1. If it is assumed that either curtain material or loose papers were located behind

this window, then ignition due to radiation alone of these items is not expected. However, a secondary fire could have been possible in the floor above the burn room due to direct flame contact, because flames were observed to cover the mezzanine floor window (W1M02) especially during PU1.

The time to INITIAL CRACKING of the glass in the burn room window, W102, was within the 3rd minute after ignition of the foam slab for all of the tests except PU4, where the window was lowered (see Section 4.4). For the first three PU tests, the small variation in this time was within the bounds of experimental variability, and as such, no specific conclusions can be drawn as to the effect of ventilation conditions on the times to initial cracking, regardless of window configuration. In addition, this result indicated that the commercially available standard glass used in this series of tests showed similar time to initial cracking.

The ALTERNATIVE WINDOW ARRANGEMENT (see Figure 3.4) used in PU3 did not have a significant effect on either the development of the fire or the external measurements taken. This arrangement only caused the venting flames to emerge from both sides of the window, while the overlap of glass remained intact. The overlap in the glass did eventually fail during the fully developed phase of the fire, after which the flames vented from the entire length of the opening, as with the STANDARD window arrangement.

CRACKING of the GLASS in W1M02, the window directly above the burn room window, occurred during the first three polyurethane tests. Only during PU1 was the glass actually dislodged. During PU4, no cracking of the glass in W1M02 occurred. With the window being the only opening in PU1, all products of combustion vented through it. As a result, a broader temperature peak occurred for PU1, compared to PU2 and PU3. The longer exposure of W1M02 to high temperatures during PU1, due to the ventilation conditions, resulted in glass dislodgment within approximately 4 minutes after the failure of the burn room window.

Results from the first three flashover fires, PU1 to PU3, provided a 2D cross-section of the plume as it vented from the burn room window, W102. Analysis of the temperature contours across this grid indicated that the plume vented out of the burn

room window and travelled up along the external wall. The path of and temperatures within the venting plume were then studied further during PU4, when a 3D thermocouple grid was constructed. Temperature contours of the entire 3D external grid highlighted that any tilting of the plume resulted in the plume missing the centre plane (corresponding to the 2D thermocouple rack) and valuable information being lost. As a result, during this series of tests, the CENTRE-LINE TEMPERATURES calculated with Law's correlations over-estimated those measured. However, the visually observed flame shapes and the predicted FLAME ENVELOPE, also based on Law's correlations, were found to be comparable. These comparisons are valuable in determining the applicability of Law's correlations developed using mainly wood crib fires, to polyurethane fires.

EXCESS FUEL FACTOR was used in an attempt to quantify external flaming. This factor was determined to be negative during this series of tests, even though external flaming was observed. While it is possible to have external flaming with a small negative excess fuel factor based on other experimental works, there is a lack of experimental evidence to validate the excess fuel factor correlation with the data from the PU tests of the present work.

HEAT FLUX CALCULATIONS were carried out using equations developed by Oleszkiewicz to determine the heat transfer from a window fire plume to the external facade of a building. However, the expression for the convective heat transfer coefficient is more suited for fuels which burn at a moderate rate, such as wood cribs, rather than polyurethane. In addition, as iterated above, due to tilting of the external plume, lower temperatures were recorded along the centre-line above the burn room window than along the true centre-line of the plume, resulting in lower calculated radiative heat flux. As such, when a comparison was made between the measured and calculated total heat flux on the external wall, the calculations were found to significantly underestimate the possible heat transfer from the venting flames to the external wall.

In summary, these tests highlighted the need to have similar ventilation class experiments to determine whether or not the results were repeatable. As a result, several factors needed to be considered. Firstly, by having repeat tests, any

inconsistencies in the measured results could be addressed. Secondly, these tests needed to be carried out on still days to minimise the uncontrollable effect of wind. Thirdly, the randomness of glass breakage needed to be eliminated. Fourthly, the continued use of the 3D external thermocouple grid increased the amount of information collected, ensuring minimal loss of important data. Fifthly, the failure and dislodgment of the window above the burn room window, highlighted the need to investigate the likelihood of secondary fires. Finally, by using a more realistic fuel source, it would be possible to obtain more realistic results which would be valuable for future performance based code development and computer model validation. No attempt was made to develop curve fits to the experimental data obtained during the polyurethane tests, because it was not possible to determine if the results were repeatable.

5. REAL FURNITURE BURNS - DISCUSSION OF RESULTS

5.1 INTRODUCTION

The experience gained from the Polyurethane Burns was applied to the Real Furniture Burns, as discussed in the *Introduction*. The eight Real Furniture Burns were designed to mimic real life fire scenarios. The contents of the room and its size were representative of a typical lounge or living room. The door and window were either opened or closed to create a Class 1 ~ through-draft condition, or a Class 2 ~ no-through draft condition. Instrumentation for the Real Furniture Burns was similar to the Polyurethane Burns. Generally, temperatures and total heat flux measurements were taken inside the burn room, along with mass loss data, concentrations of O₂, CO₂ and CO and velocity down the centre of the burn room door. Externally, heat flux transducers were placed above the burn room window (W102) and at the window above it (W1M02). The 3D external thermocouple grid, positioned above the burn room window enabled the temperature field in the venting plume to be mapped in detail.

This Chapter details the effect of the ventilation conditions on the venting plume, beginning with a discussion on Ventilation Classes in *Section 5.2*. This section is followed by the re-iteration of the Consistent External Flaming (CEF) period provided in *Section 5.3*. Tests are grouped into their respective ventilation classes and analysed in terms of temperature contours in *Section 5.4*. In *Section 5.5*, these Class distinctions and CEF averaging are used as a means to compare similarly ventilated tests to determine the repeatability of the experimental data. *Section 5.6* and *Section 5.7* cover respectively the plume characteristics, in terms of flame envelope and centre-line temperature, and the possibility of secondary fires through direct flame contact and radiative heat transfer. In *Section 5.6*, experimental results are compared with empirical approximations of plume centre-line temperature and heat flux. In *Section 5.8*, the results of Burn 3 are compared with those of Burn 4 in relation to wind effects as higher than expected winds during Burn 3 significantly altered the venting plume, compared to its original repeat case, Burn 4. Burn 1 to Burn 3 are discussed with respect to plume swirling in this section. Also discussed is the bowing of the burn room window and the related effects of the Smoke Management

System which was activated during Burn 6 and Burn 7. Conclusions reached at the end of this series of tests are presented in *Section 5.9*.

As indicated in Chapter 1, *Introduction*, and Chapter 4, *Polyurethane Burns*, the author designed and set up the external components of the Real Furniture Burns. In addition, she made major contributions to the design of the internal setup and execution of the series. Due to the experience she had gained during the Polyurethane Burns, the results of this chapter are more conclusive than those of Chapter 4.

For easy reference to internal instrumentation and burn room configuration, external instrumentation consisting of the 3D thermocouple grid and heat flux transducer locations, fuel load, environmental conditions and ventilation conditions of the Real Furniture tests, a foldout is given (Foldout 2) after the Appendices. Foldout 2 contains Figure 3.14, Figure 3.19, Figure 3.20, Table 3.5 and Table 3.6. Wherever these figures and tables are referred to in Chapter 5, they are accompanied by an asterisk.

5.2 VENTILATION CLASSES AND THE VENTING PLUME

In this study, three pairs of real furniture tests have been categorised into three ventilation classes - Class 1a (Burn 1 and Burn 2), Class 1b (Burn 5 and Burn 8) and Class 2 (Burn 4 and Burn 7). Each pair consisted of the particular two tests that had been designed to repeat each other within a given ventilation class. It was necessary to divide Class 1 into two sub-classes to take into account the differences in the internal ventilation conditions of the building, caused by the stairwell door (D9) being closed or open. Table 5.1 contains a summary of the fuel loads, window lowering criteria, environmental conditions and class specifications for the Real Furniture Burns. The pairs of tests corresponding to each class are summarised in Table 5.2 to Table 5.4. In these tables, the event history of each test is given. Ignition, burn room window cracking, window lowering, opening or failure, flashover, beginning of CEF, cracking or dislodgment of the Floor 1M window, end of CEF and termination times are listed.

Results of Burn 3 and Burn 6 are not included here. In the case of Burn 3, unexpectedly high wind during the test caused increased air entrainment, resulting in lower external temperatures, and Burn 6 did not develop to flashover due to the activation of the air handling system of the building. In Table 5.2, the time scale of Burn 1 was shifted to make the window opening time coincide with the window lowering time of Burn 2. This point is revisited in *Section 5.5*. Of the Class 1b tests, Burn 8 included combustible lining in the corridor. Externally, the only effect of the additional fuel was a slightly longer CEF period than that of Burn 5 (internally, other effects, such as higher temperatures and increased smoke in the corridor and upper floors and the maximum heat release rate in the burn room of the series, were observed as described in Alam and Beever[102]). Of the Class 2 tests, during Burn 7, the smoke management system (SMS) was activated in the building. Externally, the SMS activation did not affect the CEF averaged and non-dimensionalised temperature contours as described in *Section 5.4* and *Section 5.5*. The effect of SMS is discussed in *Section 5.8.3* with respect to ventilation condition and facilitation of flashover.

Table 5.1: Summary of fuel load, environmental conditions, WLC and Class specifications, based on Table 3.5* and Table 3.6*.

		Wood Equivalent Fuel Load Density (kg/m ²)	Window Lowering Criteria	Ambient Temperature (°C)	Average Wind Speed (m/s)	Wind Direction
Class 1a	BURN 1	26.36	Opened	15.4	1.5	ENE
	BURN 2	28.05	WLC # 1	12.1	1.6	SSE
Class 1b	BURN 5	28.21	Failed	8.3	2.1	W
	BURN 8	28.48	WLC #1	8	1.3	NNW
Class 2	BURN 4	28.32	WLC #2	11	1.6	NE
	BURN 7	27.95	WLC #1	7.7	1.2	SW

Table 5.2: Class 1a event/time histories. When an event is specific to a given test, the test number is as stated in bold and italic. *The time line was reset to 5:25 minutes for Burn 1 when the window was opened to coincide with Burn 2's window lowering time.

Event	Burn 1	Burn 2
Ignition	00:00	00:00
flames spread out and up the back of the couch	the glass cracked	2:15
smoke layer reaches the top of the window (0.4m from the ceiling)	8:25 minutes after	3:30
the centre pane of the window bows significantly	ignition, smoke	4:25
initial crack in the centre of burn room window (W102)	filled room, no	4:40
smoke reaches seat of couch (1.95m from the ceiling)	glass dislodgment	5:00
smoke level falls below bottom ledge of window/reaches floor	caused fire to die	5:20
Window OPENED/LOWERED and smoke vents from the opening	5:25*	5:25
flames reach beyond the opening	6	6:20
remanding glass in W102 dislodges - <i>Burn 1</i>	10	
flashover: where burn room temperatures reach approximately 600°C	13	7:20
flames reach on average between F3-4 and up to L3	15	9
beginning of CONSISTENT EXTERNAL FLAMING - <i>Burn 2</i>		11:25
flames reach out to F2-4 and up to L4 - <i>Burn 2</i>		15
time of greatest mass loss rate	16:45	15
beginning of CONSISTENT EXTERNAL FLAMING - <i>Burn 1</i>	18:40	
flames reach out to F2-4 and up to L4 - <i>Burn 1</i>	20	
initial dislodgment of the Floor 1M window	na	16:10
more/most of remaining glass in the Floor 1M window is dislodged	25	na
end of CEF	26:40	16:25
strength of external flames begins to lessen	27	17:25
interior of burn room becomes clearly visible	28	17:30
only small flames vent from the opening, mainly hot gases	28	19:30
contents in the room continues to burn/smoulder away	30	20
test is terminated	32	32

Table 5.3: Class 1b event/time histories. When an event is specific to a given test, the test number is as stated in bold and italic.

Event	Burn 5	Burn 8
Ignition	00:00	00:00
flames spread out and up the back of the couch	1:00	1:00
smoke layer reaches the top of the window (0.4m from the ceiling)	2:50	3:30
smoke fills upper half of the room	3:35	-
initial crack in the centre of burn room window (W102)	5:15	4:40
more cracking of the burn room window	5:47	-
smoke level falls below bottom ledge of window/reaches floor	6:10	5:00
dislodgment of centre pane in W102	6:35	-
WINDOW LOWERED and smoke vents from the opening - <i>Burn 8</i>	na	5:30
remaining glass in middle pane of W102 is dislodged	7:55	na
flames reach beyond the opening	7:55	5:45
flashover: where burn room temperatures reach approximately 600°C	9:00	7:50
beginning of CONSISTENT EXTERNAL FLAMING - <i>Burn 8</i>		8:30
initial dislodgment of the Floor 1M window	11:05	9:45
flames between F3-4 and up to L1-3 for Burn 5 and L3-4 for Burn 8	11:15	10
beginning of CONSISTENT EXTERNAL FLAMING - <i>Burn 5</i>	11:35	
flames reach out to F1-3 and up to L4-5	12	11
time of greatest mass loss rate - <i>Burn 8</i>		12:45
more/most glass in the Floor 1M window is dislodged	12:40	14:10
time of greatest mass loss rate - <i>Burn 5</i>	14:50	
end of CEF - <i>Burn 5</i>	17:35	
interior of burn room becomes clearly visible	18:50	14:15
smoke reaches Floor 3 - <i>Burn 8</i>		15
end of CEF - <i>Burn 8</i>		15:55
Floor 3 corridor is filled with smoke - <i>Burn 8</i>		17
contents in the room continue to burn/smoulder away	21	18
test is terminated	29	54

Table 5.4: Class 2 event/time histories. When an event is specific to a given test, the test number is as stated in bold and italic.

Event	Burn 4	Burn 7
Ignition	00:00	00:00
Cushion burning well, flames spread out and up its back - <i>Burn 7</i>		2:00
smoke management and stair pressurisation systems are activated	na	2:23
smoke layer reaches the top of the window (0.4m from the ceiling)	0:55	–
smoke reaches couch seat (1.95m from ceiling) and thinly fills room	2:10	3:20
Cushion burning well, flames spread out and up its back - <i>Burn 4</i>	3:00	
the centre pane of the window bows significantly	na	3:30
initial crack in the centre of burn room window (W102)	4:55	3:45
smoke level falls below bottom ledge of window/reaches floor	6:40	4:20
WINDOW LOWERED and smoke vents from the opening	9:35	4:55
flames first appear again after WLC#2 instigated - <i>Burn 4</i>	10:10	na
flames reach beyond the opening	11:50	5:45
flashover: where burn room temperatures reach 600°C ⁺	13	6:19
initial crack in the Floor 1M window	12:50	6:35
initial dislodgment of the Floor 1M window - <i>Burn 7</i>		8:20
flames reach on average between F3-4 and between L2-4	13:30	9:00
beginning of CONSISTENT EXTERNAL FLAMING	15:45	9:55
flames reach as high as L5-6, out to F2-3 and beyond P1-P5 planes	14:30	10:45
initial dislodgment of the Floor 1M window - <i>Burn 4</i>	13:20	
remaining glass in the Floor 1M window is dislodged	17:15	12:40
time of greatest mass loss rate	18:50	13:50
strength of external flames begin to lessen a little	22	14:30
interior of burn room becomes clearly visible	22	–
end of CEF period - <i>Burn 7</i>		15:55
contents in the room continue to burn/smoulder away	23	16:00
end of CEF period - <i>Burn 4</i>	23:45	
only small flames vent from the opening, mainly hot gases	–	17:00
top left hand corner of the Floor 2 window (W202) is dislodged	25:10	–
test is terminated	32	24

The following photographs in Figure 5.1 to Figure 5.6 were taken during Burn 7 and Burn 8. In sequence, these pictures represent the development of a fire as observed from outside. In Figure 5.1, the bowing of the centre pane of the burn room window is illustrated during Burn 7. Figure 5.2 to Figure 5.6 show snapshots of the growth, flashover/full-developed phase and decay of the fire. Similar photographs were obtained for all other tests, in addition to video records of both side and front views of the plume.

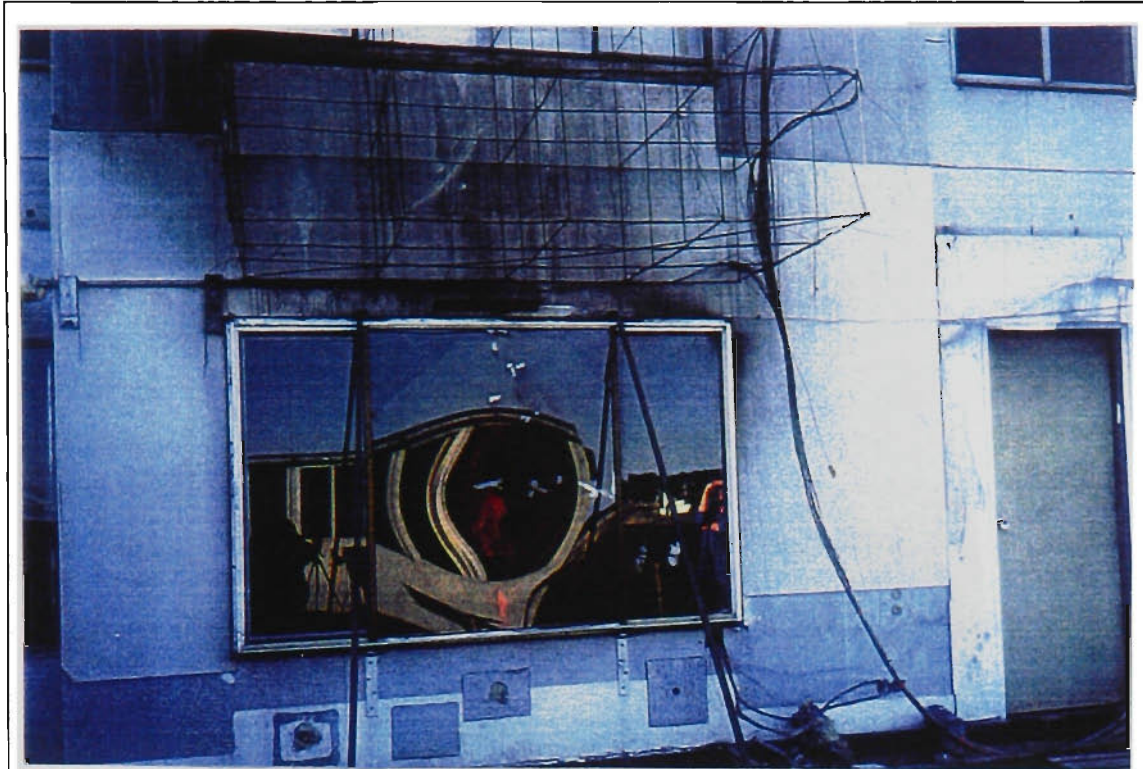


Figure 5.1: Bowing of the burn room window at approximately 3½ minutes after ignition during Burn 7 (just prior to window failure).



Figure 5.2: Growth at approximately 3½ minutes after ignition during Burn 8.



Figure 5.3: Growth phase, side view, at approximately 6½ minutes after ignition during Burn 8.

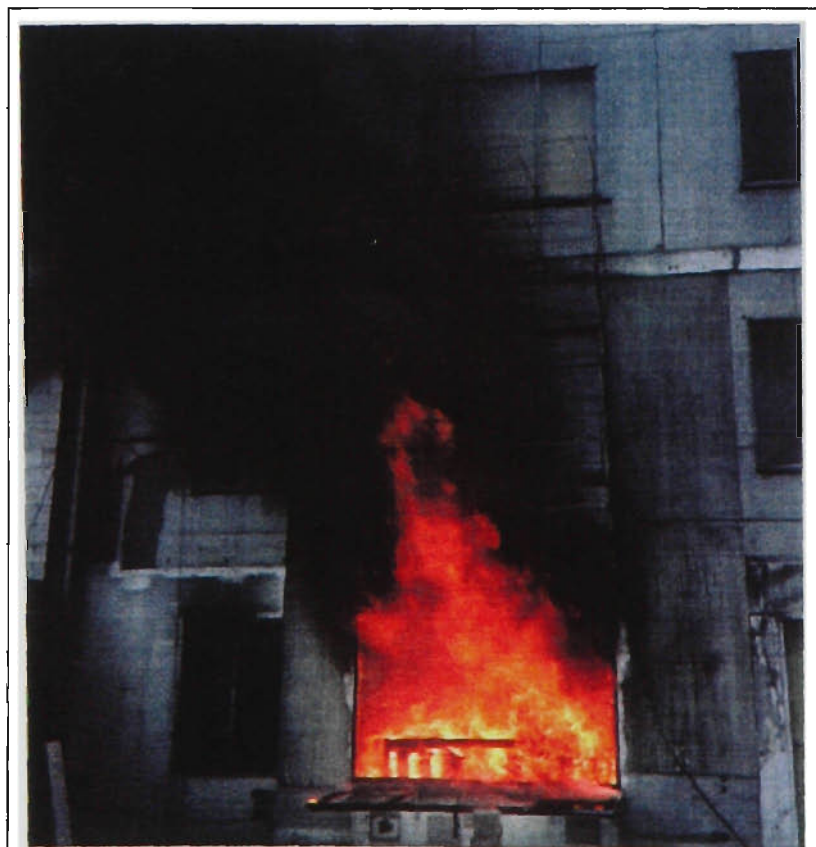


Figure 5.4: Fully developed phase, front view, at approximately 8 minutes after ignition during Burn 8.



Figure 5.5: Fully developed phase, side view, at approximately 8 minutes after ignition during Burn 8.



Figure 5.6: Decay at approximately 14 minutes after ignition during Burn 8.

To illustrate the differences between the ventilation conditions of Class 1a and Class 1b tests, Burn 2 and Burn 5 have been selected, respectively. The stairwell door (D9) was closed for Burn 2, and it was open for Burn 5. Figure 5.7 and Figure 5.8 show the air velocities during Burn 2 and Burn 5, respectively, measured at different heights above the floor at the burn room door. There was a greater volume flow rate of smoke (air/hot gases) leaving the burn room during Burn 5 compared to Burn 2, as indicated by the higher out flow (negative) velocities measured in Burn 5. The CEF averaged velocities from 2000mm to 250mm above the floor in the middle of the burn room door were -0.4, -3.2, -2.4, -1.4, -0.73, 0.7, 1.54 and 1.83m/s during Burn 5; and -2.0, -2.4, -1.7, -0.6, 0.83, 1.21, 1.77 and 1.89m/s during Burn 2. The first of these velocity readings was from a bi-directional probe located at the top of the burn room door. The following readings were from probes spaced at 250mm intervals, the last one being located 250mm above the floor. Taking a fractional door area of 0.25m x 0.82m (the door width) around each of these probes, with the exception of the first and the last ones, and assuming that the measured velocity was a representative average for the corresponding strip of area, volume flow rates of $-0.60\text{m}^3/\text{s}$ and $0.19\text{m}^3/\text{s}$ were calculated for Burn 5 and Burn 2, respectively. Around the first probe, an area of $(0.25\text{m}/2)\times 0.82\text{m}$ was taken, and for the last probe, an area of $(0.25\text{m}/2 + 0.25\text{m})\times 0.82\text{m}$ was used. The increased flow of smoke out of the burn room during Burn 5 was also matched by higher temperatures measured in the centre of the corridor and at the stairwell door (D9) during Burn 5 compared to Burn 2. These maximum temperatures were 550°C and 151°C , respectively, for Burn 5 and 408°C and 17°C , respectively, for Burn 2[102]. The higher rate of smoke outflow and the resulting higher gas temperatures in the corridor and at the stairwell door during Burn 5 can be attributed to the stairwell door's being open.

In Figure 5.9 and Figure 5.10, CEF averaged and non-dimensionalised temperature contour plots are given of Burn 2 and Burn 5 along the centre plane of the plume. In these figures the 'belly' of the plume is more pronounced for Burn 5 as compared to Burn 2. During Burn 1 and Burn 2, the burn room and stairwell doors were open and closed, respectively. During Burn 5 and Burn 8, these doors were both open. While direct wind was present only during Burn 1 and Burn 2 (as described in *Section 5.8*), the more pronounced bellying of the temperature contours during Burn 5 and Burn 8 may be attributed to the absence of direct wind and different internal ventilation conditions caused by the open stairwell door.

Consequently, the distinction between Class 1a and Class 1b tests can be linked directly to the difference in the internal ventilation conditions of the building caused by whether the stairwell door was open or closed. However, it has been recognised that it was not possible to distinguish between the contributions of wind and internal ventilation conditions to the observed effects.

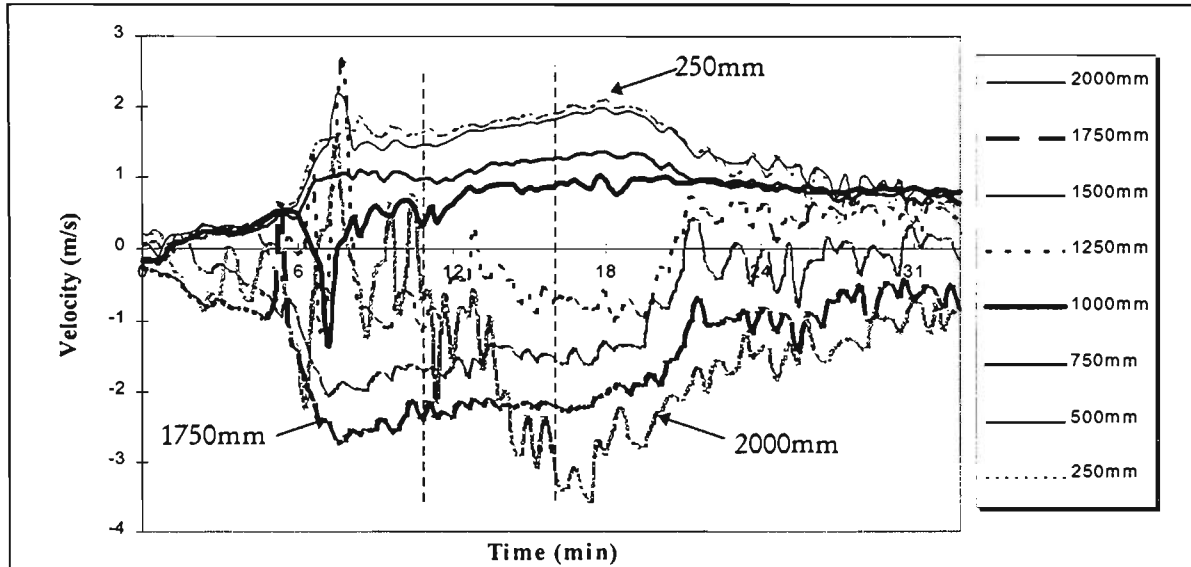


Figure 5.7: Velocity histories at the centre of the burn room door and at the indicated heights above the burn room floor for Burn 2. Negative velocities imply flow out of the burn room door. Bi-directional probe readings were temperature compensated. The dashed lines mark the beginning and end of CEF. The unmarked velocity curves, follow the descending order given in the legend with respect to the height above the floor.

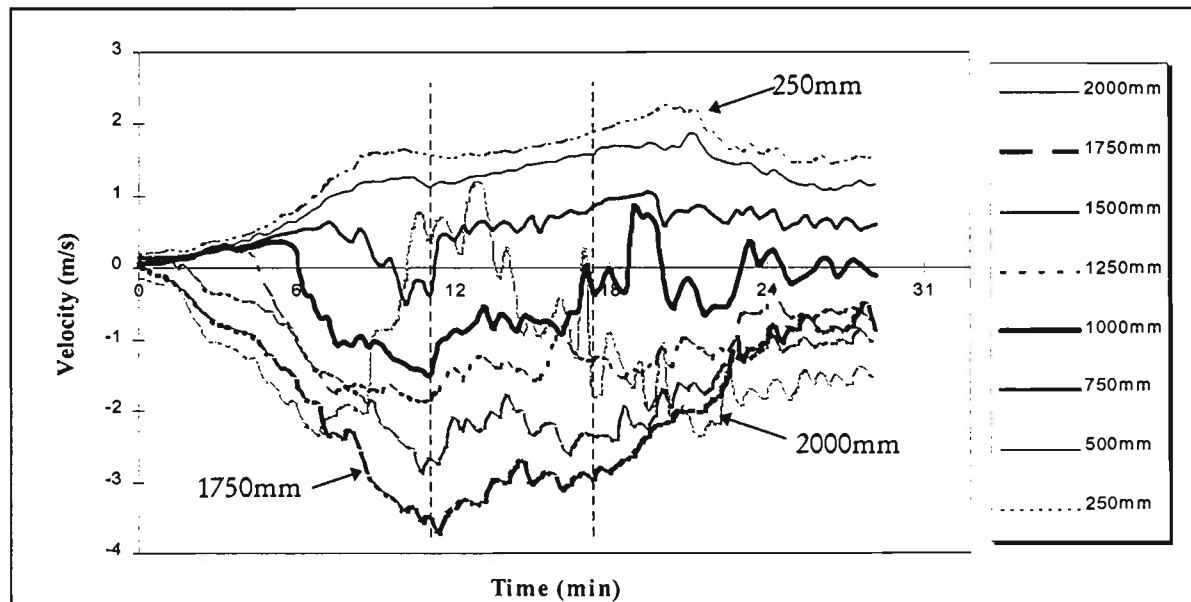


Figure 5.8: Velocity histories at the centre of the burn room door and at the indicated heights from the burn room floor for Burn 5. Negative velocities imply flow out of the burn room door. Bi-directional probe readings were temperature compensated. The dashed lines mark the beginning and end of CEF. The unmarked velocity curves, follow the descending order given in the legend with respect to the height above the floor.

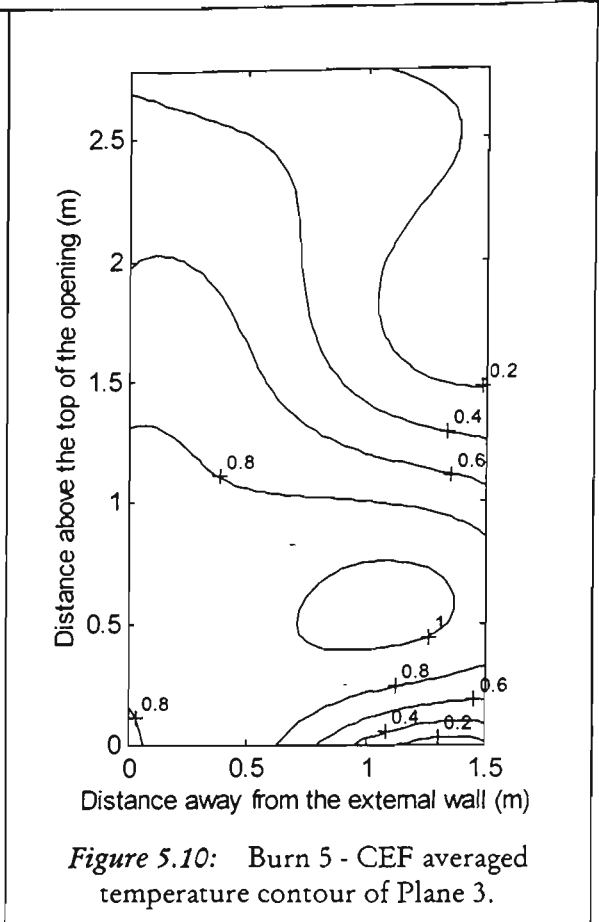
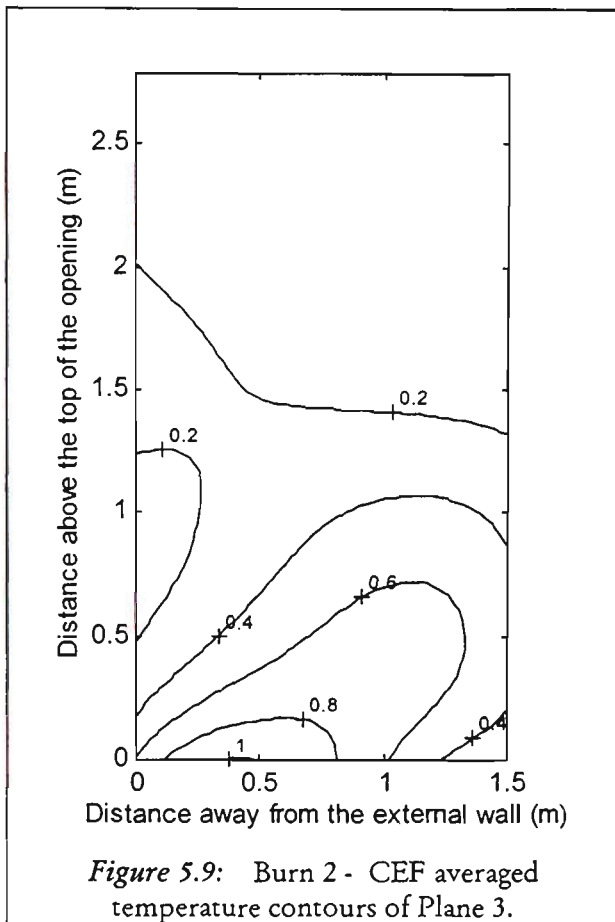


Figure 5.9: Burn 2 - CEF averaged temperature contours of Plane 3.

Figure 5.10: Burn 5 - CEF averaged temperature contour of Plane 3.

5.3 CONSISTENT EXTERNAL FLAMING (CEF)

With respect to externally venting flames, the period of time over which the data were averaged has been specified as the Consistent External Flaming (CEF) period. This period was established to take into account the portion of the fully developed fire where externally, strong consistent flames existed. Consequently, grouping of similar test data was also carried out in accordance with specific internal ventilation conditions of the building, such as whether the burn room door was open or closed. These conditions had a significant effect on the growth and development of the fire and were essentially the only significant parameters altered during the course of the tests.

As an example, the following description details the method used to determine the CEF period for Burn 2. The same approach was used to determine the CEF period of each test. For Burn 2, the upper layer temperature in the burn room reached 600°C, 7:20 minutes after ignition as marked in Figure 5.11. It is convenient to use this point in time as the onset of flashover. Even though external temperatures in excess of 600°C were also measured at this time, as shown in Figure 5.12 at Plane 3/Face 2/Level 1 ($x=1.2\text{m}$, $y=0\text{m}$, $z=0.5\text{m}$), as flames began to reach beyond the window opening, they were still intermittent. Continued observations of the test indicated that the onset of CEF occurred between when the external temperatures reached 600°C and when all the items in the room began to combust, as observed by a sudden surge of flames from the opening, approximately 11:25 minutes after ignition. The surge of flames occurred during the transition phase, flashover, and external flaming continued during the fully developed phase of the fire. This surge from the opening occurred shortly after an increase in mass loss, leading to the time of the greatest mass loss rate. The transition of flashover and beginning of CEF are marked in Figure 5.12. As shown in Figure 5.13 for Burn 2, the rate of mass loss began to increase at 11:25 minutes, marking the start of CEF. The mass loss rate peaked at approximately 15 minutes and CEF ended approximately 5 minutes after it had begun when the quasi-steady nature of the venting flames ended. The time of flashover as determined by 600°C in the room and these three stages, the beginning of CEF, the occurrence of maximum mass loss and the end of CEF, are marked in Figure 5.13. Therefore, by combining the observed behaviour of external flames with the mass loss data, the duration of CEF can be specified. The CEF period for each test is listed in Table 5.5.

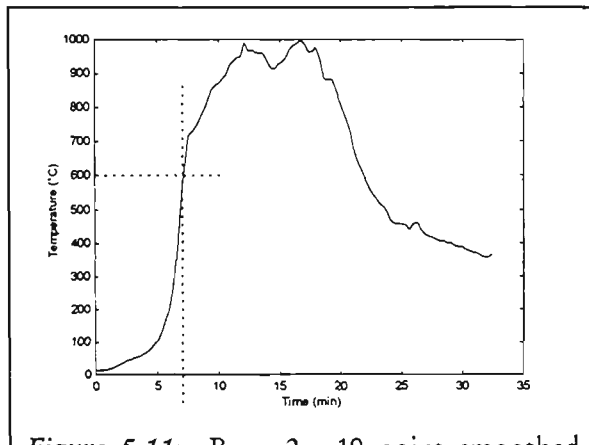


Figure 5.11: Burn 2 - 19 point smoothed upper layer temperature. The dashed line marks the beginning of flashover in the burn room.

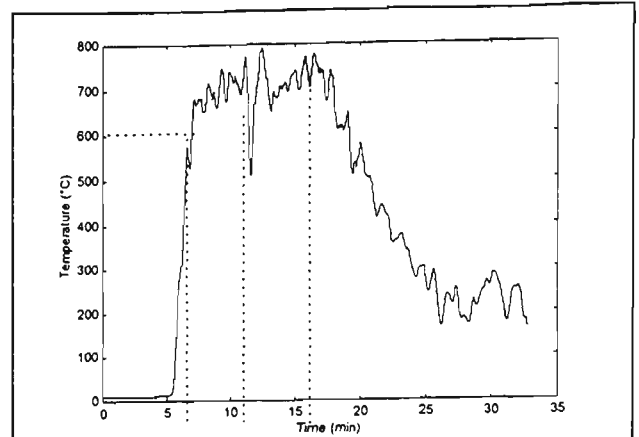


Figure 5.12: Burn 2 at $x = 1.2\text{m}$, $y = 0\text{m}$ and $z = 0.5\text{m}$ at grid location P3/L1/F2. The dashed lines mark the beginning of flashover in the burn room, beginning and end of CEF, respectively.

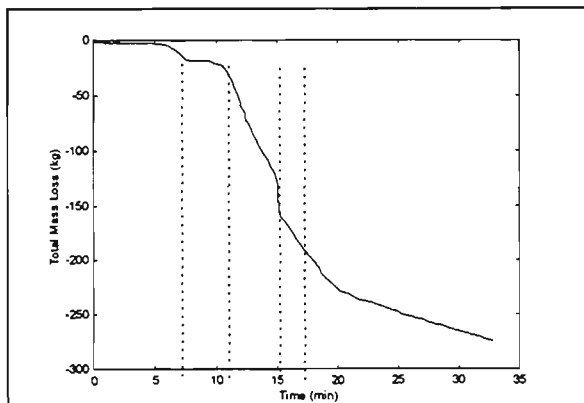


Figure 5.13: Burn 2 - 19 point smoothed Total Mass Loss. The dashed lines mark the beginning flashover and CEF, largest mass loss rate and end of CEF, respectively.

Table 5.5: Duration of CEF, T_{max} and T_{amb} used in non-dimensionalisation of the data.

	CEF Duration (min)	T_{max}	T_{amb}
BURN 1	8	913.5	15.4
BURN 2	5	810.9	12.1
BURN 5	6	949.9	8.3
BURN 8	7	978.2	8
BURN 4	8	978.8	11
BURN 7	6	865.7	7.7

To investigate further the temperature variations at a given location within the CEF period, Location P3/L1/F2 has been selected, following on from the temperature-time curve given in Figure 5.12. Figure 5.14 is a detail of Figure 5.12, illustrating the difference between the CEF averaged temperature for a given location (dashed line) and the instantaneous temperature data collected over the CEF period (solid line). At this grid location, the mean temperature is 712°C , during the CEF period. The average temperature difference between the instantaneous temperatures during CEF and the CEF averaged temperature, 712°C , is $\pm 52^{\circ}\text{C}$. The histogram given in Figure 5.15 shows that the occurrence of temperatures between these two limits, 660°C and 764°C , are high.

While it can be seen in Figure 5.14 that the temperature falls below 540°C close to the beginning of the CEF period at location P3/L1/F2, and that visible flames would not be present at this temperature, this is a rare occurrence as shown in Figure 5.15. This portion of the data is still included in the CEF period because at other locations within the 3D grid, external flames existed at this time.

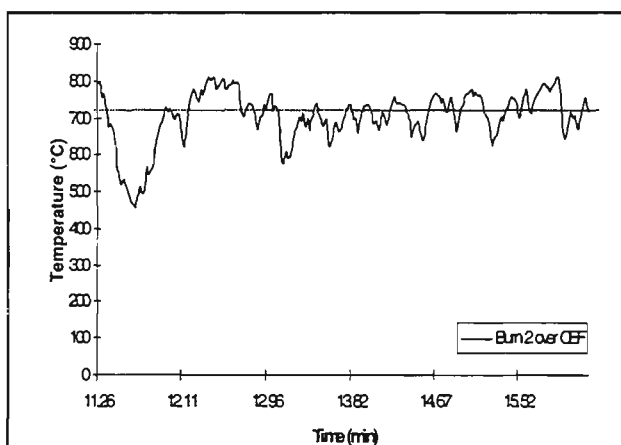


Figure 5.14: Temperature during the CEF period for Burn 2 at $x = 1.2\text{m}$, $y=0\text{m}$ and $z = 0.5\text{m}$, grid location P3/L1/F2. The dashed line marks the average temperature of 712°C used as the CEF averaged temperature for this location.

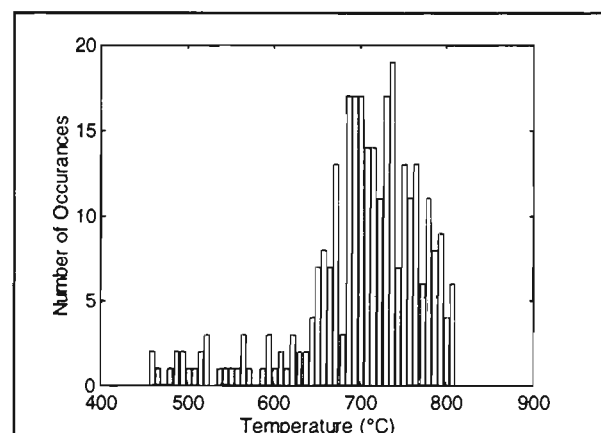


Figure 5.15: Histogram of the temperature data given in Figure 5.14 (collected during the CEF period of Burn 2 at $x = 1.2\text{m}$, $y=0\text{m}$ and $z = 0.5\text{m}$, grid location P3/L1/F2).

5.4 TEMPERATURE CONTOUR PLOTS

The temperature measurements from the selected grid sections marked in Figure 3.19 are reported in detail here. Levels 6 and 7 of the 3D external thermocouple grid were excluded from the discussion after observing that no additional information had been gained from them. Hence, only Levels 1 to 5 are included here for all tests. As indicated in *Section 5.3*, the temperature contours across these sections of the grid have been time averaged over CEF and non-dimensionalised with respect to the average ambient temperature and maximum external temperature during the corresponding CEF period. The ambient and maximum external temperatures used for non-dimensionalisation are listed in Table 5.5 for each test. For plotting, a third order spline fit was applied to the results. In this section, the CEF averaged and non-dimensionalised temperature contour plots from the following sections of the grid are presented in detail, in addition to discussing the overall (three-dimensional) temperature field within the venting plume as obtained from Level 1 to Level 5 measurements.

Plane 3 (P3): The centre plane of the grid perpendicular to the external wall. P3 was located between the top centre of the burn room window and the top of the Floor 1M window, and it extended 1.5m away from the wall. This Plane was chosen, because along this section of the wall, the effects of the venting plume were expected to be the severest. The existing data in the literature from full scale experiments correspond mostly to either Plane 3 or where Plane 3 intersects with Face 1 above the centre of the opening.

Face 1 (F1): This Face was located on the external wall, and it covered the 2.4m by 2.78m area of the external facade directly above the burn room window, W102. The width of F1, 2.4m, was the same as that of W102, and the window directly above at Floor 1M, W1M02. Face 1 extended to the top of W1M02. As Face 1 lied

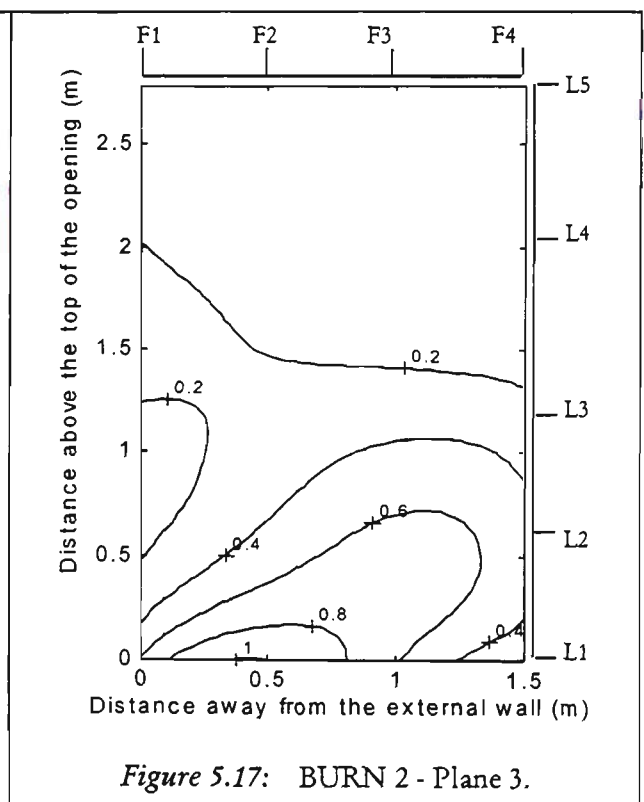
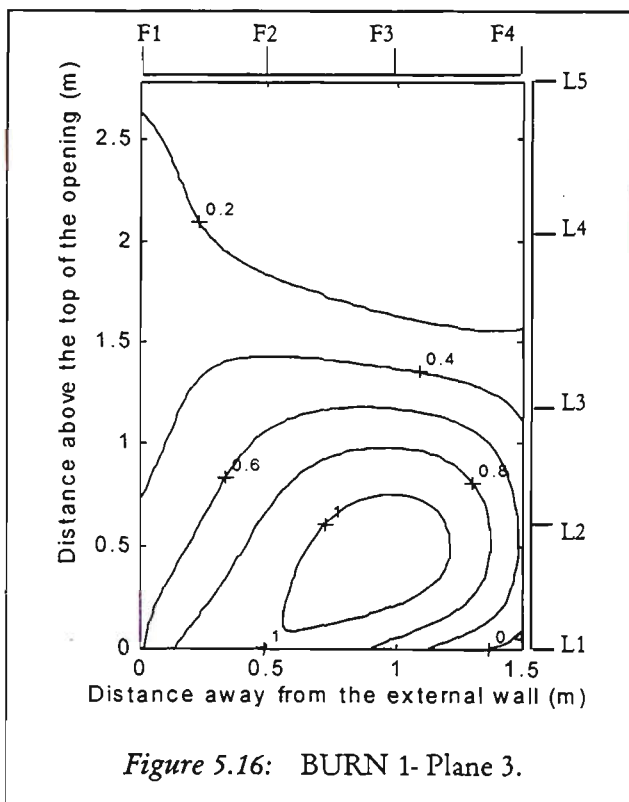
just above the burn room window, it gave an overall impression of the flames as they vented from the opening and travelled up along/beside the wall.

Level 4 (F4): This Level was at the centre of the Floor 1M window, W1M02, above the burn room window, W102, and it extended 1.5m away from the window. It was selected to illustrate the effects of the venting plume, with respect to secondary fires.

5.4.1 Ventilation Class 1a - Burn 1 & Burn 2

5.4.1.1 Plane 3

The temperature contour plots shown in Figure 5.16 and Figure 5.17 are for Plane 3 of Burn 1 and Burn 2 respectively. The contours for Burn 1 rise out from the bottom of the frame. The hottest region corresponding to the temperature contour of 1.0, is almost elliptical. This shape results from the almost 45° angle path the flames take as they emerge from the opening. Hence, a region of slightly lower temperatures forms just behind the core of the plume. The hot core lies approximately between 0.5m to 1m away from the wall or opening. As expected, the surrounding contour lines show a drop in temperature with increased vertical distance away from the opening, and horizontally beyond the core of the plume.



The temperature contours for Plane 3 of Burn 2 can also be seen to show trends similar to those of Burn 1. However, the hot core is not as developed, being hotter closer to the wall, covering a region from approximately 0.2m to 0.8m, just above Level 1. The 'follow on' from the hot core is also slightly more skewed than that of Burn 1, resulting in even lower temperatures on the external wall above the opening. Once

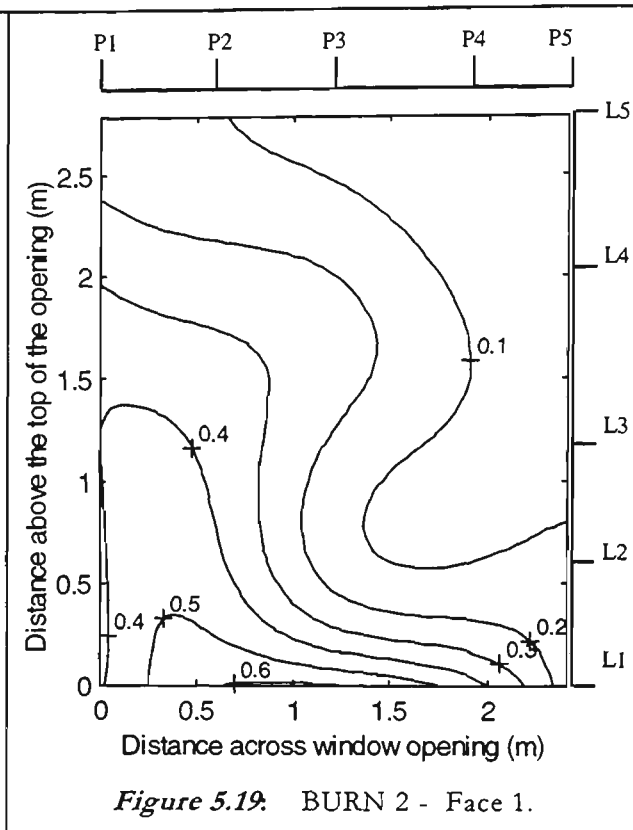
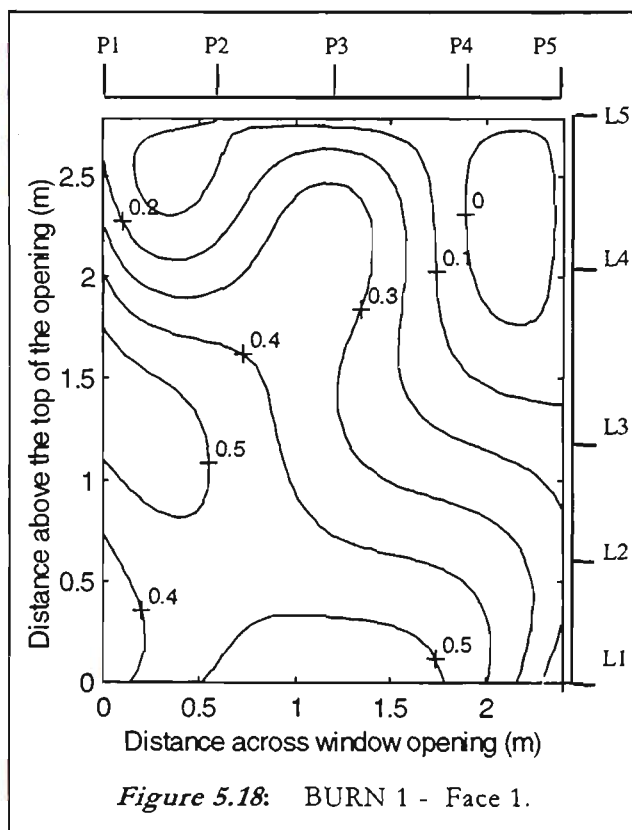
again, there is a decline in temperature with increased vertical distance. However, the drop is greater over a shorter distance. The skewness of the core has been attributed to the direction of the wind which came predominantly from the South-South-East during the course of Burn 2, as listed in Table 5.1. During Burn 1, the wind direction was primarily East-North-East. The building is positioned along the North-South cardinal axis, and the burn room window faces South as illustrated in Figure 3.10. Hence, a South-South-East wind during Burn 2, had a direct effect on the venting plume by pushing the core of the plume away from the wall, and increased air entrainment resulted in lower temperatures in the venting flames. During Burn 1, a side-ways East-North-East wind had a less direct effect on the venting plume, although the average wind speeds were comparable during both tests. The wind effects are discussed further in *Section 5.8*.

5.4.2.1 Face 1

The temperature contour plots shown in Figure 5.18 and Figure 5.19 are for Face 1 of Burn 1 and Burn 2, respectively. The contour plot of Burn 1 Face 1 also shows the drop in temperature with both vertical and horizontal distance. The hottest region starts at Level 1 and ends just below Level 2. Given that the venting plume tended towards the left (West), the temperatures at Level 1 are higher on the left side of the opening compared to the right, where a drop to 10% of the maximum temperature was recorded. Vertically, the temperature also decreased with increased distance away from the core. Moving up the wall, there is a drop to between 40% to 20% of the maximum temperature at Level 4, which corresponds to the centre of the Floor 1M window.

The overall impression of Face 1 of Burn 1 indicates a rather disorganised pattern of measured temperature, as the plume rises up the external wall. Initially, the plume tends to the left, over Level 1 to Level 3, before moving up, with the heat slowly dissipating with this rise. Before the plume centers itself again as it approaches Level 4, it cools off rapidly on both sides. The unique 'wave' pattern shown in Figure 5.19 was caused during Burn 2 by the swirling of the entire plume which vented from the top right of the opening and tended towards the left. The plume rotated clockwise with an

increasing diameter as air was entrained, and it moved across the grid to the left. The hotter under currents drew heat directly from the burn room. Up and away from the external facade, heat began to dissipate as more air was entrained into the venting plume. The swirling of the plume and subsequent 'wave' pattern were caused by a direct wind.



5.4.1.3 Level 4

The temperature contour plots shown in Figure 5.20 and Figure 5.12 are for Level 4 of Burn 1 and Burn 2, respectively. These images show that the flames tended predominantly to the left side of the opening, as also suggested in Figure 5.18 and Figure 5.19, resulting in a temperature gradient across the Floor 1M window which failed during both tests (Glass breakage is covered in *Section 5.7*).

The results from Burn 2 have been affected more by the wind speed and especially the direction compared to the other tests discussed here. This has manifested itself in the swirling of the external plume, in whole or in part during the course of these tests. The swirling of the plume was significantly greater during Burn 2 compared to Burn 1. The effect of wind on the plume can be advantageous in cooling the plume. Yet it may

also cause the plume to skew across the facade to other window openings or balconies, as discussed further in Section 5.8.

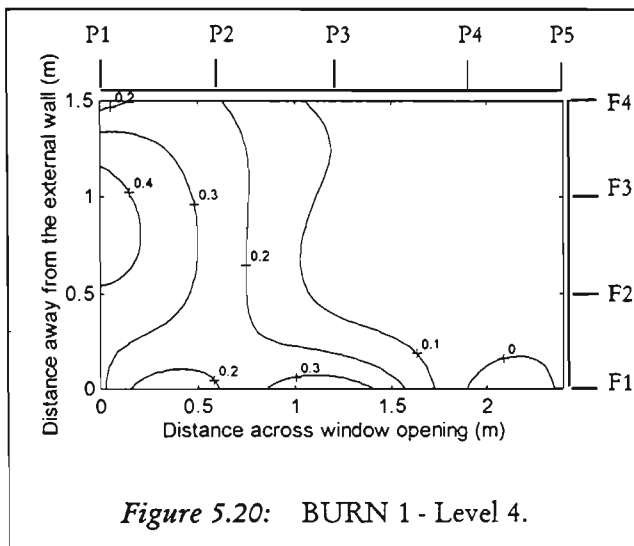


Figure 5.20: BURN 1 - Level 4.

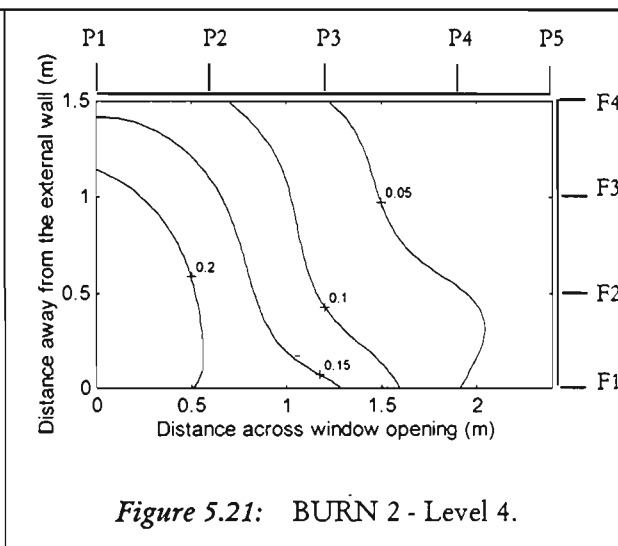


Figure 5.21: BURN 2 - Level 4.

5.4.1.4 Level 1 to Level 5

Figure 5.16 to Figure 5.21 show the Plane 3, Face 1 and Level 4 contour plots of Burn 1 and Burn 2. These plots were selected to give an indication of the flames as they emerged from the window opening. The same sections of the 3D grid, are expanded next in Figure 5.22 and Figure 5.23 which include the entire grid, from Level 1 to Level 5 to show the variation in temperature both across and within the venting plume. These dimensionless contours are also averaged over the CEF period, and they should be viewed as though one is standing in the burn room or in place of the building, rather than facing it (As indicated in Section 4.2.2, the reason for this view point is the available options in MATLAB for this type of presentation). The plume comes out of the opening across the lowest level (Level 1) and rises up through the upper levels (Levels 2 to 5). The temperature contour of 1.0 occurs in approximately the same location of Level 1 for both Burn 1 and Burn 2. However, as the flames travel upwards, they veer more quickly to the left of the grid with respect to an observer facing the building, from Level 2 to Level 5 for Burn 2. This difference has been previously attributed to a direct wind. The same trend is matched by a drop in temperature. At Level 2, the contour of 0.7 indicates a 30% drop of the maximum measured temperature at the ‘core’ between Level 1 and Level 2. This core continues as the 0.4 contour on Level 3 and as the 0.2 contour on Level 4. However, for Burn 1,

the hot core of the flames continues to rise up through the centre of Level 2, retaining the same intensity as Level 1, as indicated by the contour of 1.0. Once at Level 3, a 20% drop occurs, corresponding to the temperature contour of 0.8 which is followed by a significant drop at Level 4.

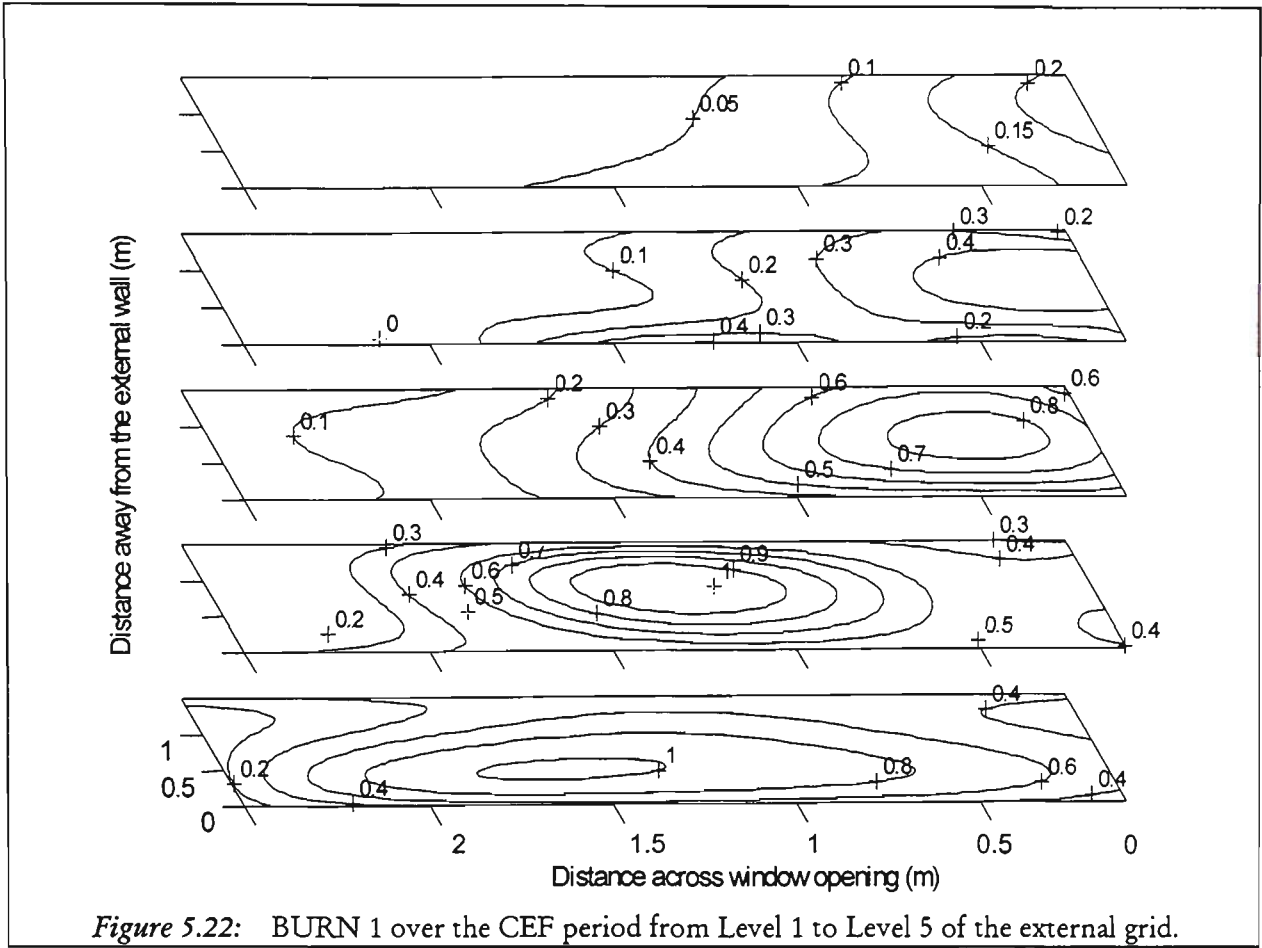


Figure 5.22: BURN 1 over the CEF period from Level 1 to Level 5 of the external grid.

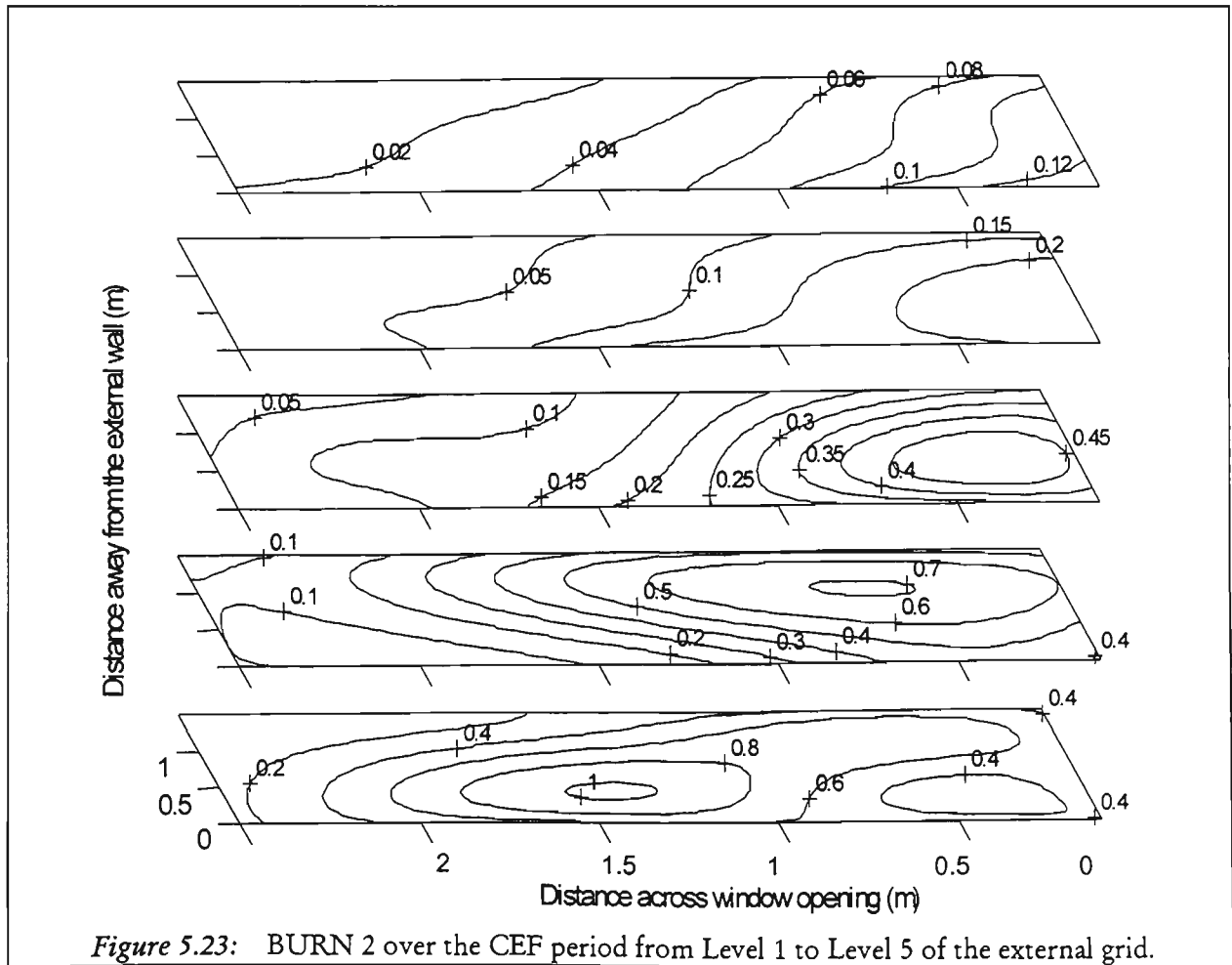


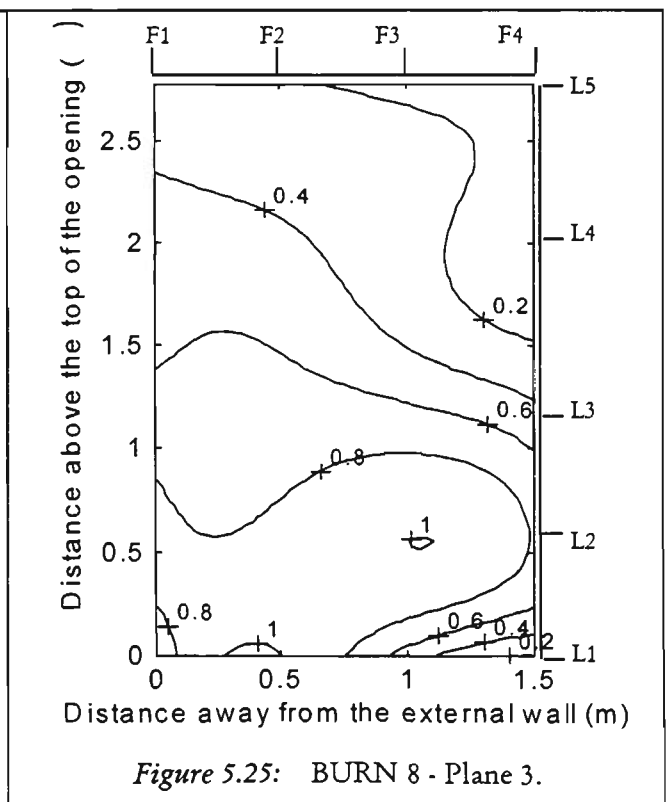
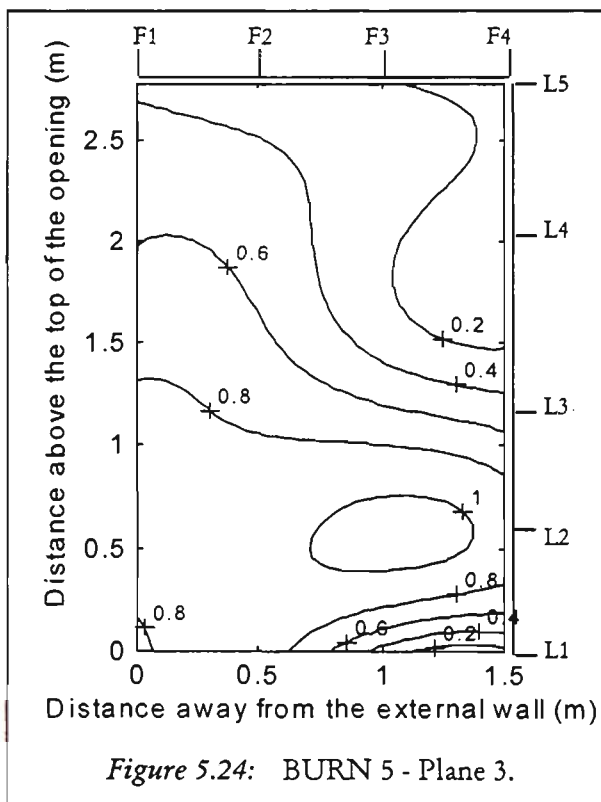
Figure 5.23: BURN 2 over the CEF period from Level 1 to Level 5 of the external grid.

5.4.2 Ventilation Class 1b - Burn 5 & Burn 8

5.4.2.1 Plane 3

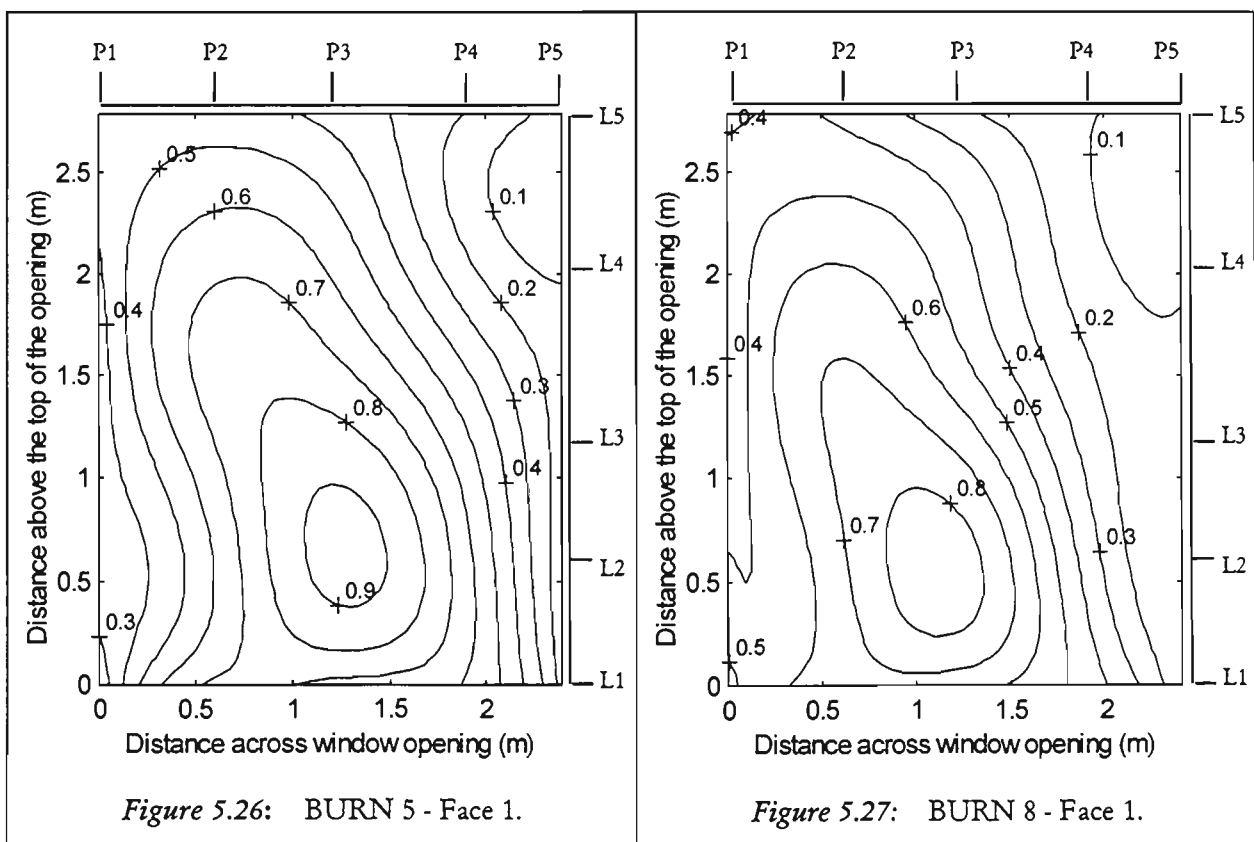
Plane 3 temperature contours are shown in Figure 5.24 and Figure 5.25 for Burn 5 and Burn 8, respectively. The temperatures between the external wall and the core of the venting plume just above the opening between Level 1 and Level 2, are considerable higher than those on Plane 3 of Burn 1 and Burn 2. This difference has been attributed to increased air entrainment into the plume during Burn 1 and Burn 2 due to direct wind interaction.

For Burn 5, the hot core of the flames was focused between 0.75m and 1.25m away from the opening, just below Level 2. For Burn 8, the 'belly' in the venting plume begins closer to the opening, focused around 0.5m away, before spilling out and across the same region as the hot core of Burn 5 (the curved path of the venting plume is referred to as *bellying* of the plume in *Section 5.6.1* and Figure 5.52). Again, there is a gradual drop in temperature with vertical distance above the core, and a more rapid decline underneath it from Face 3 to Face 4.



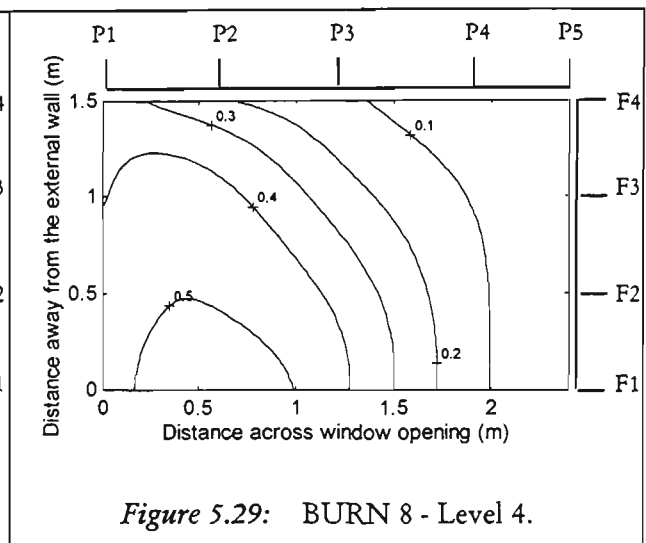
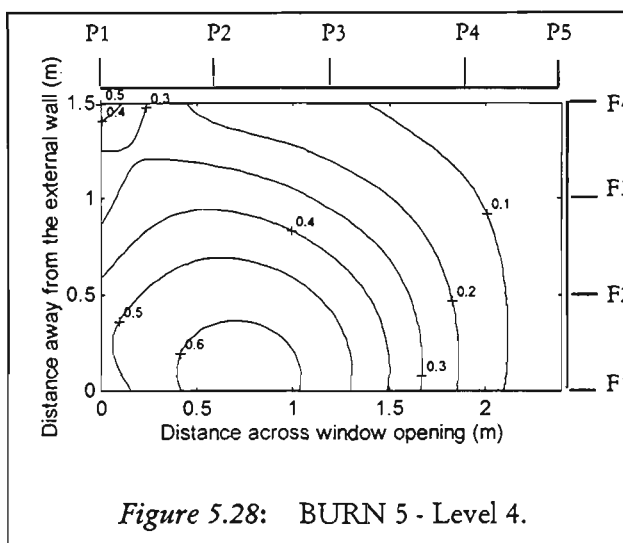
5.4.2.2 Face 1

Both Face 1 plots of Burn 5 and Burn 8, Figure 5.26 and Figure 5.27, respectively, clearly show the overall effect the venting plume has on the external facade of the building. In this case, the heat emanates from a central source, corresponding to a region where the venting flames tend towards the external wall. This hot core is focused on Level 2 between Plane 2 and Plane 3 for Burn 5; and on Level 2 centred around Plane 2 for Burn 8. Burn 5's core is proportionally hotter, with 90% of the maximum measured temperature, compared to that of Burn 8, where the core contour corresponds to 80% of the maximum measured temperature. Both regions begin just below Level 2 and end just below Level 3. Hence, the hot core on the external wall is located at approximately the same distance above the top of the burn room window during Burn 5 and Burn 8. The temperature from the venting flames decreases with distance radially away from the core. Also, in both tests, the plume exhibits a similar tendency to drift to the left, which is possibly due to local air currents over the surface of the facade.



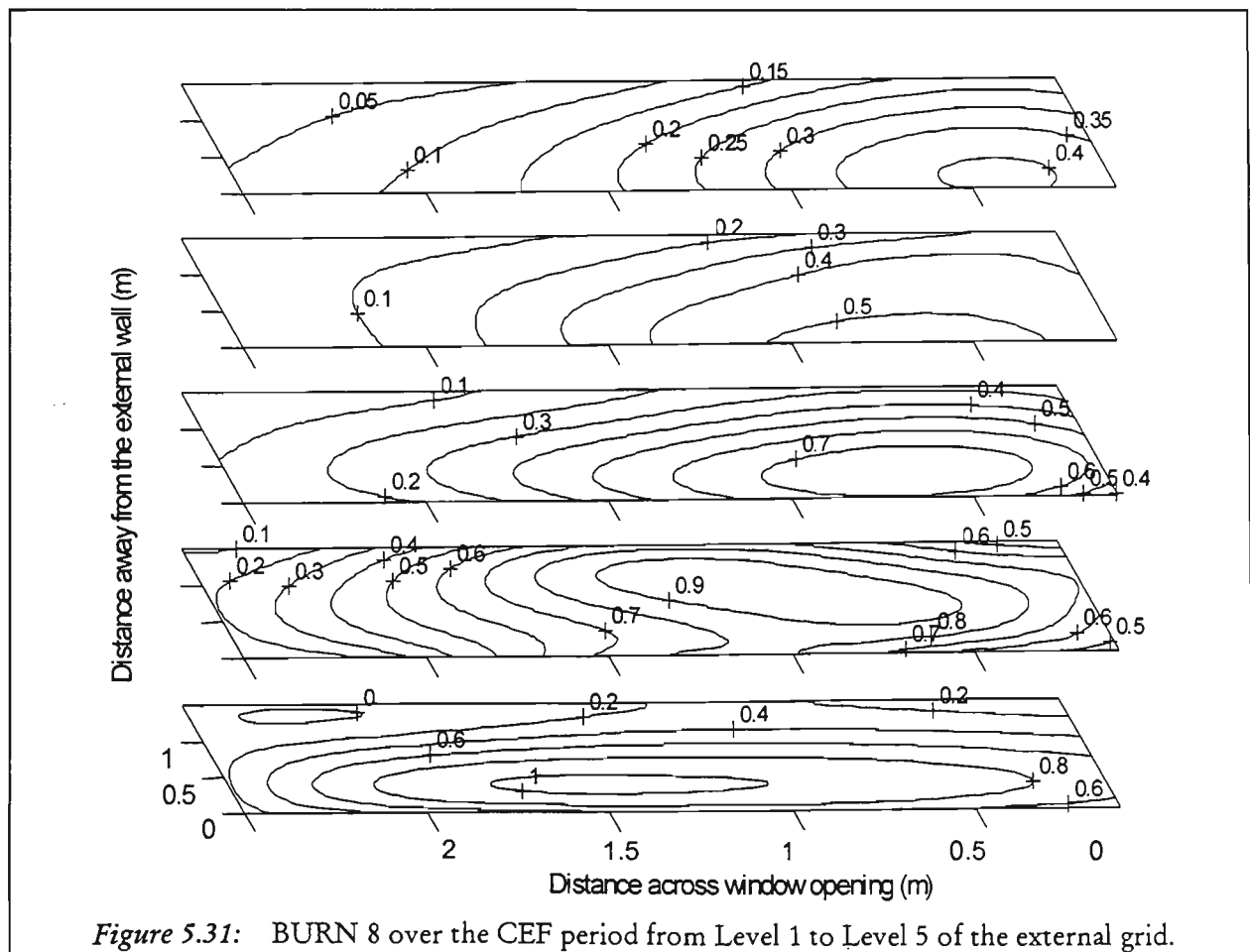
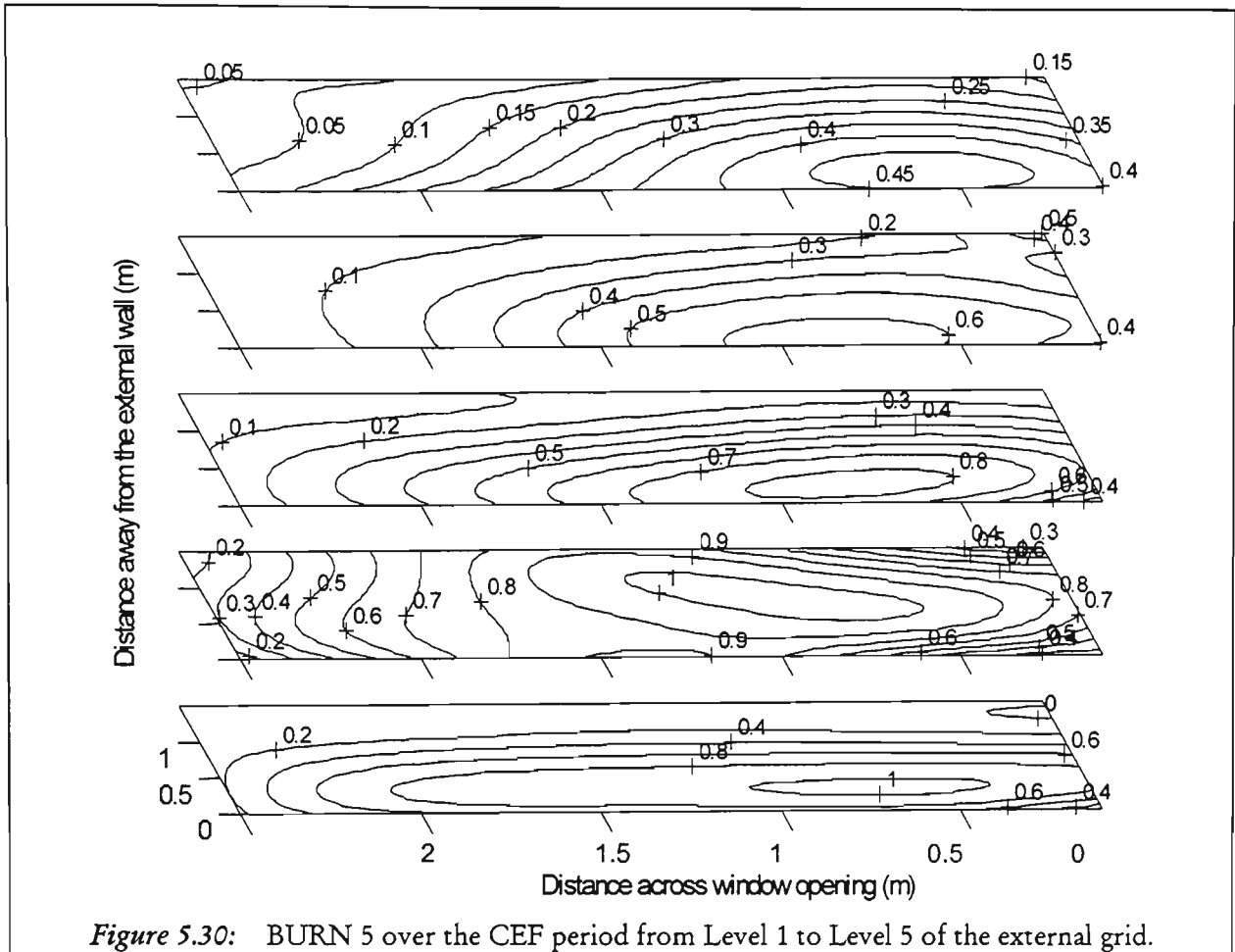
5.4.2.3 Level 4

Following from Face 1, are the plots of Level 4 for Burn 5 and Burn 8, which are given in Figure 5.28 and Figure 5.29, respectively. They also exhibit this 'drift'. The bottom edge of these figures corresponds to the centre of the Floor 1M window, W1M02, at the second floor of the building. At this location, the dimensionless temperature contours range between 10 to 60% of the maximum temperature measured. As a result of the drift to the left, the temperatures are higher on the left hand side of Level 4 compared to the right hand side, creating a significant thermal gradient across the Floor 1M window. This thermal gradient was sufficient to cause cracking and dislodgment of the Floor 1M window during Burn 5 and Burn 8. Details of glass breakage are covered in *Section 5.7*.



5.4.2.4 Level 1 to Level 5

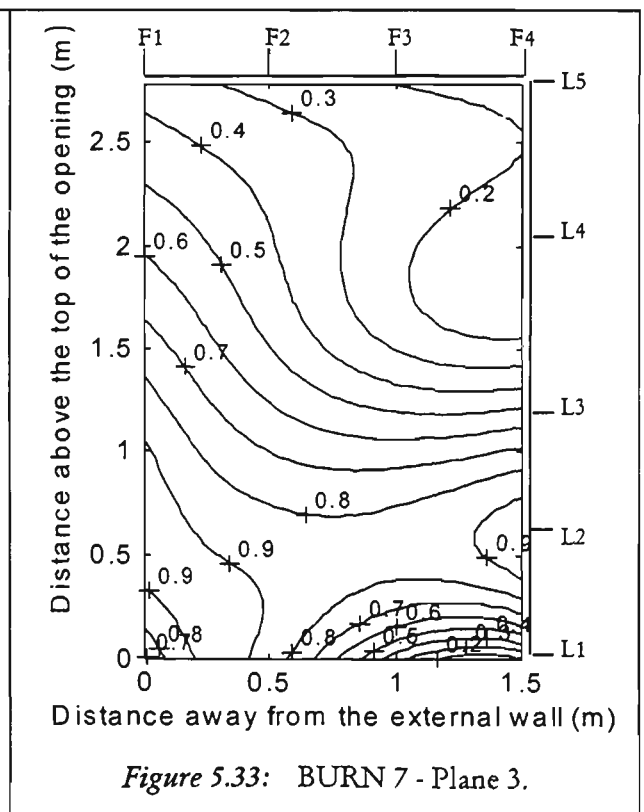
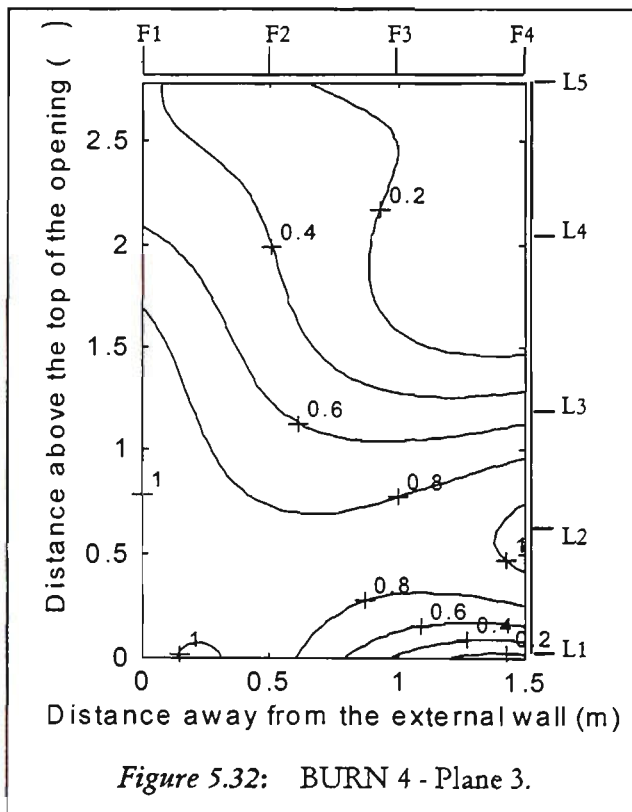
The 3D contour plots for Burn 5 and Burn 8 are given in Figure 5.30 and Figure 5.31, respectively. Once again, these figures give an impression of the entire plume as it vents from the window opening, during the CEF period. For Burn 5, the 1.0 maximum temperature contour is predominantly on the left side of Level 1, and from there, it moves up through the grid. This case is an example of how maximum temperatures of the plume may not coincide with the centre plane. For Burn 5, 80% of the maximum temperature is still being reached at Level 3, which corresponds to the bottom of the mezzanine floor window, W1M02. For Burn 8, the temperature contours are centred at Level 1, and they veer slightly to the left as they move up through the grid. The temperature at Level 3 of the grid is 70% of the maximum temperature measured, which is 10% lower than Burn 5.



5.4.3 Ventilation Class 2 - Burn 4 & Burn 7

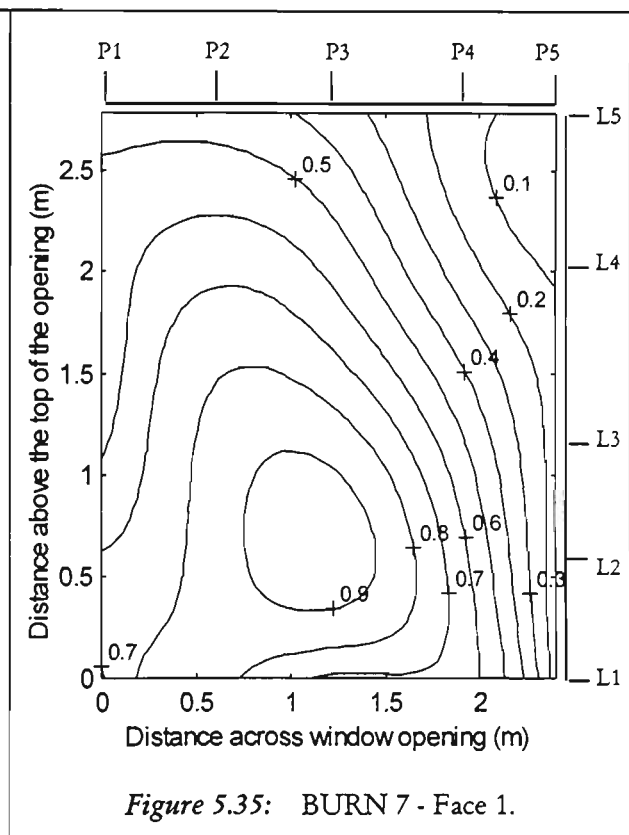
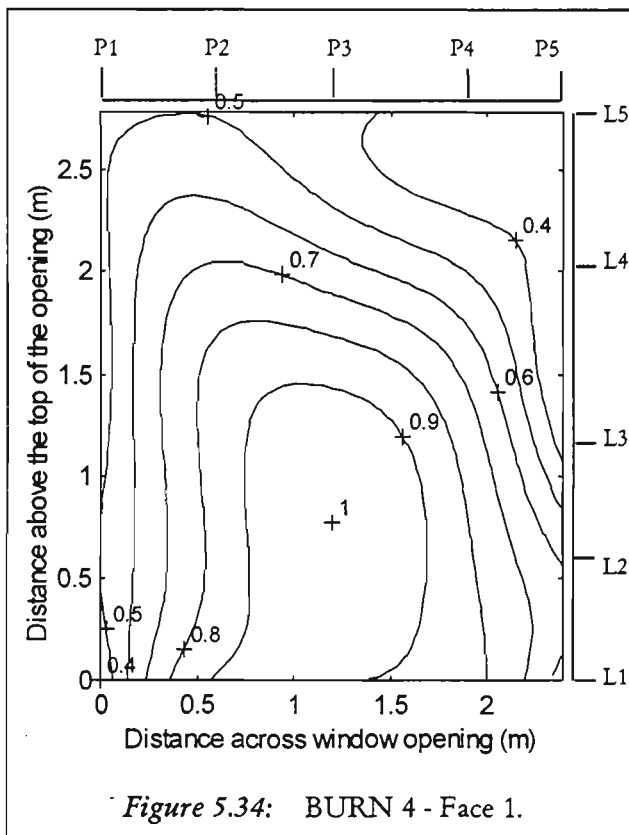
5.4.3.1 Plane 3

Plane 3 temperature contour plots shown in Figure 5.32 and Figure 5.33 are for Burn 4 and Burn 7, respectively, the repeat cases of the NO-THROUGH-DRAFT ventilation condition. The patterns shown in these figures occurred when the window was the only opening to the burn room. As such, it provided both a supply of air to the room and a means for the combustion products to vent from the room. During the early stages of both tests the entire plume vented from the upper half to two-thirds of the window. The lower part of the plume vented almost horizontally; while the upper part of the plume tilted up slightly as it vented. As the tests progressed into the CEF period, the flames grew in length and impinged back on the external wall. The single opening of Class 2 tests, resulted in the width of the venting flames exceeding the width of the window by approximately 0.5m on each side. As the only vent path, the flames also extended further away from the window than Class 1 tests .



5.4.3.2 Face 1

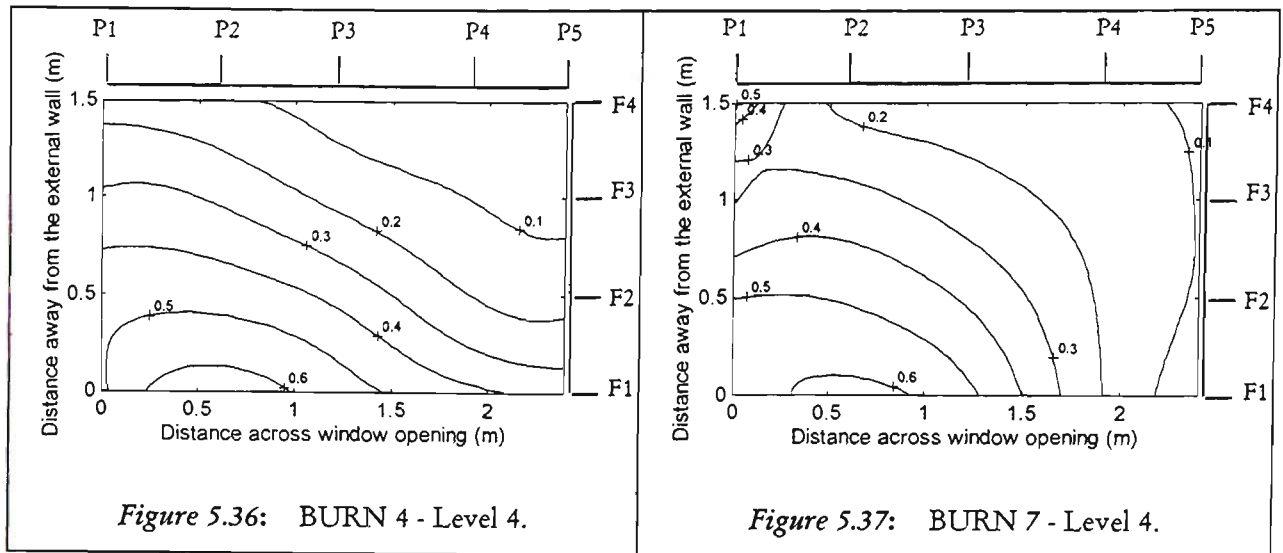
Both Face 1 plots of Burn 4 and Burn 7 show the overall effect the venting plume has on the external facade of the building. As can be seen in Figure 5.34 and Figure 5.35, there was a central hot core for both Burn 4 and Burn 7, similar to those of Burn 5 and Burn 8. These hot cores defined by the 1.0 and 0.9 temperature contours were located between Level 2 and Level 3 and focused around Plane 3, as opposed to being centred around Level 2 for Burn 5 and Burn 8. Also for Burn 4, the hot core on the wall was as hot as the venting plume itself, and this result was seen only in this test. Once again, beyond this core region, there was a rapid drop radially in temperature both across the wall and up from the core. However, especially as seen in Figure 5.34, the region below the core remained hot from its centre all the way down to Level 1.



5.4.3.3 Level 4

Following from Face 1, the plots of Level 4 for Burn 4 and Burn 7, are given in Figure 5.36 and Figure 5.37, respectively. The proportion of measured temperature on the window at this Level varies from at most 60% down to 10% of the maximum temperature. Again, there is a gradual drop away from the window, as well as across

it. The drift across Face 1 is echoed on Level 4 with greater temperature variance away from the wall on the left side (Plane 1) compared to the right side (Plane 5).



5.4.3.4 Level 1 to Level 5

Figure 5.38 and Figure 5.39 give an impression of the flames as they vent from the window opening over the CEF period. These figures show the three-dimensional temperature contour plots across Level 1 to Level 5 for Burn 4 and Burn 7, respectively. For Burn 4, a significant portion of Level 1 is bounded by the 1.0 temperature contour. This contour is closest to the wall between Face 1 (at 0m from the external wall) and Face 2 (at 0.5m from the external wall), and between from just before Plane 2 (at 0.6m across the window opening) to just after Plane 4 (at 1.8m across the window opening). The same contour then stretches out from Face 1 to Face 4 (at 1.5m) on Level 2, while narrowing to between Plane 2 to Plane 3 (at 1.2m). However, the region closest to the wall on Level 3 still has temperatures which are 80% of the maximum temperature. This hot region on Level 1 and Level 2 then begins to dissipate in the upper levels of the grid.

For Burn 7, the temperatures measured are slightly lower than those of Burn 4. They are also more focused on the left of the grid on Level 1 to Level 3. Over this portion of the grid, between 80 to 90% of the maximum temperature still exists. Over the area of the Floor 1M window, W1M02, at Level 3, the variation in measured temperature ranges from 80% to 30% of the maximum measured temperature.

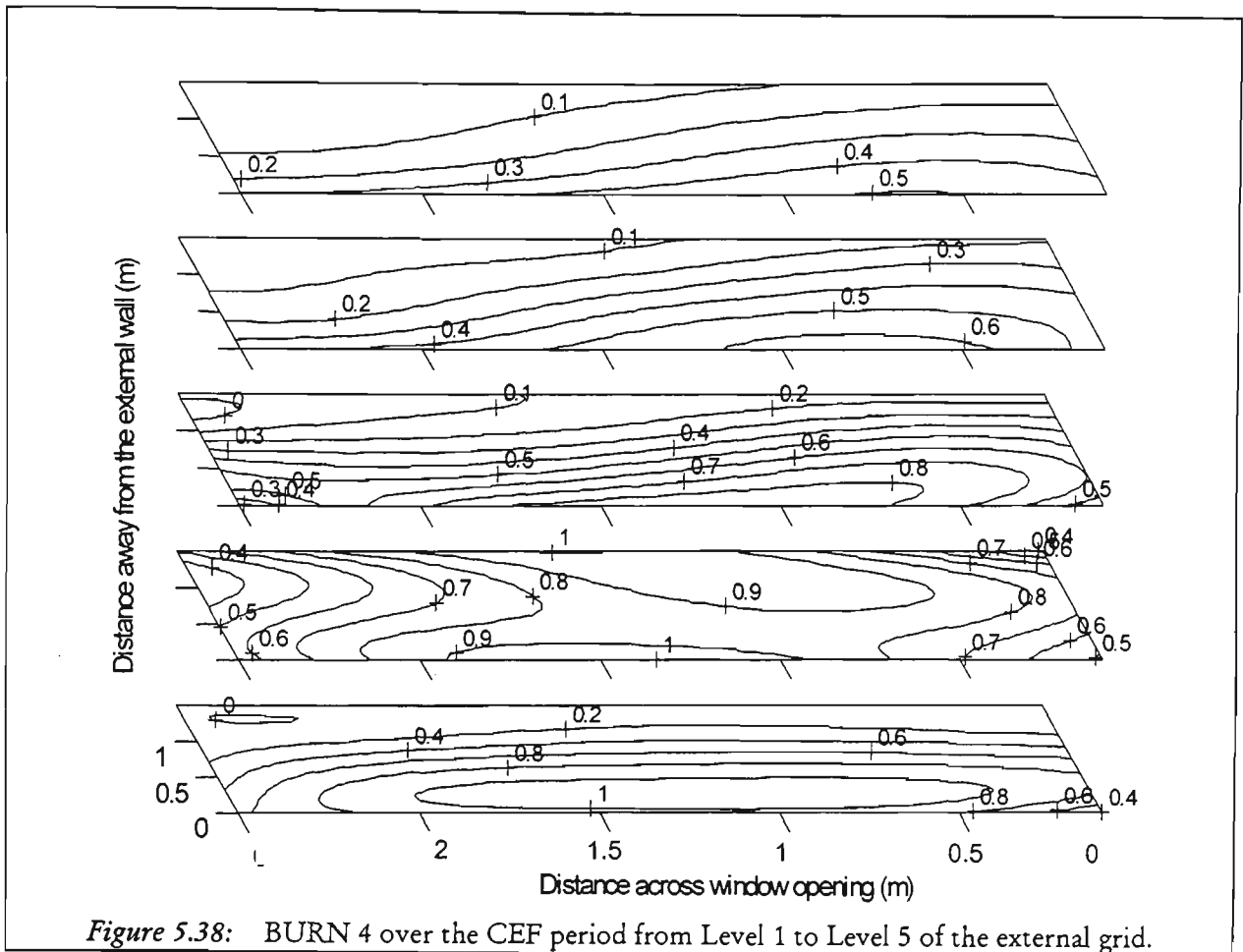


Figure 5.38: BURN 4 over the CEF period from Level 1 to Level 5 of the external grid.

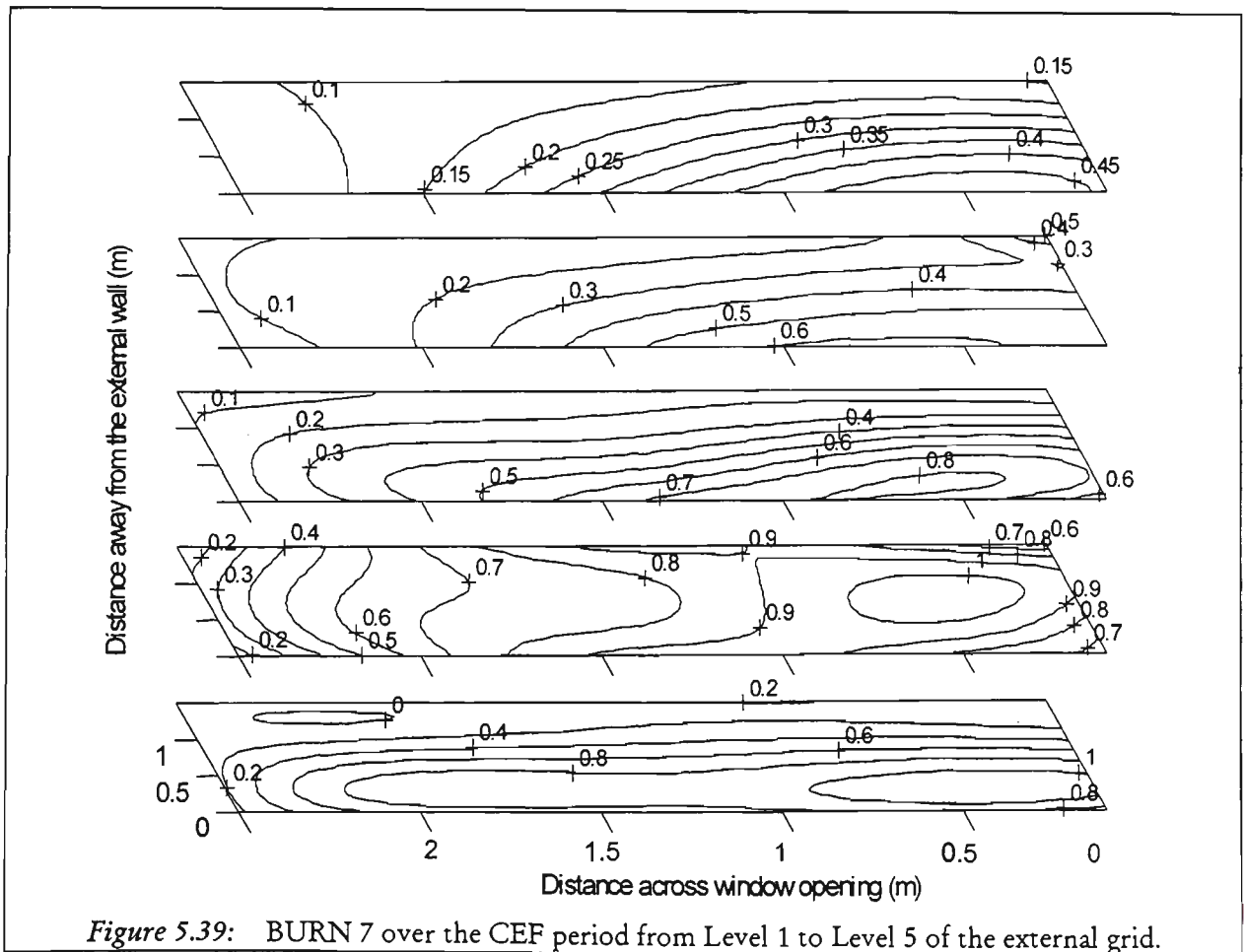


Figure 5.39: BURN 7 over the CEF period from Level 1 to Level 5 of the external grid.

5.5 REPEATABILITY

Before any conclusions can be drawn from a set of experimental data, the results must be repeatable. Repeatability ensures that the characteristics of a particular test are 'real' as measured and not caused by some unknown anomaly. The ability to determine whether or not two tests are repeats of each other, depends on by what means the comparison is made. In this study, fuel mass loss histories were chosen as an indication of the similarity of the fire development in the burn room during repeat tests. Subsequently, Plane 3, Face 1 and Level 4 temperature contours presented in the previous section, *Section 5.4*, were analysed to quantify the repeatability of the pairs of tests in each ventilation class.

5.5.1 Mass Loss Rates

One way to measure the course of fire inside a burn room, from its ignition to decay, is by monitoring fuel mass loss rate. Fuel mass loss rate is an indication of the conditions of the entire burn room at any given time, and it is not subject to spatial variations or fluctuations due to different items burning at different times. It gives an indication of how the fire is progressing and which stage it is in. In addition, fuel mass loss rate is used here in determining the CEF period of each test, and hence, it is an important parameter even in the analysis of the external data.

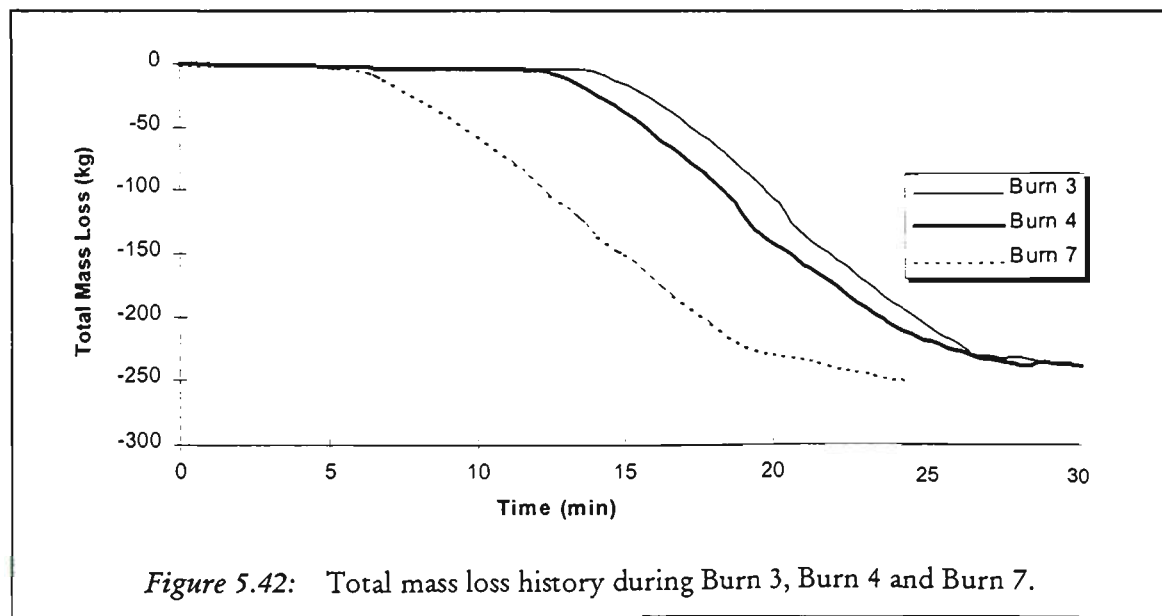
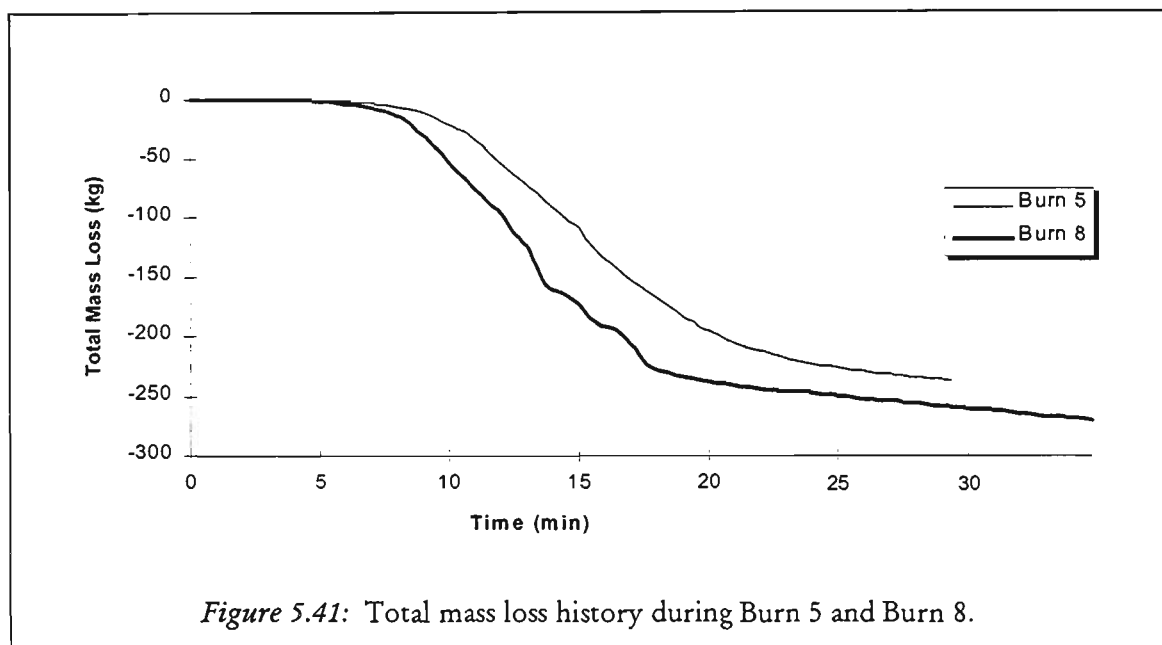
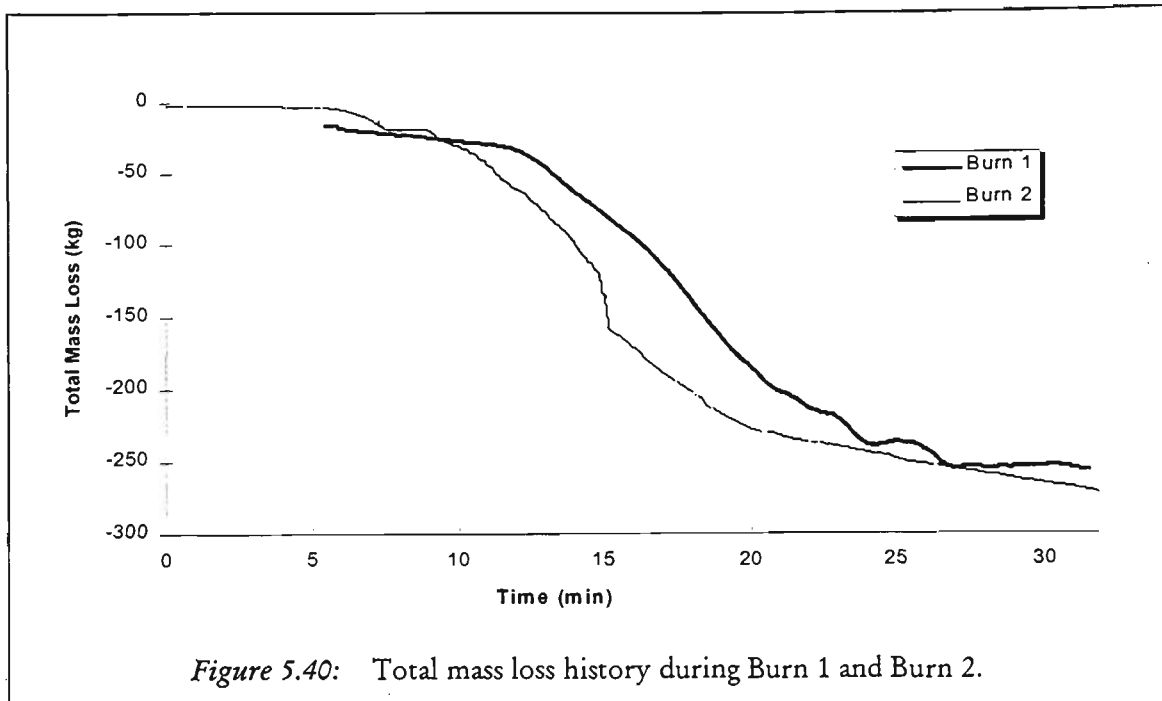
The total mass loss histories during each test are given in Figure 5.40, Figure 5.41 and Figure 5.42 for Class 1a, Class 1b and Class 2 tests, respectively. Burn 1 and Burn 2 mass loss histories are given in Figure 5.40. As indicated in *Section 5.2*, the time scale for Burn 1 was reset by matching its window opening time with the window lowering (with respect to WLC#1) time of Burn 2. Initially, Burn 1 did not develop as expected. The reason was the couch construction (strapping material retarded the flame spread to the carpet), as it was later found out. When it was noticed that the fire did not develop, the window was opened to facilitate flashover during Burn 1. As a result, the beginning portion of the mass loss curve for Burn 1 is missing from Figure 5.40. In spite of resetting the time, an offset remained between Burn 1 and Burn 2 by a few minutes. This offset is due to the time required for Burn 1 to develop after opening

the window. In Figure 5.40, the overall mass loss trends of Burn 1 and Burn 2 compare reasonably well, with the mass loss rates during the CEF period of 20kg/min for both tests.

Burn 5 and Burn 8 mass loss histories are given in Figure 5.41. Once again, this internal indicator of the fire growth compares well for Burn 5 and Burn 8, with the mass loss rate determined during the CEF period of 20kg/min and 21kg/min, respectively. Although combustible wall linings were present in the corridor in Burn 8, this significant contributor to fuel is not seen by the mass loss platforms. As a result of the combustible lining, the CEF duration was slightly longer for Burn 8 compared to Burn 5. However, the CEF averaged and non-dimensionalised external temperature contours were similar, as quantified next.

Burn 3, Burn 4 and Burn 7 mass loss histories are given in Figure 5.42. As discussed in the *Introduction*, Burn 3 and Burn 4 were originally designed as a repeat pair. As can be seen in Figure 5.42, the mass loss histories are very similar. However, due to high winds during Burn 3, the external data were not as similar. Therefore, externally, Burn 4 was grouped with Burn 7 only, which also follows the same mass loss trend as Burn 4. The average mass loss rate for Burn 3, Burn 4 and Burn 7 were 21, 20 and 18kg/min, respectively, determined during the CEF period.

It must also be noted that Burn 3 and Burn 4 were selected during this series of tests to show the repeatability of internal results, as detailed by Alam and Beever[102]. The earlier increase in mass loss for Burn 7 has been attributed to the activation of the Smoke Management System (SMS) as discussed in *Section 5.8.3*. The slightly lower mass loss rate of Burn 7 during the CEF period must also be caused by the SMS activation, due to extraction of air/hot gases.



5.5.2 Repeatability of External Temperature Measurements

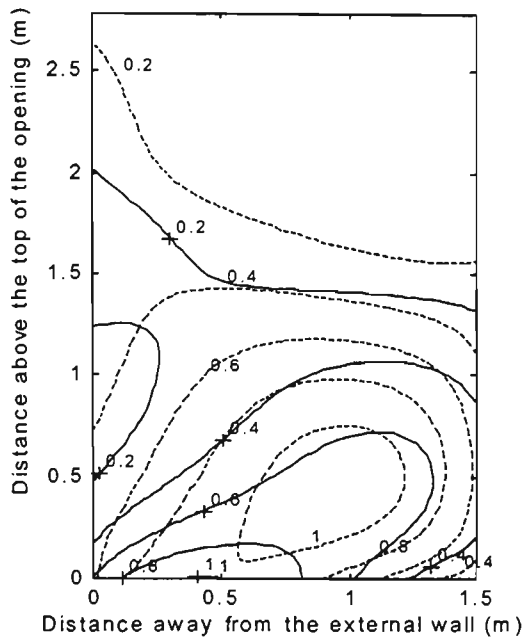
For external results, as mentioned earlier, the period of CEF was established to allow similarly ventilated tests to be compared. A detailed comparison of the CEF averaged and non-dimensionalised temperature contour plots was done in the previous section. The presentation of the data in this manner lends itself to a direct comparison of pairs of results across Plane 3, Face 1 and Level 4 of the 3D external grid. In the following, further comparison is presented with two types of contour plots in Figure 5.43a and Figure 5.43b to Figure 5.51a and Figure 5.51b. The first figure of each group of two (*figure a*), represents the combination of the data across the specified section of the 3D grid for a pair of tests within a Class. The second figure (*figure b*) represents the ***difference*** between the contour plots of the same pair of tests. The contours in the second figure (*figure b*) are the numerical difference between pairs of data used to generate either a Plane, Face or Level at a given location of the 3D grid in the first figure (*figure a*). To allow easy comparison amongst the three ventilation classes, all Plane 3 results are given in Figure 5.43 to Figure 5.45, followed by Face 1 in Figure 5.46 to Figure 5.48, and Level 4 in Figure 5.49 to Figure 5.51. Finally, a statistical analysis of the data in terms of mean difference, standard deviation and maximum difference is presented.

Beginning with the Class 1a tests, it was found that due to direct wind interaction with the venting plume, the similarity between Burn 1 and Burn 2 was difficult to estimate. The Plane 3 temperature contours, Figure 5.16 and Figure 5.17, are plotted together in Figure 5.43a. These Plane 3 contours show a similar tendency for Burn 1 and Burn 2. However, the Face 1 (Figure 5.18 and Figure 5.19 combined in Figure 5.46a) and Level 4 contours (Figure 5.20 and Figure 5.21 combined in Figure 5.49a) are not as similar. This conclusion is confirmed by the *difference plots* between Burn 1 and Burn 2 for Plane 3, Face 1 and Level 4 in Figure 5.43b, Figure 5.46b and Figure 5.49b, respectively, which display large regions of greater difference contours than the corresponding Class 1b and Class 2 difference contour plots. For this reason, Burn 1 and Burn 2 were eliminated from the averages used to determine new centre-line temperature equations for Face 1 to Face 3, in *Section 5.6.4*.

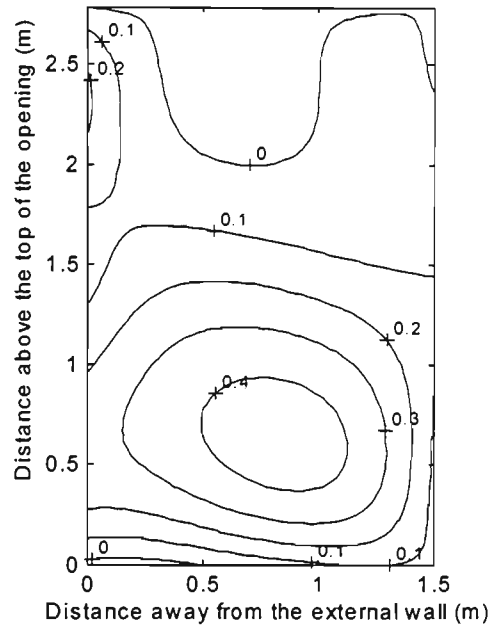
The contribution of external wind effects on Class 1a tests is difficult to quantify, the temperature contours for the Class 1b and Class 2 tests showed better comparison than the Class 1a tests, as a result of less direct wind interaction. For Class 1b and Class 2 tests, the Southern facade where the plume emerged from the burn room window was protected by either the building itself or the air-handling unit, as discussed in detail in *Section 5.8*.

In general, the temperature contours for the Class 1b tests, Burn 5 and Burn 8, repeated each other than better the Class 1a tests did. The Plane 3 contours, Figure 5.24 and Figure 5.25, plotted together in Figure 5.44a, both show a 'belly' at approximately the same location, while the Face 1 contours (Figure 5.26 and Figure 5.27 combined in Figure 5.47a) both have a hot core in the same location. The Level 4 contours (Figure 5.28 and Figure 5.29 combined in Figure 5.50a) have the hottest temperature contour on the left of the wall. The Class 1b Level 4 temperature contours are the best repeat cases amongst all Level 4 comparisons given in Figure 5.49 to Figure 5.51. The *difference plots* between Burn 5 and Burn 8 of Plane 3, Face 1 and Level 4, in Figure 5.44b, Figure 5.47b and Figure 5.50b, respectively, also show small differences.

The Class 2, Burn 4 and Burn 7, Plane 3 temperature contours, Figure 5.32 and Figure 5.33, plotted in Figure 5.45a appear to be the best repeat cases amongst all Plane 3 comparisons given in Figure 5.43 to Figure 5.45. Both contours have their maximum just above the opening, and this high temperature contour extends out away from the wall. Face 1 temperature contours (Figure 5.34 and Figure 5.35 combined in Figure 5.48a) have a hot core which reaches up and away from this centre. The Level 4 temperature contours (Figure 5.36 and Figure 5.37 combined in Figure 5.51a) are also very similar to each other. The similarity of the Class 2 tests can also be seen by the small differences in the corresponding Plane 3 (Figure 5.45b), Face 1 (Figure 5.48b), and Level 4 (Figure 5.51b) *difference plots*. While it is almost impossible to duplicate a full scale test in all details, comparing the graphical information of the external temperature contours over the CEF period which were also non-dimensionalised with respect to ambient and maximum temperatures has shown that the Class 1b and Class 2 tests were repeatable. The Class 1a tests showed similar trends.

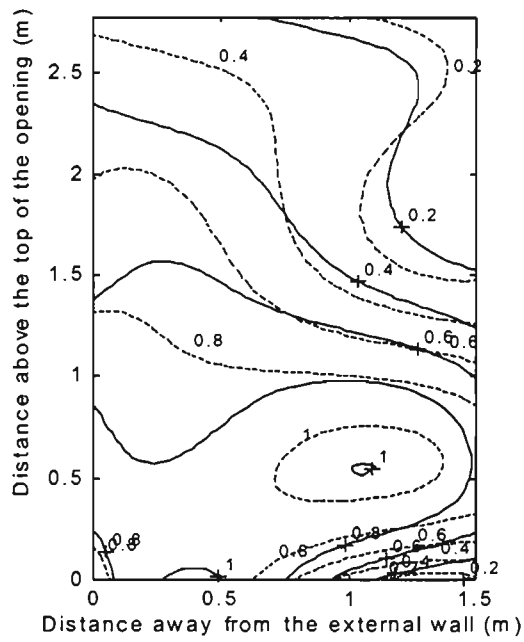


a) Burn 1 (dashed) & Burn 2 (solid).

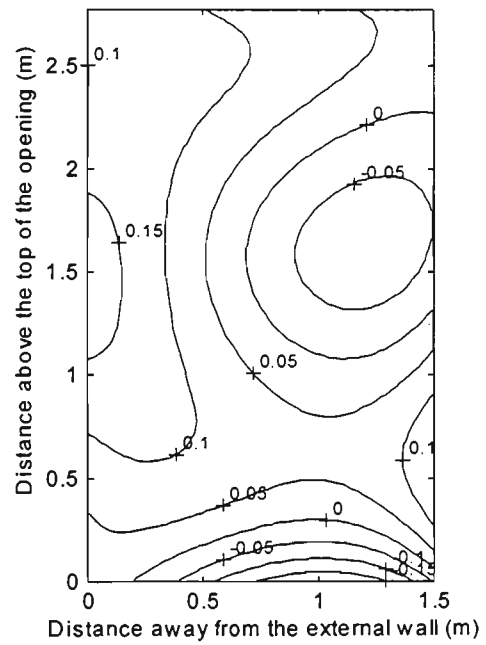


b) Difference between Burn 1 and Burn 2.

Figure 5.43: Class 1a: Plane 3.

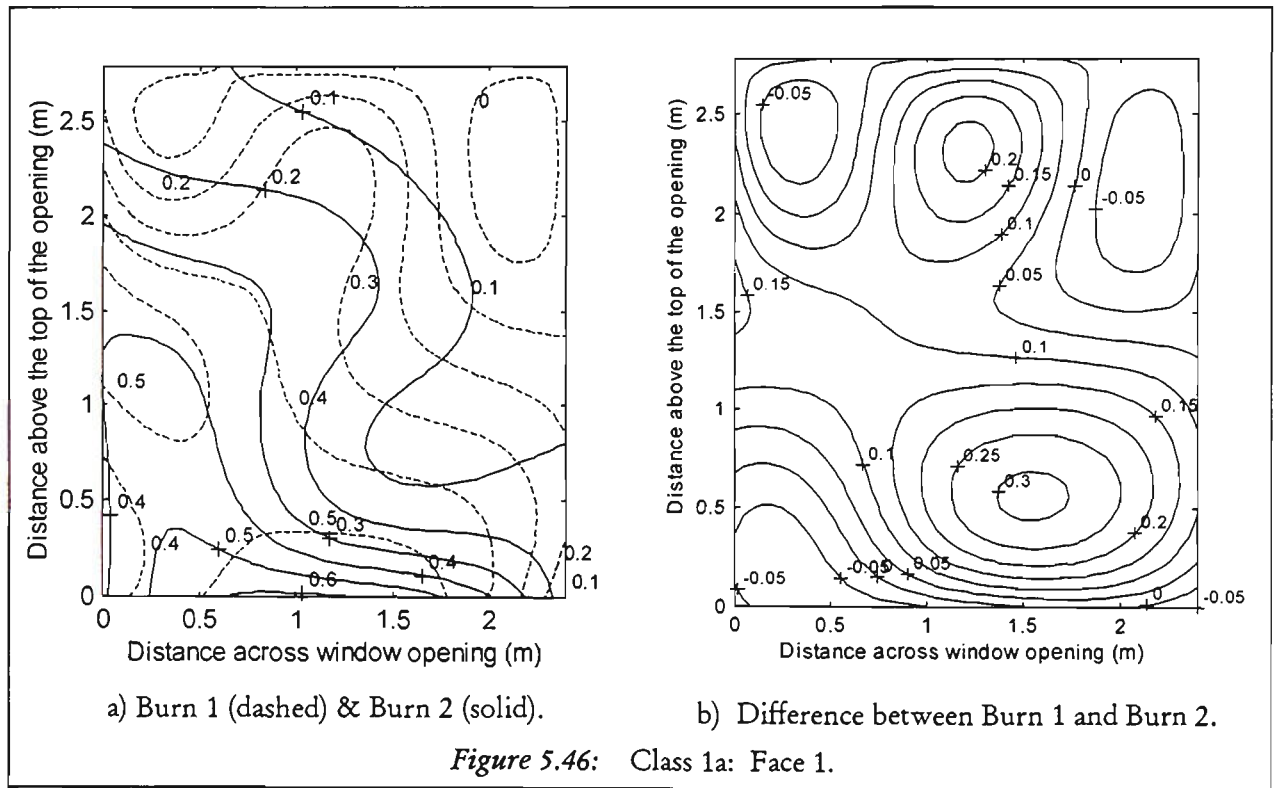
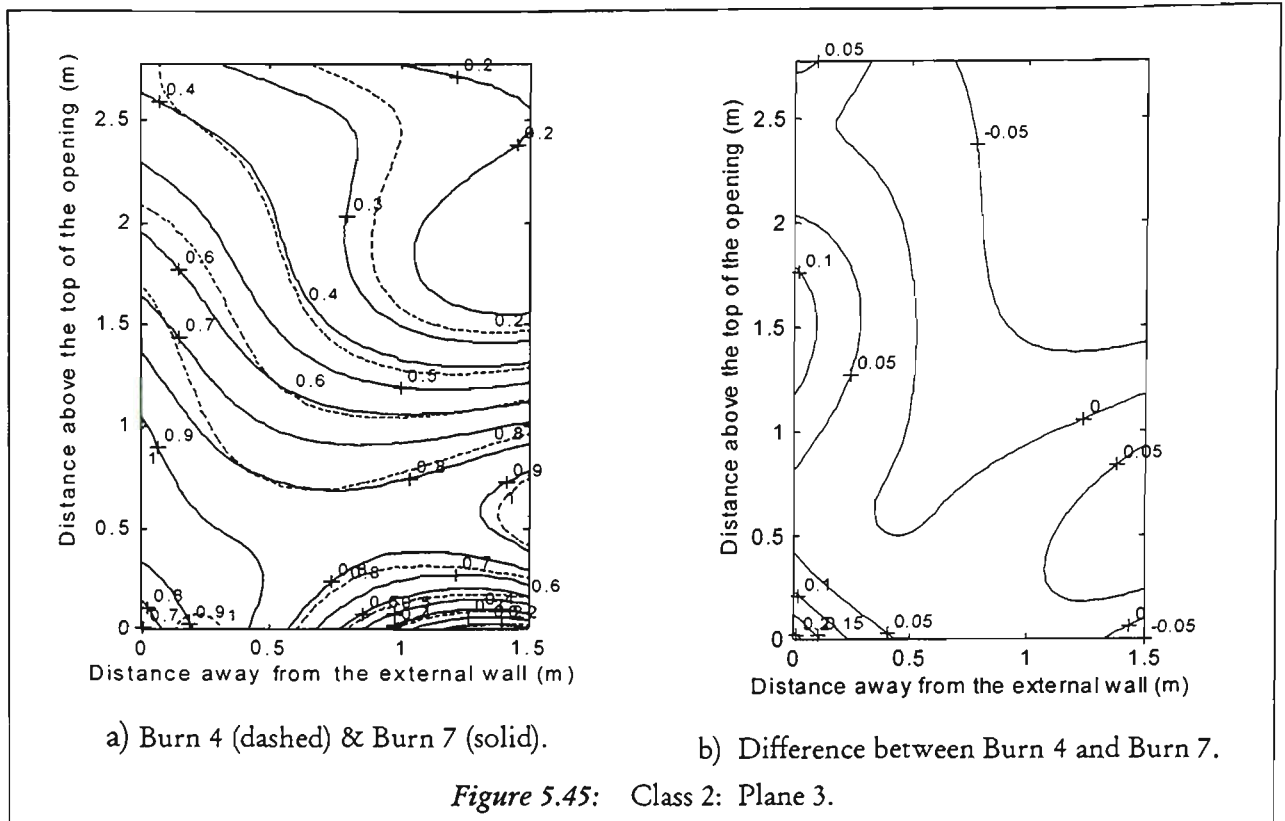


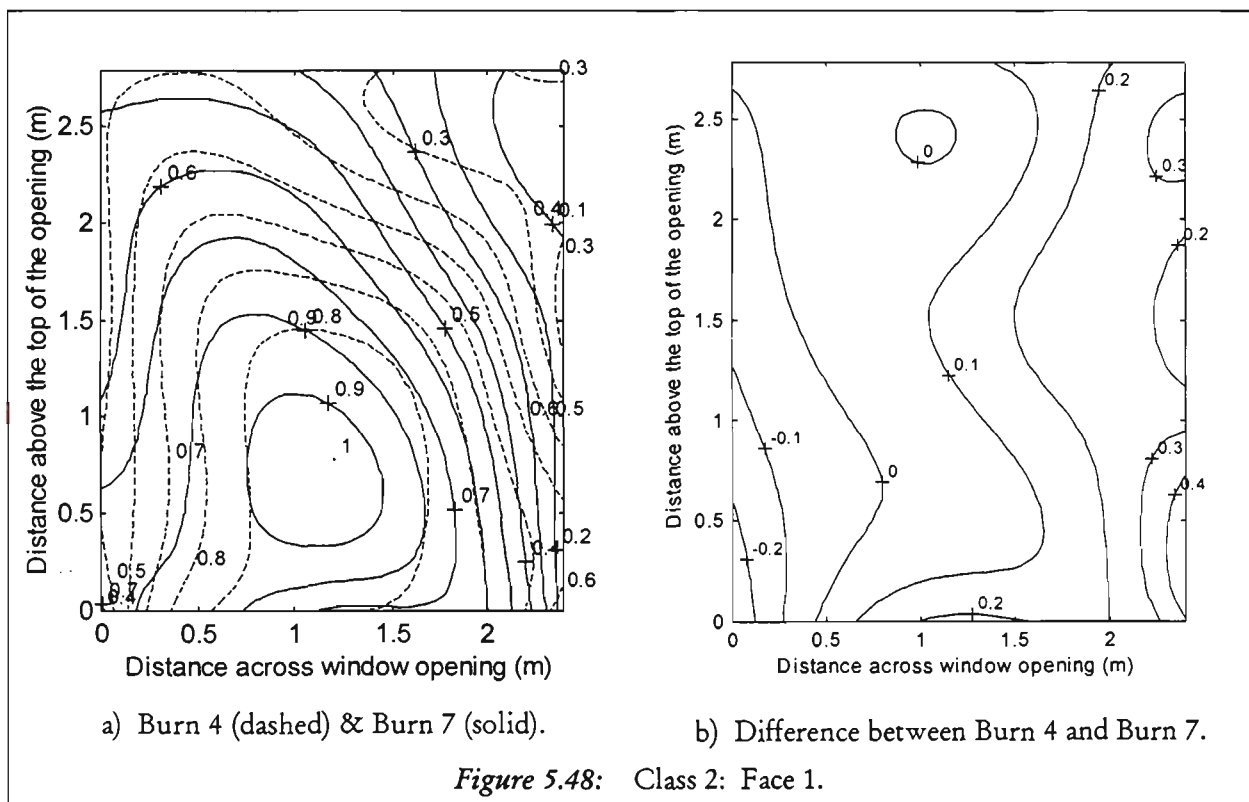
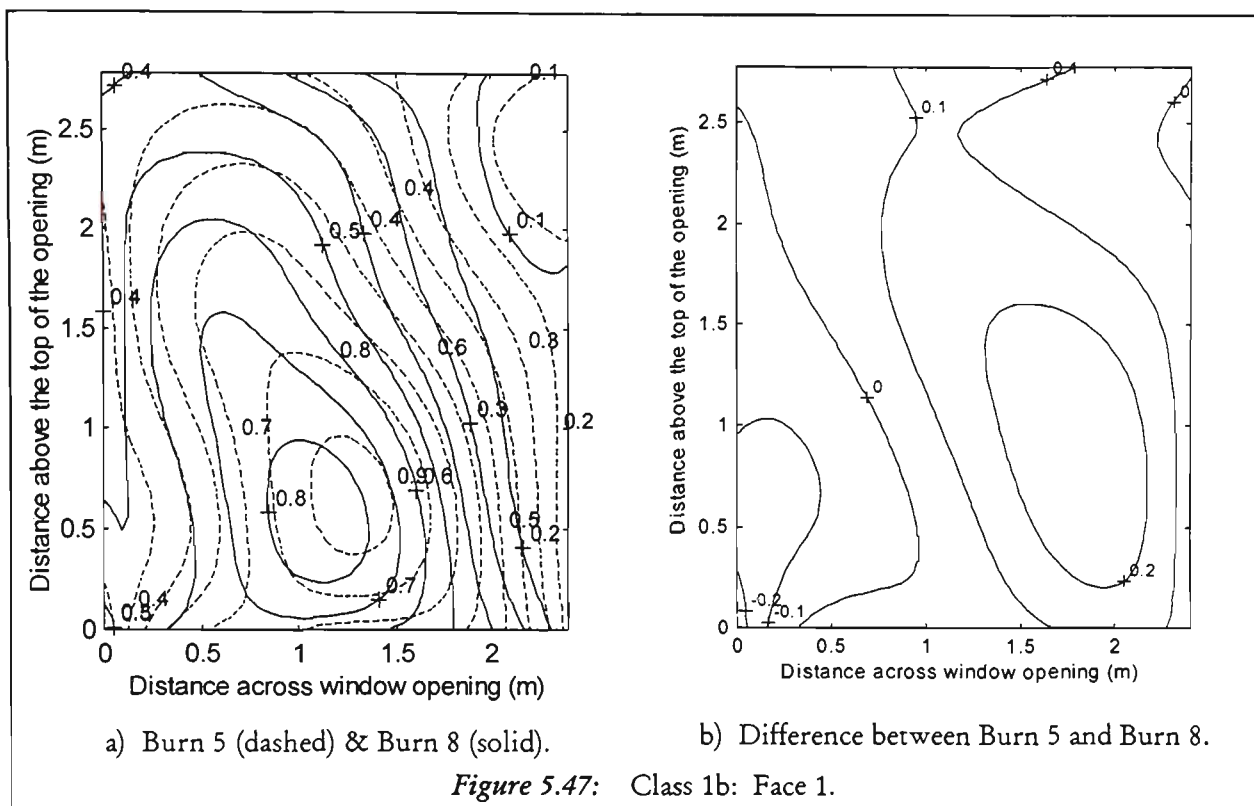
a) Burn 5 (dashed) & Burn 8 (solid).

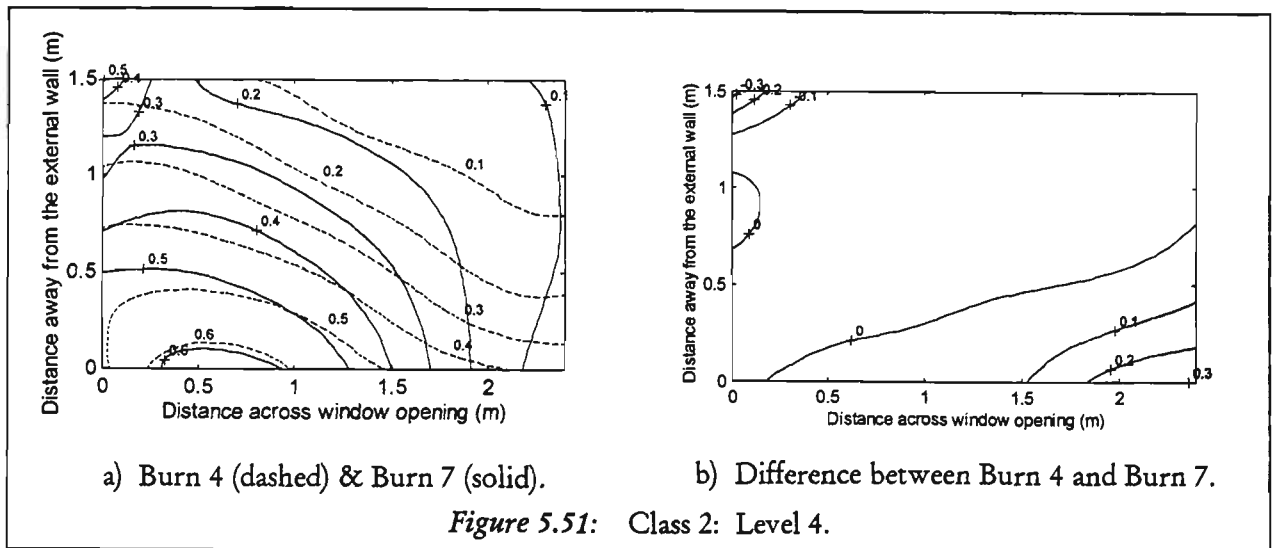
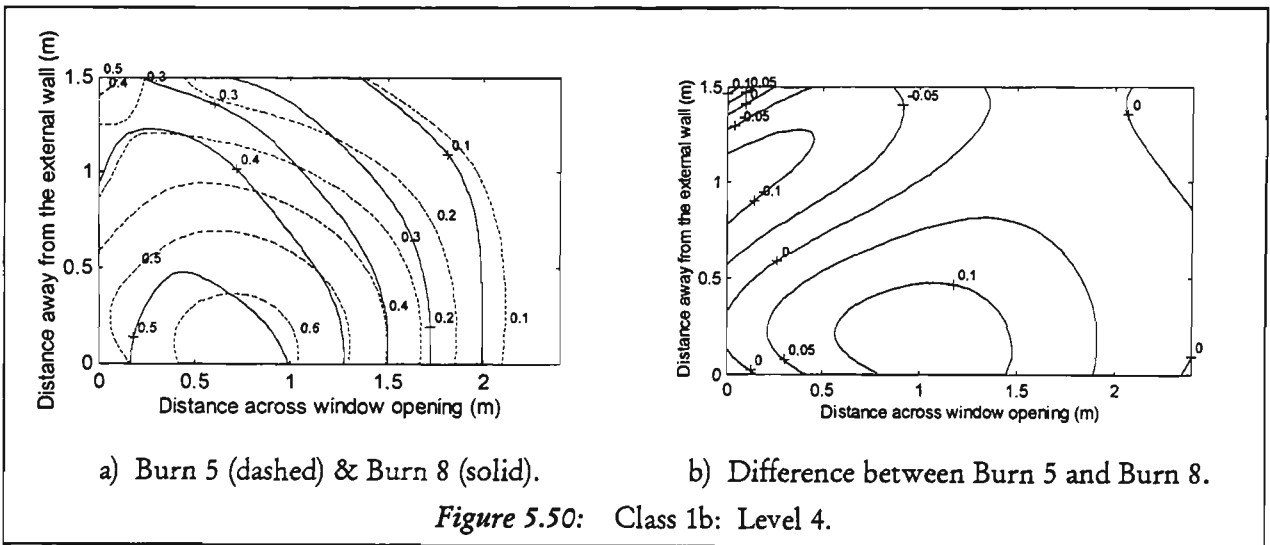
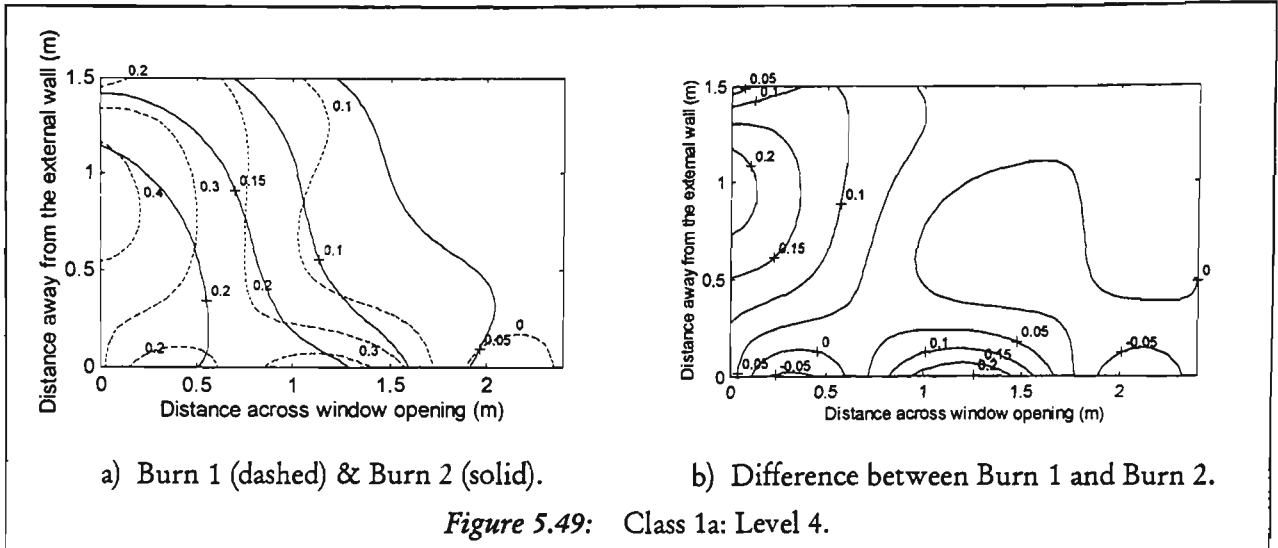


b) Difference between Burn 5 and Burn 8.

Figure 5.44: Class 1b: Plane 3.







5.5.3 Quantifying the Repeatability of External Temperature Measurements

Statistical analysis of the data for each pair of tests provided a means to quantify test repeatability in terms of mean difference, standard deviation and maximum difference. For this analysis, a comparison was made of each Class of repeat tests against their *reference*. The reference data consisted of the arithmetic average of the data collected during the repeat tests at all locations of a given section of the 3D external thermocouple grid. Following from earlier analysis, Plane 3, Face 1 and Level 4 for each pair of tests were used for comparison, with CEF averaged and non-dimensionalised data. As a result, a given pair of repeat tests has only one mean difference, standard deviation and maximum difference for each of these sections of the 3D external grid. Table 5.6 below lists the mean difference, standard deviation and maximum difference for each pair of tests with respect to its reference, for Plane 3, Face 1 and Level 4.

Considering Plane 3 for Burn 1 and Burn 2 (Class 1a), the mean difference is 0.08, with a standard deviation of 0.067 and a maximum difference of 0.23. These numbers imply that on the average, the difference between the corresponding data points of these two tests and their reference on Plane 3 is $8 \pm 6.7\%$. Although the maximum average difference is 23%, this difference is within two and three standard deviations from the mean, making it a rare occurrence. The mean difference, standard deviation and maximum difference for Burn 5 and Burn 8 (Class 1b) are 0.035, 0.021 and 0.1, respectively, for Plane 3. Therefore, the difference of Burn 5 and Burn 8 data from their reference values is on the average $3.5 \pm 2.1\%$. The maximum average difference of 10% is more than three standard deviations from the mean, making it a rarer occurrence than the maximum difference between Class 1a tests, Burn 1 and Burn 2. Lastly, for Burn 4 and Burn 7 (Class 2), the mean difference is 0.02 with a standard deviation of 0.015 (1.5%) with a maximum of 0.11 (11%) for Plane 3 with respect to their reference. The maximum for this case is also more than three standard deviations from the mean, similar to the Class 1b results. Consequently, Table 5.6 shows that statistically Burn 4 and Burn 7 (Class 2) and Burn 5 and Burn 8 (Class 1a) are more

repeatable across Plane 3 than Burn 1 and Burn 2 (Class 1a), as originally determined by a graphical comparison of the contour plots.

Similar inspection of the information presented in Table 5.6 in terms of Planes, Faces and Levels, shows that statistically, the Level 4 variations are less than those of Face 1 or Plane 3 for Class 1a and Class 1b tests. For Class 2 tests, Level 4 variations are comparable to those of Plane 3 and less than those of Face 1. The general better repeatability of Level 4 results may be explained by the temperature measurements at this level. These temperatures were at or below 600°C. Below 600°C, the radiative error associated with thermocouple measurements is expected to be negligible. Negligible error due to radiation, must have resulted in more accurate measurements and increased repeatability.

Table 5.6: Statistical analysis of experimental data of external temperature contours to determine repeatability. Mean difference (MEAN), standard deviation (STD) and maximum difference (MAX) between the reference and corresponding pairs of tests on Plane 3, Face 1 and Level 4.

			MEAN	STD	MAX
PLANE 3	Class 1a	BURN 1/BURN 2	0.080	0.068	0.23
	Class 1b	BURN 5/BURN 8	0.035	0.021	0.10
	Class 2	BURN 4/BURN 7	0.020	0.015	0.11
FACE 1	Class 1a	BURN 1/BURN 2	0.050	0.037	0.16
	Class 1b	BURN 5/BURN 8	0.051	0.036	0.14
	Class 2	BURN 4/BURN 7	0.061	0.050	0.25
LEVEL 4	Class 1a	BURN 1/BURN 2	0.025	0.027	0.11
	Class 1b	BURN 5/BURN 8	0.024	0.019	0.68
	Class 2	BURN 4/BURN 7	0.027	0.023	0.17

5.6 ESTIMATING PLUME FLAME ENVELOPE AND CENTRE-LINE TEMPERATURE

To date, most analyses of a full scale plume have been limited to results along a plane perpendicular to an external wall, vertically up from the centre of the opening. These analyses have been matched by empirical approximations which were developed by Law[21] and Law and O'Brien[30]. Their work described the expected flame envelope and centre-line temperatures of the venting plume in terms of burning rate, room and window geometry and ventilation conditions. The experimental data used to develop these approximations were obtained mainly from wood crib fires. In this study, these empirical predictions have been compared with the results of real furniture fires to extend them to more realistic living environments, in addition to comparing them with polyurethane fires in *Section 4.2.4*. These approximations are summarised in *Section 2.4.1* of the *Background*.

In the following sections, Law's[21] flame envelope approximations are compared with the observations made during each of the tests. Calculations based on her centre-line temperature equations are compared with the CEF averaged centre-line temperatures. The calculated centre-line temperatures over-estimate the measured ones. Therefore, new centre-line temperature equations are developed to describe the trends observed during these tests. Comparisons are given with Yokoi's[28] work of the centre-line temperatures, re-attachment and spandrel length, and with Sugawa and Takahashi's[72] work of the centre-line temperatures. Also included is series of three-dimensional fourth order polynomial surface fits which describe the temperature distribution across each Face of the experimental grid as an uninterrupted surface.

5.6.1 The Flame Envelope and Comparison with Other Work

While Law developed a method to describe the flame envelope for both ventilation classes, only the *no-through-draft procedure* of Class 2 has been implemented here to determine the flame envelope. This choice is due to the experimental observations of the external plume which vented out of the upper 1/2 to 2/3 of the burn room window during the CEF period, during both Class 1 and Class 2 tests. As a result, the

observed external plume during the Real Furniture Burns, was not similar to the expected through-draft plume shape shown in Figure 2.6, during Burn 1, Burn 2, Burn 5 and Burn 8, the four cases of Class 1 tests.

In Table 5.7, the dimensions of calculated flame envelope are given. The values listed in this table were calculated using Equation 2.11 to Equation 2.13, with the following values of the rate of burning and window width and height, respectively: $R=0.4\text{kg/s}$ (the maximum value calculated using Equation 2.4 to Equation 2.7), $w=2.4\text{m}$ and $h=1.5\text{m}$, respectively. Law provides three expressions to estimate the rate of burning, Equation 2.4 to Equation 2.7. All three of these expressions have been found to give approximately the same R value, $0.3 < R < 0.4 \text{ kg/s}$. The experimentally measured mass loss rates for all tests were also comparable to this range. These mass loss rates over CEF were approximately 20 kg/min (0.33 kg/s) for Burn 1, Burn 2, Burn 4 and Burn 5, and 21kg/min (0.35kg/s) and 18kg/min (0.3 kg/s) for Burn 8 and Burn 7, respectively, as discussed in *Section 5.5*. In Equation 2.4 to Equation 2.7, the window area, $A_w=3.6\text{m}^2$, the total surface area of the burn room including the window, $A_T=81\text{m}^2$, the depth of the burn room, $D_c=5.31\text{m}^2$, fire load, $L=620\text{kg}$ (wood equivalent, average of six tests) and free burning duration $\tau_F=30\text{min}$ (average of six tests) were used.

The experimental flame dimensions listed in Table 5.8 are based on visual observations. During each test, three video recorders were used, one in front of the burn room window, and one on each side. From these recordings, the height, width and depth of the plume were gauged, using the external grid as a reference. In general, the empirical envelope described in Table 5.7 has been found to contain the observed flame shape given in Table 5.8. In Table 5.8, the first two columns give the maximum height and depth of the plume before the CEF period. The last two columns are the maximum height and depth during the CEF. This distinction has been made, because the maximum height and depth occur at different stages of the fire, and it is the maximum reach of the flames which is compared to the empirically determined flame envelope given in Table 5.7. The flame height is greater during CEF, and the flame depth is larger before CEF. The reason is that the emerging flames are intermittent before CEF, allowing greater air entrainment into the plume from all sides. During

CEF, the plume attaches to the external wall, limiting air entrainment. The rate of burning is higher during CEF than before, resulting in increased combustion outside the burn room window. Due to both of these reasons, the plume has a higher vertical reach during CEF.

As stated above, the large burn room window size resulted in no-through-draft flame characteristics for the through-draft fires of Class 1. For comparison with the no-through draft flame envelope given in Table 5.7, the flame boundary was also evaluated using through draft estimates given in Equation 2.8 to Equation 2.10. Using these equations, a flame height, depth and width of 1.6m, 2.4m and 3.4m, respectively, are calculated. In Equation 2.8 to Equation 2.10, a wind speed producing the through draft of $u=3\text{m/s}$ was used. All other parameters were as specified above. The predicted through-draft flame boundary is wider and deeper than the flame boundary predicted for the no-through draft case, but it has a lower height, because the flames are assumed to emerge from the entire window opening. Unlike the values listed in Table 5.7, the predicted through-draft flame envelope does not agree with the experimentally observed ones, confirming the use of no-through draft predictions for comparison with the experimental data.

Table 5.7: Calculated flame envelope. L5 is 2.78m above the opening, F3 is 1m away from the external wall and P1 to P5 covers the 2.4m wide window.

	Calculated	Approximate grid locations
HEIGHT (m)	2.4	L5
DEPTH (m)	1.0	F3
WIDTH (m)	2.4	across P1-5

Table 5.8: Observed flame shape. L2, L3, L4, L5 and L6 are 0.59, 1.21, 2.03, 2.78 and 3.34m, respectively, above L1, which is 0.15m above the top of the burn room window. F1 to F4 are 0m to 1.5m away from the external wall at 0.5m intervals.

		Maximum height before CEF (m)		Maximum Depth before CEF (m)		Maximum height during CEF (m)		Maximum Depth during CEF (m)	
Class 1a	Burn 1	L3	1.21	F4	1.5	L4	2.03	F3-4	1-1.5
	Burn 2	L3	1.21	F3-4	1-1.5	L4	2.03	F2-3	0.5-1
Class 1b	Burn 5	L3-4	1.21-2.03	F3-4	1-1.5	L4-5	2.03-2.78	F1-3	0-1.5
	Burn 8	L2-3	0.59-1.21	F3-4	1-1.5	L5	2.78	F1-2	0.5-1
Class 2	Burn 4	L2	0.59	F4	1.5	L5-6	2.78-3.34	F2-3	0.5-1
	Burn 7	L3-4	1.21-2.03	F3-4	1-1.5	L5	2.78	F1-2	0-0.5

As indicated by the experimentally observed flame heights presented in Table 5.8, the venting plume has a greater reach on the average in Class 2 tests as compared to Class 1 tests. Observations suggest that the width of the plume is also greater than the width of the window opening for Class 2 cases. In fact, the actual width of the plume was approximately 0.5m wider on both sides of the window during most of the CEF period during these tests. For Class 1 cases, the plume width was about the window width. Law's procedure assumes the plume width for a no-through draft test to be the same as the window width; whereas for a through-draft test, slightly wider than the window width. Accordingly, a larger plume width would be expected for Class 1 cases than Class 2 cases. Experimentally, the opposite has been observed as stated above. The flame envelope developed by Law for no-through draft condition has been found to be a conservative approximation for the present through and no-through draft tests.

The actual boundaries of the venting plume are dynamic and vary across the width of the plume, as well as vertically along its centre, as illustrated in Figure 5.52 and Figure 5.53. These figures describe the bellying and the bowing of the plume, respectively. Although Law assumed a constant flame width and depth for design purposes and simplicity, she recognised that variations can exist. Oleszkiewicz[29] matched the bellying of the plume indicated in Figure 5.52, by a triangular flame envelope emerging from a window opening. This envelope is marked in Figure 5.52 by a dashed line (it was reproduced also in Figure 2.9).

Figure 5.52 and Figure 5.53 can also be interpreted as the temperature variation outside the burn room window. As explained previously, vertically along the plume, the temperature reaches a maximum slightly above and away from the opening, and then, the temperature decreases with distance. The maximum temperature occurs in the centre of the plume, and the temperature drops off on both sides of the plume. The pattern given in Figure 5.53 is similar to the temperature distribution given by Law[21, Fig.12] across a flame section, confirming this analogy.

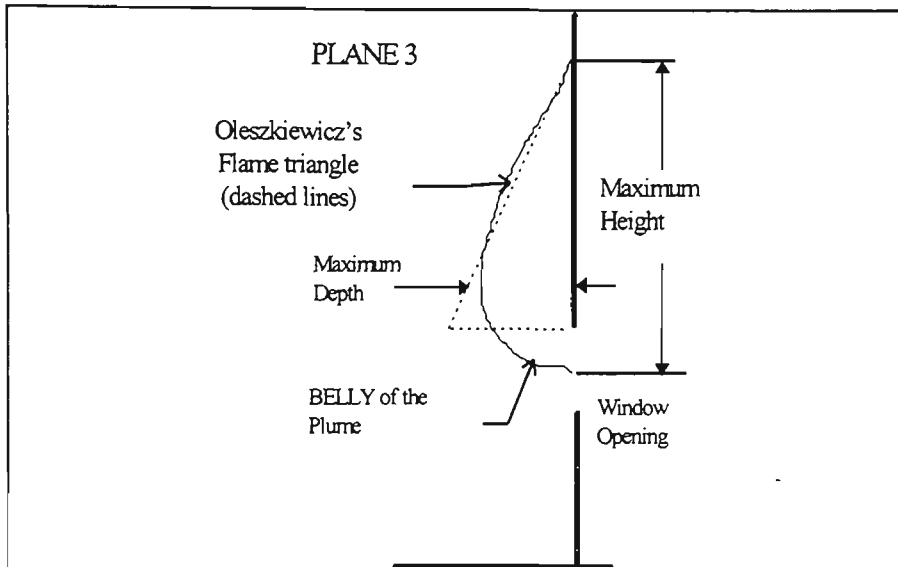


Figure 5.52: Schematic side view of the plume.

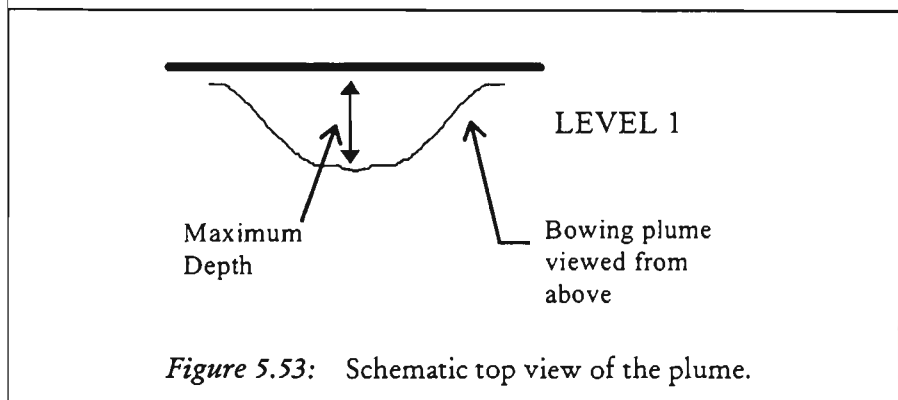


Figure 5.53: Schematic top view of the plume.

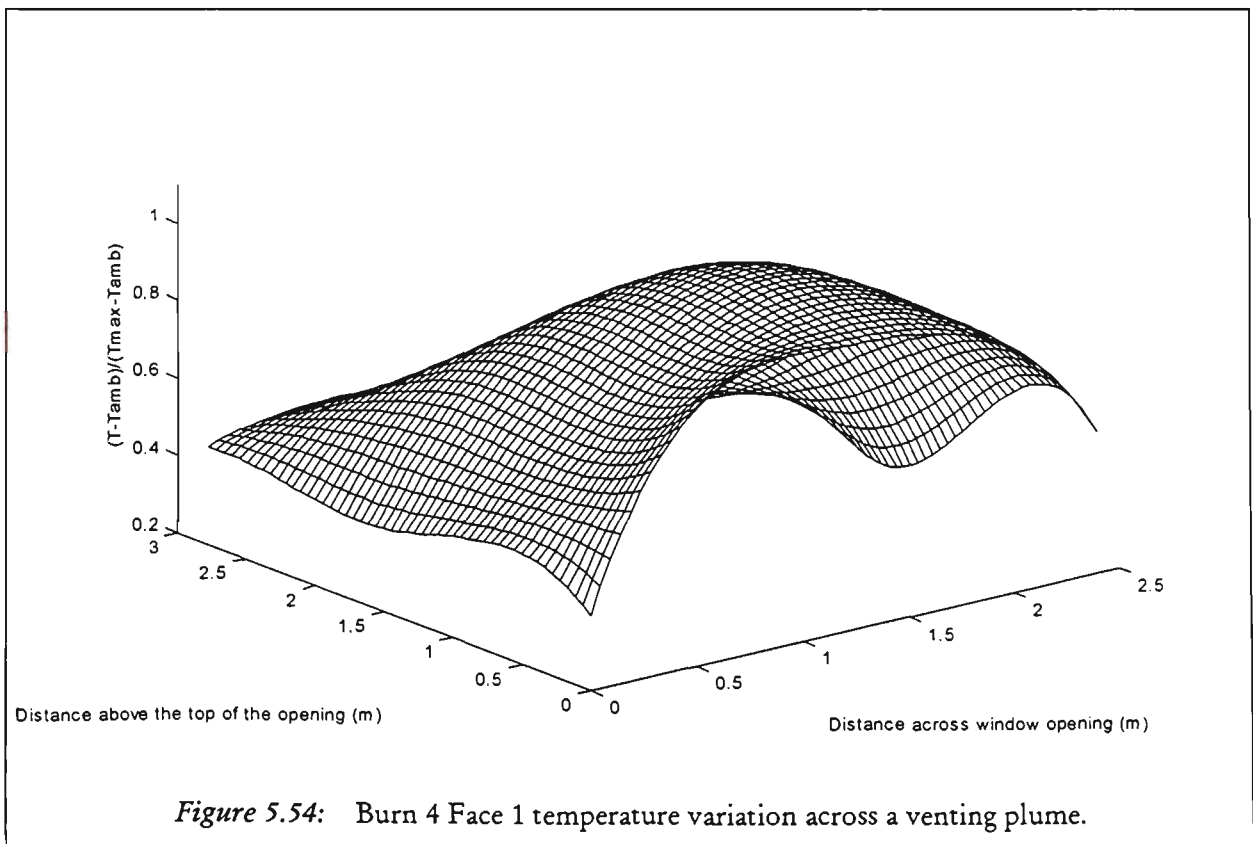


Figure 5.54: Burn 4 Face 1 temperature variation across a venting plume.

This temperature variation is illustrated further in Figure 5.54 in which a combination of the two previous figures is plotted, with a height axis of non-dimensionalised temperature. The temperature variation in Figure 5.54 illustrates that the maximum is reached just above the centre of the window. This 'maximum' drops off towards both sides of the opening.

Observations of flame heights above the burn room window are given in Law[111]. Selecting a room with a fuel load and type (consisting of wood cribs, domestic furniture and office furniture) comparable to the present ones, flame heights of 2.1m to 2.7m were observed with wind speeds varying from 0.5 to 5m/s. These flame heights are in agreement with those observed during this series of test, as indicated in Table 5.8. Greater flame heights corresponding to higher wind speeds are reported in Law[111]. Such an observation was not made in this study.

Equation 2.24 [$l_f = 0.0321(Q/D)^{2/3}$][60] provides an additional means to determine the height of the venting flames above the opening, where Q is the heat release rate ($Q = R \times \Delta H_c$, where R is the averaged CEF burning rate and ΔH_c is the *effective* heat of combustion). The CEF averaged burning rates given in Section 5.5 result in an average of 20kg/min (0.33kg/s), and the *effective* heat of combustion for this series, 19.23 MJ/kg, is provided by Alam and Beever[102, Appendix 5] for complete combustion in the burn room. Therefore, $Q = 0.33 \text{ (kg/s)} \times 19.23 \text{ (MJ/kg)} = 6.36\text{MW}$ (6,360 kW). D is the equivalent window diameter, 2.14m. These values result in a flame length of 6.9m above the top of the window opening. This calculation assumes that all heat is lost through the window, resulting in a calculated flame height just over twice that observed. As also indicated by Quintiere and Cleary[60], when Q is used as the total heat release rate in Equation 2.24, instead of the heat release rate through the window alone, it is expected that higher than experimental flame lengths would be calculated.

To determine the fraction of heat loss rate through the burn room window, Equation 2.24 has been used as follows for the present series of tests. D , the equivalent window diameter is recalculated using only the top half of the window from which the flames emerged during these tests. As such, $D = 1.51\text{m}$. Using an average observed flame height of 2.78m above the burn room window, corresponding to $l_f = 3.53\text{m}$ (as measured from the middle of the window), the heat loss through the window is calculated as 1.7 MW (1,741 kW). This value corresponds to 27% of the total heat released in the burn room.

5.6.2 The Centre-Line Temperature and Comparison with Other Work

The flame axis corresponds to the centre-line of the venting plume, beginning at the window opening and extending vertically up the external wall, in the middle of the plume, as illustrated in Figure 4.16. In Law's equations[21] which estimate centre-line temperatures, the flame temperature is assumed to be constant along the width of the window, and across the depth of the plume. It is further assumed that the flame temperature varies linearly with distance along the flame axis. Strictly speaking, these assumptions are not correct, as shown by the temperature contours given in Figure 5.16 to Figure 5.39.

In Table 5.9, the peak and average burn room temperatures are listed along with the outside plume centre-line temperatures at the intersection of Plane 3 and Face 2 at each Level. Based on the burn room window dimensions, the depth of the plume was determined to be 1.0m from the external wall, using Equation 2.12 (as also discussed in Section 4.2.4). Therefore, the centre-line corresponds to 0.5m, and it lies along the intersection of Plane 3 and Face 2. The outside values are averaged over CEF. Using Equation 2.16, the average temperature during the fully developed period inside the burn room is estimated to be 947°C, with $\eta = A_T / (A_w \sqrt{h}) = 17.5$ (Equation 2.6), and $\psi = L / \sqrt{(A_T A_w)} = 32.11$ (Equation 2.17). Taking the fully developed period to be similar to the CEF, this value falls within the range of experimental average burn room temperatures listed in Table 5.9.

In Table 5.10, the calculated plume centre-line temperatures are listed for each test. These values were calculated using Equation 2.15, with the peak and average burn room temperatures from Table 5.9, in the absence of an opening temperature, T_o . The reason for using the peak burn room temperatures in Equation 2.15 was the closeness of the estimated opening temperature, $T_o = 1067^\circ\text{C}$, calculated using Equation 2.15 to the measured peak temperatures listed in Table 5.9. The opening temperature is estimated as follows. At the flame tip, the temperature is taken to be 520°C above the ambient. Using $T_o - T_{\text{amb}} = 520 / (1 - 0.027lw/R)$ [30] with the length of the flame axis, $l = abc = 2.4 + 0.71 = 3.11\text{m}$ (as shown in Figure 5.55 below), window width $w = 2.4\text{m}$

and mass loss rate, $R=0.4\text{kg/s}$, $T_o=1067^\circ\text{C}$ is calculate for an ambient temperature of $T_{\text{amb}}=20^\circ\text{C}$. In Equation 2.15, l is the distance along the plume axis from the burn room window to the height (at each Level) where the centre-line temperature is being calculated.

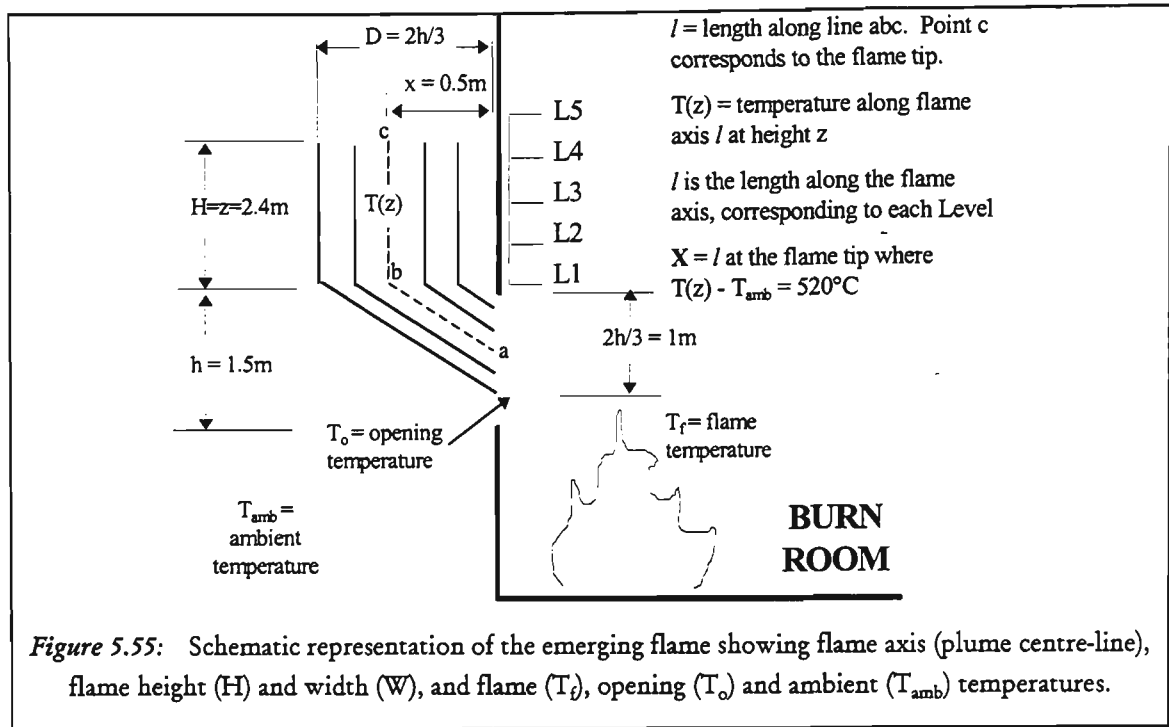


Table 5.9: Measured peak and average burn room temperatures and external centre-line temperatures averaged over CEF. The intersection of Plane 3 and Face 2 corresponds to the centre-line of the plume which was determined to be 0.5m from the external wall, as shown in Figure 5.55.

		Peak Burn Room Temperature (°C)	Average Burn Room Temperature (°C)	EXTERNAL GRID - CENTRE-LINE TEMPERATURES at the intersection of Centre Plane(P3), Face 2 (F2) and indicated Levels (°C)				
				Level 1	Level 2	Level 3	Level 4	Level 5
Class 1a	Burn 1	1001	712	790	512	255	82	45
	Burn 2	1125	831	712	272	141	76	45
Class 1b	Burn 5	1110	896	584	517	355	273	188
	Burn 8	1095	966	794	636	451	306	180
Class 2	Burn 4	1082	956	693	603	421	310	206
	Burn 7	1071	983	558	537	327	264	183

Table 5.10: Calculated center-line temperatures using Equation 2.15. The first and second numbers in each column were obtained using the peak and average burn room temperatures, respectively, from Table 5.9 in Equation 2.15. These calculated values are compared with the measured/CEF averaged ones in Table 5.9.

		Calculated Centre-Line Temperatures using Peak Burn Room Temperature / Average Burn Room Temperature				
		Level 1	Level 2	Level 3	Level 4	Level 5
Class 1a	Burn 1	864 / 615	794 / 566	695 / 496	565 / 404	446 / 320
	Burn 2	970 / 717	891 / 659	779 / 576	632 / 468	497 / 369
Class 1b	Burn 5	957 / 772	877 / 709	767 / 620	621 / 502	488 / 395
	Burn 8	944 / 833	866 / 764	757 / 668	613 / 541	481 / 425
Class 2	Burn 4	933 / 825	856 / 757	749 / 662	607 / 536	477 / 423
	Burn 7	923 / 848	847 / 777	740 / 680	600 / 551	471 / 433

Each peak burn room temperature represents a 19 point averaged value taken from a single thermocouple in the upper layer of the burn room. On the other hand, the average burn room temperatures were obtained as the time average of 70 thermocouple readings[102] (the internal thermocouple arrangement is shown in Figure 3.15). As a result, the average burn room temperatures are expected to be a better representation of the burn room temperature. Consequently, the centre-line temperatures calculated with the average burn room temperatures in Table 5.10, agree better with the measured centre-line temperatures given in Table 5.9. However, even the centre-line temperatures calculated with the measured average burn room temperatures overestimate the measured centre-line temperatures of the plume. In Table 5.9 and Table 5.10, the shaded cells correspond to the presence of observed and expected flames, respectively, as gauged by a flame tip temperature of 540°C. The shaded cells in Table 5.10 indicate that greater flame heights are expected along the centre-line than as shown by the measured temperatures given in Table 5.9. On the other hand, the observed maximum flame heights, given in Table 5.8, exceeded the levels indicated in both of these tables.

Plotted in Figure 5.56 to Figure 5.58 are the measured and calculated centre-line temperatures for Burn 1 and Burn 2, Burn 5 and Burn 8, and Burn 4 and Burn 7, using the corresponding values from Table 5.9 and Table 5.10. In these figures, the temperature of 540°C is marked by a horizontal dashed line. The measured and calculated temperatures plotted above this line correspond to the shaded cells in Table 5.9 and Table 5.10. As expected, the temperatures calculated using Equation 2.15 drop linearly with height. Although this equation is valid for temperatures exceeding

540°C, in Figure 5.56 to Figure 5.58, it is plotted for the complete experimental temperature range. The calculated centre-line temperatures are generally higher than the measured ones, with the exception of the Level 1 values for Burn 1 and Burn 2.

In Figure 5.56 to Figure 5.58, the measured temperatures also drop almost linearly with height. This tendency is seen especially in Figure 5.57 and Figure 5.58, for Class 1b and Class 2 tests, respectively. The sudden drop from Level 1 to Level 3 in the centre-line temperatures seen in Figure 5.56 for the Class 1a tests, has been attributed to direct wind interaction which occurred during these tests (A detailed discussion of Wind Effects is provided in *Section 5.8*) where increased air entrainment reduced the temperatures within the plume.

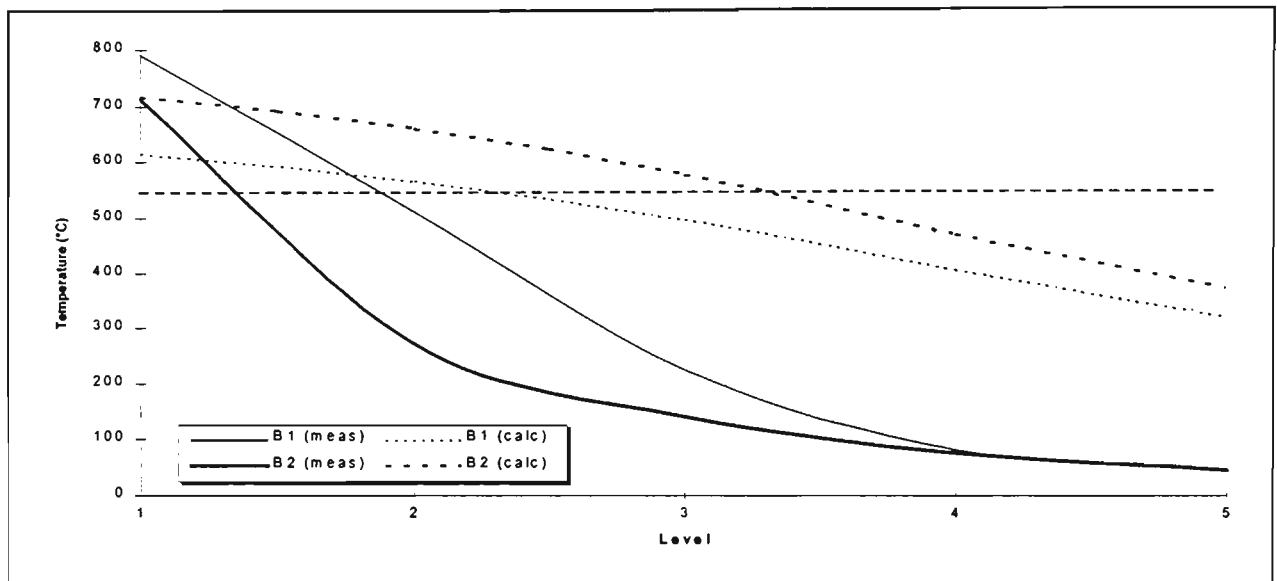


Figure 5.56: Measured and calculated center-line temperature distribution for Burn 1 and Burn 2.

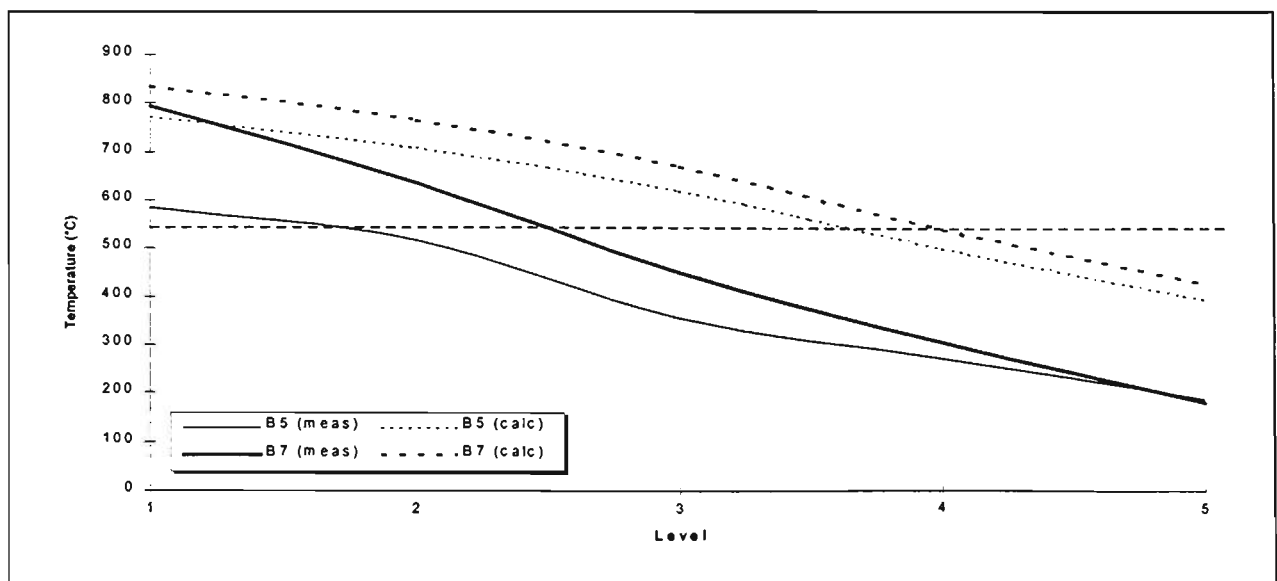


Figure 5.57: Measured and calculated center-line temperature distribution for Burn 5 and Burn 8.

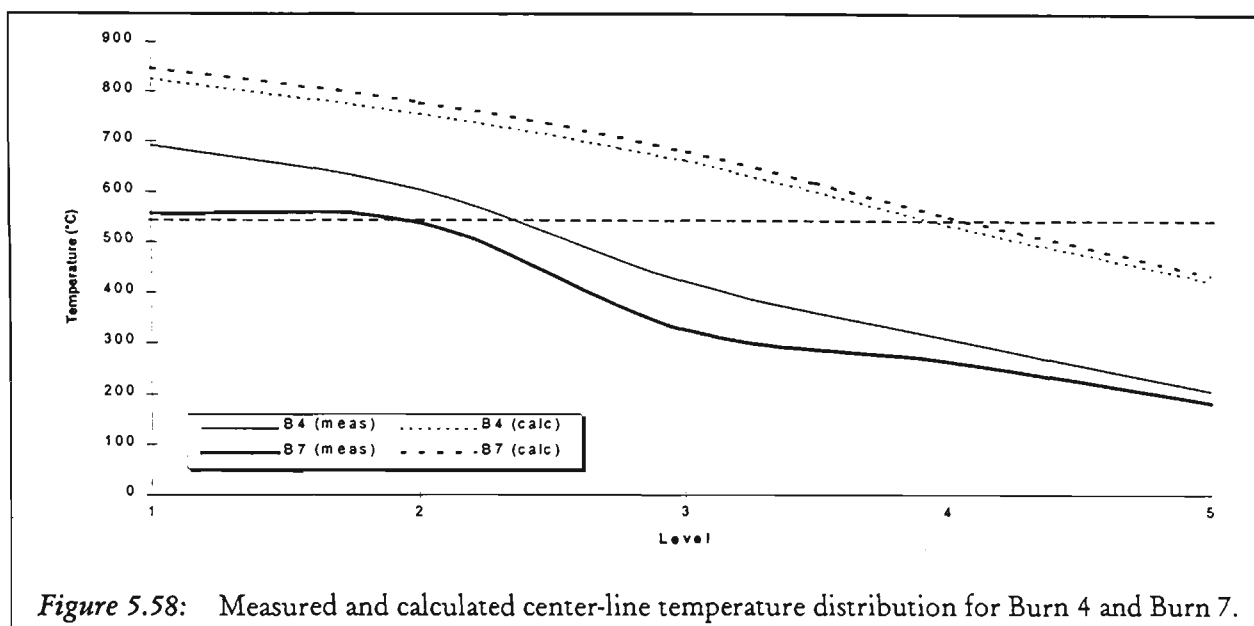


Figure 5.58: Measured and calculated center-line temperature distribution for Burn 4 and Burn 7.

Other methods of estimating the burn room temperature were also investigated to compare with the measured average burn room temperatures. A comparison has been made with Pettersson *et al.*'s[31, pp. 323-330] compartment temperature-time tables at $A_w\sqrt{h}/A_t = 0.05\text{m}^{1/2}$ (here, $A_w = 3.6\text{m}^2$ is the window area; $h = 1.5\text{m}$ is the window height and $A_t = 81\text{m}^2$ is the total enclosed area of the burn room) and with a fire load of $536\text{MJ}/\text{m}^2$. This fire load is calculated using an average fire load of $28\text{kg}/\text{m}^2$ wood equivalent (Table 5.1) and an *effective* heat of combustion of $19.23\text{MJ}/\text{kg}$ [102, Appendix 5]. With fire duration times (beginning from after the onset of flashover) corresponding to 5 and 10 minutes which fall within the experimental CEF durations as indicated in Table 5.5, the expected compartment temperatures are 565 and 798°C , respectively (after interpolating at $A_w\sqrt{h}/A_t = 0.06\text{m}^{1/2}$ for $500\text{MJ}/\text{m}^2$ and averaging the temperature values corresponding to $A_w\sqrt{h}/A_t = 0.04\text{m}^{1/2}$ and $0.06\text{m}^{1/2}$). These values are lower than the measured average burn room temperatures during CEF, listed in Table 5.9, except for that of Burn 1, and the second of these values, 798°C , is close to that of Burn 2. A comparison has also been made of the measured average burn room temperatures with the standard temperatures according to ISO 834 and NFPA No. 251 as listed by Lie[112]. Burn room temperatures of 712°C and 983°C , the minimum and maximum average values of the present tests, would require approximately 10 to 90 minutes of fire duration according to both of these standards. Although the 10-minute duration is close to the experimental CEF duration of 8 minutes during Burn 1, corresponding to the average burn room temperature of 712°C , the 90-minute duration is much longer than the CEF duration of Burn 7. During Burn 7, the CEF duration was 6 minutes corresponding to an average burn room temperature of 983°C .

The 'Method of Babrauskas'[37] can also be used to estimate temperatures in compartment fires using the following expression: $T_g = T_{amb} + (T^* - T_{amb}) \theta_1 \theta_2 \theta_3 \theta_4 \theta_5$ where T_g is the upper gas temperature, T_{amb} is the ambient air temperature (293 K) and T^* is an empirical constant (1725 K). θ_1 to θ_5 are the Burning Rate Stoichiometry, Wall Steady-State Losses, Wall Transient Losses, Opening Height Factor and Combustion Efficiency determined to be 0.97, 0.99, 0.63, 0.82 and 0.88, respectively. Each of the θ factors were determined using the following: A_w = opening area (3.6m²), h = opening height (1.5m), A_t = total surface area of the burn room, including window area (81m²), k = thermal conductivity of gypsum wall (0.48 x 10⁻³ kW/m.c), L = (gypsum layer) wall thickness (0.016m), ρ = density of gypsum wall (1440 kg/m³), c_p = specific heat of the gypsum wall (0.84 kJ/kg K) and b_p = combustion efficiency (taken to be 0.8, following Babrauskas). The equations governing θ_1 to θ_5 are listed in Appendix E. The expression above leads to an estimated gas temperature of 764°C. This value is between the average burn room temperatures of Burn 1 and Burn 2, 712°C and 831°C, respectively, but it is lower than the average burn room temperatures measured during the remaining tests.

5.6.3 Further Comparisons with Other Work: Centre-Line Temperature, Re-Attachment, Spandrel Length and Excess Fuel Factor

As discussed in Section 2.4, "Early Experimental Studies on Externally Venting Flames", Yokoi's[28] study of plumes with respect to centre-line temperatures, window shape and spandrel lengths provides one of the few sets of reliable data in this area. As such, a comparison of the present data is made with his. In addition, Sugawa and Takahashi's[72] centre-line temperature formulation is used for comparison with the experimental data. As an indication of flame height, Bullen and Thomas's [56] excess fuel factor is investigated.

Centre-Line Temperature

Using Equation 2.1 [$\Delta T_m = 24.6 Q^{2/3} Z^{-5/3}$][52], a comparison of the calculated and measured centre-line temperatures can be made. Here, ΔT_m is the temperature rise above the ambient along the centre-line and $T_{amb} = 20^\circ\text{C}$; Q is the CEF averaged heat

release rate, 6,360kW, as calculated previously in *Section 5.6.1*; Z (m) is the height above the virtual source. The virtual source is determined as follows. Assuming that the flames emerge from the upper half of the window, they occupy an area of 1.8m² (0.75mx2.4m) corresponding to an equivalent diameter of 1.51m². With a divergence angle of 15° leading to the virtual source beneath the fuel source, a corresponding vertical distance of 2.82m can be calculated. This length corresponds to the distance from the virtual source to Level 1 of the thermocouple grid. Hence, for each of the remaining levels, Z is calculated as follows: $Z = 2.82 +$ the vertical distance to each Level of the grid from Level 1. Therefore, Z_1 to Z_5 are 2.82, 3.41, 4.03, 4.85 and 5.6m. Substituting these values into Equation 2.1 results in the following centre-line temperatures:

$$T_1 = 24.6 (6,360)^{2/3} (2.82)^{-5/3} - 20 = 1480^\circ\text{C} \quad \text{at Level 1}$$

$$T_2 = 1073^\circ\text{C} \quad \text{at Level 2}$$

$$T_3 = 807^\circ\text{C} \quad \text{at Level 3}$$

$$T_4 = 588^\circ\text{C} \quad \text{at Level 4}$$

$$T_5 = 478^\circ\text{C} \quad \text{at Level 5}$$

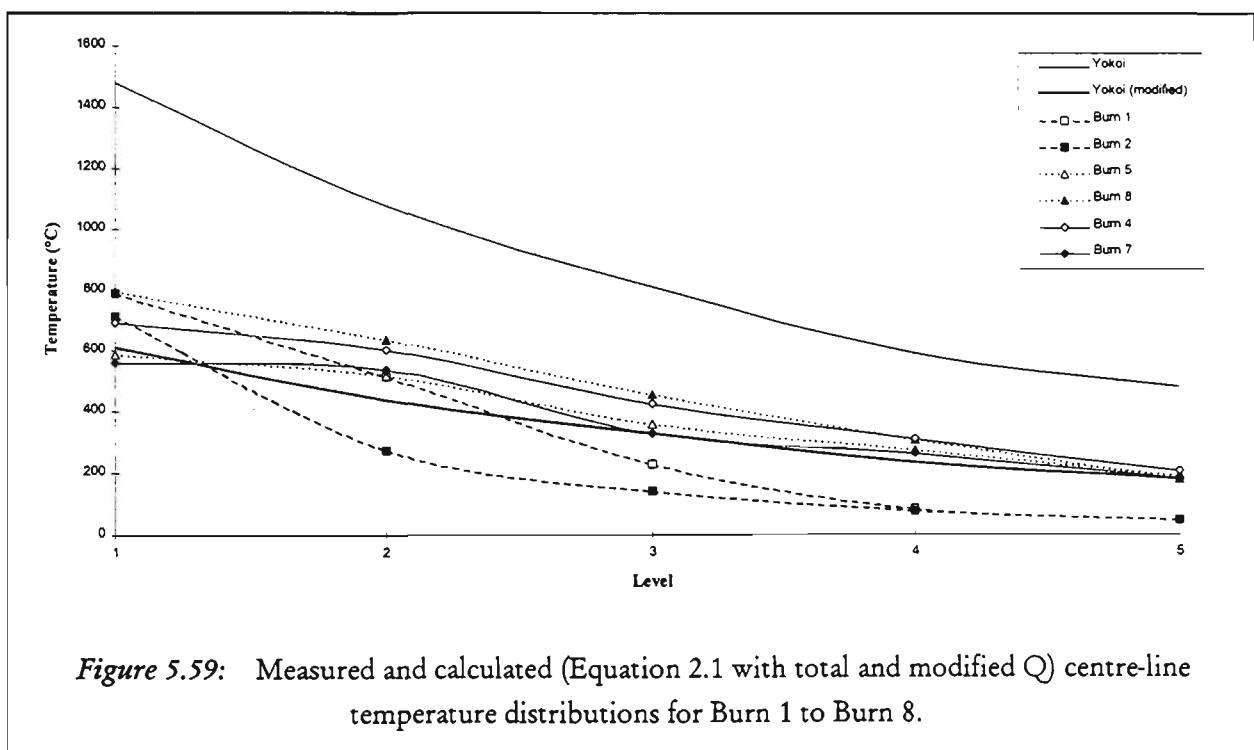
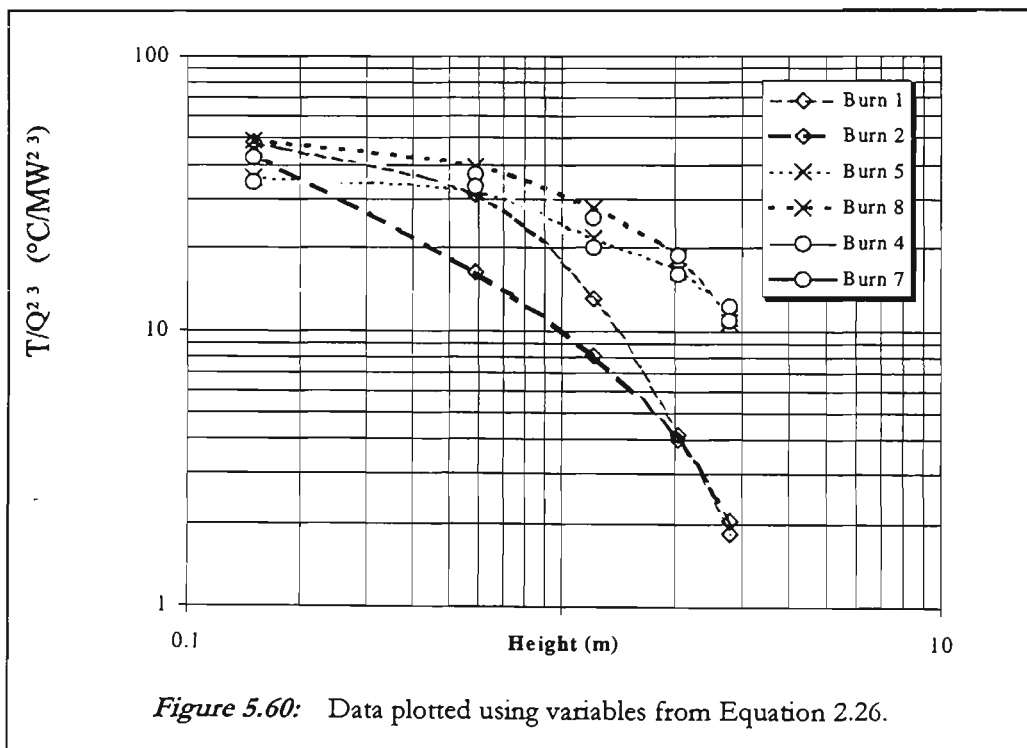


Figure 5.59: Measured and calculated (Equation 2.1 with total and modified Q) centre-line temperature distributions for Burn 1 to Burn 8.

In Figure 5.59, the centre-line temperature distributions obtained during Burn 1 to Burn 8 are compared with Yokoi's results. Equation 2.1 results in consistently higher values when a total Q of 6.36 MW is used than those measured. In Figure 5.59,

another set of calculated centre-line temperature distribution is also given, corresponding to a modified Q value of 27% of the total Q, representing the heat release rate through the burn room window as calculated in *Section 5.6.1*. This calculation was based on matching the observed flame height with the estimation given by Equation 2.24[60]. The modified line of calculated centre-line temperatures is lower than the one corresponding to the original equation, Equation 2.1. Although the modified line is closer to the measured values, its starting temperature at Level 1 is generally lower than those measured, while its ending temperature at Level 5 corresponds to those of Class 1b and Class 2 tests.

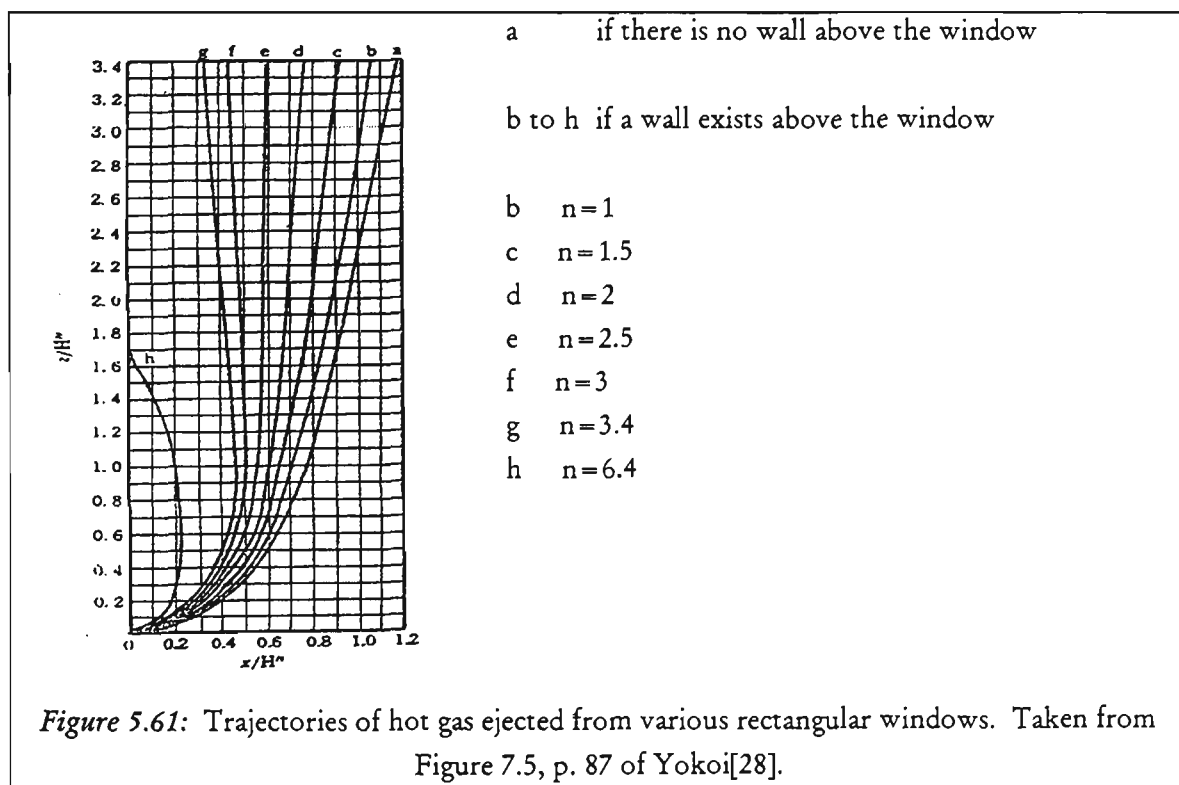
Sugawa and Takahashi's[72] representation of the centre-line temperature is given by Equation 2.26. In Figure 5.60, the centre-line temperatures measured during Burn 1 to Burn 8 are plotted using the variables of Equation 2.26, z versus $\Delta T/Q^{2/3}$ in logarithmic scale, where Q has been taken as the heat release rate through the burn room window as described above. Excluding the results of Burn 1 and Burn 2, the experimental data follow an almost linear pattern, as expected from Equation 2.26.



Re-Attachment

Equation 2.3 defines the parameter n [$n = w/(1/2h)$][28], which can be used to determine whether re-attachment of the plume above the window opening will occur. This parameter is based on the window width, w , and the height of the window from which the plume emerges, h ($w = 2.4\text{m}$, and $h = 0.75\text{m}$).

When $n \geq 6.4$ re-attachment is expected to occur as shown in Figure 5.61 below (taken from Figure 7.4, p 87 of Yokoi). Line 'h' on this figure, corresponds to the window shape in this study, where $n = 2.4 / (1/2 \times 0.75) = 6.4$. Re-attachment occurred in all tests of this series, as expected. However, it was not possible to specify an experimental re-attachment height, because there was no separation bubble above the burn room window during CEF.



Spandrel Length

The spandrel length, necessary to prevent the failure of the glass, is the distance between the top of the window from where the plume emerges and the bottom of the window on the level above. Using Table A1 (duplicate of Table 9.9 from Yokoi[28]) an approximate spandrel length can be estimated for the EB-FF (Experimental Building Fire Facility). The values in this table are based on a plume temperature of 500°C as a measure of when the window in the level above the room of fire origin will dislodge. Using a window size of $3\text{m} \times 2\text{m}$ as the closest to that of the EB-FF, and $25\text{kg}/\text{m}^2$ as

the quantity of combustibles in the room, a recommended spandrel length of 95cm is obtained from Table A1. Although the actual spandrel length between the burn room and mezzanine floor windows is 1.21m, dislodgment of the glass from the mezzanine floor window occurred during all tests. Level 3 of the external grid is positioned at the bottom of the mezzanine floor window. According to the Plane 3 contour plots presented in *Section 5.4*, temperatures measured at this height above the opening were 365°C for Burn 1 and 182°C for Burn 2, and they were in excess of 500°C for the remaining tests. Consequently, it is concluded that Yokoi's criterion is insufficient for the dislodgment of the glass from the window above the room of fire origin, because it does not account for the thermal gradient [62 - 67] across the glass leading to breakage. As a result, calculations on spandrel length using Yokoi's data underestimate the necessary spandrel length to prevent failure of the window on the level above the room of fire origin.

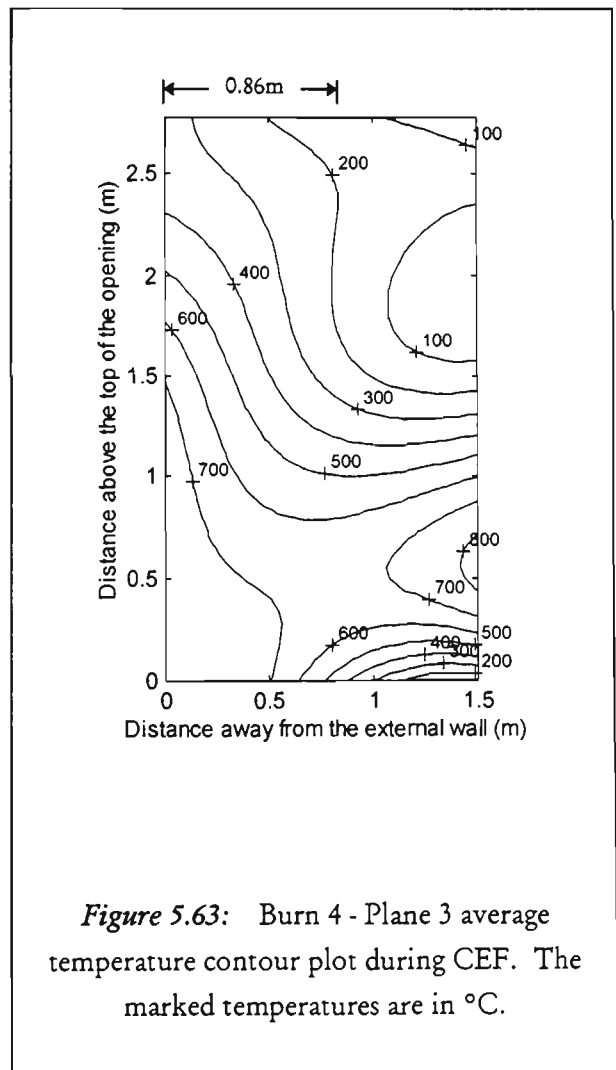
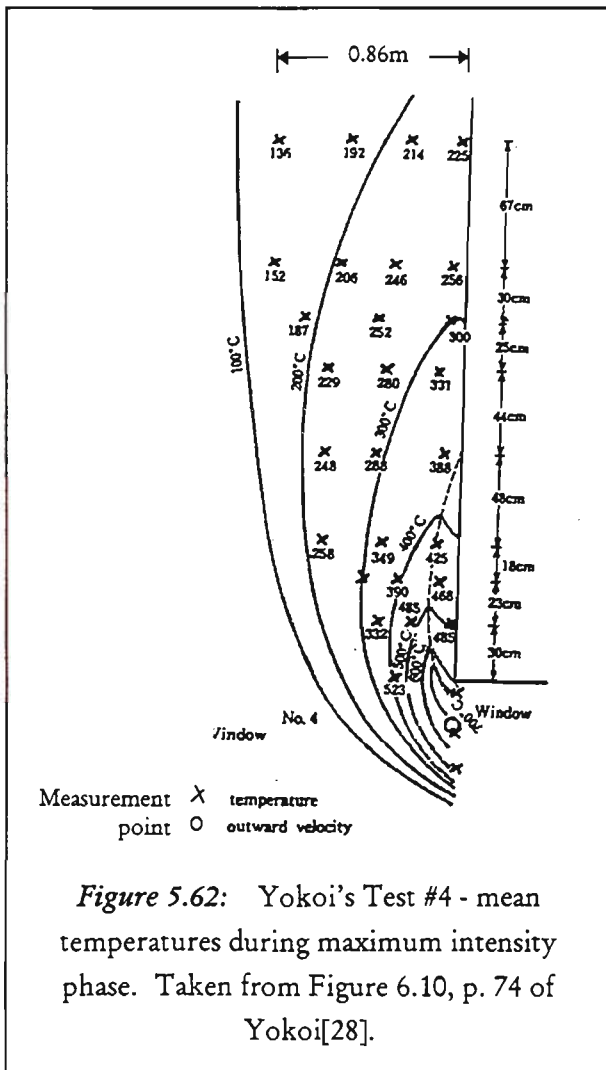
Temperature Contours

Internal ventilation conditions of Burn 4 and Burn 7 correspond to Yokoi's Test #4, a Class 2 test. Of Yokoi's full-scale tests, Test #4 is the closest to Burn 4 and Burn 7 with respect to the room and window size, fuel load and wind speed. Given the repeatability of the Class 2 tests, only Burn 4 has been used here for comparison with Yokoi's Test #4.

Yokoi's Test #4 was carried out in a concrete house at the Building Research Institute of Japan. The room measured 5 x 2.5 x 1.67m high, with a single window opening measuring 3m wide by 1m high. The weight of wood used totalled 500kg which corresponded to 40kg/m². In addition, the ceiling and the walls were lined with ply wood. Weather conditions on the day of the test were recorded as *Fine* with an Easterly wind of 1m/s. Temperatures were measured using chrome-alumel thermocouples at six locations, 30cm under the ceiling, within the burn room, and at 30 locations outside centre of the window, 0.86m away and 2.82m above the top of the opening. In Figure 5.62, the solid lines are the isotherms drawn based on temperature measurements during the maximum intensity phase (which lasted 18 minutes, internally), and the dashed line represents the maximum velocity flow path. Flames were observed to reach 5m along the external wall for approximately 2 minutes, with peak internal and external flame temperatures of approximately 810°C and 750°C, and mean outflow velocity along the plume centre-line of 4.55m/s measured using a Pitot tube.

Burn 4 temperature contours during CEF are given in Figure 5.63 for Plane 3. Plane 3 corresponds to the centre plane of the plume, located above the middle of the burn room window and perpendicular to the external wall, similar to where Yokoi's measurements were taken. In Figure 5.62 and Figure 5.63, similar horizontal and vertical distances are marked. The 700°C contour in Figure 5.63 follows a path similar to that of the line of maximum velocity in Figure 5.62. However, the temperatures along this line are much lower in Test #4. The observed flame height in Burn 4, between 2.78 to 3.34m, is lower than that of Test #4, although the peak internal and external flame temperatures are comparable.

Figure 5.63 illustrates that the plume vented differently in Burn 4 than Test #4. Higher temperatures are shown both horizontally away and vertically up from the window opening in Burn 4. The isotherms shown in Figure 5.62 represent the ideal curved path of the venting flame, with a gradual drop in temperature away from the window opening. While the temperature contours from Plane 3 of Burn 4 do not explicitly follow this shape, they also curve out and then return to the external wall.



Excess Fuel Factor

Excess fuel factor was used by Bullen and Thomas[56] to aid in their explanation of external flames. They linked the height of the external flames to the amount of unburnt fuel leaving the compartment. The larger the positive excess fuel factor, f_{ex} , is, the higher the flame height must be. As presented in Equation 2.22, $f_{ex} = 1 - m/rR$, where air mass flow rate, m is in (kg/s), r is the stoichiometric ratio and R is the rate of burning (kg/s). For the Real Furniture Burns, $r \approx 6.25$ for wood[49, p.111] and the average measured rate of burning, $R \approx 0.33$ kg/s. Using Equation 2.23 for the air mass flow rate into the room, $m = 0.5 A_w h^{1/2}$, where window area, $A_w = 3.6\text{m}^2$ and window height, $h = 1.5\text{m}$, an excess fuel factor, $f_{ex} = -0.1$ is calculated as an average value for this series of tests. Hence, similar to the PU Burns and as discussed in Drysdale[31, p347], the Real Furniture Burns indicate the presence of external flaming for an excess fuel factor less than zero. Possible discrepancies in the application of Bullen and Thomas' equation may have lead to this result. A stoichiometric ratio of 6.25 (oxygen:fuel) has been used here. Even though the majority of the fuel in the burn room was wood (as indicated by the fuel load breakdown presented in Table 3.4), this ratio does not take into account the remaining approximately 40% composition of the fuel in the room. This stoichiometric ratio is higher for many of the additional synthetic components found in the furniture, such as polyurethane ($r \approx 12.21$ air:fuel) as discussed in Section 4.2.3, of the Polyurethane Burns. As such, the stoichiometric ratio would need to be modified to take these differences into account. A higher stoichiometric ratio would result in a higher excess fuel factor.

It is not possible to compare the present results with Bullen and Thomas'[56] correlation of excess fuel factor with radiant heat flux received by the external building facade just above the window opening. The reason is that radiation heat flux measurements were not taken above the burn room window, but at the center of the Floor 1M window in the present study.

5.6.4 Centre Plane Temperature Distribution on Face 1, Face 2 & Face 3

Equation 2.15 in *Section 2.4.1*, indicates a linear temperature variation along the centre-line of the plume as shown by the dashed lines in Figure 5.56 to Figure 5.58. Although the measured temperatures do not have a linear drop with height above the burn room window in general, along the plume centre-line (at the intersection of Plane 3 and Face 2), the variation is almost linear as seen in the same figures. In the following, the CEF averaged centre plane temperatures for Plane 3/Face 1 to Plane 3/Face 3 have been used to determine a relationship between the dimensionless plume temperature along its centre and lw/R . lw/R was chosen in order to compare the resulting expression for Plane 3/Face 2 with Equation 2.15. The experimental data from the centre plane of the 3D external thermocouple grid and curves of best fit are given in Figure 5.64 to Figure 5.69.

In Figure 5.64, Figure 5.66 and Figure 5.68, the dimensionless plume temperature is plotted against lw/R along the intersection of Plane 3 with Face 1, Face 2 and Face 3, respectively, for all tests, Burn 1, Burn 2, Burn 4, Burn 5, Burn 7 and Burn 8. As explained in *Section 5.5* on Repeatability, the results from Burn 1 and Burn 2, were found to be the most dissimilar. These results are included in Figure 5.64, Figure 5.66 and Figure 5.68, but they were not used when determining the expressions below. While the selected tests belong to different classes, as explained previously, the plume vented predominantly from the upper half of the window for these tests. This typical Class 2 ventilation condition characteristic occurred also for Class 1 ventilation cases due to the large size of the burn room window. For this reason, the results from both Classes were combined for the following empirical estimates.

The average of the temperature curves for Burn 4, Burn 5, Burn 7 and Burn 8 plotted in Figure 5.64 is given in Figure 5.65 along with the best fit. The equation of the best fit to the temperature variation along the intersection of Plane 3 and Face 1 is,

$$(T_z - T_{\max}) / (T_o - T_{\text{amb}}) = 0.0003l^3 (w/R)^3 - 0.0074l^2 (w/R)^2 + 0.0297l(w/R) + 0.61 \quad \text{Equation 5.1}$$

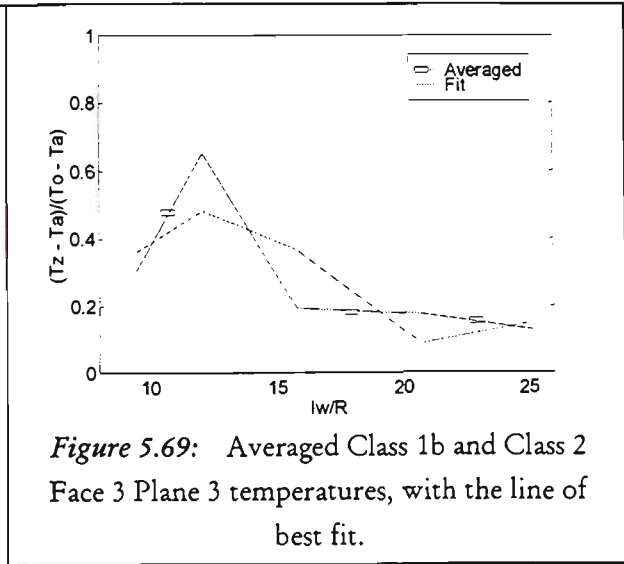
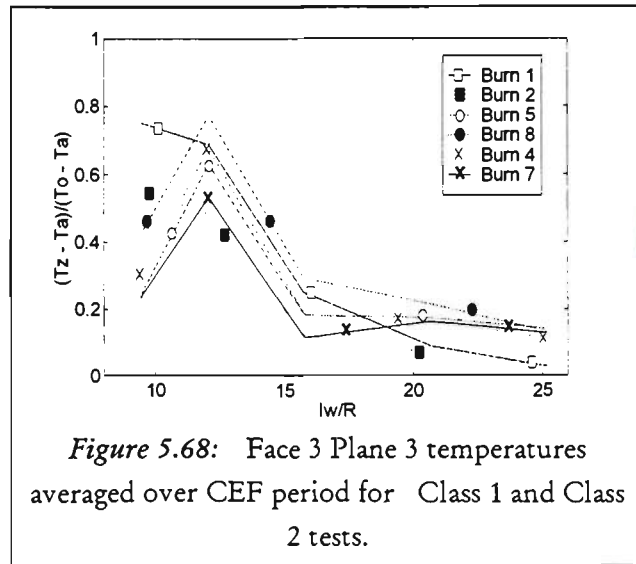
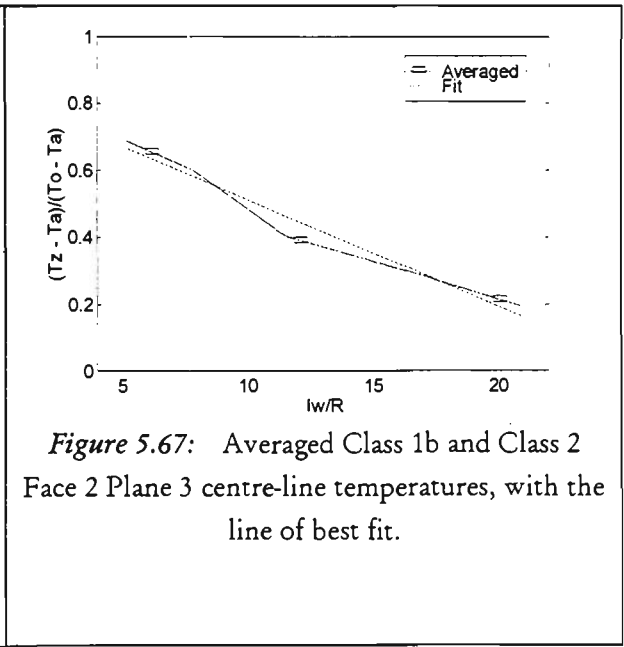
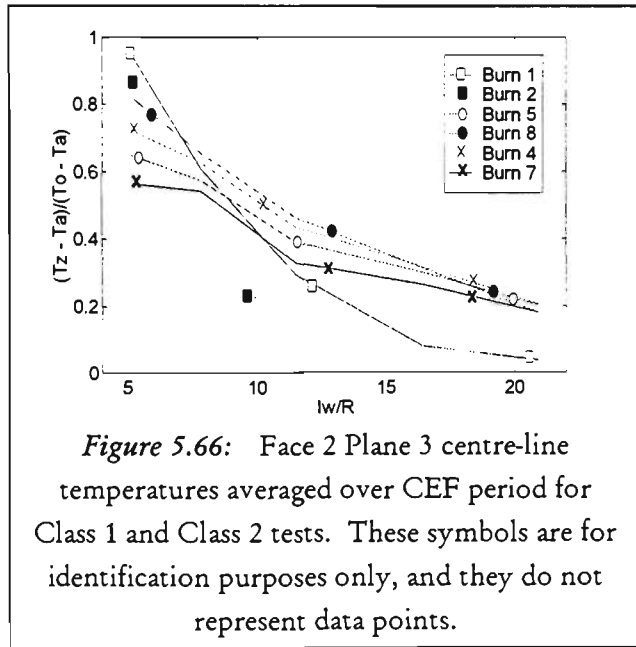
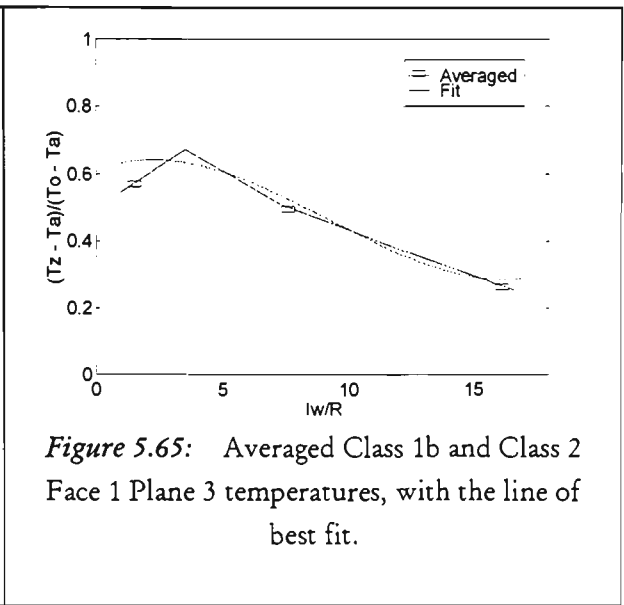
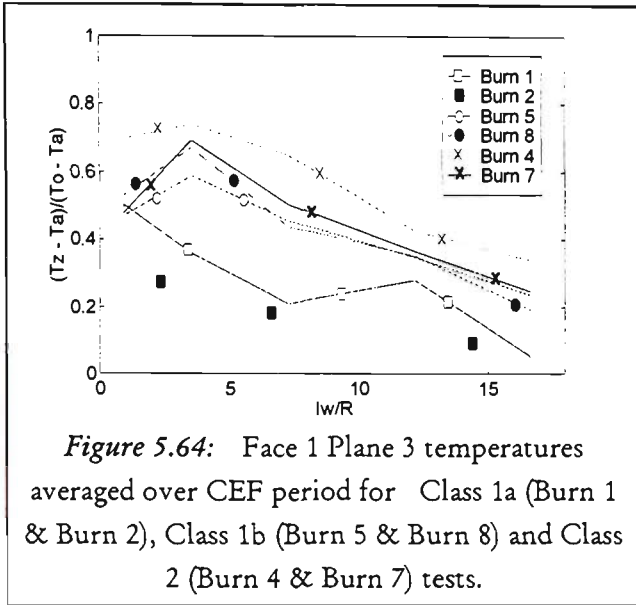
In Figure 5.66, the dimensionless centre-line temperatures along Plane 3 and Face 2 are given for Class 1b and Class 2 tests. The average of the curves for Burn 4, Burn 5, Burn 7 and Burn 8 are plotted in Figure 5.67 with the line of best fit. As mentioned previously, this variation is almost linear:

$$(T_z - T_{\max}) / (T_o - T_{\text{amb}}) = -0.0318l(w/R) + 0.829 \quad \text{Equation 5.2}$$

Equation 5.2 above is similar to Equation 2.15, with slightly modified gradient and intercept values. This similarity indicates that Law's equation developed from wood crib fires is applicable to the Real Furniture Burns.

In Figure 5.68, the dimensionless plume temperature is plotted against lw/R along Face 3 and Plane 3 for the Class 1b and Class 2 tests. The average curve for Burn 4, Burn 5, Burn 7 and Burn 8 is given in Figure 5.69 along with the curve of best fit. The equation of best fit is:

$$(T_z - T_{\max}) / (T_o - T_{\text{amb}}) = 0.0008l^3 (w/R)^3 - 0.0422 l^2 (w/R)^2 + 0.0672l(w/R) - 2.9 \quad \text{Equation 5.3}$$



5.6.5 Temperature Distribution across each Face of the Grid

Within the external plume, temperature variations exist along both the width and depth and not just the height of the plume. This variation is clearly illustrated in the 5-leveled contour plots (Figure 5.22 and Figure 5.23, Figure 5.30 and Figure 5.31, Figure 5.38 and Figure 5.39) for each of the ventilation classes. Law's equations (Equation 2.11 to Equation 2.16) give an indication of the overall reach and severity of the plume for design purposes. However, the variation of temperature within the plume is not considered except with height along the centre-line. A 3D representation of the external plume has been lacking in the literature. The following 3D polynomial fits to the temperature data across Face 1 to Face 4, have been developed to fill this gap. Such representations accomplish two objectives. The first is that the entire plume needs to be considered when ascertaining its effect on the outside environment and the external wall. Secondly, the CEF averaged and non-dimensionalised external temperature data for each ventilation class can hence be represented for easier communication of the experimental data with other researchers in the field, for performance based design code and model validation purposes.

The temperature results obtained from Face 1 of the experimental grid provide the best means to assess the impact of the venting plume on the external wall above the opening, with respect to direct flame contact. Additional temperature information gained by considering Face 2, Face 3 and Face 4 provides details regarding the structure of the plume and the variation in temperature within the plume. It is this variation which allows the transfer of heat from inside the plume to the external wall via radiation. Combined, this information can be interpreted in terms of Secondary Fires, with respect to direct flame contact and the transfer of heat, on the external wall and window above the room of fire origin, and it may be extended to assess the viability of combustible linings.

The measured temperatures have been averaged over the CEF period and non-dimensionalised. The space coordinates of the experimental results from each Face have also been non-dimensionalised in terms of the window width and height. This analysis was carried out for the purpose of generating a series of 3D fourth order polynomial fits which describe the temperature variation across each Face of the

experimental grid, thus providing a continuous empirical description of the venting plume. Each surface fit is represented as a fourth order polynomial fit. The Vandermonde matrix method[105] is used to determine the coefficients of a three-dimensional polynomial equation based on the experimental results, and a fourth order polynomial was chosen, as it provided a good approximation to the experimental results.

The following section provides the surface fits for Face 1 for Burn 2, Burn 4 and Burn 8, representing their respective ventilation classes. The comparison between the experimental results and 3D fourth order polynomial surface fits is given in the pairs of figures for Burn 2, Burn 4 and Burn 8, in Figure 5.70 to Figure 5.75. In these pairs of figures, the experimental results over Face 1 is given first in Figure 5.70, Figure 5.72 and Figure 5.74 for each test, followed by the corresponding 3D polynomial fits in Figure 5.71, Figure 5.73 and Figure 5.75, respectively. The non-dimensionalised experimental temperature is plotted against w , the window width and $2h$, twice the window height. The window width is 2.4m, and the height is 1.5m. Hence, a 2.4m x 3m region is covered above the burn room window which corresponds approximately to a Face. The 3D fourth order polynomial surface fits are plotted against non-dimensionalised x and y coordinates representing the dimensionless window and height, respectively. For non-dimensionalisation of the space co-ordinates, $w=2.4m$ and $h=1.5m$ are used for x and y , respectively.

Matrix equations have been used to simplify each polynomial. The coefficient and space variable matrices for Burn 2, Burn 4 and Burn 8, are given in Table 5.11 for Face 1. This table provides the information required to plot Figure 5.71, Figure 5.73 and Figure 5.75. The coefficients to define the fitted surfaces for Face 2 to Face 4 of Burn 2, Burn 4 and Burn 8 are given in Appendix F.

Table 5.11: Coefficients and variables of the 3D polynomial. T represents the CEF averaged and non-dimensionalised temperature (a 5 x 5 matrix) on Face 1 for Burn 2, Burn 4 and Burn 8, and x and y represent the dimensionless distance across and up from the burn room window, respectively. The window width and height of 2.4m and 1.5m were used to non-dimensionalised x and y, respectively.

Burn 2 - Face 1		
$T =$	$\begin{bmatrix} 0.029 & -0.270 & 0.727 & -0.546 & -0.041 \\ -0.189 & 1.640 & -4.287 & 3.260 & 0.173 \\ 0.336 & -2.794 & 7.132 & -5.317 & -0.442 \\ -0.137 & 1.092 & -2.613 & 1.557 & 0.535 \\ 0.037 & -0.205 & 0.297 & -0.119 & 0.384 \end{bmatrix}$	$\begin{bmatrix} y^4 x^4 & y^3 x^4 & y^2 x^4 & y x^4 & x^4 \\ y^4 x^3 & y^3 x^3 & y^2 x^3 & y x^3 & x^3 \\ y^4 x^2 & y^3 x^2 & y^2 x^2 & y x^2 & x^2 \\ y^4 x & y^3 x & y^2 x & y x & x \\ y^4 & y^3 & y^2 & y & c \end{bmatrix}$
Burn 4 - Face 1		
$T =$	$\begin{bmatrix} -0.061 & 0.432 & -1.003 & 0.818 & -0.178 \\ 0.235 & -1.838 & 4.657 & -4.088 & 0.923 \\ -0.369 & 3.029 & -7.883 & 7.029 & -1.875 \\ 0.326 & -2.366 & 5.475 & -4.468 & 1.711 \\ -0.047 & 0.313 & -0.669 & 0.484 & 0.381 \end{bmatrix}$	$\begin{bmatrix} y^4 x^4 & y^3 x^4 & y^2 x^4 & y x^4 & x^4 \\ y^4 x^3 & y^3 x^3 & y^2 x^3 & y x^3 & x^3 \\ y^4 x^2 & y^3 x^2 & y^2 x^2 & y x^2 & x^2 \\ y^4 x & y^3 x & y^2 x & y x & x \\ y^4 & y^3 & y^2 & y & c \end{bmatrix}$
Burn 8 - Face 1		
$T =$	$\begin{bmatrix} 0.228 & 1.417 & -2.874 & 1.942 & -0.058 \\ 1.181 & -7.322 & 14.706 & -9.647 & 0.273 \\ -1.901 & 11.738 & -23.096 & 14.600 & -0.633 \\ 0.957 & -5.825 & 11.109 & -6.529 & 0.616 \\ -0.080 & 0.457 & -0.818 & 0.432 & 0.453 \end{bmatrix}$	$\begin{bmatrix} y^4 x^4 & y^3 x^4 & y^2 x^4 & y x^4 & x^4 \\ y^4 x^3 & y^3 x^3 & y^2 x^3 & y x^3 & x^3 \\ y^4 x^2 & y^3 x^2 & y^2 x^2 & y x^2 & x^2 \\ y^4 x & y^3 x & y^2 x & y x & x \\ y^4 & y^3 & y^2 & y & c \end{bmatrix}$

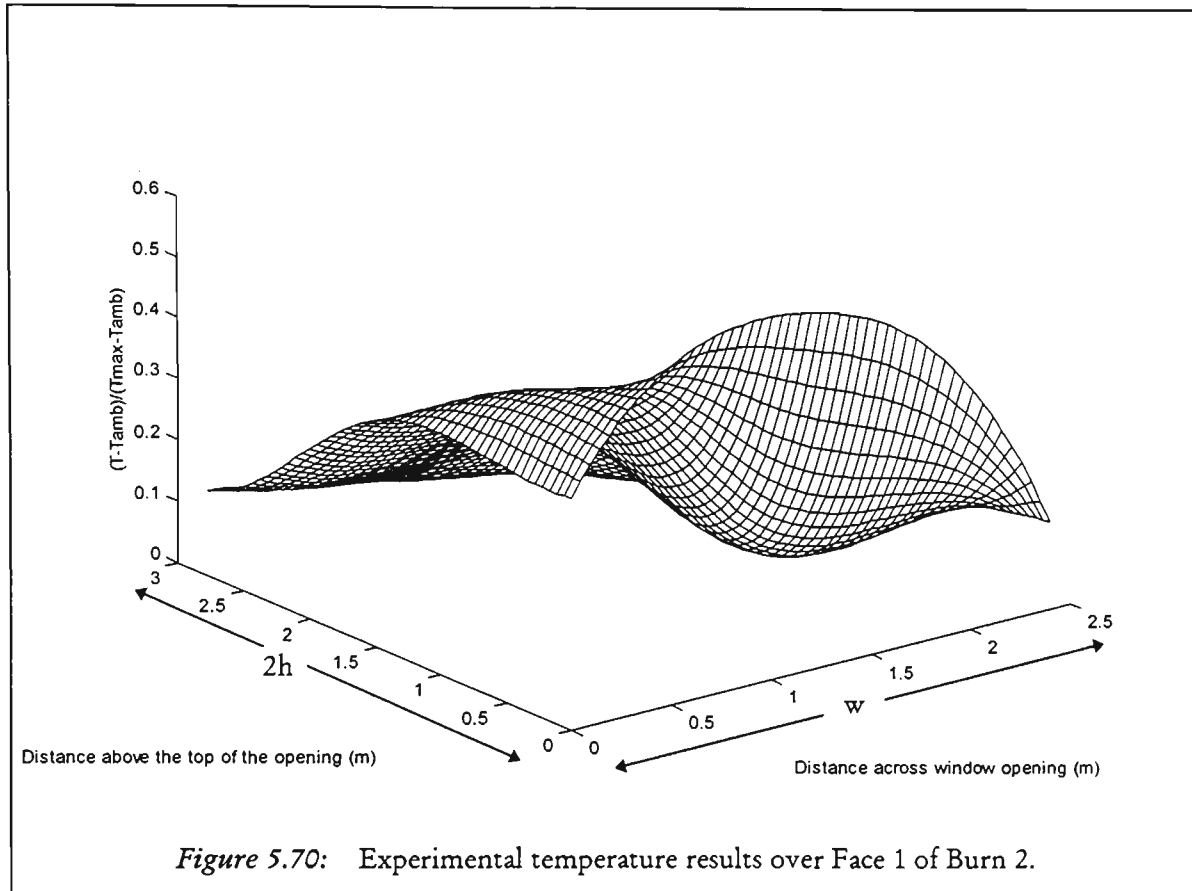


Figure 5.70: Experimental temperature results over Face 1 of Burn 2.

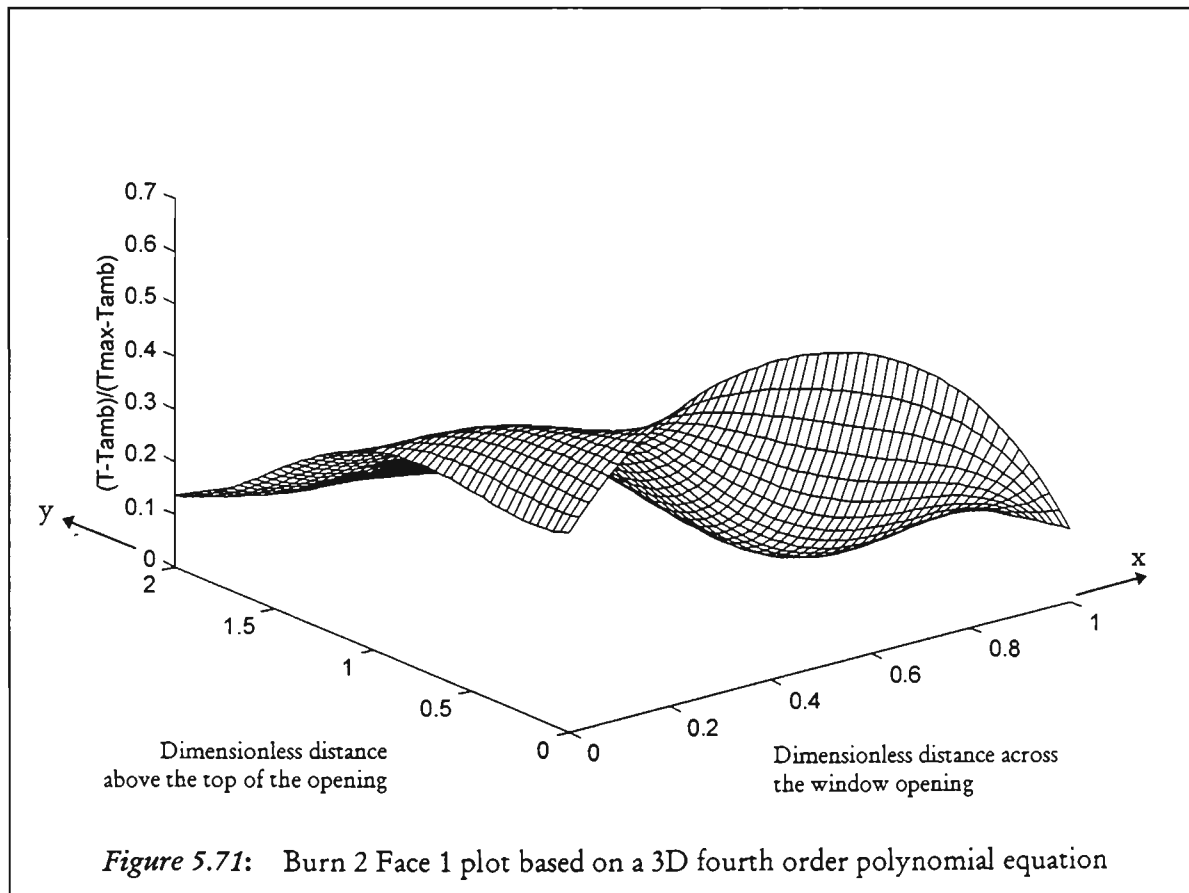
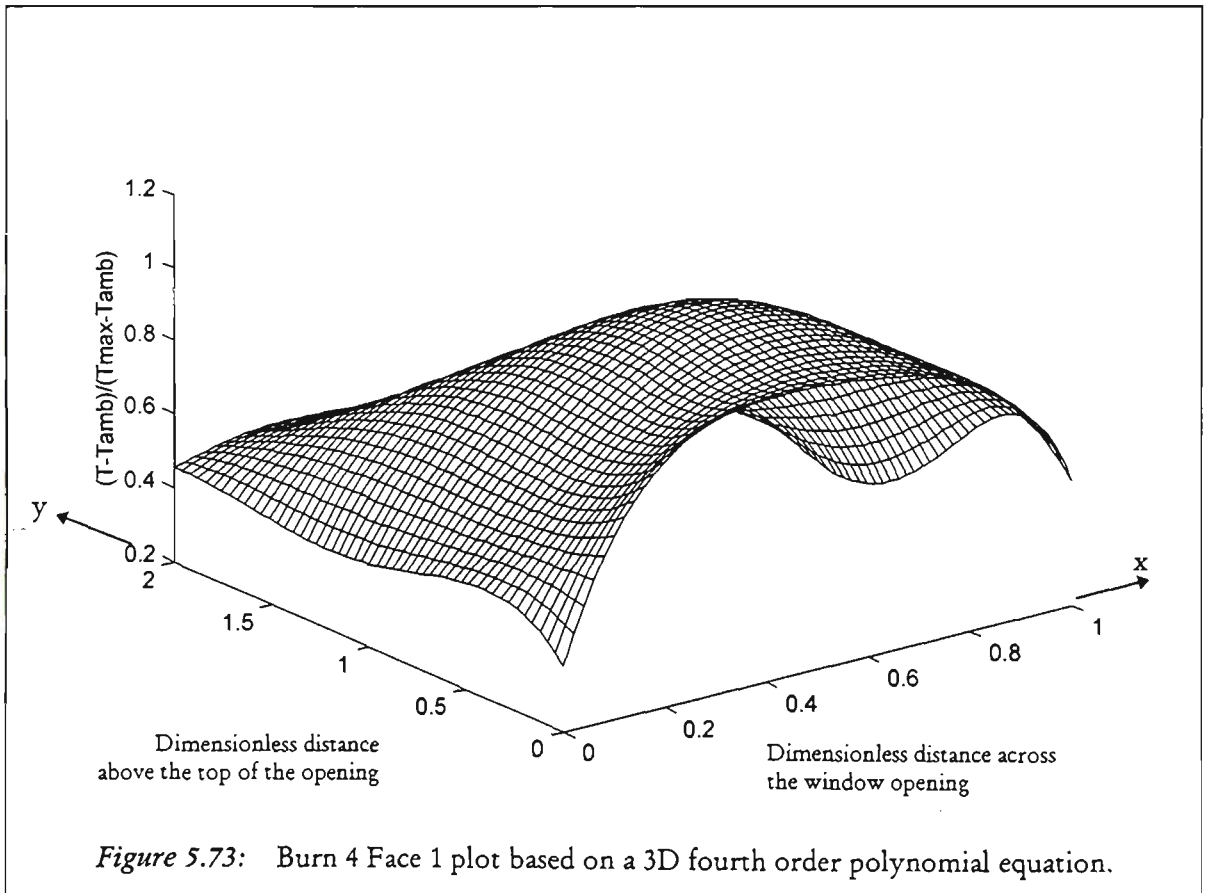
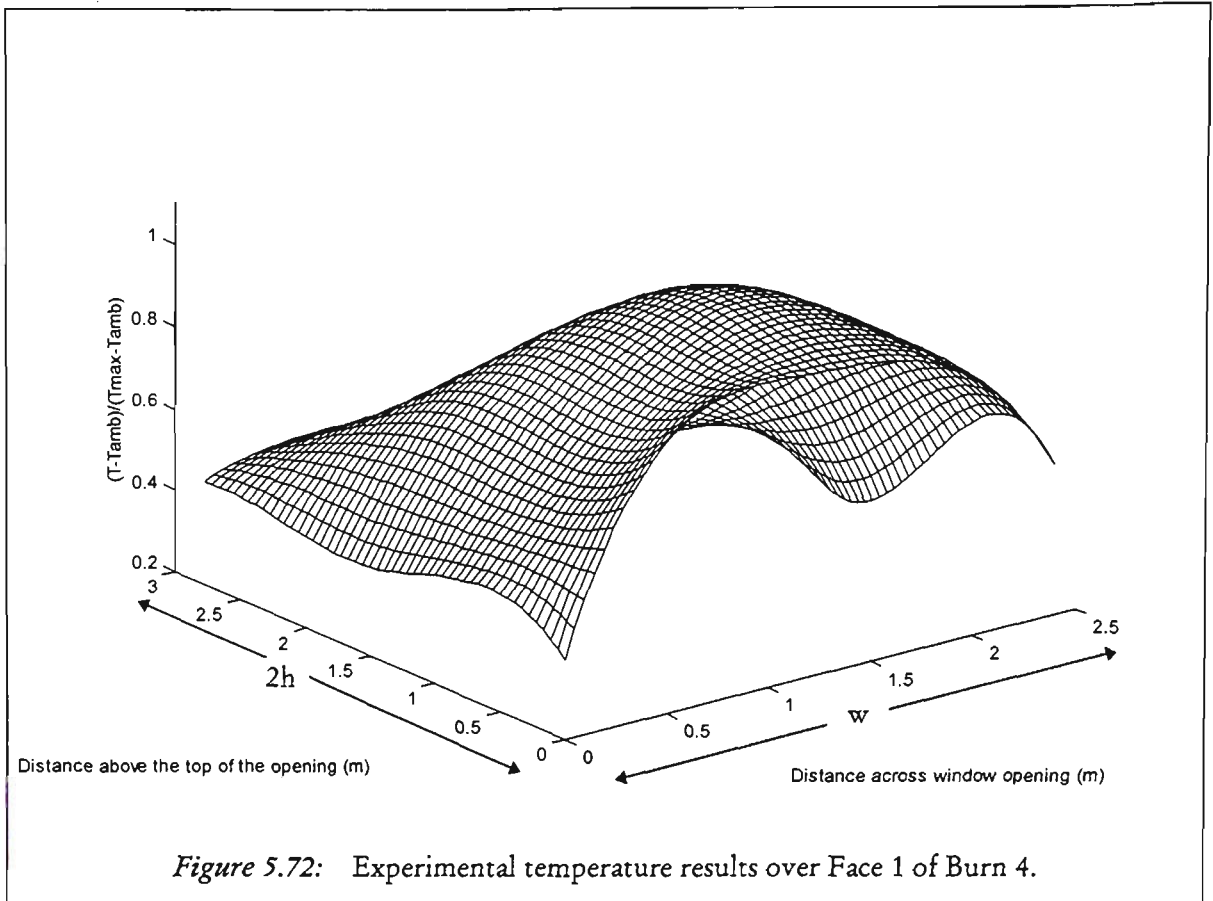
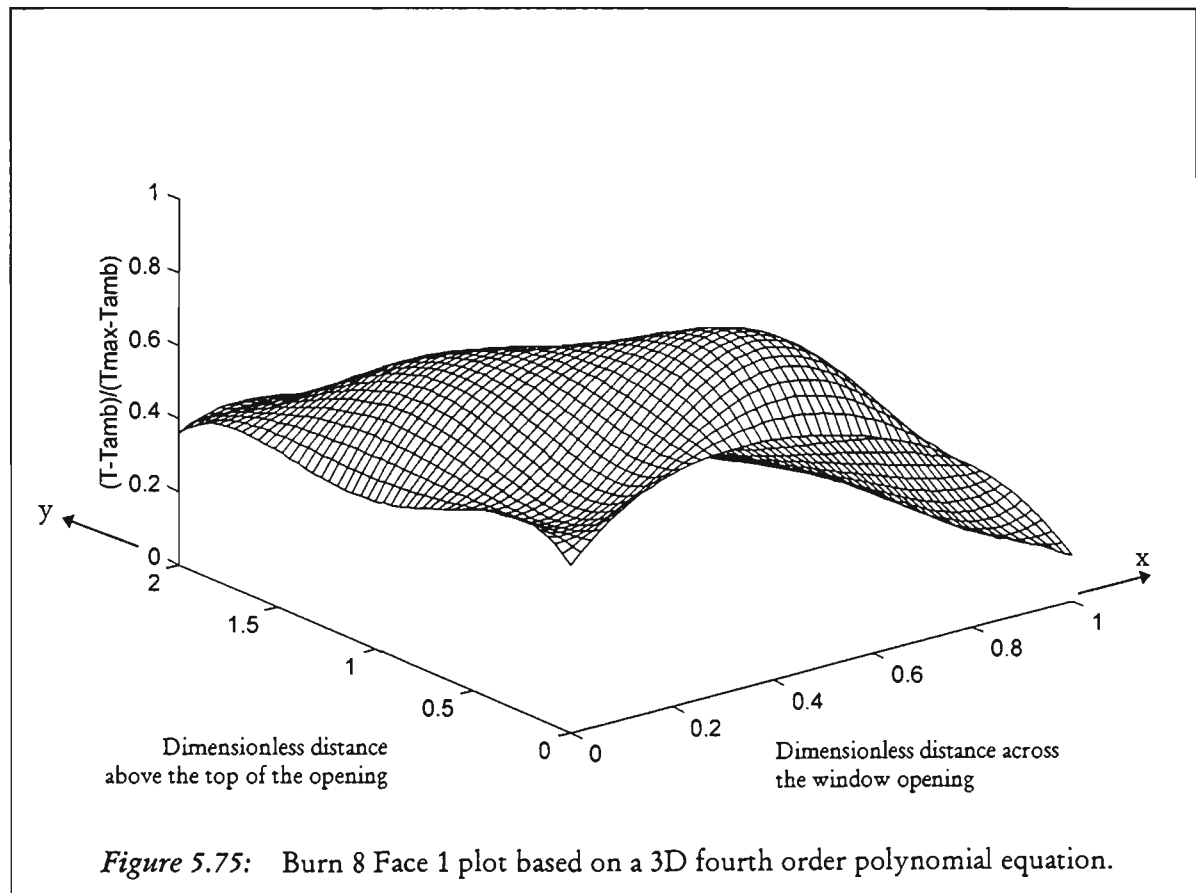
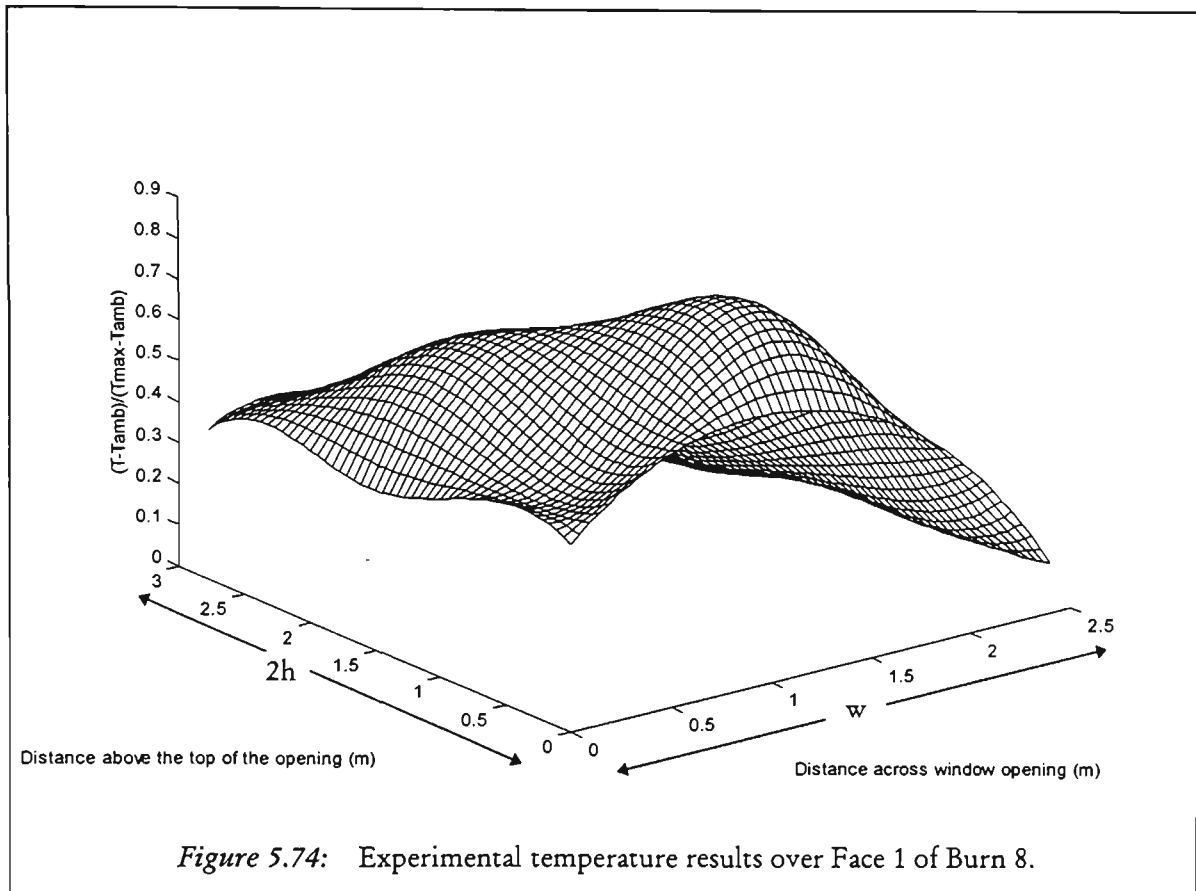


Figure 5.71: Burn 2 Face 1 plot based on a 3D fourth order polynomial equation





5.7 SECONDARY FIRES

A major concern of external flames venting from a window is the possibility of the initiation of a secondary fire. A secondary fire may start either in the floor above (or beside) the opening, or across from the opening to an adjacent building. The construction and materials used on the external facade of a building affect the way in which the fire spreads.

Two ways in which a secondary fire may begin are,

1. through direct flame contact on combustibles:
 - ◆ on the external wall itself,
 - ◆ on the adjacent walls,
 - ◆ in the floor above,

and

2. through radiative heat transfer, when it is significant enough to cause the spontaneous ignition of combustibles:
 - ◆ through upper floor windows,
 - ◆ on linings of adjacent buildings.

Combustible external linings were not tested during these tests. However, given the temperatures and total heat fluxes measured, such linings could have made any of the fires much more severe.

5.7.1 Direct Flame Contact

A venting plume, once it has breached the burn room boundary, leads to the escape of smoke and hot gases. This is soon followed by flames which often reach temperatures in excess of those reached in the burn room, due to the continued combustion of unburnt gases. The appearance of external flames and their reach has been linked to the excess fuel factor[56] which provides a means to determine what proportion of fuel burns outside the compartment, when restricted ventilation conditions do not allow complete combustion within the compartment.

The impact of the venting flames on an external wall can be gauged in terms of the structural and surface damage caused by the flames and whether the heat transfer is high enough to cause a secondary fire. The impact of external flames is also affected by the amount of air entrained into the plume, which cools the plume and reduces flame height. This was the case for Burn 1 and Burn 2 where direct wind interaction not only caused the entire plume to swirl (see *Section 5.8.2*) away from the opening, but it also caused the corresponding measured temperatures along the plume centre-line to be considerably lower at higher Levels (Level 4 and Level 5) within the plume compared to the other tests (see *Section 5.6.2*).

5.7.1.1 Window Cracking Times ~ W101 and W1M02

With respect to a secondary fire in the floor above the room of fire origin, direct flame spread can occur through an already open window, or after the window has failed due to the thermal stress caused by heating across the glass[64,65]. Flames may ignite combustibles, such as loose pieces of paper, curtains, blinds or linen in this upper floor room. As explained next, a secondary fire due to direct flame contact through a window could have taken place in the floor above the burn room during the present experiments, if it had not been prevented.

The observations listed in Table 5.2 and Table 5.4, temperatures measured along the centre Plane (P3) shown in Table 5.9, and times to window cracking and dislodgment of the mezzanine floor window (W1M02) listed in Table 5.12 are combined to reach the following conclusions. For these residential class building tests, not only did the flames reach and cover the Floor 1M window, but also for a substantial period of time, namely during the CEF period, the temperatures and duration of the exposure were severe enough to initiate a secondary fire in the floor above the room of fire origin. To prevent smoke and fire damage to the interior of the upper rooms in the building, a single sheet of 16mm fire rated plaster board was placed inside the room, covering the entire window, as indicated in the *Experimental Setup*. If this barrier had not been erected to protect the mezzanine floor room (R1M02), it would have been destroyed. Also, depending on the configuration of the openings in the mezzanine floor room, the flames could have been drawn into the room, as seen during real fires[49, p.193] and shown numerically[89]. The situation would have been aggravated further had

combustible linings been mounted on the external wall, supplying an additional source of fuel, closer to the opening on the next floor to increase the severity of the fire[74].

As seen in Table 5.12, the time to cracking of the burn room window varied from 3 to 5:30 minutes. The short durations to window cracking must be due to the proximity of the ignition source (wood crib and a couch) to the window and presence of an adequate amount of air to allow the couch to burn sufficiently to cause the glass to crack. The slight differences in these times may be due to ventilation conditions, wind and differences in glass properties[64]. As listed in Table 5.12, the time to lowering of the burn room window was around 5 minutes from ignition, with the exception of Burn 4 and Burn 5. During Burn 4, a Class 2 test, WLC#2 was met before WLC#1. Burn 3 and Burn 4 were the only tests when WLC#2 was used (Burn 3 results are not used here due to the presence of high external wind as discussed further in *Section 5.8.1*). This difference is the reason for the longer time to window lowering in Burn 4. During Burn 5, the window cracked, and glass began to dislodge before WLC#1 was met. The staged dislodgment of the glass lasted from 5:15 to 7:55 minutes from ignition.

From ignition, it took from as little as 8:20 minutes (Burn 7) to at most 16:10 minutes (Burn 2) for the glass in the Floor 1M window, W1M02, to be dislodged. This occurred just before or during the CEF period where the reach of the flames were at their greatest. The time for CEF to begin once the window was lowered was the shortest for Burn 8, a Class 1b test, followed by Burn 7 a Class 2 test. Due to the obscuration of the Floor 1M window by smoke and flames, the times from ignition to when the initial crack formed were difficult to gauge, and were determined audibly. However, dislodgment of sections of glass was observed visually. Based on the results summarised in Table 5.12, it can be concluded that for residential type buildings with standard glass windows, failure of the window in the room of fire origin takes approximately 5 minutes from ignition. Dislodgment of glass in the window on the floor above takes between 4 to 10 minutes once the burn room window has failed.

Table 5.12: Time from ignition to window cracking, flashover and CEF. Failure times include time of initial crack and of initial dislodgment of the Floor 1M window. For Burn 1, further details are given in Table 5.2. Note: na=not available, no=not observed.

	Time to Initial Crack of the Burn room window W102 (min)	Time to LOWERED, OPEN or FAILED window (min)		Time to <i>Initial Crack/ Dislodgment</i> of the Floor 1M window W1M02 (min)	Time (min) from Ignition for >600°C CEF	
BURN 1	3 (once open)	Opened	na	na	13	18:40
BURN 2	4:40	WLC #1	5:25	no / 16:10	7:20	11:25
BURN 5	5:15	Failed	5:15-7:55	no / 11:05	9	11:35
BURN 8	5:30	WLC #1	5:30	no / 9:45	7:50	8:30
BURN 4	4:55	WLC #2	9:35	12:50 / 13:20	13	15:45
BURN 7	3:45	WLC #1	4:55	6:35 / 8:20	6:19	9:55

5.7.2 Heat Transfer

While direct flame contact poses a visible risk, sufficient radiative transfer of heat through glass also causes damage. The approximate radiant heat required to ignite a second item varies from 10 to 20kW/m² for easily ignitable items such as thin curtains and loose newsprint to upholstered furniture. 40kW/m² will ignite difficult items such as wood of 1.25 cm (½ inch) or greater in thickness[108]. These values provide a rule of thumb for comparison. A method has been described by Law[21] to approximate the radiant and total heat transfer of a venting plume at various heights above an opening using a constant flame thickness. Oleszkiewicz[29] modified this approach using a triangular flame thickness to determine emissivity. The relevant equations (Equation 2.18 to Equation 2.21) are summarised in *Section 2.4.1* of the Background.

Flame emissivities calculated using Equation 2.18, [$\epsilon = 1 - \exp[-b\lambda(z)]$ where $b=0.3\text{m}^{-1}$] are presented in Table 5.13. The first column of the Table 5.13 shows the emissivity for a constant flame thickness of 1.0m as specified by Law. In the second column, a maximum flame thickness of $2h/3$ ($= 1\text{m}$) as specified by Oleszkiewicz, is used. Based on his triangular flame shape (shown in Figure 2.9), the subsequent flame thickness at each Level, were determined assuming that at Level 7 (3.89m above Level 1) the flame thickness is zero (based on visual observations made during these tests.). In the last column, for a triangle height of 3.89m, a maximum flame thickness of 1.5m is used at the base of the triangle. This value corresponds to the maximum observed flame thickness (depth) during this series of tests, as listed in Table 5.8.

Table 5.13: Flame emissivity determined using constant and variable flame thicknesses. In the last column, a triangular flame shape is used with the maximum observed flame thickness of 1.5m, as opposed to the calculated flame thickness of 1m used in the second column.

Constant Flame Thickness (LAW)	Triangular Flame Shape using $\lambda_{\max}=2h/3 = 1\text{m}$ (OLESZKIEWICZ)		Triangular Flame Shape using $\lambda_{\max}=1.5\text{m}$ (OBSERVED)	
$\lambda = 1\text{m}$	$\lambda (\max) = 1\text{m}$	emissivity	$\lambda (\max) = 1.5\text{m}$	emissivity
$\epsilon = 0.26$	$\lambda_1 = 1\text{m}$	$\epsilon_1 = 0.26$	$\lambda_1 = 1.5\text{m}$	$\epsilon_1 = 0.36$
	$\lambda_3 = 0.69\text{m}$	$\epsilon_3 = 0.19$	$\lambda_3 = 1.03\text{m}$	$\epsilon_3 = 0.27$
	$\lambda_4 = 0.48\text{m}$	$\epsilon_4 = 0.08$	$\lambda_4 = 0.72\text{m}$	$\epsilon_4 = 0.19$

To determine the radiative and convective heat transfer, the centre-line temperatures, $T(z)$, and burning rates, R , are needed. This information is provided in Table 5.14. Using Equation 2.19 [$I = \epsilon 5.6699\text{E-}8(T(z))^4$] and Equation 2.20 [$q = \alpha(T(z) - T_{\text{wall}})$]; where $\alpha = k(R/A_w)^{0.6}$ (Equation 2.21) and $A_w = 3.6\text{m}^2$, $k = 0.013$ (constant), $R = 20\text{kg/min}$ on the average, $T_{\text{wall}} = 100^\circ\text{C}$ and $T(z)$ is the centre-line temperature], the radiative, convective and total heat fluxes were determined at Level 1, Level 3 and Level 4. The resulting calculated values are compared with the experimental data in Table 5.15. These Levels were selected as they correspond to where actual heat flux measurements were taken. The measured total and radiative heat fluxes given in Table 5.15 are only along Plane 3 and Face 2 (plume centre-line) at Level 1, Level 3 and Level 4. A complete list is given in Table 5.16 of radiative and total heat flux measurements taken during the Real Furniture Burns, which include Plane 1 and Plane 5 in addition to Plane 3. All radiant and total heat flux measurements were averaged over the CEF period to allow for comparison with calculated radiation and total heat flux. The corresponding heat flux transducer locations are given in Figure 3.20* of the *Experimental Setup*. A wall temperature, T_{wall} , of 100°C was used in the calculations, as was done by Oleszkiewicz. The assumption in this choice is that after the wall temperature exceeds 100°C , the heat flux transducer will no longer function correctly as its cooling water will boil.

Table 5.14: Center-line temperatures and burning rates measured during the CEF period.

	Temperature T(z) taken at Face 2 - Plume Centre-line (°C)			Rate of Burning (kg/min)
	Level 1	Level 3	Level 4	
BURN 1	790	255	82	20
BURN 2	712	141	76	20
BURN 5	584	355	273	20
BURN 8	794	541	306	21
BURN 4	693	421	310	20
BURN 7	558	372	264	18

Table 5.15: Calculated radiative, convective and total heat flux, kW/m², at Level 1, Level 3 and Level 4. Radiative heat flux calculations were done with the emissivities listed in Table 5.13, based on flame thickness. Under the variable ϵ column, two sets of radiation heat flux values are given, corresponding to maximum flame thicknesses of 1m and 1.5m, respectively. Level 1 is just above the burn room window, Level 3 is at the bottom of the mezzanine floor window, Level 4 is at the center of the mezzanine floor window. The negative total heat flux values calculated for Level 4 Burn 1 and Burn 2, due to the calculated negative convective heat flux, are not listed. dna=data not available.

		Using Constant ϵ			Using variable ϵ (b/w $\lambda_{max} = 1m$ and $\lambda_{max} = 1.5m$)					Measured
		Radiation	Convective	Total	Radiation	Convection	Total			Total / Rad
Burn 1	Level 1	18.8	25.1	43.9	18.8	26.2	25.1	43.9	51.3	49.7
	Level 3	1.13	5.6	6.7	0.82	1.17	5.63	6.46	6.8	13.2
	Level 4	0.23	-0.7	—	0.12	0.17	-0.65	-0.5	—	6.6 / 2.6
Burn 2	Level 1	13.8	22.2	36.1	13.8	19.3	22.3	36.1	41.6	38.3
	Level 3	0.43	1.5	1.9	0.31	0.44	1.49	1.8	1.93	9.1
	Level 4	0.22	-0.8	—	0.11	0.16	-0.87	-0.8	—	4.8 / 0.7
Burn 5	Level 1	7.9	17.6	25.5	7.9	11.1	17.6	25.5	28.7	dna
	Level 3	2.3	9.3	11.6	1.64	2.34	9.3	10.9	11.6	21.7
	Level 4	1.3	6.3	7.6	0.68	0.98	6.3	6.9	7.3	2.4
Burn 8	Level 1	19.1	26.0	45.0	19.0	26.6	26.0	45.0	52.6	dna
	Level 3	6.5	13.1	19.6	4.65	6.61	13.2	17.8	19.7	20.6
	Level 4	1.7	7.7	9.4	0.85	1.23	7.72	8.5	8.95	27.9
Burn 4	Level 1	12.8	21.6	34.4	12.8	17.9	21.6	34.4	39.5	dna
	Level 3	3.4	11.7	15.1	2.46	3.50	11.7	14.1	15.2	45.1
	Level 4	1.7	7.6	9.3	0.87	1.27	7.64	8.5	8.9	25.9
Burn 7	Level 1	7.0	15.6	22.6	7.0	9.8	15.6	22.6	25.4	dna
	Level 3	2.5	7.8	10.3	1.3	1.95	7.75	9.1	9.7	31.8
	Level 4	1.2	5.6	6.8	0.63	0.92	5.99	6.2	6.5	15.7

Table 5.16: Measured heat flux, hf, in kW/m². BR-hf was located on the floor of the burn room. All heat flux measurements are of total heat flux, except where indicated. Heat flux transducer locations are illustrated in Figure 3.20*. dna=data not available.

	Grid Location	Class 1a		Class 1b		Class 2	
		BURN 1	BURN 2	BURN 5	BURN 8	BURN 4	BURN 7
hf1(rad)	L4 / P3	2.6	0.7	dna	dna	dna	dna
hf2	L4 / P3	6.6	4.8	2.4	27.9	25.9	15.7
hf3	L3 / P1	dna	3.7	2.7	6.6	5.7	4.9
hf4	L3 / P3	13.2	9.1	21.1	20.6	45.1	31.8
hf5	L3 / P5	3.2	2.8	3.7	6.4	18.3	5.2
hf6	L1 / P3	49.7	38.3	dna	dna	dna	dna
BR-hf		dna	dna	106.5	93.4	77.7	75.5

In Table 5.13 the emissivity within the plume was determined based on two assumptions, that of either a rectangular flame shape which corresponds to a constant flame thickness, or a triangular flame shape, which corresponds to a variable flame thickness. The constant flame thickness proposed by Law results in a constant flame emissivity, while the variable flame thickness proposed by Oleszkiewicz (as also observed during this series of tests), allows for the emissivity of the plume to be determined based on the thickness of the flame at various heights.

Using a constant emissivity when calculating radiative heat transfer produces consistently higher values compared to those calculated with variable emissivity which decreases with decreasing flame thickness. Regardless of the emissivity used, the calculated *radiative heat transfer* values are lower than the only available measured values for Burn 1 and Burn 2 at Level 4, as shown in Table 5.15. As a result, it is difficult to reach a definite conclusion from this comparison regarding the calculation of radiative heat transfer.

The calculated total heat flux measurements at Level 1 compare reasonably well with the measured values for Burn 1 and Burn 2 (only available for these tests). In addition, the calculated total heat flux is similar to the measured value during Burn 8 at Level 3. All other calculated total heat flux values on Level 3 and Level 4 are lower than the measured ones. It is expected that air entrainment was not as effective in cooling the lower portions of the plume (Level 1) which vented directly from the burn room

window, and that entrainment into the plume increased along its length (up to Level 4). The equations used to calculate emissivity, ϵ , and the convective heat transfer coefficient, α , do not take into account air entrainment effects and resulting variations with the external plume height.

The negative calculated convective heat transfer values at Level 4, listed in Table 5.15 for Burn 1 and Burn 2, are as a result of the measured centre-line temperatures being less than the 100°C (used as T_{wall}). These lower temperatures measured during Burn 1 and Burn 2 have been attributed to increased air entrainment due to direct wind interaction with the plume during these tests.

To estimate the uncertainty in the measured heat flux values given in Table 5.15, the error analysis of Oleszkiewicz (*Section 3.1.5.3* and *Section 3.2.6*), is applied here to this series of tests using representative values. For this purpose, the maximum external temperature of 794°C is used, measured at Face 2, Level 1 and Plane 3 in Burn 8 (Table 5.9). Similar to Oleszkiewicz's analysis, it is assumed that an erroneous measurement will correspond to an average foil temperature of 155°C for the transducer. With these two temperature values in Equation 2.20 and $R=20\text{kg}/\text{min}$ on the average, an *erroneous convective heat flux* of $23.42\text{kW}/\text{m}^2$ is calculated. For the corresponding correct measurement, an average foil temperature of 100°C is used, resulting in a *correct convective heat flux* of $26\text{kW}/\text{m}^2$. Based on these two values, an uncertainty of 7.2% is expected in convective heat flux measurements. From the calculated values listed in Table 5.15, radiative heat flux can be calculated to be between 30 to 40% of the total heat flux, corresponding to 70 to 60% convective heat flux within the total. Calculated values were used for this estimation in the absence of radiative heat flux measurements at Level 1. The reason for using the calculated Level 1 values is because better agreement is obtained between the calculated and measured total heat flux values at this Level. If 70 to 60% of the total heat flux is convective, then a measurement error of 5.0 to 4.3% can be estimated in the measured total heat flux. With this uncertainty, the calculated heat flux heat flux is within the experimental error only for Burn 1 and Burn 2 at Level 1, and Burn 8 at Level 3.

Radiation measurements were taken at Level 4, Plane 3 of the grid for Burn 1 and Burn 2. This location corresponds to the centre of the Floor 1M window. At this height above the opening, the radiative contribution of total heat transfer was 40% and 15% for Burn 1 and Burn 2, respectively. However, ignition due to radiation alone, through the Floor 1M window is not expected for Burn 1 or Burn 2, based on the numbers quoted at the beginning of this section. The calculated radiation levels just above the window opening (Level 1, Table 5.15) indicate that ignition due to radiation *alone* of wood was not possible even at this level. Given that radiative heat transfer will decrease with increased vertical distance, this range of values must be reduced significantly at Level 4. A matching drop in total heat flux from Level 1 (hf6) to Level 4 (hf2), also existed for all of the tests.

Variations in total heat flux along the bottom of the Floor 1M window can be seen when hf3, hf4 and hf5 given in Table 5.16, are compared. These measurements indicate that the total heat flux was generally higher along the centre of the venting plume. With the exception of Burn 4, a symmetry exists about the centre of the plume in all tests as indicated by the total heat flux measurements on either side of the window. This similarity exists in the measured values of hf3 and hf5 in spite of the slight tilting of the venting plume as seen in the 3D temperature contour plots (Figure 5.16, Figure 5.17, Figure 5.30, Figure 5.31 and Figure 5.39 for Burn 1, Burn 2, Burn 5, Burn 8 and Burn 7, respectively). A similar tilt existed for Burn 4 (as observed from the 3D temperature contour plot given in Figure 5.38), and the heat flux on the right of the plume centre-line is about three times that on the left. As a result, factors other than the tilting of the plume, such as the possibility of molten glass caught between the grid and the transducer, and transducer malfunction, need to be considered when comparing hf3 and hf5 readings, although these factors can not be fully accounted for. The effect of having items burning in different parts of the room with respect to the opening have been observed to influence the tilt of the venting plume, in addition to the ventilation conditions and local wind movement on the face of the building.

Total heat flux measurements presented by Oleszkiewicz[29] can be used for comparison with the present results. Experiments were carried out at the NRCC large facility as described in *Section 2.5*. The results quoted here were selected from a test

with a comparable window size (2.6m x 1.37m) and total heat release rate (6.9MW - fuel source: propane gas). Total heat flux measurements of 53.2, 33.1, 17.2 and 15.6 kW/m² were taken at 0.25, 1.5, 2.5 and 3.5m above the top centre of the opening, respectively. As shown in Table 5.16, the corresponding measurements for Burn 1 and Burn 2 at Level 1 (0.15m above the top of the opening), start from comparable values, but they drop off more quickly than Oleszkiewicz's measurements. For Burn 5 and Burn 8, and Burn 4 and Burn 7, total heat flux measurements are available at Level 3 and Level 4, only. At Level 3, on the average, the measured values of these four tests are similar to Oleszkiewicz's at 1.5m. As expected, especially Class 2 test results, those of Burn 4 and Burn 7, at Level 3 and Level 4 compare well (The chosen case of Oleszkiewicz's was a Class 2 test). Results just above the top of the window opening are only comparable with those measured for Burn 1 (see Table 5.16).

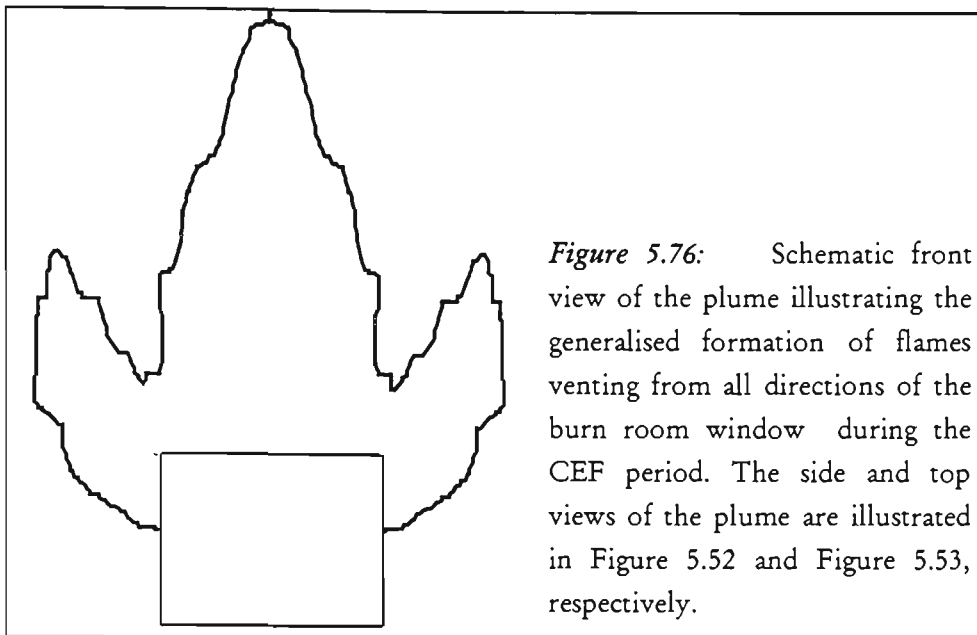
5.8 EFFECTS DUE TO WIND AND SMOKE MANAGEMENT SYSTEM

5.8.1 Burn 3

The effect of wind on external plume is twofold. Firstly, wind can cool the plume due to increased air entrainment, and hence, it can reduce the heat exposure on the external facade of the building. This effect was discussed in *Section 5.6.2*, where the centre-line temperatures of the venting plume for Burn 1 and Burn 2 were considerably lower further up from the burn room window (at Level 4 and Level 5), compared to the other tests. Secondly, in contrast, wind can help externally venting flames reach windows and openings adjacent to or on either side of those of the room of fire origin.

Although most tests in this series took place on almost still days, this was not true of Burn 3. Originally, Burn 3 and Burn 4 were designed as a repeat pair of tests, and internally, the resulting temperatures and mass loss rates were almost identical, as described in Alam and Beever[102] and in Figure 5.42. However, due to wind direction and higher speeds during Burn 3, the external results do not show this similarity. Consequently, only Burn 7 was grouped with Burn 4 with respect to external plume characteristics.

As shown in Figure 5.76, flames vent out along the top of the opening as well as from the sides. As indicated earlier, this generalised formation was observed during tests of both ventilation classes and was attributed to the large burn room window size, although during Class 2 fires, the plume width was wider. Figure 5.76 illustrates the front view of the plume schematically. The side and top views of the plume are illustrated in Figure 5.52 and Figure 5.53, respectively.



In Figure 5.77 and Figure 5.78, the centre plane, P3, temperature contour plots of Burn 3 and Burn 4, respectively, have been plotted. These contours were CEF averaged and non-dimensionalised, similar to the results presented earlier. A comparison of Figure 5.77 and Figure 5.78 allows the effects of wind during these two tests to be compared. During Burn 3, S-SSW winds with average and peak speeds of 3.5 and 5.8 m/s, respectively, were recorded; while for Burn 4, NE average and peak wind speeds of 1.6 and 2.8m/s, respectively, were measured. Hence, the wind speed was about twice as high during Burn 3 as it was during Burn 4. With the burn room window (W102) facing South, there was no barrier to prevent the interaction between the higher speed wind and the external plume during Burn 3. As a result, the plume swirled as a whole, as discussed further in *Section 5.8.2*. The wind direction and increase in wind speed disrupted the flow of the venting plume. This interruption is manifested as a “dip” in the middle of the contour plot in Figure 5.77, as well as lower temperatures along the external wall during Burn 3 as a result of increased air entrainment. The “dip” is formed around Level 2, just before Face 2, dramatically altering the temperature of the venting plume.

Without wind effects, the plume vented from the opening undisturbed during Burn 4 (and also during Burn 7). It was observed during Burn 4 that the flames vented away from the opening, and rose up slightly, sending hot exhaust gases out of the burn room. This hot stream occupied the lower third of the grid, easily covering L1 to L3. The temperature along the external wall as shown in Figure 5.78 remained high,

corresponding to the temperature contour of 1.0, due to lower air entrainment than in Burn 3 caused by lower wind speeds in Burn 4. The wind speeds measured during Burn 7 were as low as those during Burn 4, even though the wind direction differed. Hence, Burn 4 and Burn 7 results could be used for comparison of external results for Class 2 tests.

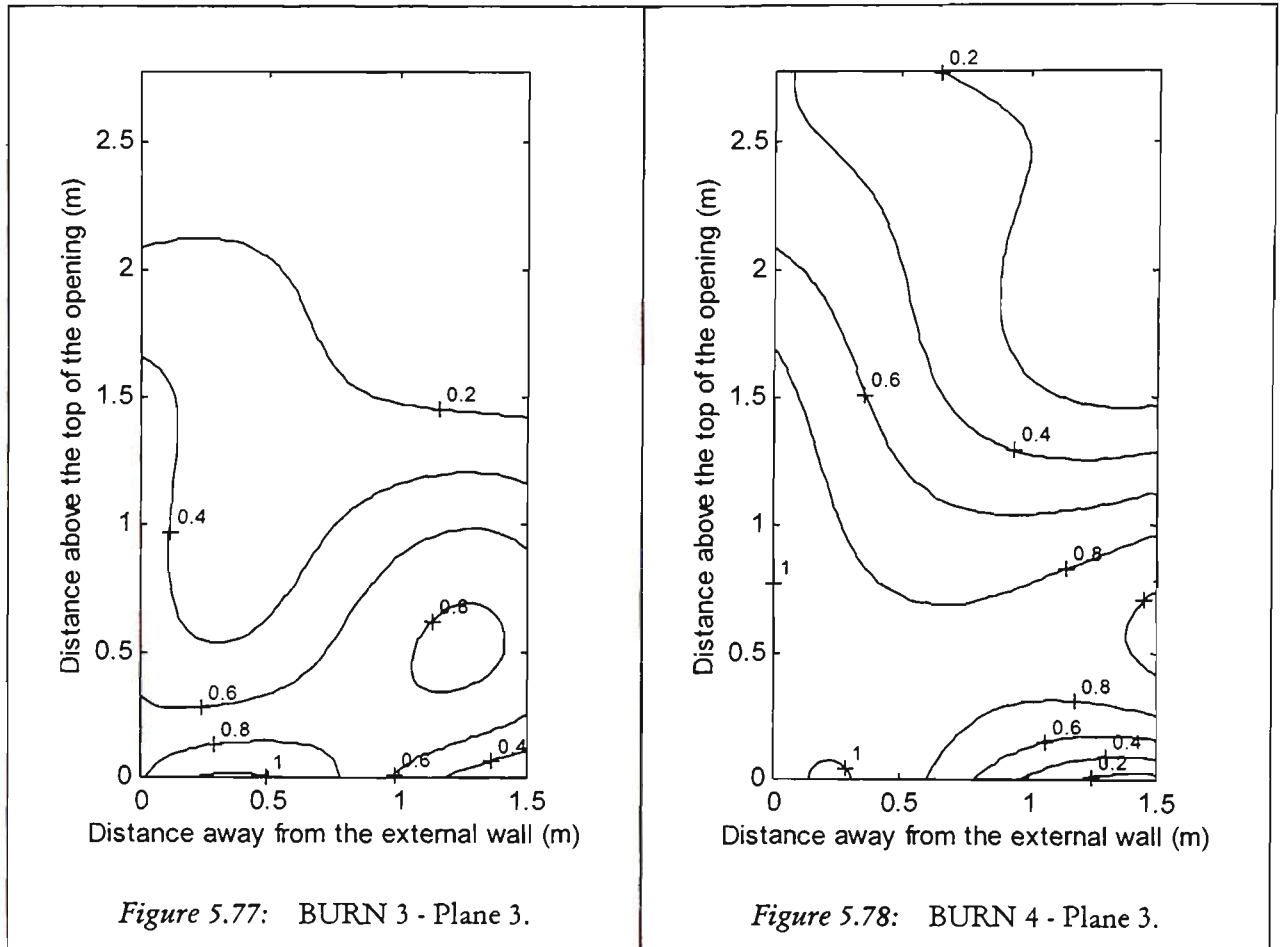


Figure 5.77: BURN 3 - Plane 3.

Figure 5.78: BURN 4 - Plane 3.

As mentioned in Section 2.6.4 “Environmental Effects”, the presence of a front (direct) or side wind can tilt the venting plume. Sugawa *et al.*[73] performed a series of small scale experiments and developed an equation to determine the tilt of a venting plume when subjected by a side wind. Using Equation 2.28 [$\sin\phi = V_{\text{wind}} / u^* (h/w)^{1/3}$] to determine the tilt of the plume for Burn 3,

$$\begin{aligned} \text{where } V_{\text{wind}} &= 3.5 \text{ m/s} && \text{(average wind speed - Burn 3)} \\ u^* &= (Qg/\rho_{\text{amb}}T_{\text{amb}}c_p w)^{1/3} && \text{(velocity based on total heat release rate)} \\ &= [(6,360 \times 9.81)/(1.21)(14.1)(1)(2.4)]^{1/3} \\ &= 11.5 \text{ m/s} \end{aligned}$$

using $c_p = 1 \text{ kJ/kg K}$ for the venting gases

$$w = 2.4 \text{ m (window width)}$$

$$h = 1.5 \text{ m (window height)}$$

$$T_{\text{amb}} = 14.1 \text{ }^{\circ}\text{C (Table 3.6*)}$$

$$Q = R \times \Delta H_c = 0.33 \times 19.23 = 6.36 \text{ MW (see Section 5.6.1)}$$

Therefore

$$\sin\phi = 3.5/[(11.5 \times (1.5/2.4)^{1/3})]$$

$$\phi \approx 20^{\circ} \text{ measured from the horizontal (70}^{\circ} \text{ from the vertical)}$$

This result is much higher than the observed tilt angle during any of the tests. Although the plume tilted to varying degrees during the eight tests, the wind was not side on (along building facade) as required by Sugawa *et al.*'s formulation. This difference may account for the higher calculated tilt angle. However, if the heat release rate is modified to include only the heat released through the burn room window, 27% of the total (as determined in Section 5.6.1) then a tilt angle of 56° from the vertical is calculated. This result compares better with the observed tilt angle of the plume which was between 15° to 30° from the vertical during the course of most tests, with the exception of Burn 1 to Burn 3, as it was difficult to estimate visually the tilt of the venting plume due to swirling during these three tests.

5.8.2 Swirling

The swirling of the venting plume has sparked the interest of many researchers, whether it is the edges of a plume, or the entire plume itself, swirling out of an opening in a building. These phenomena have been attributed to many reasons, such as a geophysical rotational force[92], the shedding of vortices around the plume and subsequent surge of hot gases towards the vent opening[90], or more simply to atmospheric pressure variations[92].

The swirling of the plume, either in part or in whole was observed in all of the cases to a certain degree. The most pronounced was for Burn 1, Burn 2 and Burn 3, where wind caused the entire plume to swirl clockwise away from the opening, creating huge spiralling sections which were at most 2.5m in diameter with a visually observed period of just over one second. An example of this is shown in Figure 5.79. Although there is no dispute that the fire and flames have a natural periodicity innate to the

combustion process itself, the swirling of the venting plume as a whole has been observed to be caused by wind, as explained next.

In Figure 5.80, the wind direction with respect to the Experimental Building-Fire Facility and the average and peak wind speeds during each test are given. The outline of the building and air-handling unit outside are illustrated in top view along with the burn room window (W102). During Burn 4 and Burn 8, the wind direction was NE and NNW, respectively. Consequently, the building acted as a barrier, preventing direct interaction between the wind and external plume. As indicated in Figure 5.80, the air-handling unit served a similar function for Burn 5 and Burn 7 during which the wind directions were W and SW, respectively. As a result, no swirling of the entire plume was observed during Burn 4, Burn 5, Burn 7 and Burn 8. During Burn 1, Burn 2 and Burn 3, the wind directions were ENE, SSE and S-SSW, respectively. Hence, direct interaction was possible between the wind and external plume. This interaction resulted in the swirling of the entire plume. Although the wind speed increased from Burn 1 to Burn 3, it was not possible to measure the effect on swirling of the increased wind speed during Burn 3.

Burn 1 and Burn 2 were designed as repeat cases for Class 1a. Although the entire external plume swirled during both of these tests, the change in wind direction and swirling of the plume caused the differences in the external results. However, the results of these tests were utilised here, since they were the only available Class 1a cases.

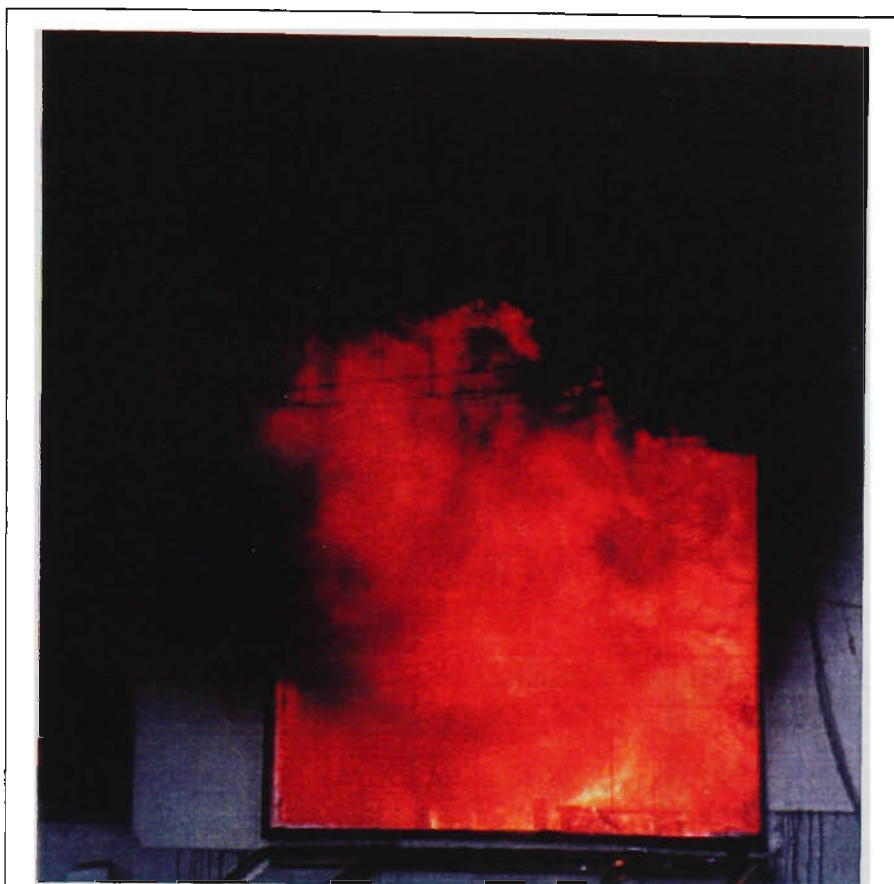


Figure 5.79: Swirling plume during Burn 2.

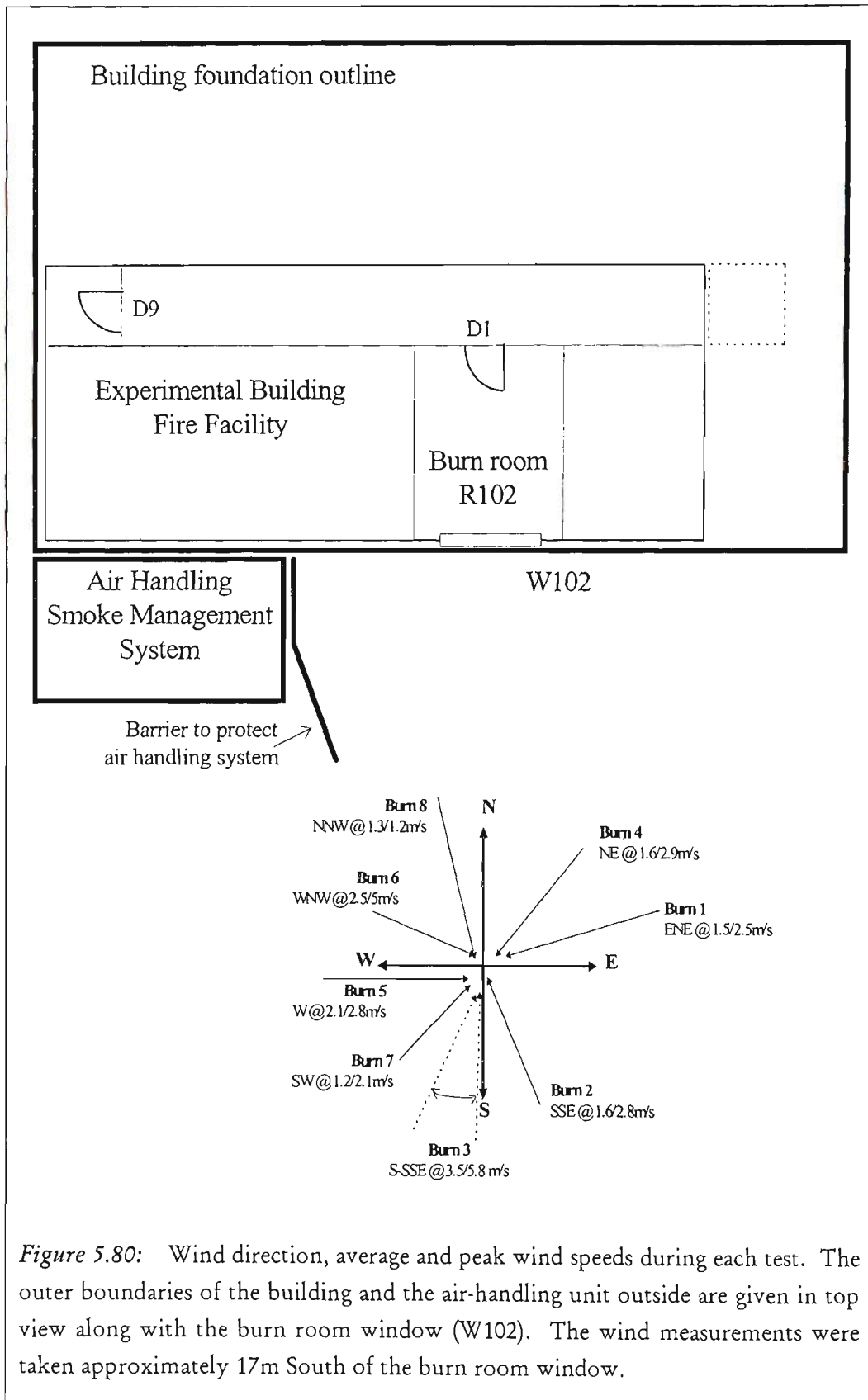


Figure 5.80: Wind direction, average and peak wind speeds during each test. The outer boundaries of the building and the air-handling unit outside are given in top view along with the burn room window (W102). The wind measurements were taken approximately 17m South of the burn room window.

5.8.3 Smoke Management Systems

Table 5.12 shows the corresponding times, from ignition, to when the window was lowered or failed, and the time it took for the window on the floor above (Floor 1M window) to crack. It can be seen that the time to cracking or failure of the window in the burn room and on the floor above was the shortest for Burn 7. This has been attributed to the activation of the Smoke Management System (SMS) for this test which caused the burn room window to bow (Bowing is discussed in detail in *Section 5.8.4*). The extraction of smoke (air/hot gases) by the SMS when the burn room door was closed caused the bowing and early failure of the burn room window. Failure of the window then allowed air into the room. As a result, the implementation of WLC #2 was not necessary for Burn 7, since WLC#1 was met (due to the bowing and early failure of the burn room window). Remembering that WLC#2 was designed to *facilitate* flashover for Class 2 tests, when the burn room door was closed, occurrence of WLC#1 was unexpected. WLC #2 was implemented during the other Class 2 tests, Burn 3 and Burn 4, to facilitate flashover which would not have occurred otherwise. This is because when both the door and the window are closed, there is not enough air in the room to sustain the fire beyond its early stages.

The use of a SMS to aid the removal of smoke from the burning environment is considered to be a viable means to slow down the progress of the fire, and delay flashover and allow time for people to evacuate the building. This point was confirmed in Burn 6, as Class 1 ventilation case, which did not flashover. Unlike Burn 7, the burn room door was open for Burn 6. The open burn room door, in combination with the pressurisation of the corridor and the use of the SMS, prevented flashover. This is because the extraction of hot gases from the room resulted in temperatures in the burn room reaching approximately 300°C under the ceiling. As a result, the fire failed to spread to other items in the burn room, as confirmed by Luo[113]. This result indicates that for this series of tests, the SMS prevented flashover for a Class 1 test, which would normally flashover, and caused flashover in a Class 2 test which would not normally flashover. These conclusions regarding the SMS as used in Burn 6 and Burn 7 have also been confirmed by Luo and Beck[114].

The second fastest time recorded for dislodgment of the glass for the Floor 1M window was for Burn 8, a Class 1b test. This has been partially attributed to the addition of

4mm plywood on the corridor walls (as combustible lining) just outside the burn room, as shown in Figure 3.18. These walls constituted approximately 11% of the total fuel mass. Also, the additional placement of combustibles in the corridor allowed excessive amount of smoke to travel within the building, reaching the third floor[102].

5.8.4 Bowing of the Burn Room Window and SMS

An example of the bowing of the centre pane of the burn room window is presented in Figure 5.1. In Table 5.17, a summary is provided of the ventilation conditions caused by the burn room and stairwell doors, D1 and D9, respectively, being open or closed in connection with bowing of the glass in W102. Also included is whether the smoke management systems was activated, as well as the wind speed and direction during each of the tests. The burn room window faced South. As a result, during all tests, except Burn 1, Burn 2 and Burn 3, the burn room window was shielded from direct external wind by either the building or the air-handling unit (the building orientation with respect to wind is illustrated in detail in *Section 5.8, Wind Effects*). Bowing of the glass occurred in both Class 1a tests (Burn 1 and Burn 2) when the stairwell door was closed, the burn room door was open and there was direct wind. During Burn 3, a Class 2 test, bowing also occurred while the stairwell and burn room doors were both closed, but direct wind was present. These observations indicate that wind interaction, due to either a side wind or direct wind, can contribute to the bowing of the burn room window. Although the closed stairwell door, D9, might have played a part in bowing of the burn room window, its effect is expected to be less, because the burn room door, D1, was closed during Burn 3. As expected, the closed burn room door during Burn 3, resulted in lower corridor temperatures (42°C) than during Burn 1 or Burn 2 (408°C)[102].

Table 5.17: Bowing of the burn room window, W102. A summary is given of the ventilation conditions, smoke management system (SMS) activation and wind speed and direction resulting in bowing of W102. D1 and D9 refer to the burn room and stairwell doors, respectively. The burn room window faces South.

Ventilation Class	Test	D1	D9	SMS	Wind Direction and Average Speed	Bowing of W102
Class 1a	BURN 1	Open	Closed	off	ENE @ 1.5m/s	Yes
	BURN 2			off	SSE @ 1.6m/s	Yes
Class 1b	BURN 5	Open	Open	off	W @ 2.1m/s	no
	BURN 6			Yes	WNW @ 2.5m/s	Yes
	BURN 8			off	NNW @ 1.3m/s	no
Class 2	BURN 3	Closed	Closed	off	S-SSW @ 3.5m/s	Yes
	BURN 4			off	NE @ 1.6m/s	no
	BURN 7			Yes	SW @ 1.2m/s	Yes

Bowing also occurred in one Class 1b test, Burn 6, during which the burn room and stairwell doors were both open, no direct wind was present and the Smoke Management System (SMS) was activated. The Smoke Management System (SMS) extracted smoke out of the burn room, generating a pressure differential within the burn room. Hence, activation of the SMS resulted in bowing of the burn room window during Burn 6. During Burn 7, a Class 2 test, both the burn room and stairwell doors were closed, no direct wind was present and the SMS was activated. Bowing of the burn room window during Burn 7 has been attributed to both the activation of the SMS and the closed stairwell door. Bowing of the burn room window was not observed during the remaining tests, Burn 4, Burn 5 and Burn 8.

5.9 CONCLUSIONS FROM THE REAL FURNITURE BURNS

Results from the Real Furniture Burns have highlighted the effects of internal ventilation conditions and external conditions on externally venting flames. A summary of Burn 1 to Burn 8 is given in Table 5.18. Included in this table are the environmental conditions, such as average ambient temperature, wind speed and direction, as well as the Window Lowering Criterion used on W102, the burn room window, and the time to initial cracking/dislodgment of the mezzanine floor (Floor 1M) window, W1M02. Consistent External Flaming durations of each test is also provided.

Table 5.18: Summary of information gathered for the Real Furniture Burns.

*Burn 8 has combustible lining in the corridor. * Burn 7 - smoke management system activated.
dna=data not available and na=not applicable.

REAL FURNITURE BURNS					
		Average Ambient Temperature, Wind Speed and Direction	Time to Lowered, Opened or Failed window (W102) (min)	Time to Initial Crack/Dislodgment of W1M02 (min)	CEF Duration (min)
Class 1a	BURN 1	15.4°C 1.5m/s @ ENE	Opened / na	dna	8
	BURN 2	12.1°C 1.6m/s @ SSE	WLC#1 / 5:25	dna / 16:10	5
Class 1b	BURN 5	8.3°C 2.1m/s @ W	Failed / 5:15-7:55	dna / 11:05	6
	BURN 8*	8°C 1.3m/s @ NW	WLC#1 / 5:30	dna / 9:45	7
Class 2	BURN 4	11°C 1.6m/s @ NE	WLC#2 / 9:35	12:50 / 13:20	8
	BURN 7*	7.7°C 1.2m/s @ SW	WLC#1 / 4:55	6:35 / 8:20	6

REPEATABILITY

The primary intention of this work to was to study in detail the nature of externally venting flames during the fully developed phase of a fire. It was intended to establish that the full-scale tests designed for this purpose were repeatable so that the results could be used with numerical models for validation purposes. To test repeatability, large amounts of temperature data were collected in a region of space, above the burn room window, where the emerging flames existed. In analysing the experimental data, several important factors became apparent with respect to **REPEATABILITY** of the tests. These factors were:

- ◆ the internal ventilation conditions,
- ◆ to average the data over CEF and subsequent non-dimensionalisation,
- ◆ window lowering criteria.

Given that the main controllable difference among groups of tests was THE INTERNAL VENTILATION CONDITIONS, it was this aspect that needed to be considered when the tests were grouped. The distinction between the internal ventilation conditions, namely *Class 1*, through draft, and *Class 2*, no-through draft, established the first step towards producing repeatable sets of results. This classification was then refined by the sub-division of Class 1 into Class 1a and Class 1b, which allowed specific differences in the internal ventilation of the building to be incorporated, beyond the open door/window and the closed door/window scenarios. Consequently, the external experimental results from the same class of tests can be compared.

Following the classification of repeat pairs of tests, an averaging method had to be developed to enable large amounts of data to be analysed. This new averaging method consisted of averaging the data over the CONSISTENT EXTERNAL FLAMING (CEF) period. Such averaging further accentuated the similarities between pairs of tests with similar ventilation conditions and again distinguished Class 1 tests into two sub-divisions. The CEF duration of each test corresponded to part of the fully developed stage of the fire, and it was determined to pose the greatest risk to the external environment, including the external wall and the window or room above the room of fire origin. Several important factors were considered in the definition of the CEF period. The CEF period started soon after there was an increase in the rate of mass loss. This point in time corresponded to shortly after flashover, followed by a surging of external flames. The CEF period ended when the mass loss rate began to decline, after the consistent flaming had finished. The data were then non-dimensionalised with respect to the maximum measured external temperature and the average ambient temperature taken during the course of the test. This non-dimensionalisation procedure allowed comparison between similar ventilation cases by reducing the effects of slight variations in the ambient and maximum external temperatures measured during each case. Ultimately, the identification of the ventilation classes, CEF averaging and non-dimensionalisation of the results allowed the REPEATABILITY of the tests to be gauged.

Finally, the WINDOW LOWERING CRITERIA (WLC) were established based on the onset of glass failure, primarily to eliminate the effect of partial dislodgment of the burn room window during the early stages of the fire's development. These criteria were established to eliminate only partial cracking/dislodgment of the burn room window. When the failure of the window occurred in stages, it was observed to influence the early stages of the fire's development during the Polyurethane Burns. Consequently, lowering the entire window when a criterion was met, regulated the early fire development. The first criterion was established to produce an 'open window' during Class 1 tests. The second criterion was designed to *facilitate* flashover for tests where the door to the burn room was closed during Class 2 tests.

Determining the REPEATABILITY OF THESE FULL-SCALE TESTS was an important step towards establishing the validity of the experimental results and the subsequent usefulness of these results for design or numerical validation purposes. Grouping the tests into the appropriate ventilation classes, averaging of the results over the CEF period, non-dimensionalisation, and eliminating the effects of partial window breakage using the WLC have allowed the repeatability of the tests to be gauged in several ways, both internally and externally. Internally, the mass loss data provided a means to gauge the fire's development in the room without spatial fluctuations or the possible effects of different items burning at different times. Once the burn room window was open, the burning rates of repeat tests averaged over CEF have been shown to be very similar, given that the fuel configuration and construction varied slightly. Burn 7 was the exception. It had a slightly lower burning rate which has been attributed to the extraction of smoke (air/hot gases) with the smoke management system which appeared to have limited/hampered the burning. Externally, the CEF averaged and non-dimensionalised temperature contours selected from the 3D grid, have shown a varying degree of similarity, being the best for Class 2 (Burn 4 & Burn 7) tests, followed by the Class 1b (Burn 5 & Burn 8) tests. While Class 1a (Burn 1 & Burn 2) tests showed similar trends, the uncontrollable influence of direct and side winds on the venting plume, which also caused it to swirl, has made these tests the least repeatable. The similarity of repeat tests gauged from a graphical comparison of external temperatures contours was confirmed by statistical analysis of the data.

COMPARISONS WITH APPROXIMATIONS - FLAME SHAPE AND TEMPERATURE

Once the repeatability of the data was established, comparison of the experimental results with the empirical approximations became meaningful to determine the flame envelope and flame temperatures along the plume axis.

The empirical equations used to determine the venting flame's height, width and depth provided a good means to determine the overall boundary of the flames during this series of Real Furniture tests, even though the approximations were developed from mostly wood crib fires. As such, the observed venting flames were contained within Law's[21] *flame envelope*. Law's flame envelope does not consider the variations across the width and depth of the external flames. The present study has highlighted such variations within the plume. As an example of these variations, it was found that the width of the fire plume was greater during Class 2 tests, compared to Class 1 tests, contrary to assumptions. Also, the bellying of the plume and its tapering off matched the stylised triangular shape described by Oleszkiewicz.

When determining the centre-line (flame axis) temperature of the venting plume, Law's empirical approximation[21] is used with the measured average burn room temperatures, in the absence of opening temperatures. Although the measured average burn room temperatures have been estimated to be close to the burn room opening temperature, higher plume centre-line temperatures were calculated using Law's method than those measured. Hence, using Law's equation overestimated the severity of the venting plume. Calculations to estimate the burn room temperatures were also carried out. Using the Pettersson[31] or Babrauskas[37] methods, resulted in burn room temperatures that compare well with those measured during this series of tests.

OTHER COMPARISONS

Comparisons have been made between the results obtained during the Real Furniture Burns and other published results in the literature. Firstly, good agreement was found between the observed flame height reported in Law[111] during a full scale fire test and those observed here for tests with comparable fuel type and load, and external wind speed. In addition, Law and Thomas's[60] estimation of the flame length based on Yokoi's data was tested. It was found that unless the proportion of heat loss through

the window could be specified, unrealistic flame lengths were calculated. This formulation was used with the experimental flame length to determine that approximately 27% of the total heat released in the room vented out of the window.

Secondly, extensive comparisons were carried out with the results of Yokoi[28]. Centre-line temperatures during Burn 1 to Burn 8 were compared with Equation 2.1[52]. This equation, based on Yokoi's[28] experimental data, was found to produce centre-line temperatures higher than those measured during the present series, when the total heat release rate was used. However, when the total heat release rate was modified, to take into account the proportion venting through the window, 27%, there was better agreement between measured and calculated centre-line temperatures. In addition, Yokoi's formulations for re-attachment and spandrel lengths were considered. Re-attachment of the plume as observed during this series of tests, confirmed the application of Yokoi's parameter n , which is based on window shape and plume height. The calculated spandrel length, based on Yokoi's experimental data, underestimated the necessary distance between windows to prevent dislodgment of the glass from an upper level window. His criterion for glass dislodgment is based on the height above the window where the plume temperature is 500°C, and thermal stress necessary to cause failure is not considered in his analysis.

Thirdly, Sugawa and Takahashi's[72] formulation to estimate centre-line temperatures based on their small scale experiments was used for comparison. Their results are plotted using the variables of Equation 2.26, z versus $\Delta T/Q^{2/3}$ in logarithmic scale. The experimental data collected during this series of tests is almost linear in this format, as expected based on the Sugawa and Takahashi formulation, with the exception of Burn 1 and Burn 2 data.

Fourthly, selected total heat flux measurements made by Oleszkiewicz[29] were compared with those taken during this series of tests. They were found to compare well with tests of similar internal ventilation conditions and comparable window size and heat release rate. Lastly, Sugawa *et al.*[73] developed from small scale experiments a correlation to determine the tilt of the venting plume when subjected to side wind. The tilt angles calculated using their equation were higher than those observed during

these tests. This disagreement was attributed in part to Sugawa *et al.*'s formulation which was developed for side-on wind conditions, only. When the heat release rate was modified to take into account the fraction of the total which vented through the window, more realistic tilt angles were calculated.

2D AND 3D EQUATIONS OF THE TEMPERATURE DISTRIBUTION WITHIN THE VENTING PLUME

The temperature variation across the centre plane (Plane 3) of the plume was investigated. Using Law's variables, the equations of best fit were developed to describe the variation in the temperature with height along the plume centre-line (Plane 3/Face 2), along the external wall (Plane 3/Face 1) and along the outer edge of the plume (Plane 3/Face 3). For this purpose, a combination of Class 1b and Class 2 results were used (Class 1a results were excluded due to lower repeatability). It was found that the temperature along the flame varied linearly. Along Plane 3/Face 1 and Plane 3/Face 3, third order polynomial equations were obtained.

Upon identifying the variations across the width, height and depth of the externally venting plume, equations were developed to describe these variations using CEF averaged non-dimensionalised Face temperature results for each Class of tests. 3D polynomial surface fits were developed for each Face of the thermocouple grid, expressed in terms of window width and height. The resulting Face 1 to Face 4 groupings of the 3D polynomial equations, allow easy communication of the experimental results of each Class of tests for code validation purposes.

These matrix equations can be adjusted with respect to the expected T_{\max} (maximum temperature), T_{amb} (ambient temperature) and window size, to determine the expected temperatures over the region directly above a burn room window. Face 1 surface fits give an indication of the temperature variations on the external wall, while the Face 2 surface fits describe the centre of the plume. Face 3 and Face 4 give an indication of the variations in temperature with increased distance away from the external wall, and towards the exposed outside environment.

SECONDARY FIRES

The possibility of the externally venting flames initiating a Secondary Fire in the room above the room of fire origin was also examined here. It was found that the duration of high temperatures as well as the reach of the venting flames posed a greater risk to flame spread through the window above the floor of fire origin than radiative ignition alone. This conclusion is based on the relatively low radiative heat flux measured on the Floor 1M window, along with thermal gradients in excess of 80°C along the window width. In all tests which developed to flashover, flames easily covered the Floor 1M window. The subsequent failure of this window, indicated that the initiation of a secondary fire is a real possibility. On the average, the burn room window failed in about 5 minutes after ignition, and the Floor 1M window dislodged between 4 to 10 minutes after the failure of the burn room window.

Oleszkiewicz's[29] method to estimate the total and radiant heat flux on the external wall due to externally venting flames was investigated. The total heat flux levels just above the burn room window were calculated to be comparable to the measured ones. This conclusion confirms the appropriateness of Oleszkiewicz's convective heat transfer coefficient for furniture fires, which was developed from wood crib fire data. The agreement between the calculated and measured total heat flux becomes worse with height above the burn room window. The radiative heat flux values calculated at the window on the floor above were lower than the measured ones. Although at such heights above the burn room window, the calculated values are lower than the measured ones, even the measured levels were still too low to cause ignition of items, such as curtain material or loose pieces of paper[108] through radiative heat transfer alone.

EXTERNAL WIND, SWIRLING OF THE VENTING PLUME AND SMS

While these tests were designed to be performed on almost 'still' days to allow repeatable results, the influence of wind on the venting plume was still apparent. Varied wind speeds and directions contributed to the swirling of the plume to varying degrees during each of the tests. Swirling of the entire plume occurred only during Burn 1, Burn 2 and Burn 3 where the entire plume swirled away from the opening,

creating huge spiralling sections approximately 2.5m in diameter with a visually observed period of just over one second. During all other tests, the venting plume was protected from direct wind interaction by either the building itself or the air-handling unit. As such, it has been concluded that although the fire and flames have a natural periodicity innate to the combustion process itself, any significant swirling of the venting plume is due to wind alone.

Another interesting manifestation was the **BOWING OF THE BURN ROOM WINDOW**. Bowing occurred during Burn 1 to Burn 3 as a result of mainly direct and side winds interaction on the Southern facade of the building. It also occurred during Burn 6 and Burn 7 when the smoke management system was activated.

The **SMOKE MANAGEMENT SYSTEM** was in operation during Burn 6, a Class 1b test, and Burn 7, a Class 2 test. For the first of these two tests, flashover did not occur. During Burn 6, the removal of smoke (air/hot gases) prevented the heat build-up in the burn room and the spread of the fire. In contrast, the activation of the SMS caused flashover during Burn 7, which would not have flashed over otherwise. This was attributed to the bowing and subsequent cracking of the burn room window, leading to Window Lowering Criteria #1 (WLC#1) being reached.

COMBUSTIBLE LINING IN THE CORRIDOR

Combustible lining was mounted from the floor to the ceiling along a portion of the corridor outside the burn room during Burn 8. When the test was completed, it was observed that only the top half (ceiling down) of the lining was burnt. Due to the increased fuel load, burn room temperatures were highest during Burn 8. The combustible lining also produced significant amounts of smoke in the corridor, reaching up to the third floor of the building. However, the external temperature contours were similar to those of Burn 5, and consequently, Burn 8 was grouped with Burn 5 for the evaluation of the externally venting plume during Class 1b tests.

6. NUMERICAL PREDICTION OF THE EXTERNAL TEMPERATURE FIELD

6.1 INTRODUCTION

The shift towards performance based design codes for the building and fire safety industry has sparked a plethora of work into the re-evaluation of the existing building design codes and fire safety requirements. Although Australia has an excellent fire safety record[115], the designs lack technical substantiation. In addition, these designs are based largely on empirical rules developed as the building codes grew, and consequently, they are not as cost effective as possible, resulting in an imbalance which causes considerable cost to the community. Hence, current design measures, although producing a superior fire safety record, do not provide a balance between *desirable protection* and *affordable cost*.

To meet the needs of performance based codes, computer models validated against realistic and repeatable experimental data must be generated. To this end, the CESARE-CFD model has been expanded for the first time to include the temperature field outside the room of fire origin to study a venting plume. This program was chosen here to align the present study with the ongoing computational efforts at CESARE. The CESARE-CFD program is a modified version of the commercially available program FURNACE, written by Kent and co-workers at the University of Sydney. In its original form, FURNACE models a pulverised coal-fired boiler or a pool fire with user specified inflow for fuel and air, and a single-port or multiple-outlet ports on the same wall. As such, the program could not simulate complex fuel geometries, or flame spread over individual items of fuel.

Major modifications[116,117,118,119,120] on this program have been carried out which allowed the program to represent a building fire more realistically. As a result, the fuel source can be either a 'solid' of any shape or arrangement within the burn room, or a propane burner. More importantly, the program now allows for the placement of 'outlet ports', representative of doors and windows on opposing walls. As explained in detail in the following section, simulations with CESARE-CFD were

performed by the author for only a selected number of cases due to the limitations of the program. To analyse the output, a post-processing program was developed in MATLAB. This program is presented in Appendix D along with other MATLAB programs. Sample input and output data files used with CESARE-CFD are given in Appendix G.

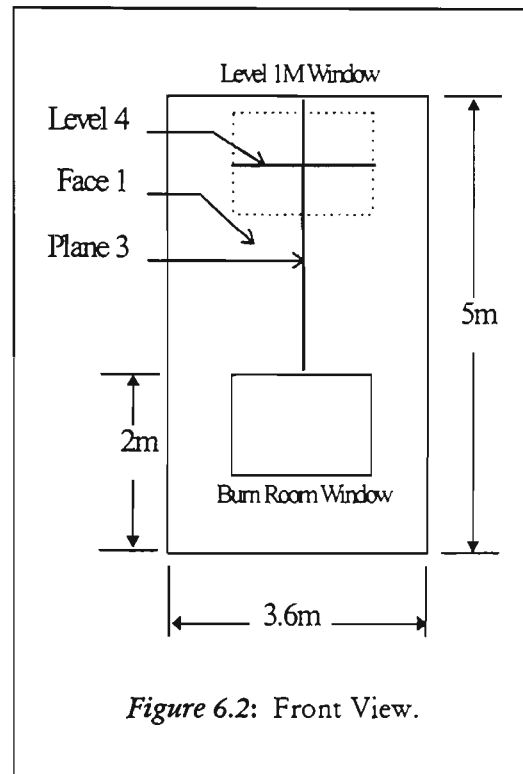
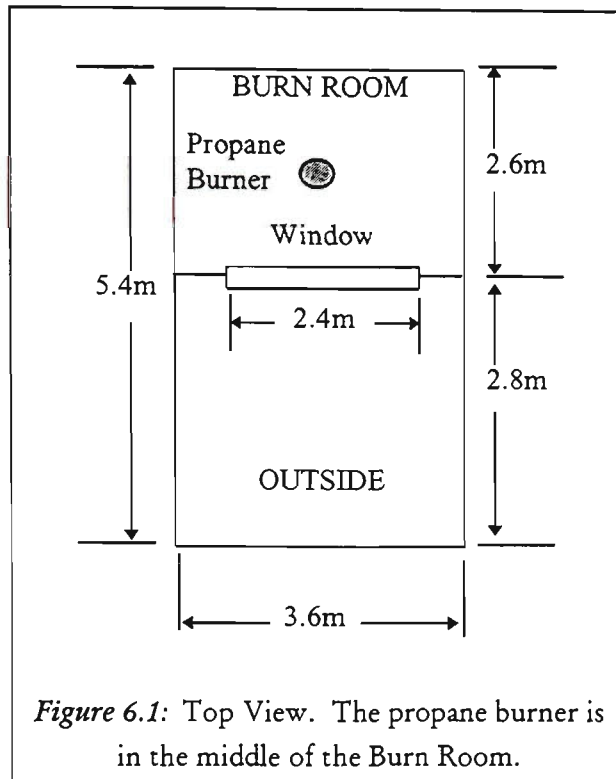
One of the advantages of numerical prediction is that complex geometries on the external facade of a building can be incorporated into the model to determine its effect on the venting plume. In addition, fire and smoke spread throughout a building can be modelled. On the other hand, a model of the external plume is only as good as the modelling of the internal conditions of the burn room, since these conditions lead to the external flames and plume. Although the CESARE-CFD can simulate up to 80% combustion of the fuel at steady-state, it cannot truly represent time-dependent flashover. Hence, the predicted external temperature fields to be presented next, must be viewed with this point in mind.

As discussed in *Section 2.7*, modelling of the venting plume has been carried out by Satoh and Kuwahara[89]. They highlighted the presence of upward moving coherent structures and their oscillatory nature in the venting plume. Their temperature and velocity contours give a general indication of these structures, and a heat release rate of 1.5MW (corresponding to a burn room temperature of approximately 700°C) results in temperatures between 400 to 500°C, reaching to a height of 1m above the window opening. The dynamic three-dimensional nature of the venting plume, was confirmed by Galea *et al.*[95], when comparison of 2D and 3D models were made. The work highlighted the limitations of 2D modelling. Continuing from their earlier work, Galea *et al.*[96] provided temperature contours of the venting plume with and without horizontal projections above the opening. Temperature contours plotted through the vertical symmetry plane and off to the side, showed the variations in temperature across the width of the window opening.

6.2 NUMERICAL RESULTS AND COMPARISON WITH EXPERIMENTAL DATA

The CESARE-CFD was run to predict the temperature field outside a burn room, with a window opening the same size as that used in both the polyurethane and real furniture experiments. The 'room' itself was standard size, 2.4 x 3.6 x 2.4 m high, with the fuel source (a gas burner) located in the centre of the room. The fuel was burned in the room with a constant mass flow rate, equivalent to 1MW (low heat release rate) and 2MW (high heat release rate). The higher of these two values was the practical limit of the program. The program was run to convergence, resulting in steady-state conditions. These steady-state numerical results were generated for comparison with the CEF averaged experimental results.

As shown in Figure 6.1 and Figure 6.2, the overall grid dimensions were 5.4 x 3.6 x 5m high, allowing a 2.8 x 3.6 x 5m high portion of the external environment to be mapped. The runs were also divided into two grid sizes, coarse and fine. The coarse grid divided the overall dimensions into 20 x 29 x 27 elements, each 0.2m in size, while the fine grid had 47 x 67 x 62 elements, each 0.08m in size. Three cases are given in the following section. These cases correspond to a low rate of burning with a coarse and fine grid, Run 1 and Run 2, respectively, and a high rate of burning with a coarse grid, Run 3. To allow for comparison of the CFD prediction with the experimental results, the equivalent portions of the CFD results, corresponding to Plane 3, Face 1 and Level 4 of the 'experimental grid', as shown in Figure 6.2, have been examined. The steady-state CFD results were non-dimensionalised similar to the CEF averaged experimental results, where the ambient temperature was 20°C and the maximum external temperature were 365°C, 525°C and 869°C for Run 1 to Run 3 (consequently, only during Run 3, external flaming is obtained). Hence, external flaming was obtained only in Run 3, using a flame tip temperature of 540°C.



In an attempt to achieve a balance between processing time and acceptable results, a comparison was made first between a coarse and a fine grid to establish grid independence of the computational results. Run 1 and Run 2 had the same rate of burning, 1MW, with the coarse grid, 0.2m element size, and the fine grid, 0.08m element size, respectively (A propane supply rate of 0.0217kg/s was used in the CESARE-CFD. With a heat of combustion (ΔH_c) of 46.45MJ/kg[121], this flow rate corresponds to a HRR of 1MW). The predicted temperature contours corresponding to Plane 3 of the experimental grid are given in Figure 6.3 and Figure 6.4 for coarse and fine grids, respectively. This Plane is perpendicular to the external wall and is located in the centre of the burn room window. It extends 1.5m away from the wall and 3m above the top of the burn room window, taking it to a height corresponding to just above the Floor 1M window. Figure 6.5 and Figure 6.6 correspond to Face 1 of the experimental grid which lies just above the external wall. It covers a 2.4m wide (window width), by 3m high (just past the top of the Floor 1M window), area of the wall. The computational results on Level 4 of the experimental grid are given in Figure 6.7 and Figure 6.8, for the coarse and fine grids, respectively. This Level is at the centre of the Floor 1M window and extends 1.5m away from it.

The steady state results were reached within 10 days on a UNIX workstation with the coarse grid, and 28 days with the fine grid. As can be seen from Figure 6.3 to Figure 6.8, the temperature contours obtained with the two grids are substantially different. However, the location of individual contours across each Plane, Level and Face is comparable. Consequently, due to the impracticality of the fine grid run time, it was decided that the coarse grid could be used with varying burning rates to produce not quantitative but qualitative results for comparison with the experimental results.

Run 3 had twice the burning rate of the previous runs, and hence, its heat release rate was closer to those of the Polyurethane Burns. Even this heat release rate, the highest possible in the CESARE-CFD, was substantially lower than that of the Real Furniture Burns (For Polyurethane Burns, the *average* mass loss rate was 5kg/min, corresponding to a HRR of 2.2MW, with a ΔH_c of 26MJ/kg. For Real Furniture Burns, the *average* mass loss rate was 20kg/min, corresponding to a HRR of 6.4MW, with an *effective* ΔH_c of 19.23 MJ/kg[102, Appendix 5] for the Real Furniture Burns.). Figure 6.9 to Figure 6.11 were generated from the results of Run 3. These figures correspond to Plane 3, Face 1 and Level 4 of the experimental grid. Due to the inherent limitations of the data acquired for the early Polyurethane Burns, and the brevity of the CEF period of PU4, a comparison of the steady-state numerical results with these experimental results was inappropriate. This conclusion is apparent from a comparison of the CFD results in Figure 6.9 to Figure 6.11 with the experimental Plane 3, Face 1 and Level 4 results of PU4, given in Figure 4.12 to Figure 4.14. Instead, a comparison was made with the experimental results from the Real Furniture Burns averaged over CEF, realising that non-dimensionalisation might not possibly rectify the differences in heat release rates. Class 2 results from Burn 4 and Burn 7 were selected for comparison. The reason for this choice was the ventilation conditions of Burn 4 and Burn 7 consisting of an open window as the only opening, and a closed door.

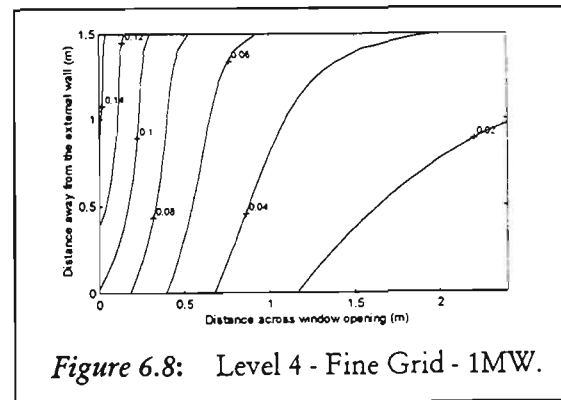
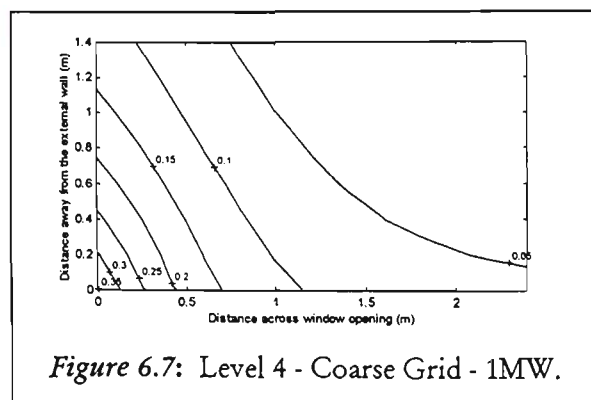
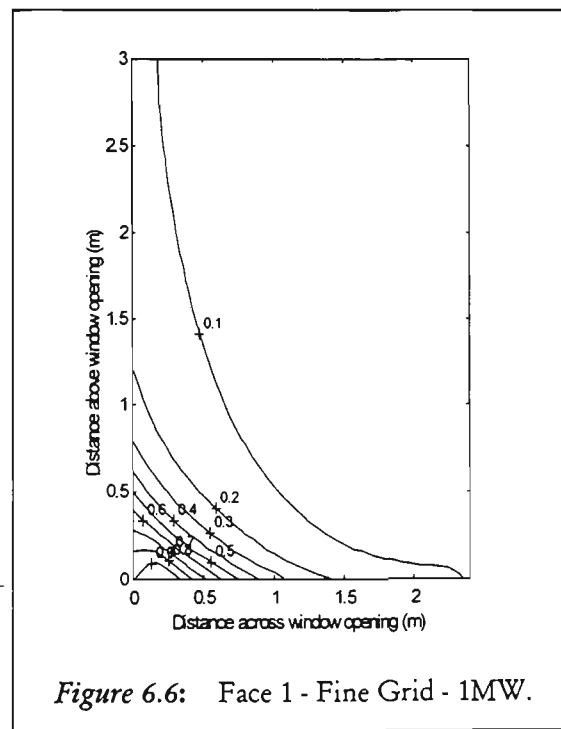
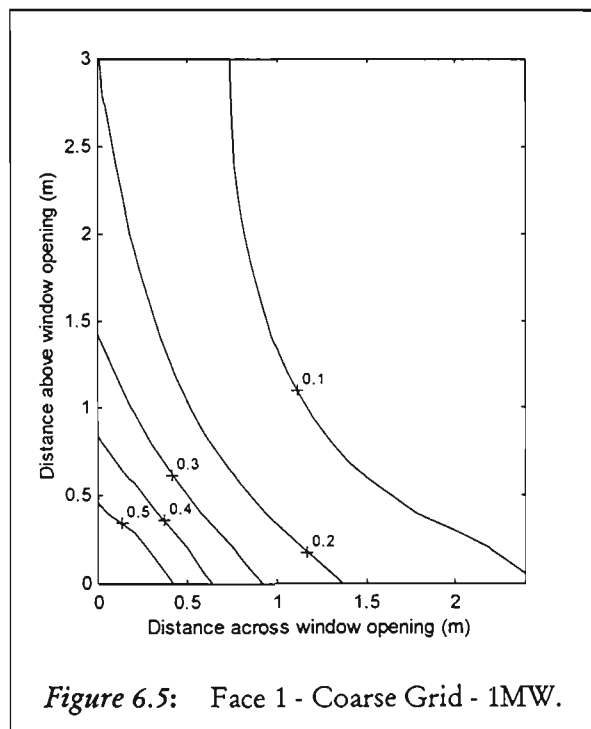
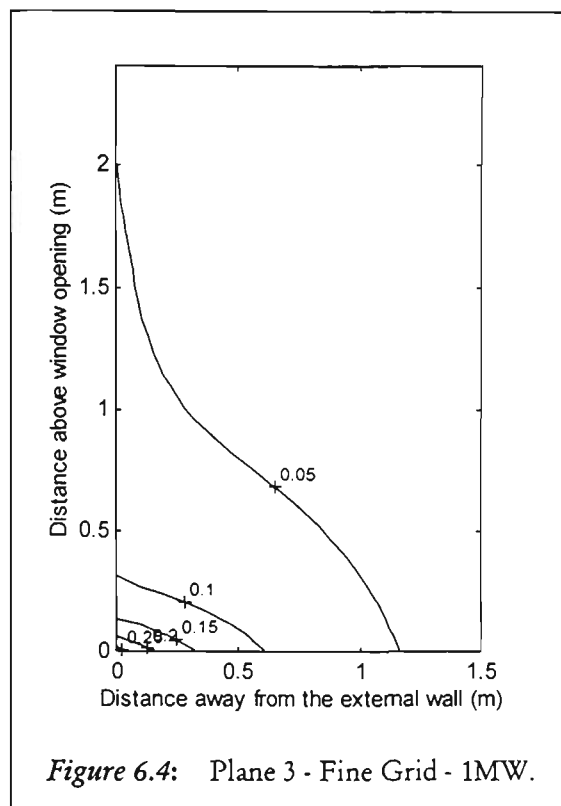
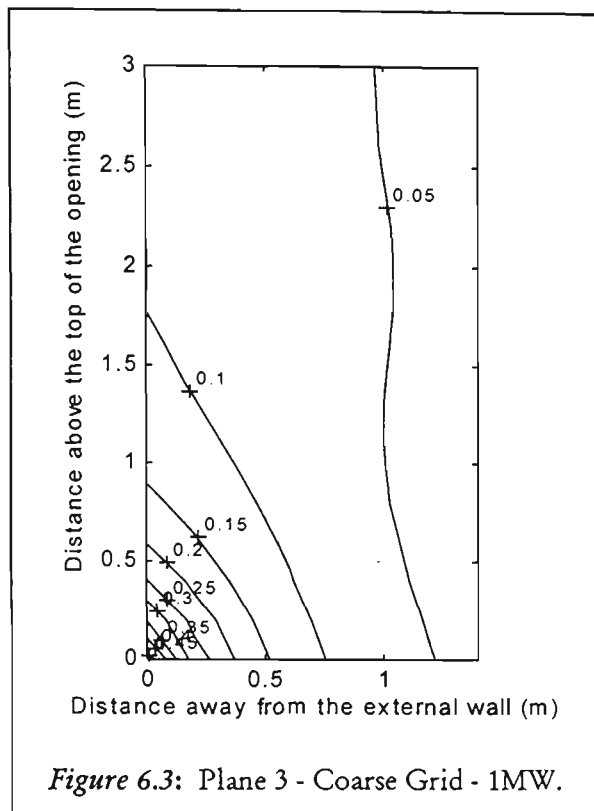
A detailed comparison has been made of the experimental Plane 3, Face 1 and Level 4 results of Burn 4 and Burn 7, given in Figure 5.32 to Figure 5.37, with the corresponding predicted results given in Figure 6.9 to Figure 6.11. This comparison has indicated that the numerically predicted results agree globally with the experimental results for Face 1 and Level 4, but not for Plane 3. Even for Face 1 and

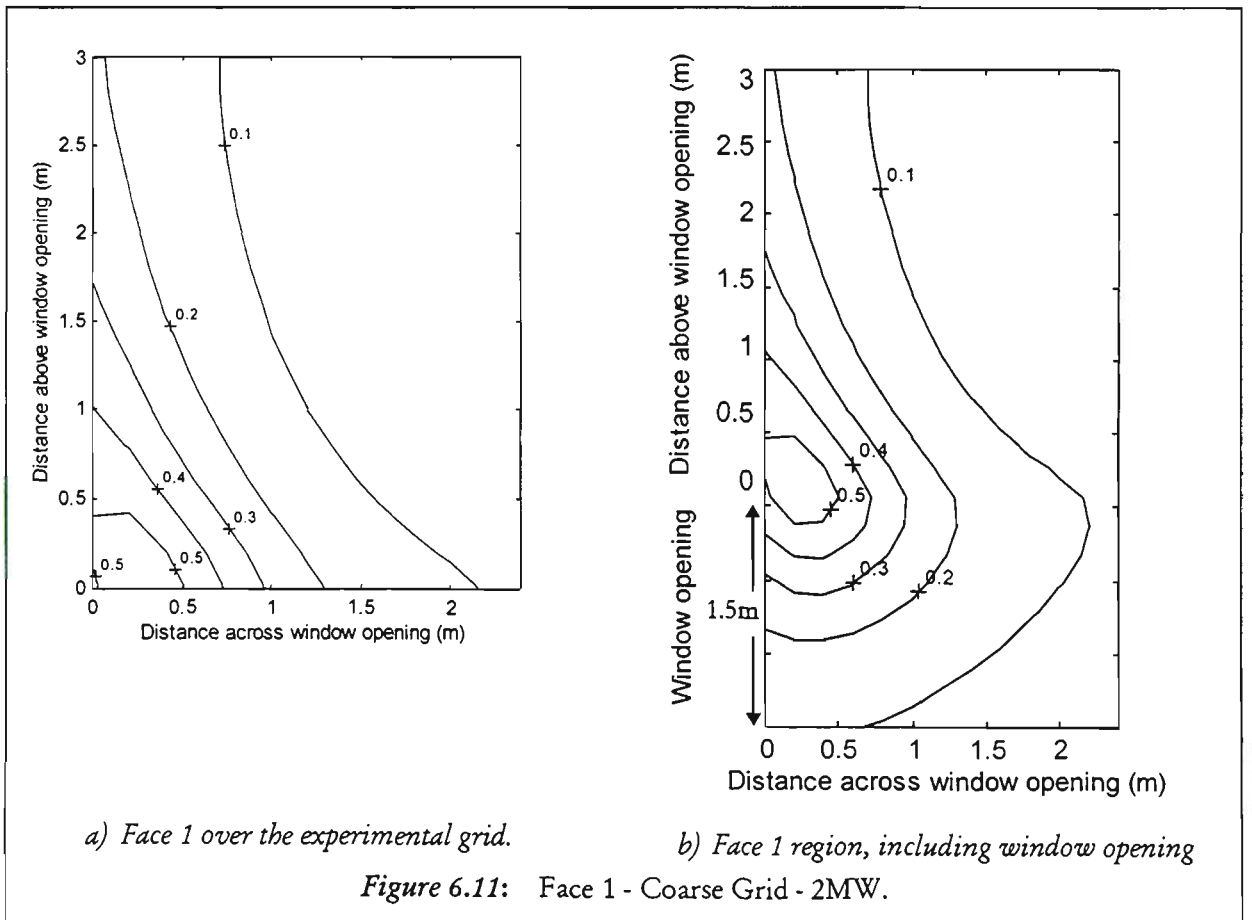
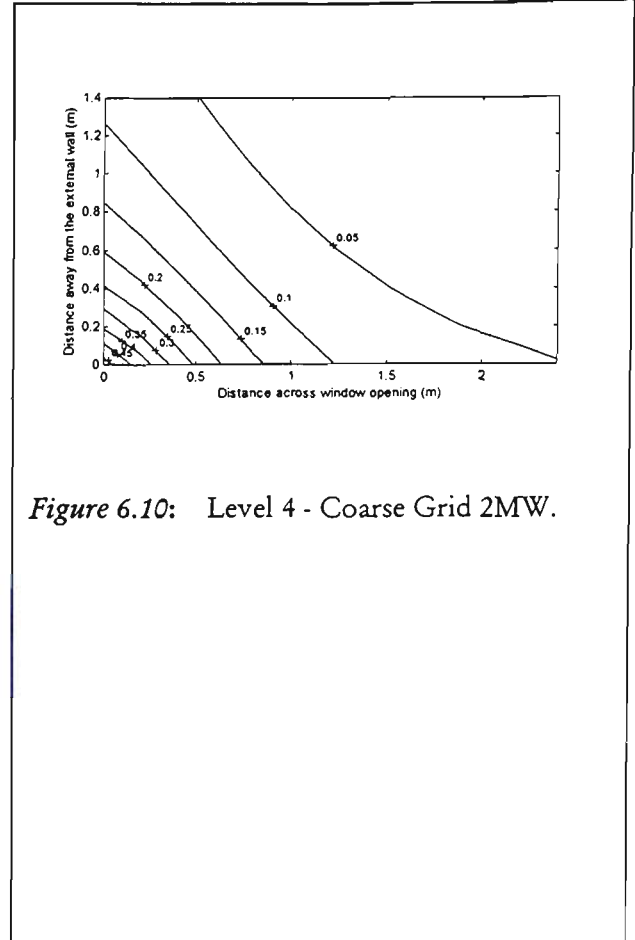
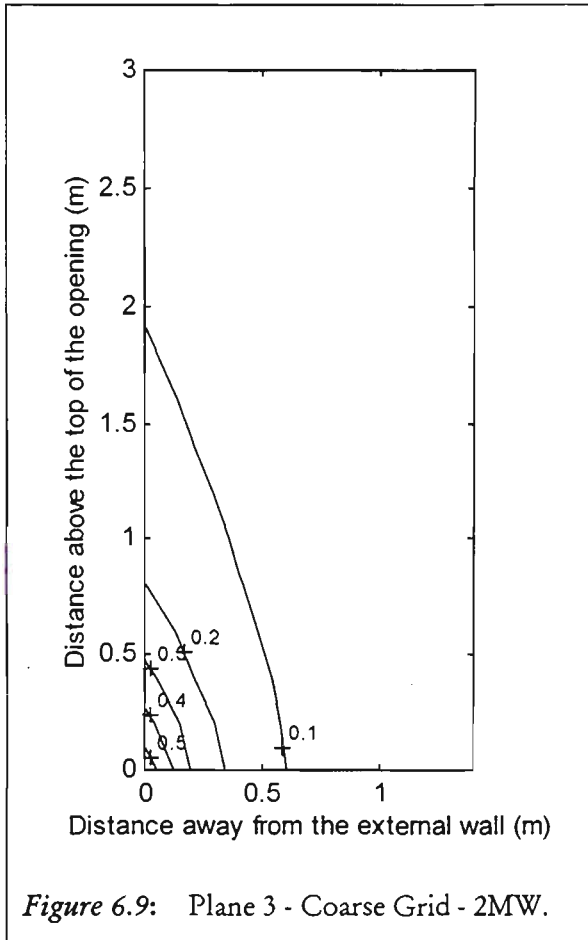
Level 4, some characteristics inherent to the experimental results are missing from the predicted results. The closed contour pattern of the experimental results on Face 1 also exists in the predicted results. However, as shown in Figure 6.11b, these closed contours are displaced towards the window with respect to the experimental results, given in Figure 5.34 and Figure 5.35. The displaced predicted contours are not closed within this limited region. The substantial ‘bellying’ of the contours in the Plane 3 plots, Figure 5.32 and Figure 5.33, which indicate a greater horizontal reach of the flames, is missing in the predicted results given in Figure 6.9. This result must be due to the inability of the program to predict the conditions within the burn room when the window is open. In addition, the predicted Level 4 contours shown in Figure 6.10 have considerably lower temperatures at this height than the experimentally measured results given in Figure 5.36 and Figure 5.37. This difference can be attributed to both the inability of the program to simulate the burn room conditions and the four-fold difference between the numerical and experimental rates of burning. Of these two factors, the former is expected to be more important than the latter. The reason is that the Plane 3, Face 1 and Level 4 predicted temperature contours in Figure 6.3, Figure 6.5 and Figure 6.7, respectively, with 1MW heat release rate are quite similar to the corresponding ones in Figure 6.9, Figure 6.10 and Figure 6.11a with 2MW heat release rate, signifying the effectiveness of non-dimensionalisation for a two-fold increase in the rate of burning.

The differences in temperature contour shapes between the numerical and experimental results can be attributed to two main reasons. The first reason is that the CESARE-CFD cannot predict the buoyancy driven turbulent convective flow that exists through the burn room under even no-through draft ventilation conditions. As a result, the bellying of the plume observed during the experiments cannot be obtained with the CESARE-CFD. The second reason must be the simple way in which turbulence is modelled within the CESARE-CFD. The basic $k-\epsilon$ model is used to treat turbulence even under the complex flow conditions expected within the room. The incorrectly predicted external temperature contours imply that the predicted streamline pattern within the plume must be equally erroneous. Inaccurate mean temperature and velocity predictions indicate that the mean flow equations are not treated properly due to the inadequate representation of the Reynolds stresses.

Therefore, turbulence modelling needs to be refined within the CESARE-CFD for better treatment of these terms.

Modelling of the venting plume by Satoh and Kuwahara[89] produced temperature profiles for a larger region of space outside the burn room window than examined here. Satoh's results are comparable to the CESARE-CFD results for the same region. Galea's[96] temperature profiles for windows without a balcony also show similar trends. While each of these predicted results contain comparable temperature profiles, indicating similar numerical modelling, they all lack some of the basic characteristics of a venting plume seen during this series of tests, starting with the bellying above the burn room window.





6.3 CONCLUSIONS FROM THE NUMERICAL PREDICTIONS

The steady-state results of the CESARE-CFD and the CEF averaged experimental results are similar for Face 1 and Level 4, but not for Plane 3. Even for Face 1 and Level 4, the similarities are qualitative, only. This comparison was possible due to the CEF averaging of the experimental data. In addition, non-dimensionalising temperature with T_{\max} (maximum measured external temperature) and T_{amb} (average ambient measured temperature) has been an appropriate means to compare numerical and experimental data for similar ventilation conditions. Without such averaging and non-dimensionalisation of the experimental data, the ability to extract useful information from the results would have been limited.

7. CONCLUSIONS

In this thesis, externally venting flames have been studied during two series of full scale flashover fires, and their characteristics have been determined in relation to internal ventilation conditions, burning rate, burn room size, secondary fires, glass breakage and wind effects. The experimental results are compared with existing empirical approximations. Some of these approximations are modified to fit the data. Once the repeatability of the tests has been established, new approximations are developed as curve fits to the experimental data for easier communication of the data for numerical prediction and code validation purposes. The repeatable experimental results are compared with limited numerical predictions. In this chapter, summaries are given of *Section 4.7, Conclusions from the Polyurethane Burns*, *Section 5.9, Conclusions from the Real Furniture Burns* and *Section 6.3, Conclusions from the Numerical Predictions*.

Polyurethane Burns: The conclusions of the first series of tests can be summarised as follows:

- ◆ With 15 to 18kg of polyurethane in a standard burn room of 2.4m x 3.6m x 2.4m, the standard glass in the burn room window (2.4m x 1.5m) took about 3 minutes to fail during PU1 to PU3. During PU4, with 16kg of polyurethane in a larger burn room of 3.6m x 5.31m x 2.4m, the burn room window was lowered 2:30 minutes after ignition, using WLC #1, indicating that the gas temperature reached 450°C next to the glass. For the ventilation class of PU4, Class 1, this condition represented when glass cracking was expected.
- ◆ The internal ventilation conditions affected the measured external temperature and heat flux patterns. During PU1, a no-through-draft Class 2 test, the burn room window was the only vent path. As a result, external temperature and heat flux histories show wider peaks than those of PU2 to PU4, through-draft Class 1 tests.
- ◆ Once the window failed, the Standard and Alternative Window arrangements were not found to have a discernible effect on the

externally venting flames during the fully developed phase of the fire, as most of the glass had dislodged prior to flashover.

- ◆ The use of the window lowering criterion and the larger burn room, increased the burning rate during PU4 compared to those of PU1 to PU3.
- ◆ Secondary fires due to direct flame contact were found to be more likely during PU1 to PU3, where cracking (and dislodgment during PU1) of glass from the window above the room of fire origin occurred. During PU4, no cracking occurred in the window above the burn room, due to the larger burn room size.
- ◆ On the average, Bullen and Thomas's[56] excess fuel factor was determined to be a low negative number, although external flames were present during these tests. Hence, with this data, their correlation cannot be validated.
- ◆ Predictions of the flame envelope using Law's[21] empirical approximations were found to be consistent with experimental data when using polyurethane as a fuel, even though these approximations were developed from mostly wood crib fires.
- ◆ Estimation of centre-line temperatures, using Law's[21] equations were found to overestimate those measured. This result has been linked to the tilting of the plume which caused it to miss the 2D rack, resulting in lower measured temperatures.
- ◆ Heat flux calculations (using measured temperatures) developed by Oleszkiewicz[29] were found to underestimated the measured total heat flux, and consequently, the possible effects of the venting plume on the external facade. This result has been attributed to the convective heat transfer co-efficient used in the calculations, which was developed for fires with moderate burning rates, such as wood crib fires, in addition to the lower measured temperatures due to the tilting plume.
- ◆ High wind speeds, above 2.5m/s, caused the venting plume to tilt, affecting both temperature measurements and heat flux calculations. Consequently, it was concluded that wind effects need to be minimised to gauge repeatability of the tests.

Real Furniture Burns: The second series of tests were carried out in a burn room of 3.6m x 5.31m x 2.4m with an average fuel load density of 28kg/m² using furniture. The burn room window size was the same as in the first series, 2.4m x 1.5m. The conclusions of this series are as follows:

- ◆ A new method has been developed to analyse multiple and long time records of experimental data of external temperature and heat flux. This method is based on time averaging each record over the corresponding Consistent External Flaming (CEF) period. CEF averaging enabled comparison of experimental data with empirical approximations and numerical predictions.
- ◆ Repeatability of the tests was gauged using Class distinctions, CEF averaging and non-dimensionalisation. It was found that the tests were very repeatable with the exception of the two Class 1a tests which were unduly influenced by wind.
- ◆ Empirical approximations of Law[21] to estimate the flame envelope resulted in dimensions consistent with the observed plume size during this series of tests.
- ◆ Empirical approximations of Law[21] to estimate centre-line temperatures were found to follow the same linear trend along the plume axis as measured during this series of tests. However, the calculated centre-line temperatures overestimated the measured centre-line temperatures.
- ◆ Similar to the first series of tests, the plume vented from the upper 1/2 to 2/3 of the burn room window during the CEF period of each test, the no-through draft Class 2 behaviour. Due to the large window size, this behaviour existed during both Class 1, through draft, and Class 2 tests.
- ◆ Re-attachment of the venting plume based on Yokoi's[28] window shape parameter, n , was found to be consistent. However, the calculated spandrel lengths underestimated the necessary distance to prevent failure of an upper level window.
- ◆ Law and Thomas's[60] flame length estimation resulted in unrealistically high vertical reach of the flames when the total heat release rate was used in the estimation as the heat loss

through the burn room window. Instead, their formulation was used with the experimentally observed flame length to determine that only about 27% of the total heat released must have vented through the window.

- ◆ Total heat flux measurements of Oleszkiewicz[29] were found to be similar to those measured here for similar internal ventilation conditions and comparable window size and heat release rate.
- ◆ Sugawa *et al.*'s[73] tilt angle estimation developed from small scale experiments, resulted in higher values than observed during these tests. This result has been attributed partly to their formulation being for side wind conditions only. When the heat release rate in their formulation was modified to account for the rate of heat released through the burn room window, 27% of the total, a tilt angle of 56° from the vertical was calculated. This value is close to the experimentally observed range of tilt angles, 15° to 30° from the vertical.
- ◆ 2D temperature variation equations were developed from the results of this series of tests (with the exception of Class 1a results which were not as repeatable as those of the other tests) to match those developed by Law. These equations express the temperature variation along the plume centre-line (intersection of Plane 3/Face 2) as well as along Plane 3/Face 1 and Plane 3/Face 3 to give an impression of the variation in temperature across the depth of the plume. Using Law's coordinates, the equation corresponding to the plume centre-line is linear, indicating a linear drop in temperature with height along the plume axis. Along Plane 3/Face 1 and Plane 3/Face 3, the temperature drop is related to the height in the form of a third order polynomial.
- ◆ Upon identifying the variations across the width, height and depth of the externally venting plume, 3D fourth order polynomial equations were developed as surface fits to the temperatures on each Face of the 3D external thermocouple grid. This representation allowed the temperature field above the burn room window to be determined in terms of the window shape,

distance away from the external wall (Face 1 to Face 4) and maximum and ambient temperatures.

- ◆ The likelihood of secondary fires was found to be high due to the measured temperatures and duration of external flames over the window above the burn room window which failed in every test that reached flashover. Limited radiative heat transfer measurements suggested that ignition due to radiation alone would not be possible.
- ◆ Regarding the possibility of a secondary fire, it has been observed that the glass in the window above the burn room window (W1M02) dislodges in about 4 to 10 minutes after the failure of the burn room window (W102) which happens approximately 5 minutes after ignition.
- ◆ All Class 1 tests developed to flashover, with the exception of one during which activation of the Smoke Management System (SMS) prevented flashover. This result has been attributed to the active removal of smoke and hot gases, which prevented the build-up of a hot-gas layer in the burn room.
- ◆ Activation of the Smoke Management System during a Class 2 test facilitated flashover which would not have otherwise occurred. This result has been attributed to the bowing and subsequent failure of the burn room window due to the activation of the smoke management system.
- ◆ Bowing of the burn room window was linked to the activation of the Smoke Management System, external wind and internal ventilation conditions. During three of the tests, bowing of the burn room window has been attributed mainly to direct or side wind and, to a smaller extent, to the closed stairwell door, which together must have resulted in greater pressure differential within the building.
- ◆ Another effect of external wind was that it caused the swirling of the entire plume. The swirling plume had an observed diameter of approximately 2.5m, slightly larger than the burn room window width, with a period of just over one second.

- ◆ Combustible wall lining in the corridor was found to contribute to higher temperatures and smoke levels within the building, with no discernible effect on the externally venting flames.

Numerical Prediction of the External Temperature Field: The following conclusions have been reached from a comparison of the experimental results with the numerical predictions:

- ◆ Steady-state numerical prediction results using CESARE-CFD were compared with the CEF averaged experimental results from two Class 2 tests of the Real Furniture Burns. Burn 4 and Burn 7 were selected for this comparison due to their ventilation conditions (closed door and open window) and the reasonable lengths of their CEF durations, in addition to being the best overall repeat cases. The numerical predictions showed only qualitative agreement with the experimental results. Quantitative differences existed in the numerical results not having the expected bellying of the plume, indicative of a greater horizontal reach. The closed contour patterns on the Faces were also missing.
- ◆ CEF averaging and non-dimensionalisation of the experimental results have been shown to be an appropriate means to compare the experimental data with the steady-state predictions.

REFERENCES

- 1 Koepping, K-P., "Prometheus", *The Encyclopedia of Religion*, M. Eliade (ed), MacMillian Publishing Company, New York, Vol. 12, pp. 4-5, 1987.
- 2 Quintiere, J., "A Perspective on Compartment Fire Growth", *Combustion Science and Technology*, Vol. 39, pp. 11-54, 1984.
- 3 Quintiere, J., "Fire Growth and Development", *The Warren Centre: Fire Safety and Engineering - International Symposium Papers*, University Printing Service, University of Sydney, pp. 39-64, 1989.
- 4 Seigel, L. G., "The Projection of Flames from Burning Buildings", *Fire Technology*, Vol. 5, No. 1, pp. 43-51, 1969.
- 5 Drysdale, D., "Mechanisms of Flashover: An Overview", *Proceedings of the Seventh International INTERFLAM '96 Conference*, pp. 155-157, 1996.
- 6 Law, M., "Fire Grading and Fire Behaviour", *Fire Safety Journal*, Vol. 17, pp. 147-153, 1991.
- 7 Belles, D. W., "External Walls of Buildings - Prevention of Fire Spread for Story to Story", *Building Standards*, Vol. 55, No. 3, May-June, pp. 7-12, 1986.
- 8 Lougheed, G. D., Yung, D., "Exposure to Adjacent Structures from Flames Issuing From a Compartment Opening", *Proceedings of the Sixth International INTERFLAM '93 Conference*, pp. 297-306, 1983.
- 9 Beever, P., "Regulations, Codes and Standards: The Fire Engineering Approach", *Proceedings of the First International ASIAFLAM 1995 Conference*, pp. 1-7, 1995.
- 10 Meacham, B. J., "Performance-Based Codes and Fire Safety Engineering Methods: Perspectives & Projects of the Society of Fire Protection Engineers", *Proceedings of the Seventh INTERFLAM '96 Conference*, pp. 545-553, 1996.
- 11 Beck, V., *et al.*, "The Warren Centre for Advanced Engineering: Fire Safety and Engineering Project Report", University Printing Service, University of Sydney, p. 7, 1989.
- 12 Jones, W. W., "A review on Compartment Fire Models", NBSIR 84-2684, *National Bureau of Standards*, Washington, DC., USA, 1983.
- 13 Beck, V. R., "Fire Safety System Design Using Risk Assessment Models: Developments in Australia", *Proceedings of the Third International Symposium on Fire Safety Science*, pp. 45-59, 1985.
- 14 Evans, D. D., "Large Fire Experiments for Fire Model Evaluations", *Proceedings of the Seventh International INTERFLAM '96 Conference*, pp. 329-334, 1996.

-
- 15 Tewarson, A., Newman, J. S., "Scale Effects on Fire Properties of Materials", *Proceedings of the First International Symposium of Fire Safety Science*, pp. 451-462, 1985.
 - 16 Babrauskas, V., Wickström, U., "The Rational Development of Bench-Scale Fire Tests for Full-Scale Fire Prediction", *Proceedings of the Second International Symposium of Fire Safety Science*, pp. 451-462, 1988.
 - 17 Kanury, A. M., "Scaling Correlations of Flashover Experiments", *Fire Safety: Science and Engineering, ASTM STP 882*, T. Z. Harmathy, Ed., American Society for Testing and Materials, Philadelphia, pp. 97-121, 1985.
 - 18 Galea, E., "On the Field Modelling Approach to the Simulation of Enclosure Fires", *Journal of Fire Protection Engineering*, Vol. 1(1), pp. 11-22, 1989.
 - 19 Oleszkiewicz, I., "Fire Exposure to Exterior Walls and Flame Spread on Combustible Cladding", *Fire Technology*, pp. 357-375, 1990.
 - 20 Yung, D., Oleszkiewicz, I., "Fire Spread Via Exterior Walls Of Buildings", *Proceedings of the Fourth Conference on Building Science and Technology*, pp. 1-12, 1988.
 - 21 Law, M., "Fire-Safety of External Building Elements - The Design Approach", *American Iron and Steel Engineering Journal*, Second Quarter, pp. 59-74, 1978.
 - 22 Oleszkiewicz, I., "Experimental Studies of Fire Spread along Building Facades", *Combined Meetings: The Combustion Institute and The National Bureau of Standards, The Center for Fire Research Annual Conference*, Gaithersburge, MD, 1987.
 - 23 Janssens, M., Tran, H. C., "Data Reduction of Room Tests for Zone Model Validation", *Journal of Fire Sciences*, Vol. 10, pp. 528-553, 1992.
 - 24 He, Y., "On Experimental Data Reduction for Zone Model Validation", *Journal of Fire Sciences*, Vol. 15, pp. 144-161, 1997
 - 25 Gewain, R. G., "Assessment of Fire Risk for Exterior Structural Members", *Fire Risk Assessment, ASTM STP 726*, G. T. Castion and T. Z. Harmathy, Eds., American Society for Testing and Materials, pp. 75-94, 1982.
 - 26 Graham, T. L., Makhviladze, G. M., and Roberts, P. J., "On the Theory of Flashover Development", *Fire Safety Journal*, Vol. 25, pp. 229-259, 1995.
 - 27 Chow, W. K., "Study of the Flashover Criteria for Compartment Fires", *Journal of Fire Sciences*, Vol. 15, pp. 95-107, 1997
-

-
- 28 Yokoi, S., "Study on the Prevention of Fire-Spread Caused by Hot Upward Current", Report of the Building Research Institute, Japan, Report # 34, 1960.
- 29 Oleszkiewicz, I., "Heat Transfer from a Window Plume to a Building Facade", HTD-Vol.123, Collected papers in Heat Transfer, Book No. H00526, pp. 75-86, 1989.
- 30 Law, M., O'Brien, T., "Fire Safety of Bare External Structural Steel", Construction Steel Research and Development Organisation, London, 1989.
- 31 Drysdale, D., "An Introduction to Fire Dynamics", John Wiley and Sons, 1986. Page numbers are as indicated within the text.
- 32 Kanury, A. M., "Ignition of Liquid Fuels", The SPFE Handbook of Fire Protection Engineering, First Edition, Philip J. DiNenno (ed), National Fire Protection Association, USA, Section 1, pp. 315, 1988.
- 33 Quintiere, J. G., "Surface Flame Spread", The SPFE Handbook of Fire Protection Engineering, First Edition, Philip J. DiNenno (ed), National Fire Protection Association, USA, Section 1, pp. 360-367, 1988.
- 34 Williams, F. A., "Mechanism of Fire Spread", *16th International Symposium on Combustion*, Pittsburgh, pp. 1281-1296, 1976.
- 35 Thomas, P. H., "The Growth of Fire - Ignition to Full Involvement", *Combustion Fundamentals of Fire*, G. Cox (Ed), Academic Press Ltd., pp. 275-296, 1995.
- 35 Hinkley, P. L., Wraight, H. G. H., Theobald, C. R., "The Contribution of Flames under Ceilings to Fire Spread in Compartments", *Fire Safety Journal*, Vol. 7, pp. 227-142, 1984.
- 37 Walton, W. D., Thomas, P. H., "Estimating Temperatures in Compartment Fires", *The SPFE Handbook of Fire Protection Engineering*, First Edition, Philip J. DiNenno (ed), National Fire Protection Association, USA, Section 2, pp. 16-32, 1988.
- 38 ISO 8421-1:1987 Fire protection - Vocabulary - Part 1: General Terms and phenomena of fire.
- 39 Waterman, T. E., "Room Flashover - Criteria and Synthesis", *Fire Technology*, Vol 4, pp. 25-31, 1968.
- 40 Johnson, P., Hatton, T., Lacey, R., (Prepared by), *Fire Safety and Engineering - Technical Papers, Part 6: Passive Systems*, The Warren Centre - University of Sydney, pp 6.13, 1989.
- 41 Cooper, L. Y., "Compartment Fire-Generated Environment and Smoke Filling", The SPFE Handbook of Fire Protection Engineering, First Edition, Philip J. DiNenno (ed), National Fire Protection Association, USA, Section 2, pp. 116-138, 1988.
-

-
- 42 Oleszkiewicz, I., "Fire Spread on Building Facades", *Proceedings of the Fifth International Fire Protection Engineering Institute*, 1989.
- 43 Hinkley, P. L., "Smoke and Heat Venting", *The SPFE Handbook of Fire Protection Engineering*, First Edition, Philip J. DiNenno (ed), National Fire Protection Association, USA, Section 2, pp. 33-43, 1988.
- 44 Oleszkiewicz, I., "Vertical Separation of Windows Using Spandrel Walls and Horizontal Projections", *Fire Technology*, Vol. 27, No. 4, pp. 334-340, November 1991.
- 45 Kung, H-C., "Cooling of Room Fires by Sprinkler Spay", *Journal of Heat Transfer*, Vol 99, pp. 353- 359, 1977.
- 46 Kim, A., "Protection of Glazing in Fire Separations by Sprinklers", *INTERFLAM '93*, pp. 83-93, 1993.
- 47 Barnett, C. R., "Fire Separation between External Walls of Buildings", *Fire Safety Science: Proceedings of the 2nd International Symposium*, pp. 841-850, 1988.
- 48 Heskestad, G., "Fire Plumes", *The SPFE Handbook of Fire Protection Engineering*, First Edition, Philip J. DiNenno (ed), National Fire Protection Association, USA, Section 1, pp 107-115, 1988.
- 49 Zukoski, E. E., "Properties of Fire Plumes", *Combustion Fundamentals of Fire*, Cox, G. (Ed) Academic Press Ltd. Page numbers are as indicated within the text., 1995.
- 50 Cetegen, B. M., Zukoski, E. E., Kubota, T., "Entrainment in the Near and Far Field of Fire Plumes", *Combustion Science and Technology*, Vol. 39, pp. 305-331, 1984.
- 51 Quintiere, J. G., Rinkinen, W. J., Jones, J. J., "The Effect of Room Openings on Fire Plume Entrainment", *Combustion Science and Technology*, Vol. 26, pp. 193-201, 1981.
- 52 Beyler, C. L., "Fire Plumes and Ceiling Jets", *Fire Safety Journal*, Vol. 11, pp. 53-75, 1986.
- 53 Thomas, P. H., "Fire, Flames and Dimensional Analysis", *Proceedings of the Third International Symposium on Fire Safety Science*, pp. 3-26, 1991.
- 54 Emmons, H. W., "Vent Flows", *The SPFE Handbook of Fire Protection Engineering*, First Edition, Philip J. DiNenno (ed), National Fire Protection Association, USA, Section 1, pp. 130-137, 1988.
- 55 Thomas, P. H., Law, M., "The Projection of Flames from Buildings on Fire", *Fire Prevention Science and Technology*, No. 10, pp. 19-26, 1972.
-

-
- 56 Bullen, M. L., Thomas, P. H., "Compartment Fires with Non-Cellulosic Fuels", *17th Symposium (International) on Combustion*, Pittsburgh, pp. 1139-1148, 1974.
- 57 Peatross, M. J., Beyler, C. L., "Ventilation Effects on Compartment Fire Characterisation", *Proceedings of the Fifth International Symposium on Fire Safety Science*, pp. 403-141, 1997.
- 58 Fleischmann, C. M., Parkes, A. R., "Effects of Ventilation on the Compartment Enhanced Mass Loss Rate", *Proceedings of the Fifth International Symposium on Fire Safety Science*, pp. 415-426, 1997.
- 59 "Fire-Safe Structural Steel - A Design Guide", American Iron and Steel Institute, 1979
- 60 Quintiere, J. G., Cleary, T. G., "Heat Flux from Flames to Vertical Surfaces" *Fire Technology*, Second Quarter, pp. 209-231, 1994.
- 61 Marchant, E. W., "Effect of Wind on Smoke Movement and Smoke Control Systems", *Fire Safety Journal*, Vol. 7, pp. 55-63, 1984.
- 62 Joshi, A. A., Pagni, P. J., "Fire Induced Fields in window Glass. I - Theory", *Fire Safety Journal*, Vol 22, pp. 25-43, 1994.
- 63 Joshi, A. A., Pagni, P. J., "Fire Induced Fields in window Glass. II - Experiments", *Fire Safety Journal*, Vol 22, pp. 25-43, 1994.
- 64 Pagni, P. J., Joshi, A. A., "Glass Breaking In Fires", *Proceedings of the Third International Symposium on Fire Safety Science*, pp. 791-802, 1991.
- 65 Skelly, M. J., Roby, R., J., "An Experimental Investigation of Glass Breakage in Compartment Fires", *Journal of Fire Protection Engineers*, Vol. 3, No. 1, pp. 25-34, 1991.
- 66 ski-Rahkonen, O., "Breaking of Window Glass Close to Fire, II: Circular Panes", *Fire and Materials*, Vol. 15, pp. 11-16, 1991.
- 67 Silcock, G. W., "An Experimental Evaluation of Glazing in Compartment Fires", *Proceedings of the Sixth International INTERFLAM '93 Conference*, pp. 747-756, 1993.
- 68 Harmathy, T. Z., "Flame Deflectors", *Building Research Note No. 96*, Division of Building Research, National Research Council of Canada, Ottawa, Canada, October, 1974.
- 69 Kashiwagi, T., Newman, D. L., "Flame Spread Over an Inclined Thin Fuel Surface", *Combustion and Flame*, Vol. 26, pp 163-177, 1976.
- 70 Drysdale, D. D., Macmillian, A. J. R., "Flame Spread on Inclined Surfaces", *Fire Safety Journal*, Vol. 18, pp. 245-254, 1992.
-

-
- 71 Fire Engineering Guidelines, Ch. 5, Section 5.5.5.2, Fire Code Reform Centre Ltd., 1996.
- 72 Sugawa, O., Takahashi, W., "Flow Behaviour of Ejected Fire Plume from an Opening with and without External Wind", *Proceedings of the First International ASIAFLAM Conference*, pp. 409-420, 1995.
- 73 Sugawa, O., Momita, D., Takahashi, W., "Flow Behaviour of Ejected Fire Flame/Plume from an Opening Effected by External Wind", *Proceedings of the Fifth International Symposium on Fire Safety Science*, pp. 249-260, 1997.
- 74 Bechtold, R., "The Role that Facades Play in Fire Spread", *Fire International*, Vol. 59, pp. 32-40, 1978.
- 75 Baum, H. R., McGrattan, K. B., Rehm, R. G., "Large Eddy Simulations of Smoke Movement in Three Dimensions", *Proceedings of the Seventh International INTERFLAM '96 Conference*, pp. 189-198, 1996.
- 76 Miles, S., Kumar, S., Cox G., "The Balcony Spill Plume - Some CFD Simulations", *Fifth International Symposium on Fire Safety Science*, pp. 237-247, 1997.
- 77 Yang, K. T., Lloyd, J. R., Kanury, A. M., Satoh, K., "Modeling of Turbulent Buoyant Flows in Aircraft Cabins", *Combustion Science and Technology*, Vol. 39, pp. 107-118, 1984.
- 78 Lockwood, F. C., Naguib, A. S., "The Prediction of the Fluctuation in the Properties of Free, Round-Jet and Turbulent Diffusion Flames", *Combustion and Flame*, Vol. 24, pp. 109-124, 1975.
- 79 Baum, H. R., McGrattan, K. B., Rehm, R. G., "Three Dimensional Simulations of Fire Plume Dynamics", *Fifth International Symposium on Fire Safety Science*, pp. 511-522, 1997.
- 80 Magnussen, B F., Hjertager, B. H., "On Mathematical Modeling of Turbulent Combustion with Special Emphasis on Soot Formation and Combustion", *Sixteenth International Symposium on Combustion*, The Combustion Institute, Pittsburgh, PA., pp. 719-729, 1977.
- 81 Chow, W. K., "Combustion Effects on a Building Fire Field Model", *4th International Symposium Transport Phenomena in Heat and Mass Transfer*, Vol. 4, pp. 1274-1285, 1991.
- 82 Quintiere, J. G., "An Approach to Modeling Wall Fire Spread in a Room", *Fire Safety Journal*, Vol. 3., pp. 201-214, 1981.
- 83 Fernandez-Pello, A. C., "Flame Spread Modelling", *Combustion and Science*, Vol. 39, pp. 119-134, 1984.
- 84 Hasemi, Y., "Thermal Modeling of Upward Wall Flame Spread", *Proceedings of the First International Symposium on Fire Safety Science*, pp. 87-96, 1985.
-

-
- 85 Delichatsios, M. M., Mathews, M. K., Delichatsios, M. A., "An Upward Fire Spread and Growth Simulation", *Proceedings of the Third International Symposium on Fire Safety Science*, pp. 207-226, 1991.
- 86 Cox, G., Kumar, S., "Field Modelling of Fire in Forced Ventilated Enclosures", *Combustion Science and Technology*, Vol. 52, pp. 7-23, 1987.
- 87 Bishop, S. R., Holnorn, P. G., Beard, A. N., Drysdale, D. D., "Dynamic Modelling of Building Fires", *Applications in Mathematical Modelling*, Vol. 17, pp. 170-183, 1993.
- 88 White, D. A., Beyler, C. L., Scheffey, J. L., Williams, F. W., "Modeling the Impact of Post-Flashover Shipboard Fires on Adjacent Spaces", *Proceedings of the Seventh International INTERFLAM '96 Conference*, pp. 225-233, 1996.
- 89 Satoh, K., Kuwahara, K., "A Numerical Study of Window-to-Window Propagation in High-Rise Building Fires", *Proceedings of the Third International Symposium on Fire Safety Science*, pp. 355-364, 1991.
- 90 Satoh, K., Llyod, J. R., et al., "A Numerical Finite-Difference Study of the Oscillatory Behaviour of Vertically Vented Compartments", *Numerical Properties and Methodologies in Heat Transfer*, Edited by T. M. Shih, Hemisphere Publishing Corporation, p 517-528, 1983.
- 91 Lakkis, I., Ghoniem, A., "Numerical Simulation of Time Dependent Phenomena in Large Fire Plumes", *International Conference on Fire Research and Engineering*, Florida, P. Lund (ed), USA, Society of Fire Protection Engineers, 1995.
- 92 Satoh, K., "Numerical Study and Experiments of Fire Whirl", *Proceedings of the Seventh International INTERFLAM '96 Conference*, pp. 393-402, 1996.
- 93 Weckman, E. J., Sobieskiak, A., "The Oscillatory Behaviour of Medium-Scale Pool Fires", *Twenty-Second International Symposium on Combustion*, The Combustion Institute, Pittsburgh, PA., pp. 1299-1310, 1988.
- 94 Kim, K. I., Ohtani, H., Uehara, Y., "Experimental Study on Oscillatory Behaviour in a Small-Scale Compartment Fire", *Fire Safety Journal*, Vol. 20, pp. 377-384, 1993.
- 95 Galea, E. R., Hoffmann, N. A., Berhane, D., "Large-Scale Fire Field Modelling - The Route to General Use via Parallel Processing", *Proceedings of the Sixth International INTERFLAM '93 Conference*, pp. 307-319, 1993.
- 96 Galea, E. R., Berhane, D., Hoffmann, N. A., "CFD Analysis of Fire Plumes From Windows with External Protrusions in High Rise Buildings", *Proceedings of the Seventh International INTERFLAM '96 Conference*, pp. 835-839, 1996.
-

-
- 97 Beck, V., He, Y., Stewart, S., Luo, M., Szmalko, E. and White, B., "Experimental Validation of the NRCC Fire Growth Model", CESARE, VUT, Internal Report No. 95/1, 1995.
- 98 Theory and Practice of Thermoelectric Thermometry, CSIRO Division of Applied Physics, Temperature Measurement Course: Book 1, pp 89-97, 1995
- 99 Jones, J. C., "On the use of Metal Sheathed Thermocouples in a Hot Gas Layer Originating from a Room Fire", *Journal of Fire Sciences*, Vol. 13, pp. 257-260, 1995.
- 100 Luo, M., He, Y., Beck, V., "Application of Field Model and Two-Zone Model to Flashover Fires in a Full-Scale Multi-Room Single Level Building", *Fire Safety Journal*, Vol 1, Part 1, pp. 1-25, 1997.
- 101 Steward, S., Experimental Building Fire Facility Manager, CESARE, Melbourne, Australia, Private communication.
- 102 Alam, T., Beever, P., "An Experimental Program Funded By FCRC", CESARE, VUT, Internal Report, 1996.
- 103 Alam, T., Project Manager of the Experimental Program Funded by the Fire Code Reform Centre, Ltd., CESARE, Melbourne, Australia, Private communication.
- 104 Beck, V., Yung, D., He, Y., Sumathipala, K., "Experimental Validation of A Fire Growth Model", *Proceedings of the Seventh Intentional INTERFLAM '96 Conference*, pp. 653-662, 1996.
- 105 "MATLAB Reference Manual", The Math Works Inc., 1992.
- 106 Tewarson, A., "Generation of Heat and Chemical Compounds in Fires", The SPFE Handbook of Fire Protection Engineering, Second Edition, National Fire Protection Association, USA, Section 3, pp. 75, 1997.
- 107 Sears, F. W, Zemansky, M. W and Yung, H. D., "University Physics", Seventh Edition, Addison-Wealey Publishing Company Inc., Appendix D, 1987.
- 108 Lilley, D. G., "Dynamics of Fire Behaviour", *30th Proceedings of the Intersociety Energy Conversion Engineering Conference*, Paper No. AP-303, ASME, pp. 485-490, 1995.
- 109 Cowles, G. S., "The Attenuation of Radiation from Building Fires through Fire-resistant Glazing", *Proceedings of the Fifth International Symposium on Fire Safety Science*, p.1357, 1997.
- 110 He, Y., "A Simple Radiation Heat Transfer Model for Prediction of Fire Growth", *Proceedings of the 6th Australasian Heat and Mass Transfer Conference*, E. Leonardi and C. V. Madhusudana (Ed), pp. 233-240, 1996.
-

-
- 111 Law, M., "Notes on the External Fire Exposure Measured at Lehrte", *Fire Safety Journal*, Vol. 4, pp. 243-246, 1981/1982.
 - 112 Lie, T. T., "Fire Temperature-Time Relations", The SPFE Handbook of Fire Protection Engineering, First Edition, Philip J. DiNenno (ed), National Fire Protection Association, USA, Section 3, pp. 81-87, 1988.
 - 113 Luo, M., "One Zone or Two Zone in the Room of Fire Origin During Fires? The Effects of the Air-Handling System", *Journal of Fire Sciences*, Vol. 15., pp. 240-260, 1997.
 - 114 Luo, M., Beck, V., "Effects of Air-Handling System on Fire Spread in a Full Scale Building", *6th Australian Heat and Mass Transfer Conference*, 9-12 December, 1996 .
 - 115 National Building Fire Safety Systems Project of the Building Regulation Review Task Force, "Microeconomic Reform: Fire Regulation - An explanatory document describing developments leading to more effective Regulations for Fire Safety", pp. 4 - 9, May 1991.
 - 116 Luo, M., "Multiple Outlet Ports", CESARE Report IR94-001, Centre for Environmental Safety and Risk Engineering, Victoria University of Technology, Melbourne, Australia, 1994.
 - 117 Luo, M., "Multiple Burning Slabs", CESARE Report IR94-002, Centre for Environmental Safety and Risk Engineering, Victoria University of Technology, Melbourne, Australia, 1994.
 - 118 Luo, M., "Heat Transfer Through Walls", CESARE Report IR94-003, Centre for Environmental Safety and Risk Engineering, Victoria University of Technology, Melbourne, Australia, 1994.
 - 119 Luo, M., "O₂ Limitation and CO, CO₂ and Unburnt Fuel Prediction", CESARE Report IR94-004, Centre for Environmental Safety and Risk Engineering, Victoria University of Technology, Melbourne, Australia, 1994.
 - 120 Luo, M., "Flame Spread Model", CESARE Report IR94-005, Centre for Environmental Safety and Risk Engineering, Victoria University of Technology, Melbourne, Australia, 1994.
 - 121 Drysdale, D. D., "Thermochemistry", The SPFE Handbook of Fire Protection Engineering, First Edition, Philip J. DiNenno (ed), National Fire Protection Association, USA, Section 1, p. 149, 1988.

APPENDICES

APPENDIX A : Calculated Spandrel Heights

The following table is a duplicate of Table 9.9, taken from Yokoi[27].

Table A1: Calculated values of the necessary spandrel height (cm)

Size of opening Horizontal (m) & Vertical (m)	Quantity of combustible in room (kg/m ²)					
	25	50	75	100	150	250
1 x 1	4 cm	4 cm	4 cm	4 cm	4 cm	4 cm
2 x 1	31	35	35	35	35	35
3 x 1	41	57	57	57	57	57
4 x 1	49	70	76	76	76	76
1 x 2	42	53	53	53	53	53
2 x 2	73	111	122	125	125	125
3 x 2	95	135	161	170	176	176
4 x 2	95	140	173	191	211	223
1 x 3	102	121	129	129	129	129
2 x 3	138	184	202	214	225	225
3 x 3	120	215	242	261	280	292
4 x 3	74	226	269	291	322	334
1 x 4	128	164	183	195	201	201
2 x 4	154	231	256	286	303	320
3 x 4	83	264	301	318	362	375
4 x 4	7	243	335	363	388	415

APPENDIX B : Experimental Building Fire Facility Plans

In Figure B1 to Figure B6, the plans are given of the Experimental Building Fire Facility (EBFF).

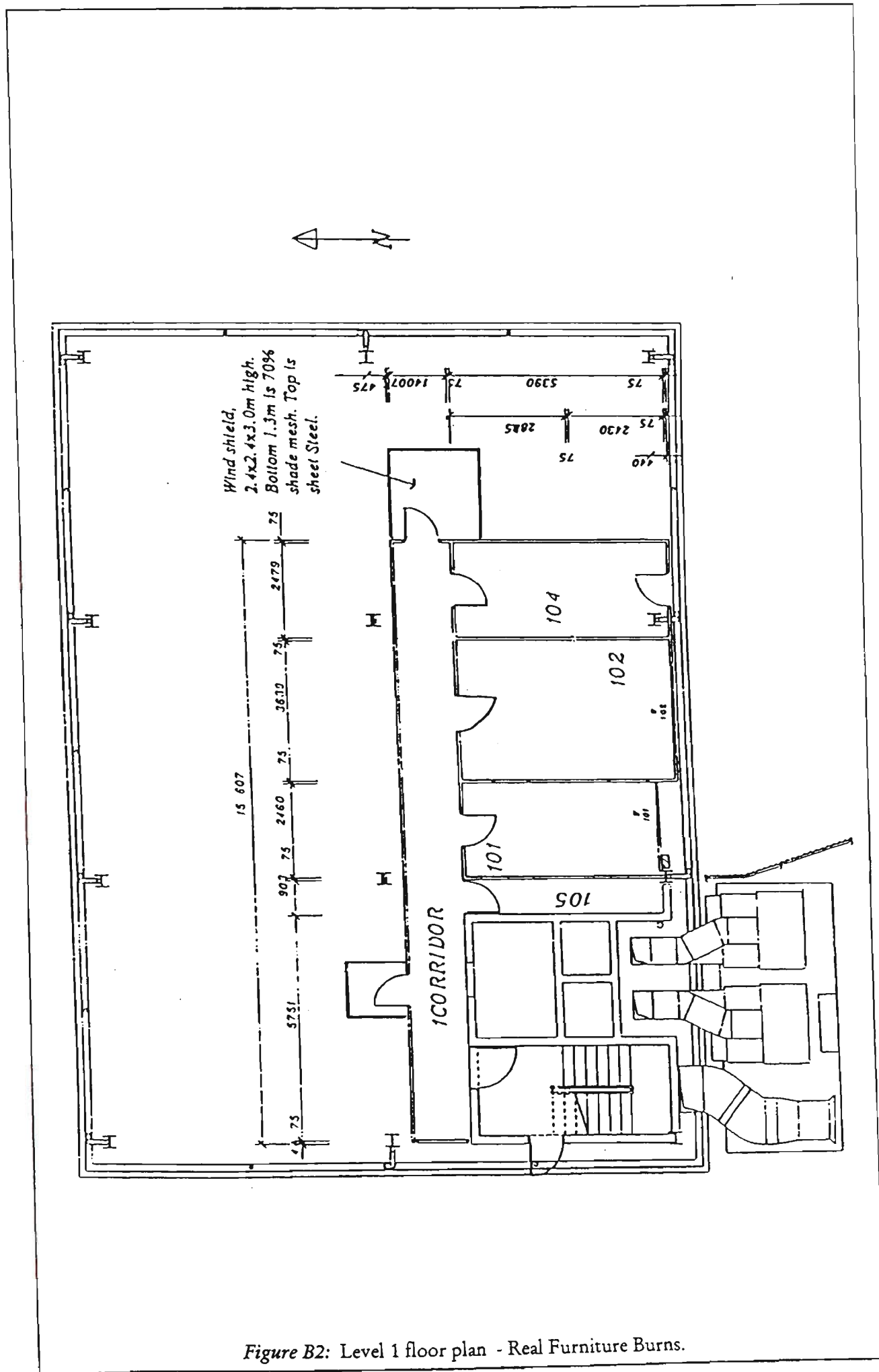


Figure B2: Level 1 floor plan - Real Furniture Burns.

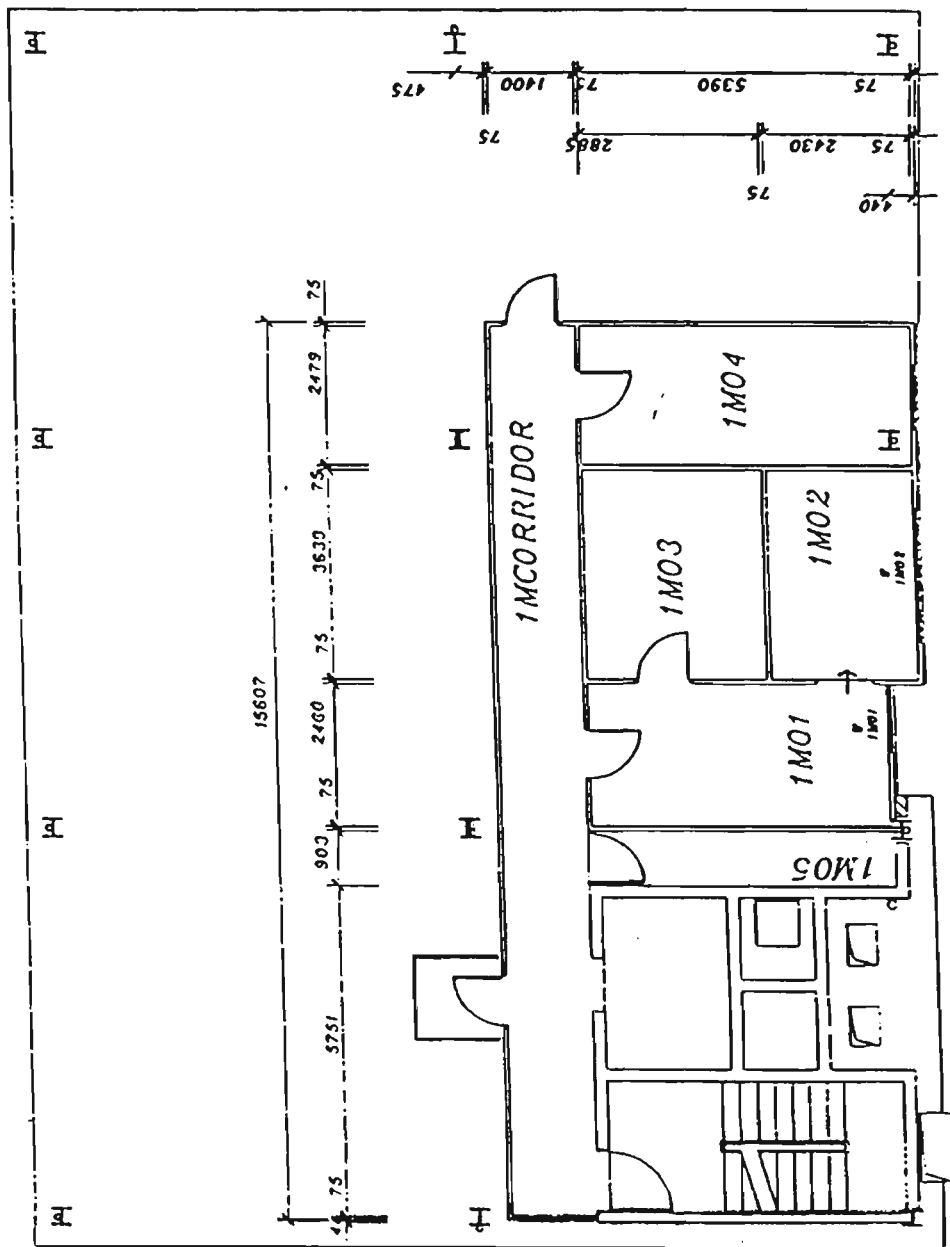


Figure B3: Level 1M floor plan.

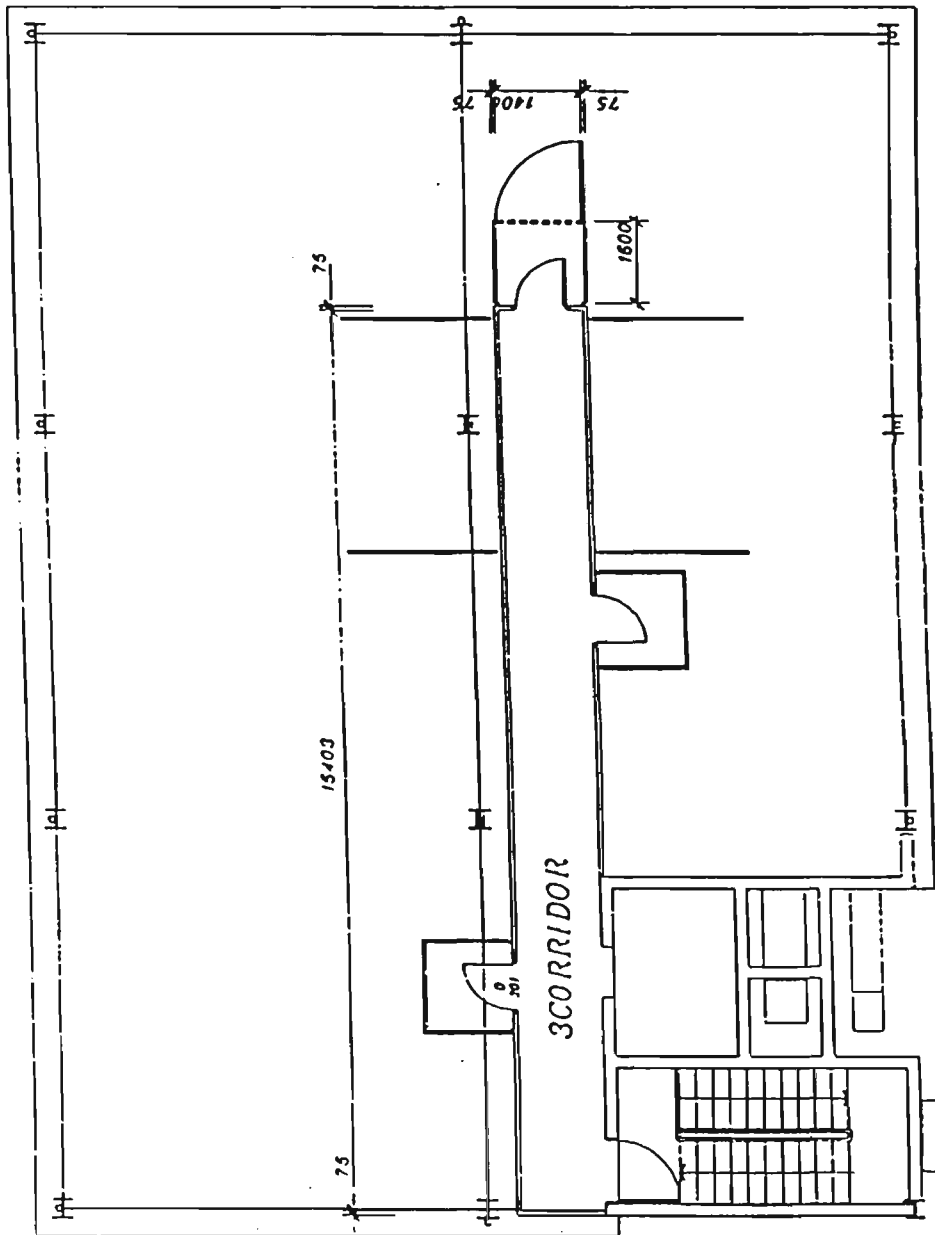
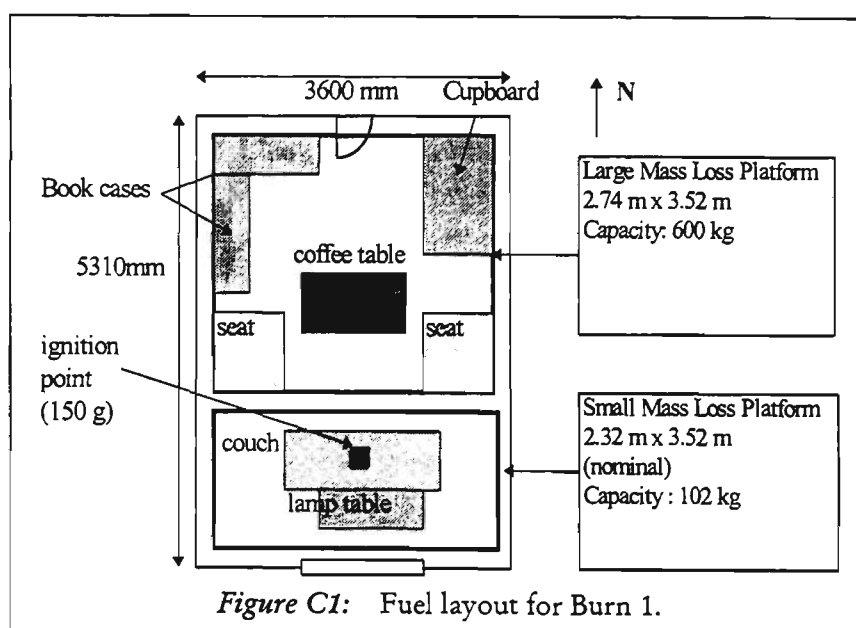


Figure B5: Level 3 floor plan.

APPENDIX C: Fuel Load and Layout for Burn 1

Table C1: Fuel Breakdown for Burn 1

	Mass (kg)	Heat of Combustion (MJ/kg)	Mass Wood Equivalent (kg)
SMALL PLATFORM			
3 Seater Couch	41.80	14.6	33.18
Lamp Table	10.60	18.4	10.60
Carpet & Underlay	18.82	53.7	54.93
<i>TOTAL</i>	<i>101.86</i>		<i>98.71</i>
LARGE PLATFORM			
Chair x 2	21.40 & 21.08	14.6 x 2	35.58
Coffee Table	21.80	18.4	21.81
Cupboard	51.54	18.4	51.54
Carpet & Underlay	36.38	53.7	115.11
Bookcase x 2	38.10 & 38.10	18.4 x 2	76.2
Books on Shelf & on Coffee Table	82.32 & 3.84	18.4	86.16
<i>TOTAL</i>	<i>396.88</i>		<i>375.45</i>
Additional Carpet & Underlay	18.2	53.7	53.11
BURN ROOM TOTAL	486.30		527.27
Equivalent Fuel load density in the burn room: 26.36 kg/m²			



APPENDIX D: MATLAB Programs

Program 1

Conversion from voltage to temperature, including cold junction correction of the data sampled using HP VEE.

Program 2

Changing CESARE's externally sampled data into MATLAB format.

Program 3

Instantaneous plot of temperature versus time for any grid location.

Program 4

Instantaneous temperature contour plots of any Plane, Level or Face of the 3-D grid.

Program 5

Non-dimensionalised and CEF averaged contour plots of any Plane, Level or Face of the 3-D grid.

Program 6

Generation and playback of Centre Plane (P3) temperature fluctuations, from ignition to decay using shaded plots.

Program 7

Calculates the coefficients of a 2D polynomial used to describe the temperature distribution across each Face of the grid.

Program 8

Allows the transfer of data generated in CESARE-CFD to be analysed in MATLAB.

Complementary functions were added to the end of this Appendix and they appear in several of the programs mentioned above. They include the ability to perform interpolation of the temperature matrix, adjusting the font size on the contour plots, and accumulative smoothing.

PROGRAM 1

```
function [temp,time] = contemp(a,b,c);

%      the HP VEE program generates three data files - volt.dat, cold.dat and sweep.dat
%      these are passed into the function contemp as variables a b and c
%      this function converts the raw voltage data, applies cold junction correction
%      and outputs a temperature (°C) matrix called TEMP
%      a corresponding TIME vector is also generated

%      ashape changes the vector 'a' (raw data) into a matrix of 112 columns
ashape=reshape(a,112,length(c));

%      re-range 'a' so that the matrix begins at LOC 29 – LOC 112
%      instead of the way the multiplexer samples the data with MUX 3 first
rearange(:,1:32)=ashape(:,17:48);
rearange(:,33:48)=ashape(:,1:16);
rearange(:,49:112)=ashape(:,49:112);
ashape=rearange;
clear rearange;

%      Converts Reference Temp (ie. cold junction readings) into a REFERENCE Voltage (milli
V)
vref = -1.853306e-2+3.89183e-2.*c+1.66451e-5.*c.^2;
vref = vref-7.87023e-8.*c.^3+2.28357e-10.*c.^4+3.57002e-13.*c.^5;
vref = vref+2.99329e-16.*c.^6-1.28498e-19.*c.^7+2.22399e-23.*c.^8;

%      conversion to micro volts
vref=vref/1000;
fprintf('\n Calculating ....')

%      This adds the reference voltage to the raw data
for k= 1:112;
    cdc(:,k)= ashape(:,k) + vref(:,1);
end

clear ashape vref;

%      here cdc has length(a) number of rows and 112 columns
%      where each column corresponds to a channel of data (ch 1 .. ch 2 .. ch 3... etc)
cdc2=reshape(cdc,length(a),1);

%      cdc2 - is now a vector where the channels are in BLOCKS
%      ie. the first block of length(a) data belongs to ch1 ... etc
%      conversion to VOLTS
cdc2=cdc2*1000000;

fprintf('\n Please wait')

%      Using the manufacture supplied equations the data is converted into temperature
temp = 2.5345e-2*cdc2 -3.439e-7*cdc2.^2;
temp = temp-1.88e-12*cdc2.^3+1.2582e-14*cdc2.^4;
temp = temp-1.4365e-18*cdc2.^5+4.695e-23*cdc2.^6;

i=find(temp > 280);

%      selects all temperatures in 'temp' that are greater than 280°C and
```

```
%      applies the second equation
fprintf('\n Almost done ...')

temp(i) = 7.45 + 2.23148e-2*cdc2(i) + 3.3631e-7*cdc2(i).^2;
temp(i) = temp(i) - 2.43219e-11*cdc2(i).^3 + 7.66105e-16*cdc2(i).^4;
temp(i) = temp(i) - 1.09973e-20*cdc2(i).^5 + 6.12544e-26*cdc2(i).^6;

%      this reshapes the variables into a 112 column matrix
t = reshape(temp,length(c),112);
temp=t;

%      THIS generates a rough time file
len=length(b);
time= ([0:1:len]/60)';
```

PROGRAM 2

```
function [stemp,stime] = scotdata(stemp,stime);

%      This function takes that 28 *.dat files sampled by CESARE
%      and changes it into matrix form - these correspond to LOC 1 – LOC 28

% this loop open MUX 4 channels corresponding to Locations 1-4
for k=17:20;
    fid=fopen(sprintf('mpx4-%d.dat',k),'rt');
    s(:,k-16)=fscanf(fid,'%f %f');
    swap = s(:,k-16);
    swap = reshape(swap,2,1762);
    stemp1(:,k-16) = swap(:,2);
    stime1(:,k-16) = swap(:,1);
clear swap;
end

%      this loop open MUX 5 channels corresponding to Locations 5-28
for j=0:23;
    fid=fopen(sprintf('mpx5-%d.dat',j),'rt');
    ss(:,j+1)=fscanf(fid,'%f %f');
    swap1 = ss(:,j+1);
    swap1 = reshape(swap1,2,1762);
    stemp2(:,j+1) = swap1(:,2);
    stime2(:,j+1) = swap1(:,1);
clear swap1;
end

%      this combines temperature data sampled by scott into STEMP & STIME
stemp(:,1:4)=stemp1(:,1:4);
stemp(:,5:28)=stemp2(:,1:24);

% stime(:,1:4)=stemp1(:,1:4);
% stime(:,5:28)=stemp2(:,1:24);

%      simple time file for all of scotts data
stime(:,1)=stime1(:,1);
stime=stime/60;
```

PROGRAM 3

```
function kwikplot(temp,time)

%      this function takes the temp and time matrix and plots
%      temperature versus time
%      in this case, for Plane 3 of Leve 1

figure(1)
plot(time,temp(:,12),'r')
hold on
plot(time,temp(:,11),'y')
plot(time,temp(:,10),'g')
plot(time,temp(:,9),'b')
legend(' Loc12 ',' Loc11 ',' Loc10 ',' Loc9 ')
set(gca,'FontSize',10);
xlabel('Time (min)')
ylabel('Temperature (°C)')
grid on
```

PROGRAM 4

```
function mapping(temp,time,stemp,stime)

%      this function plots the contour & color maps of a specific level,
%      plane or face at a specified time
%      The variable names are also simplified and a choice b/w 2 inputs or 4 is made
%      ie. temp & time with or without stemp & stime

if nargin == 2
fprintf('The following will plot a PLANE, LEVEL OR FACE at a particular time');
t=input('Please enter the time eg 5 min .... ');
    k1=find(time > (t-0.01) & time < (t+0.01));
    myt=k1(1,1);
    T=temp;
    S=temp;
    M=myt;
    N=myt;
    c=0;
end

if nargin == 4
fprintf('The following will plot a PLANE, LEVEL or FACE at a particular time');
t=input('Please enter the time eg 5 min .... ');
    k1=find(time > (t-0.01) & time < (t+0.01));
    myt=k1(1,1);
    k2=find(stime > (t-0.01) & stime < (t+0.01));
    sst=k2(1,1);
    T=temp;
    S=stemp;
    M=myt;
    N=sst;
    c=28;
end

%      This specifies the burn type as to whether there are 5 or 7 levels
%      the default value is set to zero indicating seven (7) levels
btype = 0;

%      This determines the size of the temperature matrix at fills the matrix
%      with zeros until the number of columns equals 140. This enables the
%      m file to plot data when the upper two levels are not sampled.
%      The check for 112 columns is necessary for Burn1 which has 4 input arguments
%      but also has all levels sampled. This corrects the assumption that is
%      necessary for Burns 4 & 5 where only Five (5) LEVELS are sampled: changing btype to 1.

[rr,cc] = size(T);
if cc == 112
    btype = 0;
    else if cc < 140
        btype = 1;
        T(rr,140) = 0;
    end
end
end
```

```

% % % % % % % % % % % % % % % % % % % % % % % % % % % % % %
choice=input('Please specify the 1=plane, 2=level and 3=face: ');
if choice == 1
    ans1=input('Please specify the plane number (1 - 5)');
    else if choice == 2
        if btype == 0
            ans1=input('Please specify the level number (1 - 7)');
            end
            if btype == 1
                fprintf('\n\nThe data from this burn reaches up to LEVEL 5 only. ');
                ans1=input('Please specify the level number (1 - 5)');
            end
        else if choice == 3
            ans1=input('Please specify the face number (1 - 4)');
        end
    end
end

%%%%%%%%%%%%%%
% PLANE specificaions: 1 - 5 %
%%%%%%%%%%%%%%
if choice == 1
if ans1 == 1
    P=[T(M,140-c) T(M,139-c) T(M,138-c) T(M,137-c);
        T(M,120-c) T(M,119-c) T(M,118-c) T(M,117-c);
        T(M,100-c) T(M,99-c) T(M,98-c) T(M,97-c);
        T(M,80-c) T(M,79-c) T(M,78-c) T(M,77-c);
        T(M,60-c) T(M,59-c) T(M,58-c) T(M,57-c);
        S(N,21) S(N,22) S(N,23) S(N,24);
        S(N,20) S(N,19) S(N,18) S(N,17)];
end
if ans1 == 2
    P=[T(M,136-c) T(M,135-c) T(M,134-c) T(M,133-c);
        T(M,116-c) T(M,115-c) T(M,114-c) T(M,113-c);
        T(M,96-c) T(M,95-c) T(M,94-c) T(M,93-c);
        T(M,76-c) T(M,75-c) T(M,74-c) T(M,73-c);
        T(M,56-c) T(M,55-c) T(M,54-c) T(M,53-c);
        S(N,25) S(N,26) S(N,27) S(N,28);
        S(N,16) S(N,15) S(N,14) S(N,13)];
end
if ans1 == 3
    P=[T(M,132-c) T(M,131-c) T(M,130-c) T(M,129-c);
        T(M,112-c) T(M,111-c) T(M,110-c) T(M,109-c);
        T(M,92-c) T(M,91-c) T(M,90-c) T(M,89-c);
        T(M,72-c) T(M,71-c) T(M,70-c) T(M,69-c);
        T(M,52-c) T(M,51-c) T(M,50-c) T(M,49-c);
        T(M,29-c) T(M,30-c) T(M,31-c) T(M,32-c);
        S(N,12) S(N,11) S(N,10) S(N,9)];
end
if ans1 == 4
    P=[T(M,128-c) T(M,127-c) T(M,126-c) T(M,125-c);
        T(M,108-c) T(M,107-c) T(M,106-c) T(M,105-c);
        T(M,88-c) T(M,87-c) T(M,86-c) T(M,85-c);
        T(M,68-c) T(M,67-c) T(M,66-c) T(M,65-c);
        T(M,48-c) T(M,47-c) T(M,46-c) T(M,45-c);
        T(M,33-c) T(M,34-c) T(M,35-c) T(M,36-c);
        S(N,8) S(N,7) S(N,6) S(N,5)];
end

```

```

if ans1 == 5
    P=[T(M,124-c) T(M,123-c) T(M,122-c) T(M,121-c);
        T(M,104-c) T(M,103-c) T(M,102-c) T(M,101-c);
        T(M,84-c) T(M,83-c) T(M,82-c) T(M,81-c);
        T(M,64-c) T(M,63-c) T(M,62-c) T(M,61-c);
        T(M,44-c) T(M,43-c) T(M,42-c) T(M,41-c);
        T(M,37-c) T(M,38-c) T(M,39-c) T(M,40-c);
        S(N,4) S(N,3) S(N,2) S(N,1)];
end

% This removes all the zero's padded into the matrix
[pi,pj] = find(P == 0);
if length(pi) > 5
    P(1:2,:) = [];
end
P

% DIMENSIONS
y=[3.9 3.34 2.78 2.03 1.21 .59 0.15];
z=[0 0.5 1 1.5];
if btype == 1
    y = [2.78 2.03 1.21 .59 0.15];
end

% SPLINE INTERPOLATION
[Pnew,znew,ynew]=sinterp(P,z,fliplr(y));
ynew = fliplr(ynew);

% CONTOUR MAP
figure(2)
call = contour(znew,ynew,Pnew);
% call = contour(z,y,P);
clabel(call)
smallfont;
axis('image')
set(gca,'FontSize',10);
% title(sprintf('Temperature distribution along Plane %2d at %2d (min)',ans1,t));
xlabel('Distance away from the external wall (m)')
ylabel('Distance above the top of the opening (m)')
end
%%%%%%%%%%%%%%%%%%%%%%%%%%%%%%%%%%%%%%%%%%%%%%%%%%%%%%%%%%%%%%%%%%%%%%%%
% LEVEL specifications: 1 - 7
%%%%%%%%%%%%%%%%%%%%%%%%%%%%%%%%%%%%%%%%%%%%%%%%%%%%%%%%%%%%%%%%%%%%%%%%
if choice == 2
    if ans1 == 1
        L=[S(N,20) S(N,16) S(N,12) S(N,8) S(N,4);
            S(N,19) S(N,15) S(N,11) S(N,7) S(N,3);
            S(N,18) S(N,14) S(N,10) S(N,6) S(N,2);
            S(N,17) S(N,13) S(N,9) S(N,5) S(N,1)];
    end

    if ans1 == 2
        L=[S(N,21) S(N,25) T(M,29-c) T(M,33-c) T(M,37-c);
            S(N,22) S(N,26) T(M,30-c) T(M,34-c) T(M,38-c);
            S(N,23) S(N,27) T(M,31-c) T(M,35-c) T(M,39-c);
            S(N,24) S(N,28) T(M,32-c) T(M,36-c) T(M,40-c)];
    end
end

```

```

if ans1 == 3
L=[T(M,60-c) T(M,56-c) T(M,52-c) T(M,48-c) T(M,44-c);
  T(M,59-c) T(M,55-c) T(M,51-c) T(M,47-c) T(M,43-c);
  T(M,58-c) T(M,54-c) T(M,50-c) T(M,46-c) T(M,42-c);
  T(M,57-c) T(M,53-c) T(M,49-c) T(M,45-c) T(M,41-c)];
end

if ans1 == 4
L=[T(M,80-c) T(M,76-c) T(M,72-c) T(M,68-c) T(M,64-c);
  T(M,79-c) T(M,75-c) T(M,71-c) T(M,67-c) T(M,63-c);
  T(M,78-c) T(M,74-c) T(M,70-c) T(M,66-c) T(M,62-c);
  T(M,77-c) T(M,73-c) T(M,69-c) T(M,65-c) T(M,61-c)];
end

if ans1 == 5
L=[T(M,100-c) T(M,96-c) T(M,92-c) T(M,88-c) T(M,84-c);
  T(M,99-c) T(M,95-c) T(M,91-c) T(M,87-c) T(M,83-c);
  T(M,98-c) T(M,94-c) T(M,90-c) T(M,86-c) T(M,82-c);
  T(M,97-c) T(M,93-c) T(M,89-c) T(M,85-c) T(M,81-c)];
end

if ans1 == 6
  L=[T(M,120-c) T(M,116-c) T(M,112-c) T(M,108-c) T(M,104-c);
    T(M,119-c) T(M,115-c) T(M,111-c) T(M,107-c) T(M,103-c);
    T(M,118-c) T(M,114-c) T(M,110-c) T(M,106-c) T(M,102-c);
    T(M,117-c) T(M,113-c) T(M,109-c) T(M,105-c) T(M,101-c)];
end

if ans1 == 7
L=[T(M,140-c) T(M,136-c) T(M,132-c) T(M,128-c) T(M,124-c);
  T(M,139-c) T(M,135-c) T(M,131-c) T(M,127-c) T(M,123-c);
  T(M,138-c) T(M,134-c) T(M,130-c) T(M,126-c) T(M,122-c);
  T(M,137-c) T(M,133-c) T(M,129-c) T(M,125-c) T(M,121-c)];
end
L

% DIMENSIONS
  x=[0 0.6 1.2 1.8 2.4];
  z=[0 0.5 1 1.5];

% SPLIN INTERPOLATION
  [Lnew,xnew,znew]=sinterp(L,x,z);

% CONTOUR PLOT
  figure(4)
  call = contour(xnew,znew,Lnew);
%   call = contour(x,z,L);
  clabel(call);
  smalfont;
  set(gca,'FontSize',10);
  title(sprintf('Temperature distribution along Level %2d at %2d (min)',ans1,t));
  ylabel('Distance away from the external Wall (m)')
  xlabel('Distance across window opening (m)')
end

%%%%%%%%%%
% FACE specifications: 1 - 4      %
%%%%%%%%%%

```

```

if choice == 3
    if ans1 == 1
        F=[T(M,140-c) T(M,136-c) T(M,132-c) T(M,128-c) T(M,124-c);
          T(M,120-c) T(M,116-c) T(M,112-c) T(M,108-c) T(M,104-c);
          T(M,100-c) T(M,96-c) T(M,92-c) T(M,88-c) T(M,84-c);
          T(M,80-c) T(M,76-c) T(M,72-c) T(M,68-c) T(M,64-c);
          T(M,60-c) T(M,56-c) T(M,52-c) T(M,48-c) T(M,44-c);
          S(N,21) S(N,25) T(M,29-c) T(M,33-c) T(M,37-c);
          S(N,20) S(N,16) S(N,12) S(N,8) S(N,4)];
    end
    if ans1 == 2
        F=[T(M,139-c) T(M,135-c) T(M,131-c) T(M,127-c) T(M,123-c);
          T(M,119-c) T(M,115-c) T(M,111-c) T(M,107-c) T(M,103-c);
          T(M,99-c) T(M,95-c) T(M,91-c) T(M,87-c) T(M,83-c);
          T(M,79-c) T(M,75-c) T(M,71-c) T(M,67-c) T(M,63-c);
          T(M,59-c) T(M,55-c) T(M,51-c) T(M,47-c) T(M,43-c);
          S(N,22) S(N,26) T(M,30-c) T(M,34-c) T(M,38-c);
          S(N,19) S(N,15) S(N,11) S(N,7) S(N,3)];
    end
    if ans1 == 3
        F=[T(M,138-c) T(M,134-c) T(M,130-c) T(M,126-c) T(M,122-c);
          T(M,118-c) T(M,114-c) T(M,110-c) T(M,106-c) T(M,102-c);
          T(M,98-c) T(M,94-c) T(M,90-c) T(M,86-c) T(M,82-c);
          T(M,78-c) T(M,74-c) T(M,70-c) T(M,66-c) T(M,62-c);
          T(M,58-c) T(M,54-c) T(M,50-c) T(M,46-c) T(M,42-c);
          S(N,23) S(N,27) T(M,31-c) T(M,35-c) T(M,39-c);
          S(N,18) S(N,14) S(N,10) S(N,6) S(N,2)];
    end
    if ans1 == 4
        F=[T(M,137-c) T(M,133-c) T(M,129-c) T(M,125-c) T(M,121-c);
          T(M,117-c) T(M,113-c) T(M,109-c) T(M,105-c) T(M,101-c);
          T(M,97-c) T(M,93-c) T(M,89-c) T(M,85-c) T(M,81-c);
          T(M,77-c) T(M,73-c) T(M,69-c) T(M,65-c) T(M,61-c);
          T(M,57-c) T(M,53-c) T(M,49-c) T(M,45-c) T(M,41-c);
          S(N,24) S(N,28) T(M,32-c) T(M,36-c) T(M,40-c);
          S(N,17) S(N,13) S(N,9) S(N,5) S(N,1)];
    end

```

```

% This removes all the zero's padded into the matrix

```

```

[pi,pj] = find(F == 0);

```

```

if length(pi > 5)

```

```

    F(1:2,:) = [];

```

```

end

```

```

F

```

```

% DIMENSIONS

```

```

x=[0 0.6 1.2 1.8 2.4];

```

```

y=[3.9 3.34 2.78 2.03 1.21 .59 0];

```

```

if btype == 1

```

```

    y = [2.78 2.03 1.21 .59 0];

```

```

end

```

```

% SPLINE INTERPOLATION

```

```

[Fnew,xnew,ynew]=sinterp(F,x,flipr(y));

```

```

ynew = flipr(ynew);

```

```

% CONTOUR MAP

```

```
figure(6)
call = contour(xnew,ynew,Fnew);
% call = contour(x,y,F);
clabel(call);
smalfont;
axis('image')
set(gca,'FontSize',10);
title(sprintf('Temperature distribution along Face%2d at %2d (min)',ans1,t));
xlabel('Distance across window opening (m)')
ylabel('Distance away from the external wall (m)')

end
```

PROGRAM 5

```
function cef(temp,time,stemp,stime);

%      this function has been shortned to plot the temperature contours of Level 4, Plane 3 and
%      Face 1 up to Level 5 only, over the Consistent External Flamming Period (CEF)
%      all data is non-dimensionalised against average ambient temperature
%      and maximum temp over the CEF.

if nargin == 2
fprintf('The following plots a temperaure contours over the CEF period');
select=input('Please enter burn number 2,3,4,7 or 8: ');
    if select == 2
        ts = 11.25; tamb = 12.1; tf = ts + 5;
    end
    if select == 3
        ts = 19; tamb = 12.7; tf = ts + 7;
    end
    if select == 4
        ts = 15.45; tamb = 11; tf = ts + 6;
    end
    if select == 7
        ts = 9.55; tamb = 7.7; tf = ts + 6;
    end
    if select == 8
        ts = 8.3; tamb = 8; tf = ts + 7;
    end
    k1 = find(time > (ts-0.01) & time < (ts+0.01));
    k2 = find(time > (tf-0.01) & time < (tf+0.01));
    k1 = k1(1,1);
    k2 = k2(1,1);
    newtemp = sum(temp(k1:k2,:))/(k2-k1);
    tmax = max(newtemp);
    T = (newtemp-tamb)/(tmax-tamb);
    S = T;
    c = 0;
    M = 1;
    N = 1;
end

if nargin == 4
fprintf('The following plots a temperaure contours over the CEF period');
select=input('Please enter burn number 1 or 5: ');
    if select == 1
        ts = 18.4; tf = ts + 8; tamb = 16.7;
    end
    if select == 5
        ts = 11.35; tf = ts + 6; tamb = 8.3;
    end
    k1 = find(time > (ts-0.1) & time < (ts+0.1)); k1 = k1(1,1);
    k2 = find(time > (tf-0.1) & time < (tf+0.1)); k2 = k2(1,1);
    sk1 = find(stime > (ts-0.01) & stime < (ts+0.01)); sk1 = sk1(1,1);
    sk2 = find(stime > (tf-0.01) & stime < (tf+0.01)); sk2 = sk2(1,1);
    newtemp = sum(temp(k1:k2,:))/(k2-k1);
    T = newtemp;
    tmax = max(newtemp);
    newstemp = sum(stemp(sk1:sk2,:))/(sk2-sk1);
```

```

    S = newstemp;
    tmaxx = max(newstemp);
    T = (newtemp-tamb)/(tmax-tamb);
    S = (newstemp-tamb)/(tmaxx-tamb);
    c = 28;
    M = 1;
    N = 1;
end

%%%%%%%%%%
choice = input('Please specify the 1 = plane, 2 = level and 3 = face1: ');

if choice == 1
    P = [T(M,92-c) T(M,91-c) T(M,90-c) T(M,89-c);
        T(M,72-c) T(M,71-c) T(M,70-c) T(M,69-c);
        T(M,52-c) T(M,51-c) T(M,50-c) T(M,49-c);
        T(M,29-c) T(M,30-c) T(M,31-c) T(M,32-c);
        S(N,12) S(N,11) S(N,10) S(N,9)];
end

% DIMENSIONS
z = [0 0.5 1 1.5];
y = [2.78 2.03 1.21 .59 0];

% SPLINE INTERPOLATION
[Pnew,znew,ynew] = sinterp(P,z,fliplr(y));
ynew = fliplr(ynew);
figure(2)

% CONTOUR MAP
call = contour(znew,ynew,Pnew);
% call = contour(z,y,P);
clabel(call)
smalfont;
axis('image')
set(gca,'FontSize',10);
title(sprintf('BURN %d - Plane 3',select));
xlabel('Distance away from the external wall (m)')
ylabel('Distance above the top of the opening (m)')
end
%%%%%%%%%%
if choice == 2
    L = [T(M,80-c) T(M,76-c) T(M,72-c) T(M,68-c) T(M,64-c);
        T(M,79-c) T(M,75-c) T(M,71-c) T(M,67-c) T(M,63-c);
        T(M,78-c) T(M,74-c) T(M,70-c) T(M,66-c) T(M,62-c);
        T(M,77-c) T(M,73-c) T(M,69-c) T(M,65-c) T(M,61-c)];
end

% DIMENSIONS
x = [0 0.6 1.2 1.8 2.4];
z = [0 0.5 1 1.5];

% SPLIN INTERPOLATION
[Lnew,xnew,znew] = sinterp(L,x,z);

% CONTOUR PLOT
figure(4)

```

```

    call = contour(xnew,znew,Lnew);
%   call = contour(x,z,L);
    clabel(call);
    smalfont;
    axis('image')
    set(gca,'FontSize',10);
    title(sprintf('BURN %d - Level 4',select));
    ylabel('Distance away from the external Wall (m)')
    xlabel('Distance across window opening (m)')
end
%%%%%%%%%%%%%%%%%%%%%%%%%%%%%%%%%%%%%%%%%%%%%%%%%%%%%%%%%%%%%%%%%%%%%%%%%%
if choice == 3
    F=[T(M,100-c) T(M,96-c) T(M,92-c) T(M,88-c) T(M,84-c);
      T(M,80-c) T(M,76-c) T(M,72-c) T(M,68-c) T(M,64-c);
      T(M,60-c) T(M,56-c) T(M,52-c) T(M,48-c) T(M,44-c);
      S(N,21) S(N,25) T(M,29-c) T(M,33-c) T(M,37-c);
      S(N,20) S(N,16) S(N,12) S(N,8) S(N,4)];

% DIMENSIONS
    x=[0 0.6 1.2 1.8 2.4];
    y = [2.78 2.03 1.21 .59 0];

% SPLINE INTERPOLATION
    [Fnew,xnew,ynew]=sinterp(F,x,fliplr(y));
    ynew = fliplr(ynew);

% CONTOUR MAP
    figure(6)
    mesh(xnew,ynew,Fnew);
    call = contour(xnew,ynew,Fnew);
%   call = contour(x,y,F);
    clabel(call);
    smalfont;
    axis('image')
    set(gca,'FontSize',10);
    title(sprintf('BURN %d - Face 1',select));
    xlabel('Distance across window opening (m)')
    ylabel('Distance above the top of the opening (m)')
end

```

PROGRAM 6

```
function mv = playme(temp,time,stemp,stime)

% this function generates the colour map of Plane 3 over a series of time intervals
% these can then be played back using the movie command to watch the fluctuating
% temperature contours
% for my sampling (myt) and scotts (sst)

% The variable names are also simplified and a choice b/w 2 inputs or 4
% is made. ie... temp & time with or without stemp & stime

if nargin == 2
fprintf('The following will plot a plane, level or face at a particular time');
st=input('Please enter the start time eg 5 min .... ');
    k1=find(time > (st-0.01) & time < (st+0.01));
    st=k1(1,1);
ft=input('Please enter the finish time eg 15 min .... ');
    k1=find(time > (ft-0.01) & time < (ft+0.01));
    ft=k1(1,1);

T=temp;
S=temp;
M=st;
N=st;
c=0;
end

if nargin == 4
fprintf('The following will plot a PLANE, LEVEL or FACE at a particular time');
t=input('Please enter the time eg 5 min .... ');
    k1=find(time > (t-0.05) & time < (t+0.05));
    myt=k1(1,1);
    k2=find(stime > (t-0.01) & stime < (t+0.01));
    sst=k2(1,1);
T=temp;
S=stemp;
M=myt;
N=sst;
c=28;
end

% This specifies the burn type as to whether there are 5 or 7 levels
% the default value is set to zero indicating seven (7) levels
btype = 0;

[rr,cc] = size(T);
if cc == 112
    btype = 0;
    else if cc < 140
        btype = 1;
        T(rr,140) = 0;
    end
end
end
```

```

% DIMENSIONS
y=[3.9 3.34 2.78 2.03 1.21 .59 0];
z=[0 0.5 1 1.5];
if btype == 1
    y = [2.78 2.03 1.21 .59 0];
end

% specify time step
for M=st:30:ft

M
    P3=[T(M,132-c) T(M,131-c) T(M,130-c) T(M,129-c);
        T(M,112-c) T(M,111-c) T(M,110-c) T(M,109-c);
        T(M,92-c) T(M,91-c) T(M,90-c) T(M,89-c);
        T(M,72-c) T(M,71-c) T(M,70-c) T(M,69-c);
        T(M,52-c) T(M,51-c) T(M,50-c) T(M,69-c);
        T(M,29-c) T(M,30-c) T(M,31-c) T(M,32-c);
        S(N,12) S(N,11) S(N,10) S(N,9)];

% SPLINE INTERPOLATION
[Pnew,znew,ynew]=sinterp(P3,z,fliplr(y));
ynew=fliplr(ynew);

pcolor(znew,ynew,Pnew);
set(gcf,'position',get(0,'screensize'));
shading interp;
colormap hot;
v = [0 1000];
caxis(v);
axis('image')
colorbar
h = (gcf);
mv=[mv getframe(h)];
end

clf
figure
pause
colormap hot
movie(gcf,mv,10,5)

```

PROGRAM 7

% this takes the splined data generated for the mesh plot of a face and generates a
% set of x and y vectors for plotting, based on the 51 x 51 sized temperature matrix..

```
xs = ones(51,51);  
x=linspace(0,2.4,51);  
for i = 1:51  
xs(i,:) = x;  
end
```

```
ys = ones(51,51);  
y=linspace(2.78,0,51)';  
for i = 1:51  
ys(:,i) = y;  
end
```

% P is the 51 x 51 temperature matrix, which in the following line is taken from
% Burn 8, Face 1, for a 4th power x and y polynomial. The coefficients of which are
% placed in zfit

```
P = polyfit2d(xs,ys,b8f1,4,4);  
zfit=polyval2d(P,xs,ys);
```

```
figure(1)  
mesh(xs,ys,(zfit))  
set(gca,'FontSize',10);  
set(gcf,'position',get(0,'screensize'));  
xlabel(' Distance across window opening (m)')  
ylabel(' Distance above the top of the opening (m)')  
zlabel('(T-Tamb)/(Tmax-Tamb)')
```

% polyfit2.m and polyval2d.m were written by Perry W. Stout and
% are based on the Matlab function polyfit.

PROGRAM 8

% the following loads the temperature portion of the numerically predicted data
% and reshapes it into a single column. Then x, y and z vectors are generated to plotting
% plotting and for selection of the relevant portions of the data.

% Low fuel load - Coarse Grid - RUN1

```
clear
load t1b.dat
new = reshape(t1b',5220*3,1);
```

```
clear x y z
```

```
i=1:20;
for loop=1: 29*27
x=[x;i'];
end
```

```
for loop = 1:27;
k=ones(20*29,1)*loop;
z=[z;k];
end
```

```
j = 0;
for loop = 1:27*29;
j = j+1;
y = [y;ones(20,1)*j];
if j == 29;
    j = 0;
end;
end;
```

```
nogo = find(y>=16);
x(nogo) = [];
y(nogo) = [];
z(nogo) = [];
new(nogo) = [];
```

```
% eliminate sections of the results that
% correspond to the inside of the room and
% the sides of the 'grid'
nogo = find(z==1);
x(nogo) = [];
y(nogo) = [];
z(nogo) = [];
new(nogo) = [];
```

```
nogo = find(z==27);
x(nogo) = [];
y(nogo) = [];
z(nogo) = [];
new(nogo) = [];
```

```
nogo = find(x==1);
x(nogo) = [];
y(nogo) = [];
z(nogo) = [];
new(nogo) = [];
```

```
nogo = find(x==20);
x(nogo) = [];
y(nogo) = [];
z(nogo) = [];
new(nogo) = [];
```

```
nogo = find(y==1);
x(nogo) = [];
y(nogo) = [];
z(nogo) = [];
new(nogo) = [];
```

```
nogo = find(z<=10);
x(nogo) = [];
y(nogo) = [];
z(nogo) = [];
new(nogo) = [];
```

```
nogo = find(y<=7);
x(nogo) = [];
y(nogo) = [];
z(nogo) = [];
new(nogo) = [];
```

```
nogo = find(x<=3);
x(nogo) = [];
y(nogo) = [];
z(nogo) = [];
new(nogo) = [];
```

```
nogo = find(x>=17);
x(nogo) = [];
y(nogo) = [];
z(nogo) = [];
new(nogo) = [];
```

```
xx=[0:0.2:2.4];
yy=[0:0.2:1.5];
zz=[0:0.2:3];
```

```
% plots the equivant to Plane 3
figure(1)
planeindex = find(x==9);
region = new(planeindex);
nondim = (region - 20.)/(max(new)-20.);
call = contour(yy,zz,flipr(reshape(nondim,8,16)),'k');
clabel(call)
view(0,90)
smalfont;
axis('image')
set(gca,'FontSize',10);
```

```
xlabel('Distance away from the external wall (m)')
ylabel('Distance above the top of the opening (m)')
```

```
% plots the equivalent to Level 4
figure(2)
levelindex = find(z==18);
region = new(levelindex);
nondim = (region - 20.)/(max(new)-20.);
call = contour(xx,yy,flipud(reshape(nondim,13,8)),'k');
clabel(call)
view(0,90)
smallfont;
axis('image')
set(gca,'FontSize',10);
xlabel('Distance across window opening (m)')
ylabel('Distance away from the external wall (m)')
```

```
% plots the equivalent of Face 1
figure(3)
faceindex = find(y==14);
region = new(faceindex);
nondim = (region - 20.)/(max(new)-20.);
call = contour(xx,zz,(reshape(nondim,13,16)),'k');
clabel(call)
view(0,90)
smallfont;
axis('image')
set(gca,'FontSize',10);
xlabel('Distance across window opening (m)')
ylabel('Distance above window opening (m)')
```

APPENDIX E: Method of Babrauskas Estimating Compartment Temperature

The 'Method of Babrauskas'[36] can also be used to estimate temperatures in compartment fires using:

$$T_g = T_{amb} + (T^* - T_{amb}) \theta_1 \theta_2 \theta_3 \theta_4 \theta_5 \quad \text{Equation 5.2}$$

where T_g is the upper gas temperature, T_{amb} is the ambient air temperature (293 K) and T^* is an empirical constant (1725 K).

Burning Rate Stoichiometry: θ_1

$$\theta_1 = 1.0 + 0.51 \ln \phi \quad \text{for } \phi < 1$$

$$\theta_1 = 1.0 - 0.05 (\ln \phi)^{5/3} \quad \text{for } \phi > 1$$

$$\phi = \dot{Q} / (1500 A_w \sqrt{h})$$

where \dot{Q} = energy (heat) release rate (kW).

A_w is the area of the opening (m^2).

h is the height of the opening in meters.

Wall Steady-State Losses: θ_2

$$\theta_2 = 1.0 - 0.94 \exp [-54 (A_w \sqrt{h} / A_T)^{2/3} (L / k)^{1/3}]$$

where L is the wall thickness (m).

A_T is the total area of the compartment (m^2).

k is the thermal conductivity of the wall (kW/m K).

Wall Transient Losses: θ_3

$$\theta_3 = 1.0 - 0.92 \exp [-150 (A_w \sqrt{h} / A_T)^{0.6} (t / k \rho c_p)^{0.4}]$$

$$t = 2.92 \times 10^{-6} (k \rho c_p) (A_w \sqrt{h} / A_T)^{1.5}$$

where ρ is the density (kg/m^3).

c_p is the specific heat of the wall (kJ/kg K).

Opening Height Factor: θ_4

$$\theta_4 = 1.0 - 0.205h^{-0.3}$$

where h is the height of the opening (m).

Combustion Efficiency: θ_5

$$\theta_5 = 1.0 + 0.5 \ln b_p$$

where b_p is the maximum combustion efficiency which ranges from 0.5 to 0.9.

Each of the θ factors were determined using the following:

T_{amb} = ambient temperature (20°C)

A_w = opening area (3.6m²)

h = opening height (1.5m)

A_T = total surface area of the burn room, including window area (81m²)

k = thermal conductivity of gypsum wall (0.48 x 10⁻³ kW/m.c)

L = wall thickness (0.016m)

ρ = density of the gypsum wall (1440 kg/m³)

c_p = specific heat of the wall (0.84 kJ/kg K)

b_p = combustion efficiency (assume 0.8)

APPENDIX F: Co-efficients for each Face for Burns 2, 4 and 8

Table F1: Co-efficients for Faces 2, 3 and 4 of Burn 2.

BURN 2					
Face 2	0.0349	-0.0919	0.3193	-1.0484	0.5591
	0.1010	0.0946	-3.0336	6.6241	-3.0526
	-0.0221	-1.1530	7.2400	-12.5049	4.9361
	-0.0739	1.1077	-4.5732	6.4950	-2.1801
	0.0681	-0.3907	0.6583	-0.4518	0.6109
Face 3	-0.1523	0.9114	-1.6793	0.8982	-0.0060
	0.6995	-4.1634	7.6025	-4.0353	0.1507
	-0.9143	5.3847	-9.6970	5.2415	-0.7168
	0.2573	-1.4826	2.6673	-1.7778	0.7434
	-0.0012	0.0828	-0.4031	0.3582	0.5237
Face 4	-0.0543	0.3792	-0.8691	0.6789	-0.0797
	0.2429	-1.7176	3.9867	-3.1948	0.4847
	-0.2587	1.9265	-4.7168	4.1263	-0.9775
	-0.0527	0.1472	0.2280	-0.8412	0.5105
	0.0260	-0.0688	-0.1221	0.2108	0.3726

Table F2: Co-efficients for Faces 2, 3 and 4 of Burn 4.

BURN 4					
Face 2	-0.0663	0.3434	-0.5396	0.3264	-0.1588
	0.4223	-2.2528	3.6079	-1.8906	0.6537
	-0.7549	4.0993	-6.6323	3.2189	-1.0330
	0.3338	-1.7780	2.7283	-1.1813	0.6999
	0.0468	-0.2874	0.5508	-0.4864	0.8189
Face 3	-0.0726	0.4394	-0.7958	0.3609	0.0370
	0.3488	-2.1100	3.7988	-1.6676	-0.1522
	-0.4147	2.4531	-4.1676	1.4383	0.0467
	0.0093	0.0527	-0.5413	0.8751	0.1646
	-0.1609	1.0961	-2.5040	1.9366	0.2765
Face 4	-0.0057	0.0668	-0.2282	0.2375	-0.0050
	0.0760	-0.6114	1.6449	-1.4553	0.0205
	-0.0703	0.5274	-1.3803	1.2439	-0.0821
	-0.2207	1.5582	-3.5363	2.4960	0.1245
	-0.1577	1.0121	-2.1427	1.5613	0.0326

Table F3: Co-efficients for Faces 2, 3 and 4 of Burn 8.

BURN 8					
Face 2	0.0823	-0.4171	-0.6310	0.3339	-0.1394
	0.3928	-1.9139	2.5681	-0.8573	0.4724
	-0.5863	2.6919	-2.9003	-0.1060	-0.7020
	0.2613	-1.0686	0.6233	0.7657	0.6731
	0.0292	-0.1803	0.3245	-0.2523	0.6814
Face 3	-0.1167	0.7490	-1.5229	0.9190	0.0511
	0.5614	-3.6133	7.3310	-4.3476	-0.2241
	-0.7556	4.8435	-9.6680	5.4578	0.1087
	0.2162	-1.3337	2.4309	-1.0938	0.1985
	-0.1303	0.8674	-1.9349	1.4522	0.3637
Face 4	-0.1375	0.8724	-1.7917	1.1571	0.0681
	0.7089	-4.4231	8.9067	-5.6500	-0.2356
	-1.0804	6.4845	-12.4288	7.4800	0.0989
	0.4880	-2.5957	4.1537	-1.9961	0.1782
	-0.2108	1.2467	-2.4080	1.6401	0.0671

APPENDIX G: Sample Input and Output from CESARE-CFD

Sample Input: Taken from the 2MW Coarse Grid Run

```

.....
rad grid changed
.....
4000 <- No. of iterations
false <- unsteady state solution
2 <- units of time interval 1 = sec. 2 = min. 3 = hr.
10 <- additional time (in units above)
-----
# comb-model: 1,mixture fraction; 0, eddy dissipation and soot generation comb
.....Program Control.....
uvw p k-e f g h prop traj dispn comb. radn burnslab
1 1 1 1 1 1 0 0 1 1 0
comb-model Order - Limited h,f, corr.int.
1 1 1 0

.....Under Relaxation Factors.....
u v w p te ed f g h visc den
0.5 0.5 0.5 0.5 0.50 0.50 0.5 0.50 0.50 0.5 0.5
sup svp swp smap shp srh balance hcor fcor
0.40 0.40 0.40 0.4 0.4 0.4 1.0 0.5 0.5

.....Number of Solution Sweeps.....
u v w p te ed f g h
6 6 6 40 6 6 6 6 6

..... PRINTout Tables.....
3 <- Print as i, j or k planes 1, 2 or 3
u v w p visc den te ed f g
0 0 0 0 0 0 0 0 0 0
temp h sup svp swp smap shp srh cpm cpt
0 0 0 0 0 0 0 1 0 0
VO2 traj trajend block Qwall
0 0 0 0 0

.....PLOT Output Files.....
1 <- 0 = binary output 1 = formatted output
uvw p visc te ed f g h O2 T Pconc traj prod Uwall
1 0 0 0 0 1 0 1 1 1 1 0 0 0

----- OTHER PARAMETERS -----
.....
1 1 <- in, out Temperature units 0 = Kelvin; 1 = Centigrade

```

0 <- screen display 0 = fluids 1 = combustion
 0 <- igniterset: automatic = 0; on = 1; off = -1.
 70. <- percentage combustion for igniter cut in
 1.8 4.4 2.0 <- Monitoring location x y z
 5 <- Call interval for trajectories
 1 <- First trajectory call
 3 <- Call interval for g equation
 5 <- Call interval for radiation (multiple of traj interval)
 1 <- Number of particle start locations (1 or 4)
 2 <- Number of track paths per start location
 100 <- Maximum number of steps in each trajectory
 0.2 5.0 <- Trajectory min. and max grid step
 0 <- 1 for mainly horizontal, 0 for vertical buoyant flow
 10 <- intermediate keep.oi output interval

=====

////////////////////// BASE GRID //////////////////////////////////////

=====

X max. cells west wall east wall (1 cell for 2D)

.....

 18 0.0 3.6

Fine regions No. x-min x-max (gaps will be filled)

.....

Y max. cells south wall north wall

.....

 27 0.0 5.4

Fine regions No. y-min y-max (gaps will be filled)

.....

Z max. cells bottom wall top wall

.....

 25 0.0 5.

Fine regions No. z-min z-max (gaps will be filled)

.....

=====

 BOUNDARIES BOUNDARIES

.....

300. <- Default WALL TEMPERATURE

-1. <- Default Wall coefficient (kW/m^2) (-ve = automatic)

=====

AMBIENT TEMP, WALL THERMAL PROPERTY, HEAT TRANSFER COEFF, AND WALL THICKNESS

.....

#AMBIENT TEMP(C) THER. CONDUCTIVITY(J/m-C) HTC (J/m^2-C) WALL THICK(m)

 20.0 0.8 20 0.2

ADD/SUBTRACT/SYMMETRY B = 0/ -2/ -3/

Ucoeff > 0. prescribed heat flux;

Ucoeff < 0. wall functions used.

Ucoeff = 0. adiabatic

For simulating the transient conditions, the wall temperature need calculate.

Identify the wall type, i.e. the wall connect to outside and the wall inside

idw = -2 external boundary, default external wall defined in SETBLOCK

idw = -1 internal boundary

idw = -6 burning slab which is defined in BLOCKASSIGN,GRID.F

TRAPEZIUM with depth in direction X (=1), Y (=2), or Z (=3) deg kW/m²/C

1 | Xmin Xmax | Ymin Zmin Zmax | Ymax Zmin Zmax B idw T Ucoeff

#-1 | Xmin Xmax | Zmin Ymin Ymax | Zmax Ymin Ymax B T Ucoeff

2 | Ymin Ymax | Xmin Zmin Zmax | Xmax Zmin Zmax B T Ucoeff

#-2 | Ymin Ymax | Zmin Xmin Xmax | Zmax Xmin Xmax B idw T Ucoeff

3 | Zmin Zmax | Xmin Ymin Ymax | Xmax Ymin Ymax B T Ucoeff

#-3 | Zmin Zmax | Ymin Xmin Xmax | Ymax Xmin Xmax B T Ucoeff

FRUSTRUM on axis X (=11), y (=22), or Z (=33)

11| Yaxis Zaxis | Xmin Rmin Rmax | Xmax Rmin Rmax B idw T Ucoeff

22| Xaxis Zaxis | Ymin Rmin Rmax | Ymax Rmin Rmax B T Ucoeff

33| Xaxis Yaxis | Zmin Rmin Rmax | Zmax Rmin Rmax B T Ucoeff

DOME

axis = + - 111 axis along X, curved surface in + - X direction

axis = + - 222 axis along Y, curved surface in + - Y direction

axis = + - 333 axis along Z, curved surface in + - Z direction

Axis Xcen Ycen Zcen Rmin Rmax 0 0 0 B idw T Ucoeff

=====

1 | Xmin Xmax | Ymin Zmin xZmax | Ymax Zmin Zmax B idw T Ucoeff

1 .0 3.6 3. 2.4 5. 5.4 2.4 5. -2 -2 300.0 -1

1 .0 3.6 3. 0 5. 3.2 0. 5. -2 -1 300.0 -1

1 .6 3. 3. 0.5 2. 3.2 0.5 2. 0 -1 50.0 -1

1 .0 0. 0.2 0. 5. 3. 0. 5. -3 -2 50.0 -1

1 3.6 3.6 0.2 0. 5. 3. 0. 5. -3 -2 50.0 -1

=====

BURNING SLABS B = -6

Ucoeff > 0. prescribed heat flux;

Ucoeff < 0. wall functions used.

Ucoeff = 0. adiabatic

TRAPEZIUM with depth in direction X (=1), Y (=2), or Z (=3) deg kW/m²/C

#SLAB NO| 1 | Xmin Xmax | Ymin Zmin Zmax | Ymax Zmin Zmax B T Ucoeff

-1 | Xmin Xmax | Zmin Ymin Ymax | Zmax Ymin Ymax B T Ucoeff

```

# 2 |Ymin Ymax | Xmin Zmin Zmax | Xmax Zmin Zmax B T Ucoeff
# -2 |Ymin Ymax | Zmin Xmin Xmax | Zmax Xmin Xmax B T Ucoeff
# 3 |Zmin Zmax | Xmin Ymin Ymax | Xmax Ymin Ymax B T Ucoeff
# -3 |Zmin Zmax | Ymin Xmin Xmax | Ymax Xmin Xmax B T Ucoeff

```

FRUSTRUM on axis X (=11), y (=22), or Z (=33)

```

# 11 |Yaxis Zaxis|Xmin Rmin Rmax | Xmax Rmin Rmax B T Ucoeff
# 22 |Xaxis Zaxis|Ymin Rmin Rmax | Ymax Rmin Rmax B T Ucoeff
# 33 |Xaxis Yaxis|Zmin Rmin Rmax | Zmax Rmin Rmax B T Ucoeff

```

DOME

axis = + - 111 axis along X, curved surface in + - X direction
axis = + - 222 axis along Y, curved surface in + - Y direction
axis = + - 333 axis along Z, curved surface in + - Z direction

```

# Axis Xcen Ycen Zcen Rmin Rmax 0 0 0 B T Ucoeff
#SLAB NO| 1 |Xmin Xmax | Ymin Zmin Zmax | Ymax Zmin Zmax B T Ucoeff

```

```

.....
# 1 33 4.4 1.2 .4 .0 .5 .4 .0 .5 -6 50 -1

```

=====F

REE STREAMS

wall No. xmin - xmax ymin - ymax zmin - zmax Temp

```

-----
u v w rms/mean scale (m)
-----

```

=====

BALANCE/OUTLET PORT

```

.....
false <-- uniform mass flux at balance port
true <-- Inflow or reverse flow is fresh
20.0 <-- inflow temperature
0.0 <-- inflow mixture fraction
0.3 <-- inflow turbulence rms/reference velocity
0.2 <-- inflow turbulence length scale/sqrt port area
2.0 <-- inflow reference velocity

```

Rectangular - cartesian or skewed planes

Plane Axis: 0 not skewed; 1 along X; 2 along Y; 3 along Z;

Port No Wall No. Axis x1 - x2 y1 - y2 z1 - z2

```

.....
1 6 0 .0 3.6 0. 3.0 5. 5.
2 3 0 .4 3.2 0. .0 0.4 4.6
-----

```

Axisymmetric - cartesian planes

Port No Wall No X-centre Y-centre Z-centre R-min. R-max.

```

.....
-----

```

=====

FORCED FLOW PORTS

=====

Separate Port No. for each fluid and location (i = 1 for 2-D)
 Wall numbers: 1=west, 2= east, 3=south, 4=north, 5=bot, 6=top.

Rectangular - cartesian or skewed planes
 Plane Axis: 0 not skewed; 1 along X; 2 along Y; 3 along Z;
 Port No. Wall No. Axis x1 - x2 y1 - y2 z1 - z2

# fuel port									
1	5	0	1.5	2.1	4.2	4.6	0.2	0.2	
2	4	0	1.5	2.1	5.4	5.4	0.	0.4	

Axisymmetric Ports Cartesian Planes
 Port No. Wall No. x-cen y-cen z-cen min.rad. max.rad

=====

PORT INLET CONDITIONS

.....

0.08 <- inlet turbulence rms / normal vel.
 0.02 <- Turb. length scale / sqrt of port area.

port No.	T factor	diff. (kg/s)	fluid (kg/s)	p.f. frac.	mixture [u/n v/n w/n 0]	[either tang/n rad/n 0 1]	[or]
1	20.0	1.0	0.0434	0.0	1.	0.	0. 0. 0
2	20.0	1.0	.5	0.0	.0	0.	0. 0. 0

=====

FUEL ULTIMATE ANALYSIS MASS FRACTIONS

.....

0.8 <- Carbon
 0.15 <- Hydrogen
 0.05 <- Nitrogen
 0.0 <- Sulphur
 0.0 <- Oxygen
 0.0 <- Water
 0.0 <- Ash
 46000.0 <- Specific energy LHV daf coal or wet gas (kJ/kg)
 44.0 <- Fuel gas or volatiles molecular weight
 1.8e+5 <- Soot burning activation energy (kJ/kmol)
 6.27e+0 <- Soot burning preexponential factor (kg/(m²-s-Paⁿ))

BURNING SLAB NO. 1

```

# position for fire spread routine (same position as in ports handling section)
#para. cntr.point  init.fire  maxfuel  maxfuel  heat of
#towall          size (m)   size(m)  load(kg)  evaprat.
#nwall xcen ycen zcen radmin0 radmax0 radfuel  fuelload deltahv
.....
5  4.4 1.2 .35 0. .05 .5 2.9 280.5
0.005 <- (M.F.) O2 limit.Fuel burn continues if O2 is higher
# than OLTD. This value must be great than 0, or floating in PDF

```

PARTICLES

```

.....
1400. <- Particle density (kg/m^3)
4 <- Number of coal particle sizes

```

Particle diameters (m)

```

.....
188.1e-6 137.3e-6 97.3e-6 72.4e-6

```

Size mass fractions

```

.....
0.1 0.1 0.1 0.7

```

RADIATION CONDITIONS

```

.....
4.9 <- CAPP coefficient (modified by Anthony)
0.13 <- scattering coefficient
0.4 <- additional absorption coefficient (m^-1)
0.4 .0 0 4 .0 <- in region x1,y1,z1 x2,y2,z2
2 <- Number of theta angle divisions.
4 <- Number of phi angle divisions
false <- Radiation grid is flow grid

```

RADIATION GRID

```

.....
10 <- Number of X cells nir
X cell boundaries nir + 1 required
.....
0. .4 .7 1.1 1.5 1.8 2.1 2.5 2.9 3.2 3.6

```

```

.....
10 <- Number of Y dells njr
Y cell boundaries njr + 1 required
.....
3.2 3.4 3.7 3.9 4.1 4.4 4.6 4.8 5.0 5.2 5.4

```

12 <- Number of Z cells nkr
Z cell boundaries nkr + 1 required

.0 .2 .4 .6 .8 1.0 1.2 1.4 1.6 1.8 2.0 2.2 2.4

Radiation Boundary Conditions

Cartesian Walls Axis=0 Face = +,- 1 facing +,- axes
Skew walls rotated about X Axis=1 Face = +,- 1 facing +,- Z axis
or Y Axis=2 Face = +,- 1 facing +,- Z axis
or Z Axis=3 Face = +,- 1 facing +,- Y axis

Axis	Face	X1	X2	Y1	Y2	Z1	Z2	T	Emissivity
------	------	----	----	----	----	----	----	---	------------

walls

0	1	0	0	3.2	5.4	0	2.4	20.0	0.9
0	1	0	3.6	3.2	3.2	0	2.4	20.0	0.9
0	-1	3.6	3.6	3.2	5.4	0	2.4	20.0	0.9
0	-1	0	3.6	5.4	5.4	0	2.4	20.0	0.9

corridor end

floor

0	1	0.0	3.6	3.2	5.4	0	0	20.0	0.9
---	---	-----	-----	-----	-----	---	---	------	-----

ceiling

0	-1	0	3.6	3.2	5.4	2.4	2.4	20.0	0.9
---	----	---	-----	-----	-----	-----	-----	------	-----

Single particle tracking data

false <- Tracks wanted
true <- dispersion
2 <- number of particle sizes
particle diameters (m) are

200.0e-6 10.0e-6

x	y	z	starting locations (m) are
---	---	---	----------------------------

3.	4.	5.0
----	----	-----

4.	3.	2.0
----	----	-----

47.7689958161999	46.2943648405389	45.3281349368999
44.7562274635671	44.4798926967845	44.4083851997052
44.4470506755459	44.4990474938319	44.5276386563644
44.7566254466417	50.0000000000000	50.0000000000000
99.7299572991740	85.7962707271627	76.3405657330866
68.9746287180281	62.9505480232875	58.0316435309087
54.0973656939376	51.0449551482595	48.7626086619060
47.1287371039557	46.0214520753088	45.3283068807373
44.9494387922105	44.7924174988278	44.7638247446830
44.7747239416794	44.7994969959773	45.0407114530472
50.0000000000000	50.0000000000000	101.745211017123
88.1158487797958	78.8167106788786	71.4482570356096
65.3368155111482	60.2831655840698	56.1886188883345
52.9636945760237	50.5064070275951	48.7035746175648
47.4399307138664	46.6069474167427	46.1062427387335
45.8463725104825	45.7376172449918	45.7000416971076
45.7197751445256	45.9959407365387	50.0000000000000
50.0000000000000	104.128133079541	90.9742338593025
81.9315305032809	74.6247656035794	68.4617113760279
63.2887987359197	59.0348915165844	55.6281670747851
52.9797250693973	50.9871888590824	49.5439232083926
48.5473597442558	47.9026856304181	47.5212674161657
47.3180332474369	47.2215535533330	47.2294300748172
47.5465726161518	50.0000000000000	50.0000000000000
106.750324240901	94.2822254226609	85.6534122368867
78.5201077531713	72.3751423733332	67.1187054410949
62.7157888350612	59.1199953039276	56.2615825158499
54.0533120649362	52.4002836082616	51.2084013509491
50.3887425732241	49.8575726372258	49.5359295303678
49.3613739380751	49.3431848540241	49.6962143068611
50.0000000000000	50.0000000000000	109.500109778301
97.9605622559405	89.9467098444495	83.1476003211272
77.1350714181903	71.8651433626187	67.3463899091608
63.5668297900216	60.4839504294847	58.0317949398556
56.1316318616401	54.7013085281463	53.6611066443354
52.9358059203704	52.4563411565347	52.1724414992590
52.1065344121259	52.4845707951108	50.0000000000000
50.0000000000000	112.263660556870	101.907634952477
94.7414169906182	88.4867477379399	82.7740636709862
77.6066770639704	73.0391392762867	69.1022892788492
65.7904450587678	63.0668049406941	60.8745224489878
59.1479285263372	57.8213517049535	56.8345099003454
56.1363392848334	55.6965880701459	55.5551151566486
55.9497146953950	50.0000000000000	50.0000000000000
114.917490566840	105.962585732556	99.8820399684261
94.4174829894108	89.2218100523995	84.3216280109366
79.8106162558821	75.7681129578462	72.2383838807911
69.2246852495182	66.6975602109968	64.6102708926731
62.9148589806880	61.5750017620442	60.5729505526797
59.9146246967463	59.6676994825467	60.0884952884452
50.0000000000000	50.0000000000000	117.343109997215
109.846130837235	105.013564985509	100.553130741654

FOLDOUT 1 - POLYURETHANE BURNS

The following information was taken from Chapter 3 - Experimental Setup.

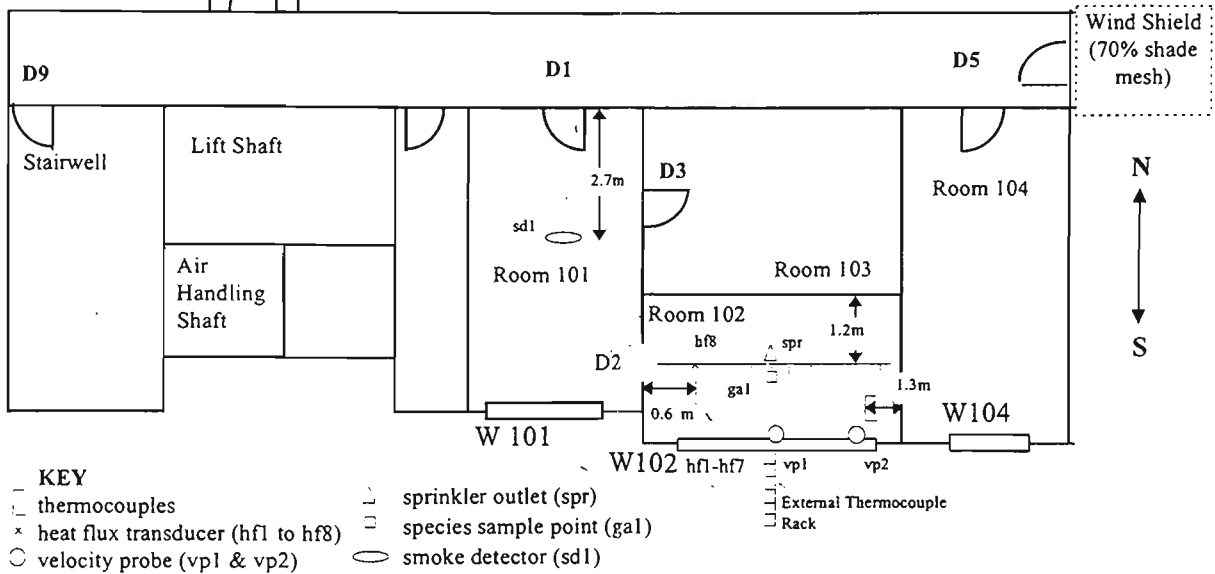


Figure 3.1: Floor 1 - Plan view including instrumentation within the standard burn room for PU1 to PU3. The key for symbols representing different instrument is given in the figure.

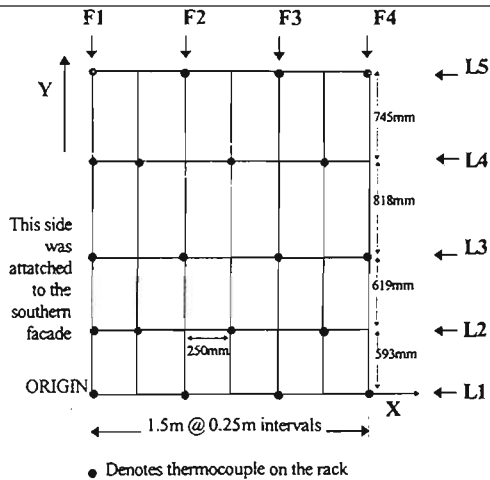


Figure 3.7: External 2D thermocouple rack. F denotes a Face, and L denotes a Level. F1 is parallel to the external facade and L1 corresponds to the top of the burn room window.

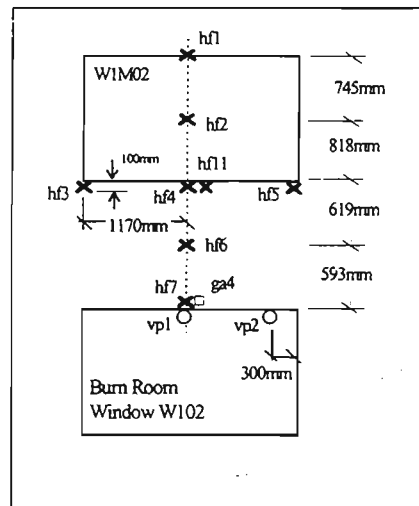


Figure 3.9: Southern elevation - external instrumentation. The dashed line indicates the edge-view of the 2D external thermocouple rack.

Combination of *Table 3.1: Fuel Load*, *Table 3.2: Environmental Conditions* and *Table 3.3: Ventilation Conditions*.

Test	Fuel Load (kg)	Environmental Conditions	D2	D1	D9	D5	W102	Ventilation Class
PU1	17.78	WNW @ 4.33 m/s	Open	Closed	Closed	Closed	Closed	Class 2
PU2	16.02	ENE @ 2.53 m/s	Open	Open	Open	Closed	Closed	Class 1b
PU3	15.06	ENE @ 3.72 m/s	Open	Open	Closed	Open	Closed	Class 1a
PU4	16.22	NNE @ 2.98 m/s	--	Open	Open	Closed	Closed	Class 1b

FOLDOUT 2 - REAL FURNITURE BURNS

The following information was taken from Chapter 3 - Experimental Setup.

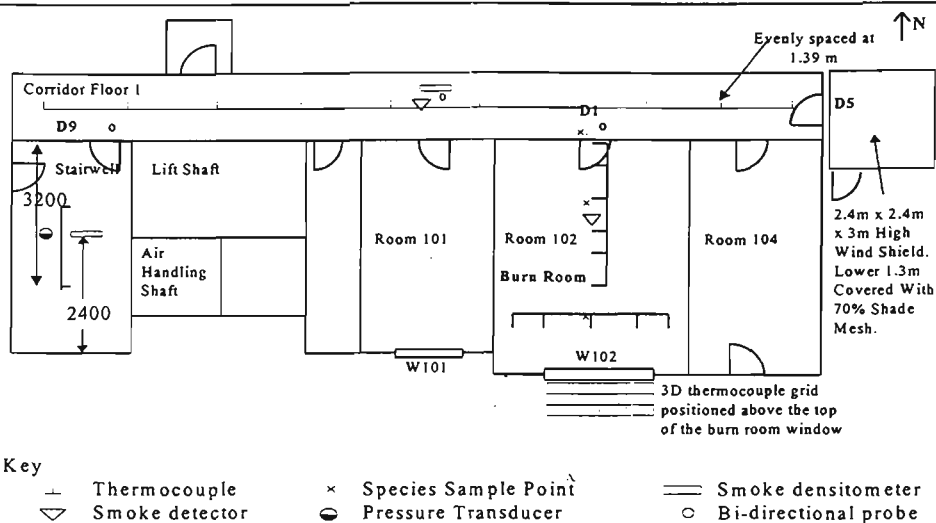


Figure 3.14: Instrumentation layout on Floor 1, including external 3D thermocouple rack.

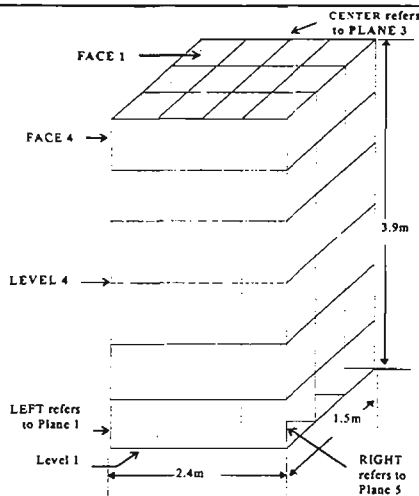
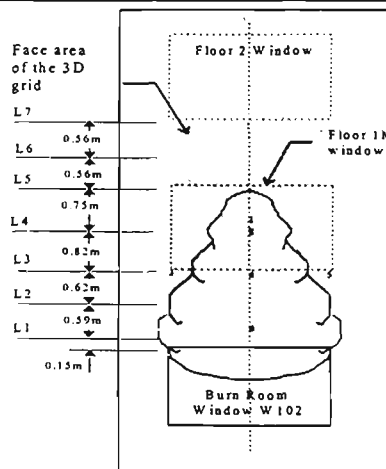


Figure 3.19: External 3D thermocouple grid. A thermocouple was attached 5cm away from each grid point



1-6: Heat Flux Transducer Locations

Figure 3.20: Locations of the external heat flux transducers

Combination of Table 3.5: Fuel load, ventilation conditions and WLC, and Table 3.6: Environmental Conditions.

Test	Wood Equivalent Fuel Load (kg/m ²)	Burn Room Door (D1)	Stairwell Door (D9)	Additional Factors, Ventilation Class and WLC	Average wind Speed and Direction
BURN 1	26.36	Open	Closed	Window opened, fuel type and distribution in Appendix C, Class 1a	ENE @ 1.5 m/s
BURN 2	28.05	Open	Closed	New fuel distribution, with similar fuel load as Burn 1, WLC#1, Class 1a	SSE @ 1.6 m/s
BURN 3	27.65	Closed	Closed	WLC#2, Class 2	S-SSW @ 3.5 m/s
BURN 4	28.32	Closed	Closed	WLC#2, Class 2	NE @ 1.6 m/s
BURN 5	28.21	Open	Open	Window failed, Class 1b	W @ 2.1 m/s
BURN 6	27.90	Open	Open	WLC#1, Smoke Management System on, no flashover, Class 1b	WNW @ 2.5 m/s
BURN 7	27.95	Closed	Closed	WLC#1, Smoke Management System on, flashover occurred, Class 2	SW @ 1.2 m/s
BURN 8	28.48	Open	Open	WLC#1, combustible linings in corridor, Class 1b	NNW @ 1.3 m/s

